

# Climate change impacts on the flow regimes of rivers in Bhutan and possible consequences for hydropower development

*Stein Beldring (Ed.)*

4  
2011

R  
E  
P  
O  
R  
T





# **Climate change impacts on the flow regimes of rivers in Bhutan and possible consequences for hydropower development**

## **Report no. 4 – 2011**

# **Climate change impacts on the flow regimes of rivers in Bhutan and possible consequences for hydropower development**

Published by: Norwegian Water Resources and Energy Directorate

**Editor:** Stein Beldring

Authors: Stein Beldring and Astrid Voksø

Print: Norwegian Water Resources and Energy Directorate

**Number**

**printed:** 70

Cover photo: Punakha Dzong, Bhutan, photo by Henny vanLanen

**ISSN:** 1502-3540

**ISBN:** 978-82-410-0751-4

**Key words:** Hindu Kush-Himalayan region, Bhutan, climate change, hydrology, hydropower

Norwegian Water Resources and Energy Directorate  
Middelthunsgate 29  
P.O. Box 5091 Majorstua  
N 0301 OSLO  
NORWAY

Telephone: +47 22 95 95 95

Fax: +47 22 95 90 00

E-mail: [nve@nve.no](mailto:nve@nve.no)

Internet: [www.nve.no](http://www.nve.no)

May 2011



# Contents

Preface.....	4
Summary .....	5
1 Introduction.....	7
2 Study area and data.....	9
3 Climate change .....	15
4 Hydrological modelling .....	18
5 Hydrological modelling with input from climate models .....	26
6 Climate change impacts on hydrological regimes in Bhutan.	29
7 Possible impacts on hydropower development .....	40
8 Conclusions .....	45
Acknowledgements .....	49
References.....	50
Appendix A Evaluation of hydrological model with observed meteorological data input .....	54
Appendix B Evaluation of hydrological model with input from climate projection Echam B1 .....	59
Appendix C Seasonal precipitation change and mean daily streamflow for climate projections Echam A2 and B1 .....	66
Appendix D Hydrological model results for period 1981-2100 based on climate projection Echam A2 .....	85
Appendix E Maps of hydrological model results for Bhutan based on climate projection Echam A2 .....	109
Appendix F Flow duration curves based on climate projection Echam B1 .....	117

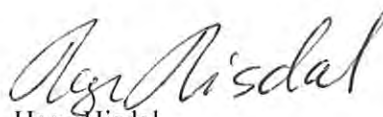
# Preface

The main objective of this study is to assess the impacts of climate change on the runoff regime of the rivers of the Kingdom of Bhutan to provide valuable information for the country's hydropower development programme. Production of electricity by hydropower is dependent on runoff, and possible changes in hydrological processes are therefore of large economical importance. Assessment of the future hydrological regime is a production chain where changes in external forcing caused by greenhouse gas emissions are introduced into climate models (global general circulation models and regional climate models). The climate model results are used for driving hydrological models that determine time series of hydrological state variables and fluxes for present and future climate conditions. These time series and their statistics, e.g. annual or seasonal mean and extreme values, are a useful way of communicating the results from modelling hydrological impacts of climate change. The results presented in this report have been produced by the Norwegian Water Resources and Energy Directorate. This study was funded by the Norwegian Agency for Development Cooperation (Norad), a directorate under the Norwegian Ministry of Foreign Affairs and the Department of Energy of the Royal Government of Bhutan, within the project Strengthening of the Energy Sector Phase III, Activity 3: Support to Hydromet Services Division for Sustainable Data Provision to Accelerated Hydropower Development.

Oslo, June 2011



Morten Johnsrud  
Director  
Hydrology Department



Hege Hisdal  
Head of Section  
Hydrological Modelling Section

# Summary

The main objective of this study is to assess the impacts of climate change on the hydrological regime of the rivers of the Kingdom of Bhutan to provide information for the country's hydropower development programme. A spatially distributed hydrological model was used for describing hydrological processes including glacier mass balance, snow storage, subsurface water storage and streamflow (river flow). Observed precipitation, temperature and streamflow from the station network of the Department of Energy of the Royal Government of Bhutan, Hydromet Services Division were used for calibrating and running the hydrological model for the period 1991-2008. Results from climate model simulations with two emission scenarios for greenhouse gas concentrations in the atmosphere were used to determine precipitation and temperature time series for the meteorological station sites for the period 1981-2100. These precipitation and temperature time series were used as input to hydrological modelling for the period 1981-2100. Hydrological model results for the water balance and streamflow of 17 catchments in Bhutan and for the entire land surface of Bhutan was considered in this study, with particular emphasis on the control period 1981-2010 and the projection periods 2021-2050 and 2071-2100. The hydrological model simulations are transient, i.e. the hydrological model was run from 1981 until 2100, while results for the control and projection periods were extracted from the transient simulations. The hydrological model has a high precision with regard to simulating streamflow, both with input from observed meteorological data or with input from climate model data.

Increasing concentrations of greenhouse gases in the atmosphere changes the radiation balance of the earth-atmosphere system, resulting in increasing ground temperatures and changes in cloud cover, precipitation, air humidity, radiation, wind and other meteorological elements. These changes will lead to changes in the land phase of the hydrological cycle with impacts on glacier mass balance, snow storage, soil moisture in the unsaturated zone, groundwater storage, evapotranspiration and runoff.

The change in mean annual temperature from 1981 to 2050 averaged over the area studied in this work is approximately 1.4 °C, while the change in mean annual temperature from 1981 to 2100 is 2.5 °C and 4.9 °C for each of the two emission scenarios for greenhouse gases, respectively. The changes in mean annual precipitation sums from 1981-2010 to 2021-2050 and 2071-2100 are mostly negative and the changes in precipitation are larger by the end of the century than by the middle. Large negative changes are more frequent in southern parts of Bhutan. Precipitation changes are small for the winter (December, January, February), spring (March, April, May) and autumn (September, October, November) seasons. For the summer season (June, July, August) the changes are negative.

Glacier mass balance is negative for most areas for the period 1981-2100, resulting in decreasing glacier ice volumes and glacier covered areas. Until the middle of the 21<sup>st</sup> century negative glacier mass balance is not sufficiently large to melt more than small fractions of the glacier covered areas completely, but by the end of the century large areas that are glacier covered at present will be completely devoid of glacier ice. The contribution to streamflow from glacier ice melt water will remain mostly unchanged during the first half of the 21<sup>st</sup> century, while it will diminish during the second half.

For most catchments streamflow is not changing much from 1981-2010 to 2021-2050. However, as a result of smaller precipitation amounts, in particular during summer, there is a reduction in streamflow for catchments with small glacier covered fraction since they will not receive a contribution to runoff from melting ice. The catchments with largest glacier covered fraction will experience increased streamflow caused by increased contribution to runoff from glacier ice melt. For the period 2071-2100 there is a decline in precipitation compared to the period 1981-2010. In combination with a reduction in glacier volume and area this leads to a large reduction in streamflow. Catchments with a negligible glacier covered fraction will also experience reduced streamflow, but this is a result of precipitation change.

Mean annual discharge available for hydropower production has been estimated assuming a run-of-river hydropower plant at the outlet of each catchment with turbines with a capacity for annual inflow in the range 20 % - 200 % of mean annual inflow for the period 1981-2010. The change in mean annual discharge available for hydropower production from 1981-2010 to 2021-2050 varies between 13 % decrease and 7 % increase for all catchments and both emission scenarios for greenhouse gases. The change in mean annual discharge available for hydropower production from 1981-2010 to 2071-2100 is influenced by reduced contribution to streamflow from glacier ice melt. This leads to a decline in mean annual discharge available for hydropower production compared to the period 1981-2010 varying from -76 % to -4 %, the rate of change depending on the initial ice covered fractions of the catchments. The difference in mean annual discharge available for hydropower production between the two climate projections is now larger. Higher temperature increase for climate projection ECHAM A2 results in more rapid melting of glacier ice than for climate projection ECHAM B1 and larger contribution to streamflow as long as the glaciers are present, but also to earlier disappearance of glacier ice and consequently reduced streamflow when the glacier covered area is smaller.

The glacier covered areas of the catchments were treated as time-variant with initial ice volumes and glacier covered areas modified by model mass balance. Streamflow downstream of areas with glaciers will decline if glacier covered areas and the contribution to runoff from melting glacier ice is reduced. Hydrological model simulations with constant glacier covered areas were performed as a sensitivity analysis. They show a strong increase in streamflow and mean annual discharge by the end of the 21<sup>st</sup> century as a result of increasing temperatures leading to higher glacier ice melt rates. Until the middle of the century there is only a small difference between the two sets of model results, as model simulations with time-variant glacier covered areas have only led to a small reduction of glacier ice volume and area.

The annual cycle of meteorological processes in Bhutan will not change during the 21<sup>st</sup> century in the sense that the largest amounts of precipitation will still occur during summer and the smallest during winter. At high altitudes temperature will remain below freezing point during the winter and precipitation will accumulate as snow. The annual cycle of streamflow follows the same pattern as in the present climate with low flow during winter and high flow during summer as a result of the combined effect of snowmelt and larger amounts of precipitation in the summer season than in the rest of the year. There is a relatively small change in the magnitude of streamflow until the middle of the 21<sup>st</sup> century, whereas changes are larger by the end of the 21<sup>st</sup> century due to reduced contribution from melting of glacier ice.

# 1 Introduction

The Hindu Kush-Himalayan region extends 3,500 km over all or part of eight countries from Afghanistan in the west to Myanmar in the east. It is the source of ten large Asian river systems – the Amu Darya, Indus, Ganges, Brahmaputra, Irrawaddy, Salween, Mekong, Yangtze, Yellow River, and Tarim, and provides water, ecosystem services, and the basis for livelihoods to a population of around 210.53 million people in the region. The basins of these rivers provide water to 1.3 billion people, a fifth of the world's population. Some of the streamflow in these rivers comes from melting of snow and glacier ice, some from storage in lakes, wetlands and the subsurface, and the remaining part from the summer monsoon which dominates the climate in this region. During the monsoon season, most of the streamflow in the lower parts of the area comes directly from rainfall. The region is characterised by an extreme variability in precipitation patterns. Precipitation is generally decreasing from the east to the west as a result of the weakening of the summer monsoon as it moves westward along the Himalayan range (Armstrong, 2010).

Global warming of the surface temperature by approximately 0.75 °C has been observed over the last 100 years (Trenberth et al., 2007). Warming in the Hindu Kush-Himalayan region has been greater than the global average, for example 0.6 °C per decade in Nepal (Eriksson et al., 2009). Different emission scenarios for greenhouse gases project a further increase of global temperature of 1 °C to 6 °C (Meehl et al., 2007). Globally averaged water vapour concentrations, evaporation and precipitation are projected to increase, with subsequent impacts on land surface hydrology including glacier mass balance and snow storage. The Hindu Kush-Himalayan region has the largest area covered by glaciers outside the polar regions, representing one of the worlds largest storehouses of freshwater. The major concentrations of glaciers are spread across about 12 mountain ranges forming the headwaters of almost all the major rivers in the central, south, and south-eastern Asian mainland (Armstrong, 2010). A substantial proportion of annual precipitation falls as snow and glacier ice and snow melt in addition to monsoon rainfall yield the major contribution to annual streamflow. With rising temperatures caused by anthropogenic greenhouse gas emissions, snow storage and snow melt will become less important, while glacier ice melt in the Himalayas is projected to increase. This will affect water resources within the next two to three decades and lead to increased flooding. This will be followed by decreased river flows as the glaciers recede (Sharma et al., 2009). Freshwater availability in central, south, eastern and south-eastern Asia, particularly in large river basins, is projected to decrease due to climate change which, along with population growth and increasing demand arising from higher standards of living, could adversely affect more than a billion people by the 2050s. Coastal areas, especially heavily-populated mega-delta regions in south, eastern and south-eastern Asia, will be at greatest risk due to increased flooding from the sea and, in some mega-deltas, flooding from the rivers. Climate change will have large impacts on agriculture. It is projected that crop yields could increase up to 20 % in eastern and south-eastern Asia while they could decrease up to 30 % in central and southern Asia by the mid 21<sup>st</sup> century. Together, and considering the influence of rapid population growth and urbanisation, the risk of hunger is projected to remain very high in several developing countries (Cruz et al., 2007).

Water plays a significant role for important sectors in the Hindu Kush-Himalayan region, e.g. hydropower, agriculture, water supply and tourism. Furthermore, hydrological processes at the land surface influence the natural environment at a range of spatial and temporal scales through their impacts on biological activity and water chemistry. Water is also a primary weathering agent for rocks and soils, breaking them down, dissolving them, and transporting the resulting sediments and dissolved solids to the sea. Freshwater discharge, latent and sensible heat fluxes, glacier mass balance and snow cover influence the global climate through feedback effects involving atmospheric and ocean circulation (Peixoto and Oort, 1992). Climate change impact studies in natural and social sciences where water resources exert a major control on the phenomena under consideration must consider changes in mean values, seasonal variability and extremes of water availability including glacier ice, snow, subsurface moisture conditions, lakes and streamflow.

The objective of this study is to assess the impacts of climate change on the hydrological regime of the rivers of the Kingdom of Bhutan to provide information for the country's hydropower development programme. A spatially distributed hydrological model was used for describing hydrological processes including glacier mass balance, snow storage, subsurface water storage and streamflow. Observed precipitation, temperature and streamflow from the station network of the Department of Energy of the Royal Government of Bhutan, Hydromet Services Division were used for calibrating and running the hydrological model for the period 1991-2008. Results from climate model simulations with two emission scenarios for greenhouse gas concentrations in the atmosphere were used to determine precipitation and temperature time series for the meteorological station sites for the period 1981-2100. Hydrological model results for 17 catchments in Bhutan and for the entire land surface of Bhutan was considered in this study, with particular emphasis on the periods 1981-2010, 2021-2050 and 2071-2100.

The Fourth Assessment Report of the Intergovernmental Panel on Climate Change (IPCC) (Cruz et al., 2007) predict that negative mass balance in mountain regions may eventually lead to disappearance of glaciers with subsequent large impacts on the seasonality and volume of streamflow. In the Hindu Kush-Himalayan region, where snow and ice melt from glaciers is often a significant contributor to dry season flow, there are indications that climate change might have serious effects on seasonal as well as annual runoff. In recent years glaciers have been receding, which might have a long-term effect on the amount of snow and ice available for glacial fed flows. This in turn can cause reduction in dry season runoff which can have serious effects on hydropower production and development in the rivers of Bhutan, which are typically run-of-river hydropower plants with little or no storage. Although deglaciation may result in declining streamflow in the long run, some areas may benefit from increased water availability during the next decades (Rees et al., 2004). In addition to the effect on hydropower production, receding glaciers also often cause lakes of various sizes to form, either on the glacier surface or in front of the receding glacier. These lakes are often dammed by ice-filled moraines and, when reaching critical levels, the lakes are suddenly emptied, often within a few hours, and often with disastrous effect downstream (Mool et al., 2001). Such phenomena are not considered in this study. The hydrological model simulations consider the water balance and interactions between the land surface and the atmosphere of the hydrological cycle, providing information about hydrological state variables and fluxes, e.g. glacier mass balance, snow storage, groundwater storage evaporation, and streamflow.

## 2 Study area and data

Bhutan is situated in the eastern Himalayas approximately between latitudes 26.5° N to 28° N and longitudes 88.5° E to 92° E. It is 340 km in length with an area of approximately 40000 km<sup>2</sup>. It is bordered by the Tibetan plateau of China in the northern and the Indian states of Sikkim in the west, West Bengal and Assam in the south, and Arunachal Pradesh in the east. The terrain is mostly mountainous with elevations ranging from 200 m a.s.l. to above 7000 m a.s.l. The population of Bhutan is estimated to be 600,000 (Mool et al., 2001).

The reversal of circulation associated with the development of winter high pressure and summer low pressure over the landmass of Asia interacts with the topography and the migration of the intertropical convergence zone to produce a particularly strong seasonality of precipitation in much of Asia and Africa called the monsoon. The intertropical convergence zone is the belt of high precipitation where warm easterly winds from both hemispheres carrying large amounts of moisture evaporated from the tropical zones converge. One of the most pronounced orographic precipitation formation effects globally occurs in conjunction with the monsoon over the Indian subcontinent. In summer, a northward shift in the position of the intertropical convergence zone and accompanying changes in circulation patterns induce moist southerly winds from the Bay of Bengal. These winds converge and rise over India north of Bangladesh, producing heavy rains that dominate the climate of Bhutan (Dingman, 1994).

Climatically Bhutan can be divided into three broad zones: subtropical in the southern foothills with temperatures ranging between 15 °C to 30 °C year round, temperate in the middle valleys or inner hills, and alpine with year-round snowfall in the northern parts. Generally, southern foothills are hot and humid during the summer and quite cool in winter. The middle valleys are cold in winter and warm in summer. Generally the monsoon starts in June and lasts until the beginning of September. The period from November to March is usually dry. Mean annual rainfall varies from approximately 2500 to 5500 mm in the southern foothills, from 1000 to 2500 mm in the inner valleys, and from 500 to 1000 mm in the northern part of the country (Mool et al., 2001). Figures 2.1 and 2.2 present mean daily temperatures and mean monthly precipitation sums for meteorological stations 1333 Druyagang (1140 m a.s.l.) and 1339 Phobjikha (2860 m a.s.l.) in main river basin number 13, river Punatsangchhu (Sankosh in India). Station 1333 is located in the southern part of the river basin, while station 1339 is located in the east of the central part of the river basin.

The rivers of Bhutan flow from the Himalayas in the north to River Brahmaputra in the south, mainly through six main river basins numbered 11, 12, 13, 14, 15, 16 and 17 in Figure 2.4. Four smaller river basins (numbers 22, 23, 24 and 25) interspersed between the main river basins in the southern part of Bhutan also drain to River Brahmaputra. River Punatsangchhu in main river basin number 13 is the longest river in Bhutan with a length of about 250 km. The hydrological regime is characterised by low flow in the winter during periods with small precipitation amounts and low temperatures resulting in accumulation of snow at high altitudes, and high flow during summer caused by monsoon precipitation and melting of glacier ice and snow. The annual cycle of observed streamflow is illustrated in Appendices A and B.

The geology and landforms of Bhutan are shaped by the collision between the Indian sub-continent and Eurasia. The Hindu Kush-Himalayan region is situated in the part the earth with the greatest diversity of geology and topography where the world's highest mountains, the Himalayas raise abruptly from the flat, densely populated Ganges plains in northern India to elevations above 8000 m a.s.l.. To the north of the Himalayas, the Tibetan plateau has been raised to an elevation of 5000 m a.s.l. The Tibetan plateau is drained by to the east by a series of great rivers that arise in nearly parallel channels, but eventually fan out into rich deltas along an arc extending from the Bay of Bengal to the Yellow Sea. The Brahmaputra which drains into the Bay of Bengal after its confluence with the Ganges is one of these rivers (Molnar and Tapponnier, 1977).

The dominant land cover of Bhutan is forest, and it occupies 72.5 % of the country. Agricultural land constitutes 7.7 % of the total area, while pasture covers 3.9 %. Glaciers and snow cover 7.5 %. The remaining 8.4 % is made up of various types of land cover, including settlement areas of 0.1 %. There are more than 600 glaciers in Bhutan with an area of approximately 1300 km<sup>2</sup> and a total ice volume of 127 km<sup>3</sup>. The glaciers are located at elevations above 4000 m a.s.l. More than 2600 glacial lakes covering an area of approximately 100 km<sup>2</sup>, located either on the glacier surface or in the front of receding glaciers may produce devastating floods if they are suddenly emptied (Mool et al., 2001).

Digital elevation data and land use data used in this study were based on information from the Department of Survey and Land Records and the Department of Agriculture of the Royal Government of Bhutan. Glacier covered areas and glacier ice volume data were based on information from the Department of Geology and Mines of the Royal Government of Bhutan and the International Centre for Integrated Mountain Development (ICIMOD) (Mool et al., 2001). The digital elevation model and land use data have a resolution of 25 • 25 metres and were generated from base maps in scale 1:50.000 for Bhutan. For areas outside the boundary of Bhutan digital elevation data and land use data were based on NASA Shuttle Radar Topographic Mission (SRTM) (<http://www2.jpl.nasa.gov/srtm>) and International Geosphere Biosphere Project land cover classification (<http://www.igbp.net/page.php?pid=328>). The SRTM data has a resolution of 90 metres at the equator. Figure 2.3 presents an elevation map of Bhutan and upstream catchment areas.

The observed meteorological and hydrological data used in this study were based on the station network of the Department of Energy of the Royal Government of Bhutan, Hydromet Services Division. The meteorological precipitation and temperature records and the hydrological streamflow records were controlled. Precipitation, temperature and streamflow records with good quality were used in this study, while data with obvious errors were rejected. In all 55 meteorological stations with precipitations data, 53 meteorological stations with temperature data and 17 hydrological stations with streamflow data were used. The streamflow gauging stations are located within the main river basins of Bhutan numbered 11 to 17 from west to east. Three main river basins include catchment areas upstream of the boundary between Bhutan and China. Figure 2.4 presents a map of Bhutan with main river basins, hydrological gauging stations and catchment boundaries. The characteristics of the catchments of the hydrological stations are presented in Tables 2.1 and 2.2. The first two digits in the station numbers refer to the main river basin number. Hydrological modelling was performed for the entire catchments area upstream of the hydrological stations, i.e. including areas outside Bhutan.



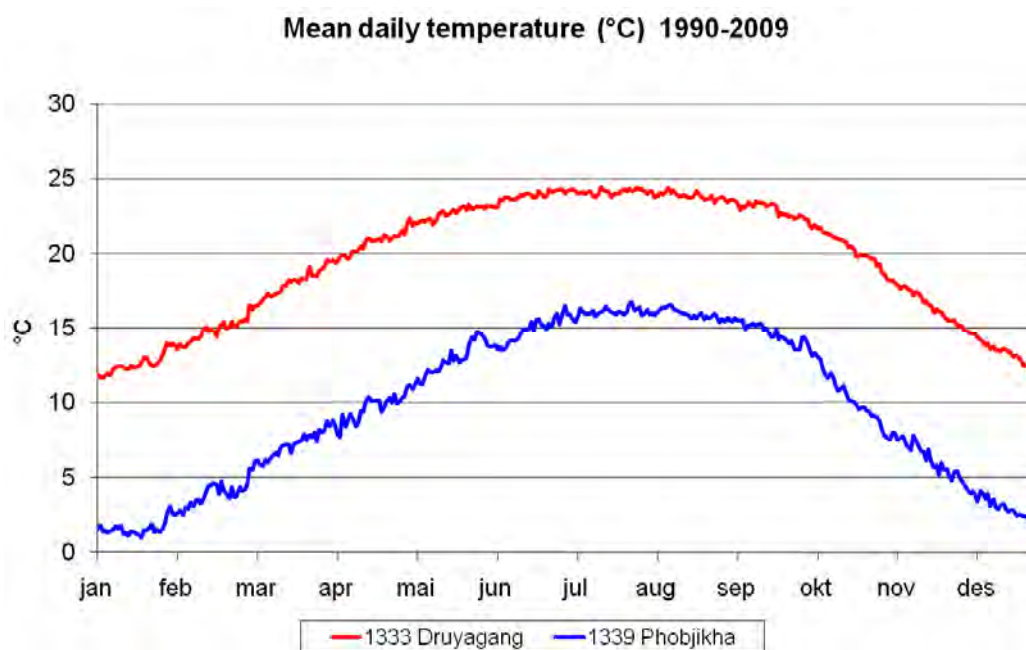


Figure 2.1. Mean daily temperature for meteorological stations 1333 Druyagang (1140 m a.s.l.) and 1339 Phobjikha (2860 m a.s.l.) for period 1990-2009.

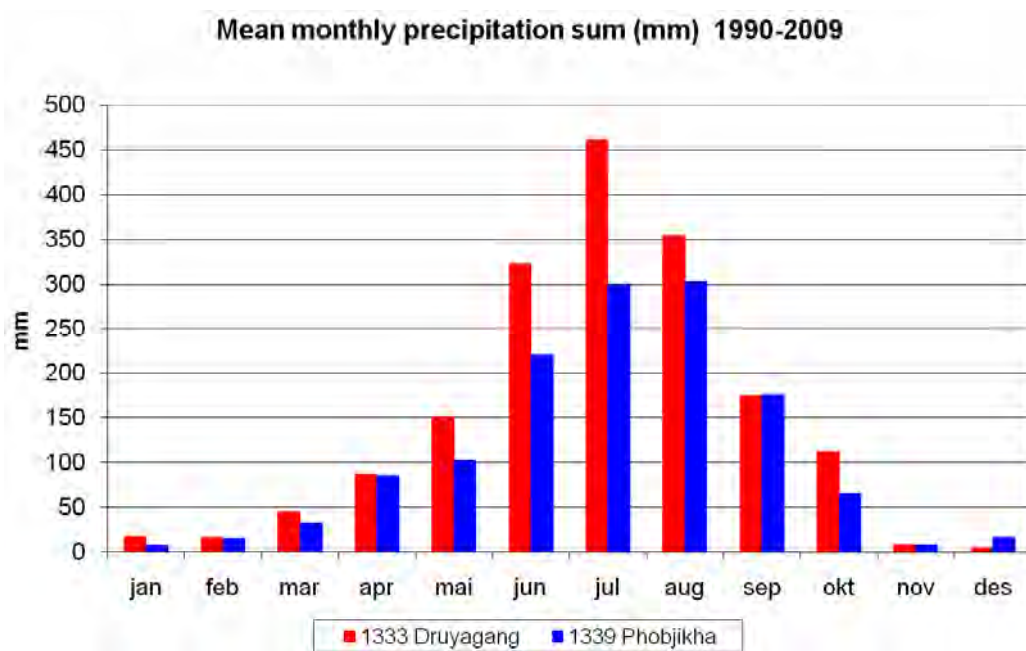


Figure 2.2. Mean monthly precipitation sum for meteorological stations 1333 Druyagang (1140 m a.s.l.) and 1339 Phobjikha (2860 m a.s.l.) for period 1990-2009.

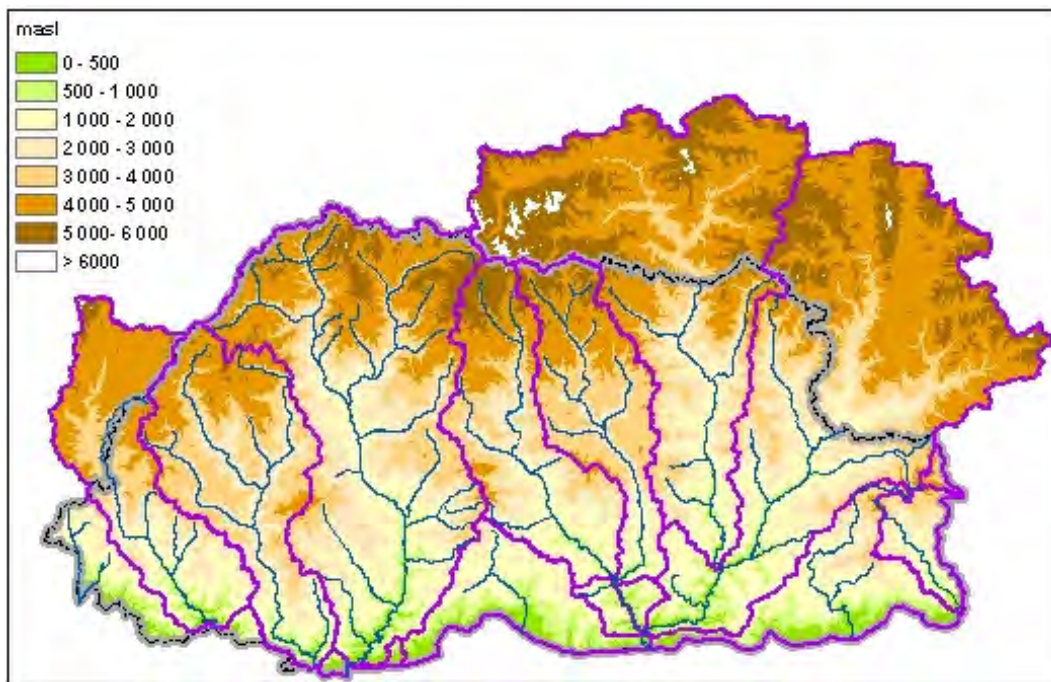


Figure 2.3. Elevation map of Bhutan and upstream catchment areas.

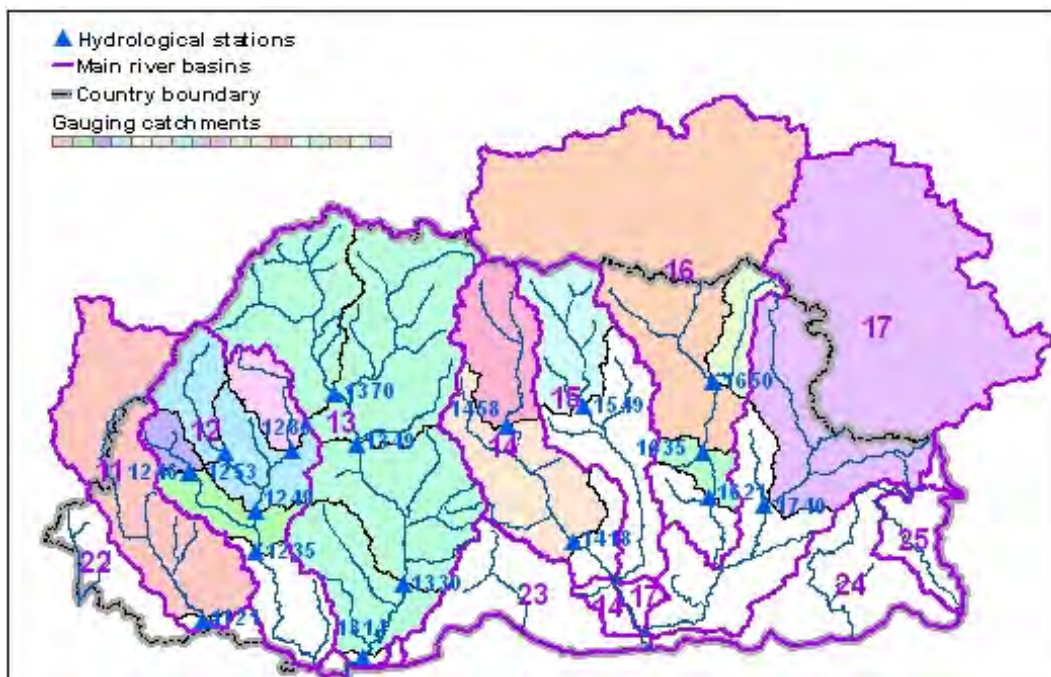


Figure 2.4. Map of Bhutan with main river basins, hydrological gauging stations and catchment boundaries. Three main river basins include catchment areas upstream of the boundary between Bhutan and China.

**Table 2.1 Hydrological gauging stations, river name, station elevation and highest elevation of upstream catchment.**

<b>Station no.</b>	<b>Name</b>	<b>River</b>	<b>Station elevation (m a.s.l.)</b>	<b>Highest elevation (m a.s.l.)</b>
1121	Doyagang	Amochhu	355	6991
1235	Chimakoti	Wangchhu	1820	7079
1246	Haa	Haachhu	2700	5587
1249	Damchhu	Wangchhu	1990	7079
1253	Paro	Parochhu	2255	7079
1280	Lungtenphug	Thimpuchhu	2260	5683
1314	Kerabari	Punatsangchhu	150	7104
1330*)	Dobani	Punatsangchhu	265	7104
1349	Wangdirapids	Wangdirapids	1190	7104
1370	Yebesa	Mochhu	1230	6700
1418	Tingtibi	Mangdechhu	530	7353
1458	Bjizam	Mangdechhu	1848	7353
1549	Kurjey	Chamkherchhu	2600	7031
1621	Kurizampa	Kurichhu	540	7352
1635	Autsho	Kurichhu	814	7352
1650	Sumpa	Kurichhu	1145	6375
1740	Uzorong	Gongrichhu	554	6475

\*) Station 1330 Dobani represents the same catchment area as station 1332 Turitar.

**Table 2.2 Hydrological stations, river, area and glacier covered fraction of upstream catchment.**

<b>Station no.</b>	<b>Name</b>	<b>River</b>	<b>Upstream catchment area (km<sup>2</sup>)</b>	<b>Glacier covered fraction (%)</b>
1121	Doyagang	Amochhu	3700	0.7
1235	Chimakoti	Wangchhu	3573	4.3
1246	Haa	Haachhu	323	0.7
1249	Damchhu	Wangchhu	2532	6.0
1253	Paro	Parochhu	820	11.3
1280	Lungtenphug	Thimpuchhu	662	6.8
1314	Kerabari	Punatsangchhu	9618	11.4
1330*)	Dobani	Punatsangchhu	8056	13.6
1349	Wangdirapids	Wangdirapids	5643	19.3
1370	Yebesa	Mochhu	2307	17.4
1418	Tingtibi	Mangdechhu	3325	12.4
1458	Bjizam	Mangdechhu	1390	28.7
1549	Kurjey	Chamkherchhu	1361	14.3
1621	Kurizampa	Kurichhu	8988	9.4
1635	Autsho	Kurichhu	8547	9.9
1650	Sumpa	Kurichhu	660	25.5
1740	Uzorong	Gongrichhu	9174	3.4

\*) Station 1330 Dobani represents the same catchment area as station 1332 Turitar.

### 3 Climate change

A large amount of observations give a picture of global warming and other changes in the climate system. Changes in the climate occur as a result both of internal variability within the climate system and external factors (both natural and anthropogenic). The major influence of external factors is related to the increasing concentrations of greenhouse gases which affect the atmospheric absorption properties of longwave radiation, thereby leading to increased radiative forcing that tend to warm the lower atmosphere and the earth's surface (Solomon et al. 2007). This temperature increase is illustrated for the catchments used for hydrological modelling in this study in Figure 6.1. The temperature increase will be accompanied by changes in cloud cover, precipitation, air humidity, radiation, wind and other meteorological elements. These effects will lead to changes in the land phase of the hydrological cycle with impacts on glacier mass balance, snow storage, soil moisture in the unsaturated zone, groundwater storage, evaporation and runoff. Assessment of the future hydrological regime is a production chain where changes in external forcing caused by greenhouse gas emissions are introduced into general circulation models and regional climate models. The climate model results are used for driving hydrological models that determine time series or statistics of hydrological state variables and fluxes for present and future climate conditions. Results from the Max Planck Institute atmosphere-ocean general circulation model ECHAM5/MPIOM (henceforth denoted Echam) (Jungclauss et al., 2006; Roeckner et al., 2006) have been used for assessment of climate change impacts on water resources in Bhutan.

Assumptions about future greenhouse gas emissions were based on the IPCC Special Report on Emission Scenarios (SRES) A2 and B1 scenarios (Nakićenović et al., 2000). Projected atmospheric greenhouse gas concentrations are lower in the B1 than in the A2 scenario. The suite of climate models considered by the Fourth Assessment Report of the Intergovernmental Panel on Climate Change (IPCC) project an average increase in global mean surface air temperature by the middle of the 21<sup>st</sup> century of approximately +1.3 °C for the B1 scenario and +1.7 °C for the A2 scenario relative to 1980 to 1999. By the end of the century the temperature rise is larger, with a mean value of +1.8 °C and +3.4 °C for the B1 and A2 scenarios, respectively (Meehl et al., 2007).

Atmosphere-ocean general circulation models remain the primary source of information of regional information on the range of possible future climates. Warming in the 21<sup>st</sup> century is likely to be well above the global mean in central Asia, the Tibetan plateau and northern Asia, above the global mean in eastern and southern Asia, and similar to the global mean in south-eastern Asia. It is very likely that summer heat waves in eastern Asia will be of longer duration, more intense, and more frequent. It is very likely that there will be fewer very cold days in eastern Asia and southern Asia. Boreal winter precipitation is very likely to increase in northern Asia and the Tibetan plateau, and likely to increase in central Asia, eastern Asia and south-eastern Asia, whereas it is likely to decrease in southern Asia. Summer precipitation is likely to increase in northern Asia, the Tibetan plateau, eastern and southern Asia and most of south-eastern Asia, but it is likely to decrease in central Asia. An increase in the frequency of intense precipitation events in parts of southern Asia, and in eastern Asia, is very likely (Christensen et al., 2007). Bhutan is situated in the northern part of the region denoted southern Asia, to the south of the Tibetan plateau.

Climate model projections Echem A2 and Echem B1 downscaled to a 0.5 degree grid for the Hindu Kush-Himalayan region by the Water and Global Change project (WATCH) (Hagemann et al., in press) funded by the European Union were used as input to the hydrological model. Historical or present climate was represented by a control period 1981-2010, while future climate for the projection periods 2021-2050 and 2071-2100 were considered. The hydrological model simulations are transient, i.e. the hydrological model was run from 1981 until 2100, while results for the control and projection periods were extracted from the transient simulations.

When focusing on the hydrological cycle, global general circulation models are too coarse to provide regional and local details of the climate at a spatial scale suitable for climate change impact studies (Bronstert, 2004). Different downscaling methods have been developed to overcome this problem, dynamically, empirically or these two techniques in combination (e.g. Giorgi et al., 2001), in order to enhance regional detail and obtain higher spatial resolution. However, even though a regional pattern with focus on a shift in the future climate compared to present may be satisfactory for assessments on large spatial scales, the uncertainty of regional climate model projections, especially the precipitation estimates, render them useless for hydrological climate change impact studies. Daily values of at site measurements of temperature and precipitation are in most circumstances the best source of input to hydrological models. Estimates of temperature and precipitation must therefore be transferred from regional climate models to selected locations. Wood et al. (2004) stated that “a minimum standard of any useful downscaling method for hydrological applications needs the historic (observed) conditions to be reproducible”. Different methods have been used to solve this problem; the delta change, or perturbation method has been widely used to adjust climate change projections to meteorological station sites (Middelkoop et al., 2001; Reynard et al, 2001, Lettenmaier et al., 1999). The delta change approach does not capture changes in the frequency of temperature and precipitation events, and it is therefore questionable whether hydrological model results for future climate projections based on this method can be trusted, in particular for extreme events. Methods that correct climate model output with the aim of reproducing the statistical properties of observed data at meteorological station sites or at the grid points of global data sets have proven to be a better procedure for improving the climate model simulations.

A statistical bias correction method for global climate simulations developed by Piani et al. (2010) were used to downscale daily precipitation and temperature output from the global climate model Echem with emission scenarios A2 and B1 to a 0.5 • 0.5 degree grid in the Hindu Kush-Himalayan region as part of the WATCH project. This method corrects the bias of climate model simulations compared to observed data to produce data sets that have the same statistical frequency distribution as the observations. Projections of daily precipitation and temperature for the period 1961-2100 were used as input to hydrological model simulations. The downscaled precipitation and temperature data from the WATCH project were interpolated to the sites of the meteorological stations of Hydromet Services Division and finally subject to a correction for bias in mean annual values before being used as input to the hydrological model.

Although the level of simplification is higher in hydrological models than in atmospheric models, they describe the essential characteristics of the precipitation-runoff process, the volumes of water stored as glacier ice, snow and subsurface water are correctly

reproduced, and they provide realistic simulations of evaporation, and more importantly, streamflow, the only variable in the climate system which integrates processes at the scale of catchments or river basins. Hydrological models which are to be used for climate change impact studies must perform well under conditions of non-stationarity as defined by Klemeš (1986). Non-stationarity means that a significant change in climate, land use or other basin characteristics occurs. In view of the natural variability of the landscape and the non-linearity of the processes involved, the parameterisation procedure of hydrological models used for climate change impact studies must reflect the significant and systematic variations in the land surface properties, e.g. by using representative parameter values for different soil types, vegetation types or geological layers. This implies repeated application of a hydrological model everywhere within a region using a global set of parameters (Gottschalk et al., 2001). The procedure for hydrological modelling that was applied in this study fulfils these requirements.

Due to the absence of directly measured catchment characteristics, natural variability and non-linearity of the processes involved, calibration is necessary to adjust the hydrological model to improve its ability to reproduce the observed hydrological data. This involves adjusting the observed precipitation and temperature data at meteorological station sites in order to correct gauge undercatch and the variability of precipitation and temperature with elevation. All these corrections result in a model parameter set that determines the behaviour of the hydrological model for a specific catchment or area of the land surface. The gridded climate model data from the WATCH project were downscaled to meteorological station sites in order for the hydrological model to use the same set of model parameters for simulations with input from observed meteorological data and climate model projections.

Deglaciation is a problem that must be dealt with when climate change impacts on water resources in the Hindu Kush-Himalayan region are considered. Glacier melt is occurring every year in the summer season, even when glacier mass balance is positive. This is a normal phenomenon, the glacier gains mass from accumulation of snow in the winter when the temperature is below the freezing point of water, whereas ice and snow melts during the ablation season in the summer when temperature is above the freezing point. However, accumulation and ablation does not necessarily occur simultaneously at all elevations of a glacier. Glaciers ice moves downhill in response to the force of gravity, eventually reaching lower elevations where melting takes place. The difference between accumulation and ablation for a given year describes the annual net mass balance. Many glaciers in the Hindu Kush-Himalayan region are retreating, however glaciers at the highest elevations, above 4000 m a.s.l., have not responded to recent climate warming in the same way as glaciers that extend to lower elevations because glaciers at higher elevation remain below the freezing point during much of the year, even in the presence of a warmer climate. Where consistent results from model studies exist, they indicate little loss in total meltwater available from glaciers over the next decades. Increased temperatures could be compensated by increased precipitation falling as snow at higher elevations, as a possible result of a strengthened monsoon (Armstrong, 2009). In the long run temperature increase will eventually lead to negative mass balance at increasingly higher elevations with the inevitable results that glaciers covered areas are reduced and the contribution to streamflow in the Hindu Kush-Himalayan region from melting glacier ice declines after a peak occurring in the course of a few decades (Eriksson et al., 2009).

## 4 Hydrological modelling

The observed meteorological data and the downscaled global climate model results were used for driving a spatially distributed version of the HBV hydrological model (Beldring et al. 2003), yielding results for hydrological variables and fluxes for present and future conditions. The HBV model has previously been applied in hydrological regimes in many parts of the world, including the Hindu Kush-Himalayan region (Bergström, 1995). The water balance algorithms of the model were described by Bergström (1995) and Sælthun (1996). The model is spatially distributed since every model element has unique characteristics that determine its parameters, input data are distributed, water balance computations are performed separately for each model element, and finally, only those parts of the model structure that are necessary are used for each element. The HBV model used in this study performs water balance calculations for 1 by 1 km<sup>2</sup> grid cell landscape elements characterized by their elevation and land use. Each grid cell may be divided into a maximum of four land surface classes; two land use zones with different vegetations, a lake area and a glacier area. The model is run with daily time steps, using precipitation and air temperature data as input. It has components for accumulation, sub-grid scale distribution and ablation of snow, interception storage, sub-grid scale distribution of soil moisture storage, evapotranspiration, groundwater storage and runoff response, lake evapotranspiration and glacier mass balance. Potential evapotranspiration is a function of air temperature, however, the effects of seasonally varying vegetation characteristics are considered. The routing of runoff through the river network is an important component of distributed hydrological models when time series of flows from large drainage basins are considered (Naden, 1993). Beldring et al. (2003) showed that for catchments smaller than approximately 6000 km<sup>2</sup>, the river networks of the catchments did not influence the dynamics of daily streamflow to an extent which necessitates inclusion of a routing procedure in the hydrological model. Although catchments as large as 10000 km<sup>2</sup> have been investigated in this study, the absence of lakes and the steep topography of Bhutan have the consequence that land surface properties and the characteristics of precipitation, snowmelt and glacier ice melt events control the shape of daily streamflow hydrographs. Hence no routing procedure was applied in this study.

Due to the absence of directly measured catchment characteristics, natural variability and non-linearity of the processes involved, calibration is necessary to adjust the model parameters to improve the model's ability to reproduce the observed hydrological data. Bergström and Sandberg (1983), Lindström et al. (1997) and Colleuille et al. (2008) examined the performance of the HBV model for several water balance components, including snow storage, soil moisture in the unsaturated zone, groundwater storage and runoff using observed data on these processes. Runoff and evapotranspiration fluxes determined by the HBV model are usually realistic when observed precipitation, temperature and streamflow data are available for model calibration. The parameter values assigned to the computational elements of the hydrological model should reflect that hydrological processes are sensitive to spatial variations in soil properties (e.g. Merz and Plate, 1997) and vegetation characteristics (e.g. Matheussen et al., 2000) through their control on storage of water, runoff events, evapotranspiration, snow and ice glacier ice accumulation and melt. The digital elevation data and land use data described in Chapter 2 were used for describing the properties of the landscape elements of the model. The land use data were assigned to the classes presented in Table 4.1. The model was run



with specific parameters for each land use class controlling snow processes, interception storage, evapotranspiration processes, soil moisture storage, groundwater storage and runoff response. Lake evaporation and glacier mass balance were controlled by parameters with the same values for all model elements.

**Table 4.1 Land use classes based on land use data described in Chapter 2.**

Main class	Sub class
Agriculture	Agriculture
Forest	Broadleaf forest
Forest	Coniferous forest
Forest	Scrub forest
Erosion	Erosion
Erosion	Landslide
Wetland	Wetland
Rock outcrops	Rock outcrops
Pasture	Pasture
Urban	Urban
Glacier	Glacier

The hydrological model was calibrated using a multi-criteria calibration strategy where the residuals between model-simulated and observed daily streamflow from several sub-catchments within a watercourse were considered simultaneously. The possibility of finding a robust parameter set increases if all operational modes of the model are activated during calibration, which requires at least 10 years of data for calibration (Sorooshian and Gupta, 1995). Available information about meteorological and hydrological processes for the period 1996-2005 from the 17 gauged sub-catchments analysed in this study were used, however some meteorological records or streamflow records are too short to allow simulation and calibration for the entire period. One model parameter set for all sub-catchments within each individual main watercourse was determined by calibrating the model with the restriction that the same parameter values are used for all computational elements of the model that fall into the same class for land surface properties. Individual model elements act as hydrological response units, i.e. patches in the landscape mosaic having a common climate, land use and pedological, topographical and geological conditions controlling their hydrological process dynamics (Gottschalk et al., 2001). This calibration procedure rests on the hypothesis that model elements with identical landscape characteristics have similar hydrological behaviour, and should consequently be assigned the same parameter values. Beldring et al. (2003) showed that the hydrological model performs well under non-stationary conditions through parameterisation of the processes that control runoff and evapotranspiration

fluxes, and by application of this process-adequate spatial discretisation scheme. The nonlinear parameter estimation method PEST (Doherty et al., 1998) was used for automatic model calibration. PEST adjusts the parameters of a model between specified lower and upper bounds until the sum of squares of residuals between selected model outputs and a complementary set of observed data are reduced to a minimum. The parameter set determined for one specific watercourse during this calibration procedure was applied for all hydrological model runs, regardless of which period or climate projection that was considered. The same precipitation and temperature stations were applied in all model runs for one specific catchment or main river river basin.

Precipitation and temperature values for the model grid cells were determined by inverse distance interpolation of observations from the three closest precipitation stations and the two closest temperature stations. Differences in precipitation and temperature caused by elevation were corrected by precipitation-elevation gradients and temperature lapse rates. There is considerable uncertainty with regard to the variations of precipitation with elevation in the mountainous terrain of Bhutan. Specific precipitation-elevation gradients and temperature lapse rates were therefore determined for each of the 17 sub-catchments, and these values were used for all grid cells within a sub-catchment. Few mountain stations necessitate use of these general gradients. The precipitation-elevation gradients were positive for elevations below 2600 m a.s.l. and negative above, as drying out of ascending air occurs in high mountain areas due to orographically induced precipitation (Daly et al., 1994). The change from a positive to a negative gradient at the elevation of 2600 metres is based on long term mean of precipitation data from meteorological stations in Bhutan and similar results from Pradhan (2008). The temperature lapse rates for days with and without precipitation were also determined by calibration, however, the same values were used for all model grid cells within each specific main water course.

The distributed hydrological model was run with input from observed meteorological data and from the downscaled climate model data with daily time steps, producing datasets of precipitation (mm/day), temperature (°C), snow storage (mm water equivalent), evaporation (mm/day), soil moisture deficit (mm), glacier mass balance (mm water equivalent/day), water stored in the upper groundwater zone (mm), water stored in the lower groundwater zone (mm), runoff (mm/day) and streamflow (m<sup>3</sup>/s) for all sub-catchments. A regionally applicable set of parameters was determined for each of the 7 main watercourses by calibrating the hydrological model with the restriction that the same parameter values are used for all grid cells that fall into the same class for land surface properties, assuming that model elements with identical landscape characteristics have similar hydrological behaviour.

The purpose of calibration is to adjust the model parameters with the aim of reproducing observed data. Therefore, in order to have confidence in a hydrological model, its performance must be validated. Model performance is usually evaluated by considering one or more objective statistics or functions of the residuals between model simulated output and observed sub-catchment output. The objective functions used in this study were the Nash-Sutcliffe and Bias statistics of the residuals, which have a low correlation (Węglarczyk, 1998). The Nash-Sutcliffe efficiency criterion ranges from minus infinity to 1.0 with higher values indicating better agreement. It measures the fraction of the variance of observed values explained by the model. Bias (relative volume error) measures the tendency of model simulated values to be larger or smaller than their

observed counterpart. Although the Nash-Sutcliffe efficiency criterion is frequently used for evaluating the performance of hydrological models, it favours a good match between observed and modelled high flows, while sacrificing to some extent matching of below-mean flows. It is for this reason that two different measures of model performance were considered. Results for model performance (Nash-Sutcliffe and Bias statistics) using observed precipitation and temperature data for the calibration period 1996-2005 are shown in Table 4.2. An independent period should be used for evaluating model performance under non-stationary conditions (Klemeš, 1986). The meteorological and hydrological records are too short to allow a sufficiently long independent period. Therefore, model performance was evaluated using observed precipitation and temperature data for the period 1991-2008. The results are shown in Table 4.3. This period is longer than the calibration period 1996-2005, however some meteorological records or streamflow records are too short to allow simulation and evaluation for the entire period. Graphs displaying model simulation results for daily streamflow for the period 1991-2008 for several sub-catchments are presented in Appendix A. Model results are good, although floods and low flows are not always correctly simulated.

**Table 4.2 HBV model performance for daily streamflow for the calibration period 1996-2005 with observed meteorological data as input.**

Station no.	Name	River	Nash-Sutcliffe efficiency	Bias
1121	Doyagang	Amochhu	0.89	-0.05
1235	Chimakoti	Wangchhu	0.84	0.01
1246	Haa	Haachhu	0.66	-0.19
1249	Damchhu	Wangchhu	0.73	-0.06
1253	Paro	Parochhu	0.71	0.0
1280	Lungtenphug	Thimpuchhu	0.77	-0.07
1314	Kerabari	Punatsangchhu	0.72	-0.15
1330	Dobani	Punatsangchhu	0.75	0.05
1349	Wangdirapids	Wangdirapids	0.73	0.08
1370	Yebesa	Mochhu	0.75	0.04
1418	Tingtibi	Mangdechhu	0.73	-0.05
1458	Bjizam	Mangdechhu	0.72	-0.04
1549	Kurjey	Chamkherchhu	0.82	0.0
1621	Kurizampa	Kurichhu	0.80	-0.05
1635	Autsho	Kurichhu	0.65	-0.12
1650	Sumpa	Kurichhu	0.73	-0.01
1740	Uzorong	Gongrichhu	0.80	0.0

**Table 4.3 HBV model performance for daily streamflow for the period 1991-2008 with observed meteorological data as input.**

Station no.	Name	River	Nash-Sutcliffe efficiency	Bias
1121	Doyagang	Amochhu	0.83	-0.01
1235	Chimakoti	Wangchhu	0.84	0.01
1246	Haa	Haachhu	0.65	-0.20
1249	Damchhu	Wangchhu	0.74	-0.07
1253	Paro	Parochhu	0.72	-0.01
1280	Lungtenphug	Thimpuchhu	0.78	-0.04
1314	Kerabari	Punatsangchhu	0.72	-0.15
1330	Dobani	Punatsangchhu	0.75	0.05
1349	Wangdirapids	Wangdirapids	0.73	0.08
1370	Yebesa	Mochhu	0.75	0.04
1418	Tingtibi	Mangdechhu	0.74	-0.06
1458	Bjizam	Mangdechhu	0.68	0.0
1549	Kurjey	Chamkherchhu	0.79	0.03
1621	Kurizampa	Kurichhu	0.73	0.04
1635	Autsho	Kurichhu	0.66	-0.13
1650	Sumpa	Kurichhu	0.72	-0.02
1740	Uzorong	Gongrichhu	0.77	0.01

Glacier mass balance simulations were performed by the hydrological model. The glacier mass balance was negative, ranging from -0.7 to -0.4 metres water equivalent per year for the period 1991-2008, using observed meteorological data as input to the hydrological model. This is in agreement with other studies from the Hindu Kush-Himalayan region, e.g. Berthier et al. (2007) who found a negative mass balance between -0.85 and -0.7 metres water equivalent per year in western Himalaya (India) for the period 1999-2004.

The glacier covered areas of the model grid cells are treated in two ways: (1) as constant assuming an inexhaustible reservoir of ice; or (2) as time-variant with initial ice volumes modified by model mass balance, but without glacier dynamics. For the period 1981-2010 the model was run with constant glacier covered area, whereas for the period 2011-2100 the model was run in both ways; with constant glacier covered areas, and with time-variant glacier covered areas, allowing the elevation of the ice surface to increase or decrease due to net accumulation or ablation. When the model is run with time-variant glacier covered areas the net annual mass balance is added to the initial ice volume in

each model grid cell. If net ablation exceeds initial ice volumes the glacier covered area of model grid cells are replaced by bedrock with an elevation adjusted for the removal of the initial ice volume. The initial glacier covered areas and the ice volumes of the glaciers at the beginning of year 2011 were based on data from the Department of Geology and Mines of the Royal Government of Bhutan and ICIMOD (Mool et al., 2001).

Table 4.4 present mean annual minimum and maximum streamflow based on observed streamflow data and hydrological model results with input from observed meteorological data. The extreme values simulated by the hydrological model are not correct. This is a general problem with hydrological models, frequently occurring values are better described by the hydrological model than less frequent values.

**Table 4.4 Mean annual minimum and maximum of daily streamflow (m<sup>3</sup>/s) for the period 1991-2008 based on observed data\*) and hydrological model results with observed meteorological data as input.**

Station no.	Mean annual minimum of observed daily streamflow (m <sup>3</sup> /s)	Mean annual minimum of hydrological model daily streamflow (m <sup>3</sup> /s)	Mean annual maximum of observed daily streamflow (m <sup>3</sup> /s)	Mean annual maximum of hydrological model daily streamflow (m <sup>3</sup> /s)
1121	32	53	1116	740
1235	21	17	510	462
1246	2.0	1.2	29	22
1249	12	7.6	273	237
1253	5.9	4.3	154	184
1280	3.8	2.9	107	82
1314	105	25	2755	2073
1330	76	20	1548	1596
1349	61	14	1219	1267
1370	22	5.2	508	478
1418	38	10	591	427
1458	13	3.1	306	184
1549	10	3.4	232	183
1621	63	23	1034	834
1635	62	18	837	535
1650	13	2.0	193	110
1740	71	67	1161	994

\*) The period with observed streamflow data is not the same for all catchments.

In addition to the model parameter sets used for hydrological modelling of the individual sub-catchments described above, a study of climate change impacts on water resources for the entire land surface of Bhutan was also performed. In this case the model was calibrated for the period 1996-2005 using observed data from all 17 sub-catchments within the 7 main watercourses in Bhutan. A regionally applicable set of parameters was determined using a multi-criteria calibration strategy where the residuals between model-simulated and observed daily streamflow from all 17 sub-catchments were considered simultaneously. The same parameter values were used for all grid cells that fall into the same class for land surface properties, assuming that model elements with identical landscape characteristics have similar hydrological behaviour. Also, precipitation-elevation gradients and temperature lapse rates were identical for all computational elements of the model. These model simulations were used for producing the maps of water resources for the periods 1981-2010, 2021-2050 and 2071-2100 presented in Appendix E.

In order for a precipitation-runoff model to simulate the relationship between input, state variables and output with minimal uncertainty, it is necessary to select appropriate values for the model parameters. In general, there are many combinations of model parameter sets that may be equally “good” in reproducing observed data, in particular when only one aspect of model performance is considered. This problem arises due to errors in model structure, boundary conditions and observed data. Since the information contained in the rainfall-runoff relationship is not sufficient to allow identification of complex models, hydrological model uncertainty may be assessed by considering multiple parameter sets that are equally good in reproducing observed data (Beldring, 2002; Wilby and Harris, 2006). Assessment of model uncertainty using multiple parameter sets that are equally good takes into account the uncertainty caused by imperfect model structure, boundary conditions and observed data used during model calibration. An investigation of the uncertainty of the HBV model was performed using simulations for present-day and future climates with multiple parameter sets. These parameter sets were determined by calibration with the aim of reproducing observed streamflow with the same precision. Observed meteorological and hydrological data were used for generating 100 parameter sets for several catchments with the condition that Nash-Sutcliffe efficiency criterion must be at least 0.75 and Bias (relative volume error) must be less than 0.1 (10 %).

Figure 4.1 shows results for this calibration procedure for catchment 1650 Sumpa for the period 1997-2006. Multi-year mean daily streamflow, i.e. the average of each day of the year for all years based on hydrological model results with precipitation and temperature input from observed meteorological data are compared to multi-year mean daily values for observed streamflow data. The results show that there is a spread in model results, but the simulations are still relatively close to the observed data indicating a small uncertainty caused by hydrological model structure and observed data. The glacier covered areas of the model are treated as constant, but although the net glacier mass balance is negative, it is not sufficiently large to melt any part of the glacier covered areas completely during this period. Model results for this catchment and period do therefore not depend on whether the glacier covered areas of the model are treated as constant or time-variant with initial ice volumes modified by model mass balance results for glacier covered grid cells. Results from other catchments show similar behaviour.

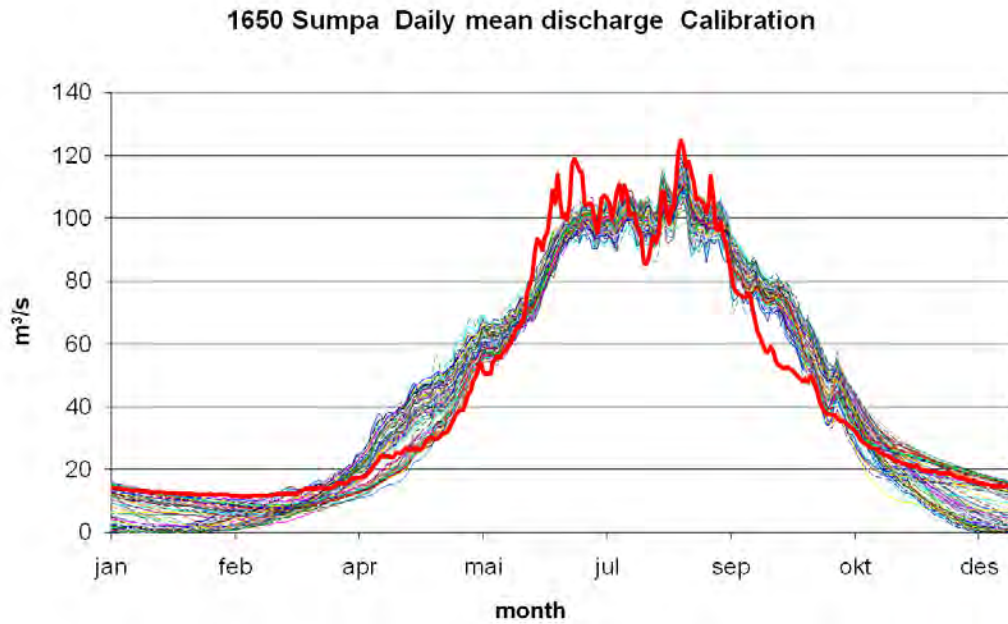


Figure 4.1. Multi-year mean daily streamflow ( $\text{m}^3/\text{s}$ ) for the period 1997-2006 based on hydrological model results for catchment 1650 Sumpa with precipitation and temperature input from observed meteorological data. Results from model calibration with 100 parameter sets calibrated with the condition that Nash-Sutcliffe efficiency criterion must be at least 0.75 and Bias (relative volume error) must be less than 0.1 (10 %) are shown as thin lines. Multi-year mean daily values for observed streamflow for the period 1997-2006 are shown with a bold red line. The glacier covered areas of the model are treated as constant.

## 5 Hydrological modelling with input from climate models

The climate model signal reproduces the statistical properties of the historical climate, not the day to day variations. This means that the downscaled climate model time series for precipitation and temperature must be considered as individual realizations of the historical climate that differ from the observed records. The long term statistics of precipitation and temperature based on the climate model signal are equal to the long term statistics of the observed data, but the daily values are different. Therefore, when the downscaled climate model signal is used to drive the hydrological model the resulting hydrological time series cannot be compared to the day to day variations of observed data. A comparison has been performed between streamflow time series from the hydrological model and the corresponding observed data after aggregation to a monthly time scale for the period 1991-2008. The two climate model projections based on the A2 and B1 emission scenarios are equal until year 2000 and the differences between the two are relatively small during the years 2001-2010. Therefore, the two sets of hydrological model simulations based on downscaled climate model results have more or less the same properties. The results for model performance (Nash-Sutcliffe and Bias statistics) for monthly streamflow for the period 1991-2008 are presented in Table 5.1. Graphs displaying model simulation results for monthly streamflow and multi-year mean monthly streamflow, i.e. the average of each calendar month for all years for the period 1991-2008 for several sub-catchments based on input data from climate projection Echem B1 are presented in Appendix B.

The downscaled climate model results for precipitation and temperature were subject to adjustment as described in Chapter 3 in order to correct the Bias in annual mean values in comparison with observed data. These corrected data were used as input to the hydrological model. Model simulation results for daily streamflow were aggregated to monthly values before comparison with observed data. The criteria of model performance presented in Table 5.1 shows that the agreement between observed data and hydrological model simulation are not as good as when observed precipitation and temperature data are used as input to the hydrological model, nevertheless the main characteristics of annual streamflow hydrographs are reproduced. Table 5.2 shows that mean annual streamflow based on observed data and hydrological model results based on input from climate projections Echem A2 and Echem B1 are not identical, but the errors are generally less than 10 %. The graphs presented in Appendix B confirm this conclusion, monthly streamflow and multi-year mean monthly streamflow simulated with the hydrological model follows the same annual cycle as the observed data. In spite of the fact that the day-to-day variations of observed data are not reproduced by the climate model signal, the strong seasonal character of meteorological conditions in Bhutan is reproduced and consequently the hydrological model reproduces the seasonal character of observed streamflow. Furthermore, glacier mass balance simulations for the period 1991-2008 were in the same range as when the model was run with observed meteorological data as input, i.e. between -0.7 and -0.4 metres water equivalent per year. The results for climate projection Echem A2 have the same characteristics as the results for climate projection Echem B1. These results confirm that the downscaled and Bias corrected climate model results for precipitation and temperature provide a reasonable approximation to observed



meteorological data. This confirms the reliability of the climate projections for the remaining part of the 21<sup>st</sup> century that were used in this study.

The extreme values simulated by the hydrological model are not correct. The graphs presented in Appendix B show that maximum monthly streamflow occurs one or two months too early in several catchments, which indicates a problem when the annual maximum flood is to be determined. However, the impacts on total streamflow available for hydropower production need not be influenced by this. Furthermore, low flow during winter is underestimated in several catchments. Tables 4.4 and 6.1, 6.2, 6.3 and 6.4 present mean annual minimum and maximum streamflow based on observed streamflow data and hydrological model results with input from observed meteorological data and climate projections Echam A2 and Echam B1. There is a deviation between model results and observed data for the period 1991-2008.

**Table 5.1 HBV model performance for the period 1991-2008 with downscaled climate model data as input. Hydrological model results and observed streamflow data\*) have been aggregated to monthly values.**

Station no.	Echam A2 Nash-Sutcliffe efficiency	Echam A2 Bias	Echam B1 Nash-Sutcliffe efficiency	Echam B1 Bias
1121	0.53	0.07	0.20	0.0
1235	0.42	-0.05	0.52	-0.05
1246	0.01	-0.07	0.29	-0.08
1249	0.38	-0.02	0.42	-0.03
1253	0.57	0.0	0.59	0.02
1280	0.57	0.0	0.63	-0.01
1314	0.31	-0.04	0.30	-0.06
1330	0.52	-0.05	0.63	-0.07
1349	0.61	0.0	0.68	-0.01
1370	0.68	-0.08	0.72	-0.09
1418	0.45	-0.01	0.55	-0.02
1458	0.66	0.0	0.72	0.0
1549	0.70	-0.03	0.70	0.0
1621	0.52	0.07	0.58	0.09
1635	0.67	-0.08	0.69	-0.08
1650	0.70	0.04	0.71	0.05
1740	0.63	-0.04	0.74	-0.04

\*) The period with observed streamflow data is not the same for all catchments.

**Table 5.2 Mean annual streamflow (m<sup>3</sup>/s) for the period 1991-2008 based on observed data\*) and hydrological model results for the period 1981-2010 with precipitation and temperature input from climate projections Echam A2 and Echam B1 downscaled to meteorological station sites. The glacier covered areas of the model are treated as constant.**

Station no.	Name	Observed streamflow (m <sup>3</sup> /s)	Echam A2 1981-2010 streamflow (m <sup>3</sup> /s)	Echam B1 1981-2010 streamflow (m <sup>3</sup> /s)
1121	Doyagang	198	164	183
1235	Chimakoti	99	90	92
1246	Haa	6.5	5.9	6.1
1249	Damchhu	62	53	56
1253	Paro	26	22	22
1280	Lungtenphug	23	22	23
1314	Kerabari	498	441	446
1330	Dobani	371	341	343
1349	Wangdirapids	294	290	291
1370	Yebesa	120	108	108
1418	Tingtibi	147	139	140
1458	Bjizam	66	63	63
1549	Kurjey	54	50	52
1621	Kurizampa	281	292	296
1635	Autsho	232	209	211
1650	Sumpa	48	48	49
1740	Uzorong	315	291	295

\*) The period with observed streamflow data is not the same for all catchments.

## 6 Climate change impacts on hydrological regimes in Bhutan

The results presented in this chapter are based on transient simulations with the hydrological model, i.e. the model was run from 1981 until 2100, while results for the control period 1981-2010 and the projection periods 2021-2050 and 2071-2100 were extracted from the transient simulation results.

The graphs in Appendices C and D and the maps in Appendix E present results for meteorological and hydrological processes based on hydrological modelling with input from climate projections Echam A2 and Echam B1 downscaled to meteorological station sites. Graphs of streamflow present values from the total area upstream of catchments, whereas graphs for temperature, precipitation, evaporation, snow water equivalent, soil moisture deficit and groundwater storage are the results from averaging all model grid cells in the area between the outlet of a catchment and the upstream sub-catchments, or alternatively the water divide.

The temperature change caused by increased concentrations of greenhouse gases in the atmosphere is illustrated in Figure 6.1. The temperatures for each of the 17 catchments are determined by the HBV model based on temperature time series downscaled to meteorological station sites. Temperature values for the model grid cells were determined by inverse distance interpolation of observations from the two closest temperature stations. Differences in temperature caused by elevation were corrected by temperature lapse rates determined during model calibration. The temperature time series shown in Figure 6.1 are the results from averaging all model grid cells within each sub-catchment. The seasonal variation of temperature and the increase in long term annual mean values are visible. Only model grid cells in the area between the outlet of a catchment and the upstream sub-catchments, or alternatively the water divide were used. This means that in those main water courses where nested sub-catchments were considered the sub-catchments represent the area between the hydrological stations. Therefore, each model grid cell is only used once during this averaging procedure. Figure 6.1 illustrates that emission scenario A2 which has a higher concentration of greenhouse gases than emission scenario B1 leads to a larger temperature increase. The change in mean annual temperature from 1981 to 2050 averaged over all 17 sub-catchments studied in this work is approximately 1.4 °C for both climate projections. The change in mean annual temperature from 1981 to 2100 averaged over all sub-catchments is approximately 4.9 °C for climate projection Echam A2 and 2.5 °C for climate projection Echam B1. This temperature increase will be accompanied by changes in cloud cover, precipitation, air humidity, radiation, wind and other meteorological elements. These changes will lead to changes in the land phase of the hydrological cycle with impacts on glacier mass balance, snow storage, soil moisture in the unsaturated zone, groundwater storage, evapotranspiration and runoff. The maps of changes in mean annual temperature from 1981-2010 to 2021-2050 and 2071-2100 for climate projection Echam A2 shown in Figures E5 and E6 in Appendix E confirm the results for temperature changes shown in Figure 6.1

The map of mean annual temperature for 1981-2010 in Figure E1 indicates that mean annual temperature is negative at the highest elevations of Bhutan, otherwise positive. Temperature time series for catchments 1330 Dobani and 1370 Yebesa for climate projection Echam A2 shown in Figures D1 and D5 in Appendix D are consistent with these results. The trends in these two temperature time series were found to be significant at the 5 % level based on Student's t-test.

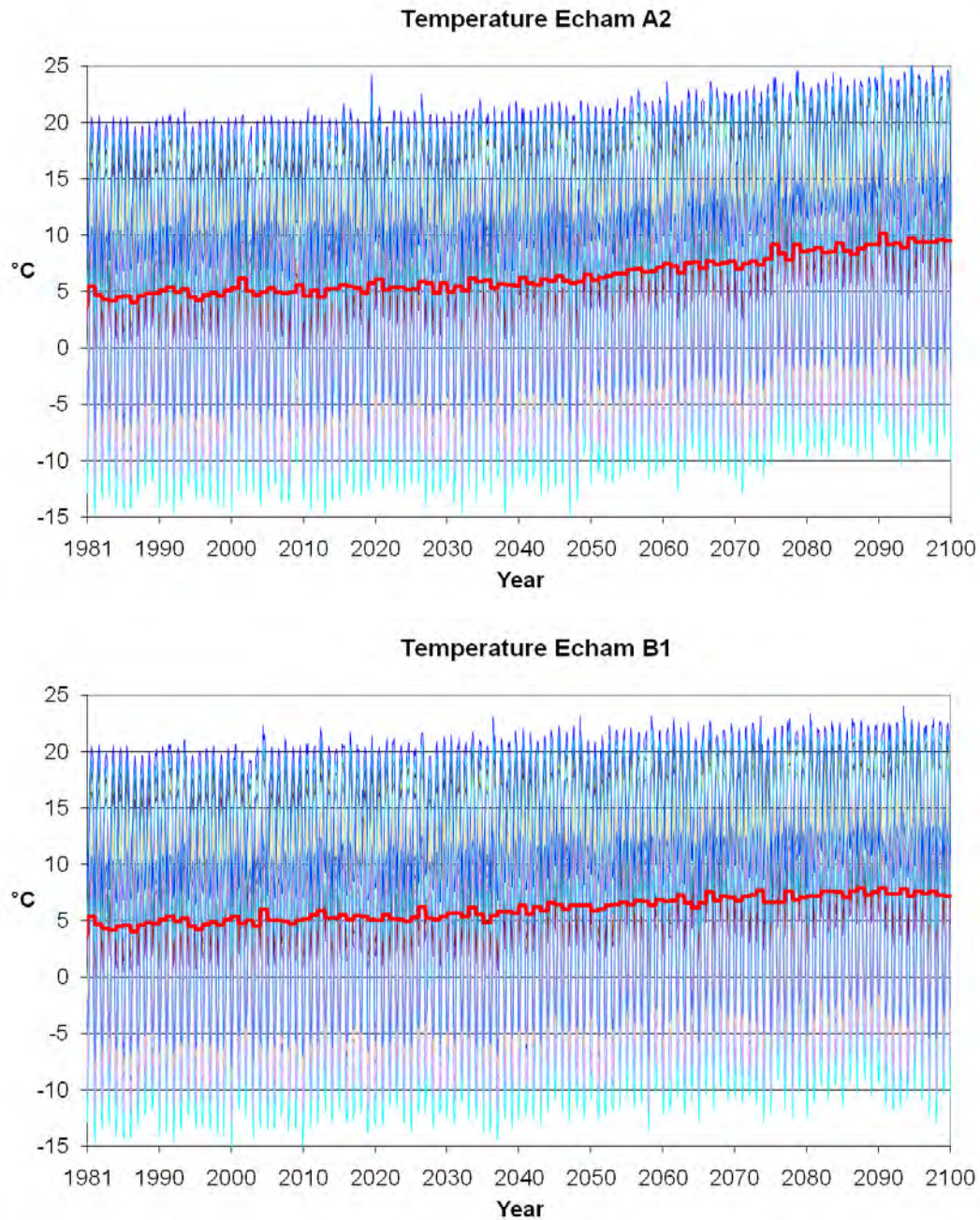


Figure 6.1. Monthly mean temperatures (°C) for the period 1981-2010 for 17 catchments in Bhutan (Table 2.1) for climate projections Echam A2 (top) and Echam B1 (bottom). Annual mean temperatures (°C) averaged over all catchments are shown with a bold red line.

Appendix C shows that precipitation change from the control period 1981-2010 to the projection periods 2021-2050 and 2071-2100 is small for the winter (December, January, February), spring (March, April, May) and autumn (September, October, November) seasons with mean change between -0.2 mm/day and 0.2 mm/day for both climate projections Echam A2 and Echam B1. For the summer season (June, July, August) the change is negative, with values in the range from -3 mm/day to -0.3 mm/day from 1981-2010 to 2021-2050 for both climate projections. Precipitation change for the summer season is between -5 mm/day and -0.5 mm/day from 1981-2010 to 2071-2100 for climate projection Echam A2 and between -0.5 mm/day and 0.5 mm/day from 1981-2010 to 2071-2100 for climate projection Echam B1. Large negative change is more frequent in southern parts of Bhutan.

The map with precipitation results presented in Figure E2 shows that mean annual precipitation sums for 1981-2010 varies from above 5000 mm/year in the southern, low-lying parts of Bhutan to below 500 mm/year in the northern, high-altitude parts. The changes in mean annual precipitation sums from 1981-2010 to 2021-2050 and 2071-2100 presented in Figures E7 and E8 are mostly negative, in the range from below 300 mm to zero. The change in precipitation is larger by the end of the century than by the middle. Negative trends in precipitation time series for catchments 1330 Dobani and 1370 Yebesa for climate projection Echam A2 shown in Figures D1 and D5 are consistent with these results. The trends in the precipitation time series for 1330 Dobani were found to be significant at the 5 % level based on Student's t-test.

The map in Figure E4 presents the mean of annual maximum snow water equivalent for the period 1981-2010 based on hydrological modelling with input from climate projection Echam A2. There is no snow storage in low-lying areas, whereas mean annual maximum snow water equivalent may be larger than 500 mm of water in high-altitude areas. The changes in snow storage presented in Figures E11 and E12 will lead to annual maximum values for snow water equivalent by the end of the century which is only one third of the values in the control climate 1981-2010. Snow storage time series for catchments 1330 Dobani and 1370 Yebesa for climate projection Echam A2 shown in Figures D2 and D6 are consistent with these results. The trends in these two snow storage time series were found to be significant at the 5 % level based on Student's t-test.

Time series of evaporation, soil moisture deficit and groundwater storage for catchments 1330 Dobani and 1370 Yebesa for climate projection Echam A2 that are shown in Figures D2, D3, D6 and D7 confirm the results above. Increasing temperatures result in a positive trend in evaporation in spite of reduced precipitation, while the combined effect of increasing temperature and reduces precipitation leads to increased soil moisture deficit, and a negative trend in groundwater storage. In areas without glacier ice that melts, less water will be available for infiltration in the soil profile, whereas more water will be lost through evaporation. Soil moisture deficit will increase and groundwater storage will decrease. With the exception of evaporation for catchment 1330 Dobani, the trends are positive at the 5 % level based on Student's t-test.

The glacier covered areas of the catchments were treated in two ways by the hydrological model: (1) as constant assuming an inexhaustible reservoir of ice; or (2) as time-variant with initial ice volumes and glacier covered areas modified by model mass balance. Streamflow downstream of areas with glaciers will decline if glacier covered areas and

the contribution to runoff from melting glacier ice is reduced. The initial glacier covered areas and the ice volumes of the glaciers were based on data from the Department of Geology and Mines of the Royal Government of Bhutan and ICIMOD (Mool et al., 2001). These data were assumed to be valid for the start of 2011. For the period 1981-2010 the model was run with constant glacier covered areas, whereas for the period 2011-2100 the model was run in both ways; with constant glacier covered areas, and with time-variant glacier covered areas, allowing the elevation of the ice surface to increase or decrease due to net accumulation or ablation. It is not realistic to apply fixed glacier covered areas since model results for glacier mass balance are negative for most elevations in Bhutan during the entire period 1981-2100. The hydrological model did not change ice covered areas at all for the period 1981-2010 when time-variant glacier covered areas were applied and consequently it was run with constant glacier covered areas for this period, assuming that information about initial ice volumes and glacier covered areas applies for the year 2011. For the period 2011-2100 the simulations with constant glacier covered areas are considered as a sensitivity analysis.

Appendix C shows that hydrological model results for streamflow with constant and time-variant glacier covered areas are equal for the period 1981-2010. There are small differences between simulations with input from climate projections Echam A2 and Echam B1 during this period, which is to be expected as the two climate model projections are equal until year 2000 and the differences between the two are relatively small during the years 2001-2010.

For most catchments streamflow is not changing much from 1981-2010 to 2021-2050. However, as a result of smaller precipitation amounts, in particular during summer, there is a reduction in streamflow for catchments with small glacier covered fraction since they will not receive a contribution to runoff from melting ice. The differences for simulations with input from climate projections Echam A2 and Echam B1 are small, but smaller precipitation amounts for EchamA2 leads to smaller streamflow than Echam B1. The two catchments with largest glacier covered fraction, 1458 Bjizam and 1650 Sumpa will experience increased streamflow caused by increased contribution to runoff from glacier ice melt.

The differences between streamflow for 2021-2050 for simulations with constant and time-variant glacier covered areas are small, a consequence of the fact that until the middle of the 21<sup>st</sup> century negative glacier mass balance is not sufficiently large to melt more than small fractions of the glacier covered areas completely. For catchments with a large glacier covered fraction there is a difference, most pronounced for catchment 1280 Lungtenphug. The results for this particular catchment is a consequence of the fact that elevations are small compared to other glacier covered catchments, resulting in higher temperatures and more rapid melting of glacier ice.

For the period 2071-2100 there is a decline in precipitation compared to the period 1981-2010, most noticeable for the climate projection Echam A2. In combination with a reduction in glacier volume and area for hydrological model simulations with time-variant glacier covered areas this leads to a large reduction in streamflow. Catchments 1121 Doyagang and 1246 Haa which both have a negligible glacier covered fraction will also experience reduced streamflow, but this is a result of precipitation change. Stream-

flow for the period 2071-2100 is in general smaller for climate projection Echam A2 than Echam B1, since Echam A2 have the smallest precipitation amounts.

Hydrological model simulations with constant glacier covered areas result in larger streamflow for the period 2071-2100 except for catchments 1235 Chimakoti, 1249 Damchhu and 1740 Uzorong which have a small glacier covered fraction and will experience unchanged or slightly reduced streamflow. For catchments 1121 Doyagang and 1246 Haa which both have negligible glacier covered areas results are identical to hydrological model simulations with time-variant glacier covered areas, i.e. reduced streamflow. For catchments with small or negligible glacier covered area the streamflow is larger for hydrological model simulation based on climate projection Echam B1 which yields larger precipitation amounts. For the catchments with large glacier covered fractions streamflow is larger for climate projection Echam A2 than for climate projection Echam B1 due to higher temperatures resulting in larger glacier ice melt.

The graphs presented in Appendix D confirm the results for streamflow during the periods 2021-2050 and 2071-2100 based on hydrological model simulations with constant and time-variant glacier covered areas. The maps in Appendix E are based on hydrological model simulations with constant glacier covered areas for the period 1981-2010 and time-variant glacier covered areas for the period 2011-2100. The map with runoff results presented in Figure E3 shows that mean annual runoff for 1981-2010 varies from above 5000 mm/year in the southern, low-lying parts of Bhutan to below 500 mm/year in the northern, high-altitude parts with glacier areas having higher runoff than surrounding areas. The changes in mean annual runoff sums from 1981-2010 to 2021-2050 and 2071-2100 presented in Figures E9 and E10 are mostly negative, in the range from below 300 mm to zero. However, for glacier covered areas runoff will increase as a result of negative glacier mass balance. The changes in runoff are larger by the end of the century than by the middle. The maps in Figures E13 and E14 show that glacier ice volumes and glacier covered areas will decline. The results shown by the maps for runoff and glacier ice volume and glacier covered areas are consistent with maps for other water balance elements presented in Appendix E and time series for water balance elements presented in Appendices C and E.

Assessment of hydrological model uncertainty for catchment 1650 Sumpa with precipitation and temperature input from climate projections Echam A2 and Echam B1 are presented in Figure 6.2. Multi-year mean daily streamflow ( $\text{m}^3/\text{s}$ ), i.e. the average of each day of the year for all years based on 100 parameter sets calibrated with the condition that Nash-Sutcliffe efficiency criterion must be at least 0.75 and Bias (relative volume error) must be less than 0.1 (10 %) are shown. The model was run for all combination of parameter set and climate projection for the periods 1981-2010 with glacier covered areas treated as constant and 2021-2050 with glacier covered areas treated as time-variant with initial ice volumes modified by model mass balance results. The results show that there is a spread in model results, indicating that there is an uncertainty caused by hydrological model structure, the data used for calibrating the model and the climate projections. However, there is consistency in the results in the sense that the hydrological model simulations from different parameter sets are grouped in a narrow band, meaning that they point to the same conclusion. Comparison with Figure 4.1 shows that model simulations for the calibration data have a smaller deviation than simulation results with climate model data as input. Also, comparison between Figure 4.1 and the top

graph in Figure 6.2 confirm that hydrological modelling with input from climate model projections for the control period are realistic. The uncertainty for projections of future climate would be larger if several emission scenarios for greenhouse gases, climate models or downscaling methods had been applied. Also, introduction of other hydrological model structures would increase the uncertainty of projections of future hydrological conditions. Results from other catchments show similar behaviour.

The hydrological model is not able to provide correct simulations of mean annual minimum and maximum daily streamflow when observed meteorological data are used as input. The same problem arises when climate model data downscaled to meteorological station sites are used as input to the hydrological model. However, hydrological model results may still be used to determine the relative change from the control period 1981-2010 to the projection periods 2021-2050 and 2071-2100 for climate projections Echem A2 and Echem B1. Tables 6.1, 6.2, 6.3 and 6.4 present mean annual minimum and maximum daily streamflow based on hydrological model results with input from climate projections Echem A2 and Echem B1. The hydrological model was run with constant glacier covered areas for the period 1981-2010 and with time-variant glacier covered areas for the periods 2021-2050 and 2071-2100. The hydrological model was also run with fixed glacier covered areas for the period 2071-2100.

The results for mean annual minimum streamflow show a small change from 1981-2010 to 2021-2050 with a mean value of 2 % increase for Echem A2 and 9 % decrease for Echem B1. For the period 2071-2100 there is a larger change from the control period with a decrease in mean annual minimum streamflow with a mean value of 19 % for Echem A2 and 18 % for Echem B1 when glacier covered areas are treated as time-variant, whereas there is a mean increase of 4 % for both Echem A2 and Echem B1 when glacier covered areas are treated as constant. Hydrological model simulations with time-variant glacier covered areas for periods 2021-2050 and 2071-2100 result in a decline in mean annual minimum streamflow. The reduction is larger for the period 2071-2100 than for the period 2021-2050 as a result of negative mass balance and reduction in glacier ice volume and area. Hydrological model simulations for period 2071-2100 with constant glacier covered area result in increasing mean annual minimum streamflow for many catchments as a result of higher temperatures and larger contribution from glacier ice melt. Catchments with a large glacier covered fraction experience a larger increase.

The results for mean annual maximum streamflow show a small change from 1981-2010 to 2021-2050 with a mean value of 2 % increase for both Echem A2 and Echem B1. The change from the 1981-2010 to 2071-2100 is larger with a decrease in mean annual maximum streamflow from the control period with a mean value of 22 % for Echem A2 and 6 % for Echem B1 when glacier covered areas are treated as time-variant, whereas there is a mean increase of 6 % for Echem A2 and a mean increase of 18 % for Echem B1 when glacier covered areas are treated as constant. Hydrological model simulations for periods 2021-2050 with time-variant glacier covered areas and 2071-2100 with constant glacier covered areas result in increasing mean annual maximum streamflow for most catchments and there is a tendency for larger increase for catchments with a large glacier covered fraction. Hydrological model simulations for period 2071-2100 with time-variant glacier covered areas result in a decline in mean annual maximum streamflow for most catchments as a result of negative mass balance and reduction in glacier covered areas.



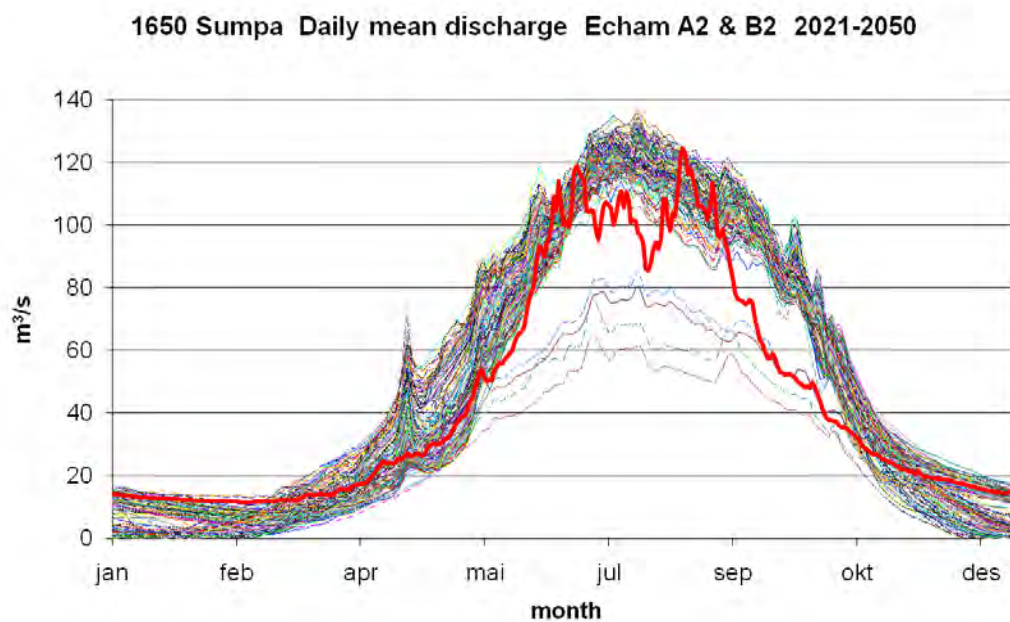
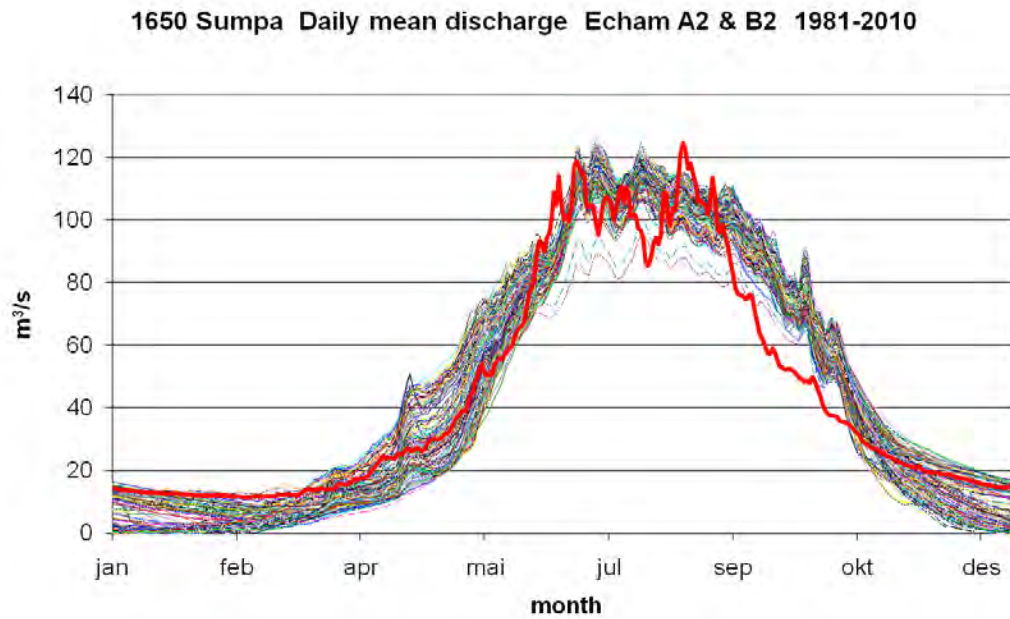


Figure 6.2. Multi-year mean daily streamflow ( $\text{m}^3/\text{s}$ ) based on hydrological model results for catchment 1650 Sumpa with precipitation and temperature input from climate projections Echam A2 and Echam B1. Results from model simulations with 100 parameter sets calibrated with the condition that Nash-Sutcliffe efficiency criterion must be at least 0.75 and Bias (relative volume error) must be less than 0.1 (10 %) are shown as thin lines. Multi-year mean daily values for observed streamflow for the period 1997-2006 are shown with a bold red line. Top: Simulations for the period 1981-2010 with glacier covered areas treated as constant. Bottom: Simulations for 2021-2050 with glacier covered areas treated as time-variant with initial ice volumes modified by model mass balance results.

**Table 6.1** Mean annual minimum of daily streamflow (m<sup>3</sup>/s) for the periods 1981-2010, 2021-2050 and 2071-2100 based on hydrological model results with precipitation and temperature input from climate projection Echam A2. The glacier covered areas of the model are treated as constant, or time-variant with initial ice volumes modified by model mass balance results.

Station no.	Echam A2 1981-2010 constant glacier area	Echam A2 2021-2050 time-variant glacier area	Echam A2 2071-2100 time-variant glacier area	Echam A2 2071-2100 constant glacier area
1121	40	40	37	37
1235	11	12	9.7	11
1246	1.0	1.0	0.9	0.9
1249	5.7	5.9	5.0	5.2
1253	3.6	3.6	3.0	3.3
1280	2.0	1.9	1.5	2.0
1314	21	21	17	22
1330	14	14	11	14
1349	9.7	9.8	8.3	11
1370	3.8	3.8	3.3	4.2
1418	9.4	9.4	7.6	8.4
1458	3.4	3.4	2.8	3.4
1549	2.6	2.7	2.4	3.4
1621	18	17	12	19
1635	15	14	9.8	16
1650	1.6	1.6	0.7	2.0
1740	57	59	56	66

**Table 6.2 Mean annual minimum of daily streamflow (m<sup>3</sup>/s) for the periods 1981-2010, 2021-2050 and 2071-2100 based on hydrological model results with precipitation and temperature input from climate projection Echam B1. The glacier covered areas of the model are treated as constant, or time-variant with initial ice volumes modified by model mass balance results.**

<b>Station no.</b>	<b>Echam B1 1981-2010 constant glacier area</b>	<b>Echam B1 2021-2050 time-variant glacier area</b>	<b>Echam B1 2071-2100 time-variant glacier area</b>	<b>Echam B1 2071-2100 constant glacier area</b>
1121	47	43	43	43
1235	13	11	11	11
1246	1.1	1.0	1.0	1.0
1249	6.7	6.0	5.8	5.9
1253	3.9	3.5	3.3	3.5
1280	2.3	1.9	1.8	2.1
1314	24	21	19	22
1330	15	14	13	14
1349	11	9.8	9.1	11
1370	4.0	3.8	3.6	4.2
1418	10	9.4	8.4	8.9
1458	3.6	3.4	3.0	3.3
1549	2.8	2.7	2.6	3.1
1621	19	17	13	18
1635	16	14	11	16
1650	1.7	1.6	0.8	1.8
1740	60	60	59	66

**Table 6.3** Mean annual maximum of daily streamflow (m<sup>3</sup>/s) for the periods 1981-2010, 2021-2050 and 2071-2100 based on hydrological model results with precipitation and temperature input from climate projection Echam A2. The glacier covered areas of the model are treated as constant, or time-variant with initial ice volumes modified by model mass balance results.

Station no.	Echam A2 1981-2010 constant glacier area	Echam A2 2021-2050 time-variant glacier area	Echam A2 2071-2100 time-variant glacier area	Echam A2 2071-2100 constant glacier area
1121	670	678	635	635
1235	613	601	474	537
1246	34	31	21	21
1249	340	342	275	304
1253	101	98	77	106
1280	113	98	79	110
1314	3252	3429	3051	3473
1330	2206	2325	1804	2323
1349	1617	1709	1253	1778
1370	577	607	432	621
1418	592	625	547	670
1458	229	261	208	338
1549	235	246	183	266
1621	946	980	762	1042
1635	616	643	436	719
1650	122	125	40	159
1740	1085	1121	1030	1120

**Table 6.4 Mean annual maximum of daily streamflow (m<sup>3</sup>/s) for the periods 1981-2010, 2021-2050 and 2071-2100 based on hydrological model results with precipitation and temperature input from climate projection Echam B1. The glacier covered areas of the model are treated as constant, or time-variant with initial ice volumes modified by model mass balance results.**

<b>Station no.</b>	<b>Echam B1 1981-2010 constant glacier area</b>	<b>Echam B1 2021-2050 time-variant glacier area</b>	<b>Echam B1 2071-2100 time-variant glacier area</b>	<b>Echam B1 2071-2100 constant glacier area</b>
1121	708	716	764	764
1235	602	529	618	674
1246	32	27	28	28
1249	344	320	364	387
1253	96	87	92	116
1280	111	88	99	128
1314	3205	3213	3659	4015
1330	2149	2141	2179	2641
1349	1574	1589	1486	1946
1370	556	564	511	673
1418	580	603	605	699
1458	227	255	203	301
1549	235	233	232	301
1621	939	945	853	1105
1635	612	617	484	738
1650	121	122	45	149
1740	1068	1097	1207	1284

## 7 Possible impacts on hydropower development

The flow duration curve is a cumulative frequency curve which summarizes the variability of a streamflow time series. Streamflow data are plotted along the vertical axis while the horizontal axis shows their exceedance probabilities, i.e. the fraction of time over the entire record that different streamflow values are exceeded. The steepness of the curve gives a visual impression of the temporal variability of the streamflow time series. The steeper the curve, the more variable are the data. An index of the relative variability of streamflow can be extracted from the flow duration curve as the ratio of flow associated with a high or low exceedance probability to a flow associated with a moderate exceedance probability, e.g. the ratio between the streamflow exceeded 95 % of the time and the streamflow exceeded 50 % of the time.

Figure 7.1 presents the flow duration curve for catchment 1349 Wangdirapids for the period 1981-2010 based on hydrological modelling with input from climate projection Echem B1 downscaled to meteorological station sites. The hydrological model was run with constant glacier covered areas. The streamflow values have been normalized by dividing by mean annual streamflow which is  $291 \text{ m}^3/\text{s}$ . The maximum value plotted in the graph is 300 % of mean annual streamflow, although this particular flow duration curve comprises streamflow data with an upper limit of  $2841 \text{ m}^3/\text{s}$  or 976 % of the mean annual value. The flow duration curve is the red curve in Figure 6.1. It shows that mean annual streamflow is exceeded 40 % of the time.

The flow duration curve can be used for estimating the integrated volume of discharge below a given streamflow value, called sum lower integrated. The green curve in Figure 7.1 shows the fraction of total discharge volume below a given streamflow value. It shows that 3.5 % of the total discharge volume occurs at a streamflow lower than  $58 \text{ m}^3/\text{s}$ , corresponding to 20 % of mean annual streamflow.

The flow duration curve can be used for estimating the fraction of the integrated volume of discharge that can be diverted by a construction with installed capacity equal to a given streamflow value. The blue curve in Figure 7.1 shows that 83 % of the total discharge volume can be diverted by a construction with capacity  $580 \text{ m}^3/\text{s}$ , corresponding to 200 % of mean annual streamflow.

The data presented in figure 7.1 can be used for estimating mean annual discharge available for hydropower production assuming a run-of-river hydropower plant at the outlet of the catchment with operational range between minimum turbine discharge and maximum turbine discharge. By setting sum lower integrated equal to minimum turbine discharge and installed capacity equal to maximum turbine discharge, the mean annual discharge available for hydropower production is the product of mean annual streamflow and the difference between installed capacity and sum lower integrated. This method is restricted to run-of-river situations where the head varies with the flow. It overestimates the actual hydropower that can be developed at the site because turbine efficiencies are assumed constant and operational constraints can reduce hydropower generation (McMahon, 1993).

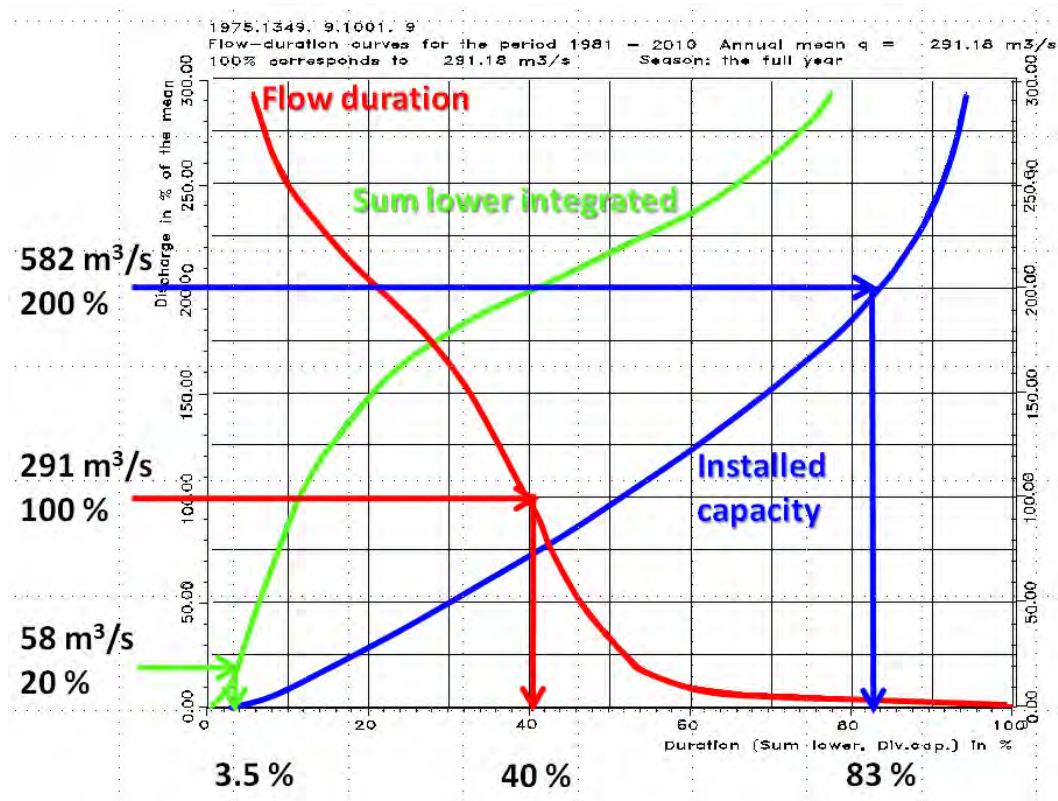


Figure 7.1 Curves for flow duration (red), sum lower (green) and diversion capacity (blue) for catchment 1349 Wangdirapids based on hydrological model results for streamflow with precipitation and temperature input from climate projection Echam B1 for the period 1981-2010. The streamflow values have been normalized by dividing by mean annual streamflow which is 291 m³/s. The glacier covered areas of the hydrological model are treated as constant.

Assuming a hydropower plant with capacity for annual inflow in the range 20 % - 200 % of mean annual inflow in the period 1981-2010 for the data presented in Figure 7.1, the mean annual discharge available for hydropower production is  $291 \text{ m}^3/\text{s} \cdot (0.83 - 0.035) = 7319 \cdot 10^6 \text{ m}^3/\text{year}$ . This means that 79.5 % of mean annual discharge is lost from hydropower production.

Appendix F presents flow duration curves, sum lower integrated curves and installed capacity curves for the periods 1981-2010, 2021-2050 and 2071-2100 based on hydrological modelling with input from climate projection Echam B1 downscaled to meteorological station sites. The hydrological model was run with constant glacier covered areas for the period 1981-2010, with time-variant glacier covered areas with initial ice volumes for glacier covered grid cells modified by model mass balance results for the period 2021-2050 and with both constant and glacier covered areas for the period 2071-2100. This resulted in four sets of curves for each catchment.

Tables 7.1, 7.2, 7.3 and 7.4 presents mean annual discharge available for hydropower production based on hydrological model results with precipitation and temperature input from climate projections Echam A2 and Echam B1 downscaled to meteorological station

sites assuming a run-of-river hydropower plant at the outlet of each catchment with turbines with a capacity for annual inflow in the range 20 % - 200 % of mean annual inflow for the period 1981-2010. The hydrological model was run with constant glacier covered areas for the period 1981-2010, with time-variant glacier covered areas with initial ice volumes for glacier covered grid cells modified by model mass balance results for the period 2021-2050 and with both constant and glacier covered areas for the period 2071-2100. The hydrological model simulations are transient, i.e. the hydrological model is run from 1981 until 2100, while results for the control and projection periods were extracted from the transient simulations.

Tables 7.1 and 7.2 show that differences between simulations of mean annual discharge available for hydropower production with input from climate projections Echem A2 and Echem B1 during the period 1981-2010 is less than 5 % for most catchments, which is to be expected as the two climate model projections are equal until year 2000 and the differences between the two are relatively small during the years 2001-2010.

The change in mean annual discharge available for hydropower production from 1981-2010 to 2021-2050 varies between 9 % decrease and 6 % increase for climate projections Echem A2 and between 13 % decrease and 7 % increase for climate projection Echem B1. The exception in both cases is catchment 1280 Lungtenphug which has a decrease of 32 % for A2 and a decrease of 35 % for B1. The results for this particular catchment is a consequence of the fact that elevations are small compared to other glacier covered catchments, resulting in higher temperatures and more rapid melting of glacier ice. The difference in mean annual discharge available for hydropower production between the two climate projections is small.

When glacier covered areas are treated as time-variant there is a reduction in glacier ice volume and area for the period 2071-2100. Combined with smaller precipitation amounts this leads to a decline in mean annual discharge available for hydropower production compared to the period 1981-2010 varying from -76 % to -4 %, the rate of change depending on the initial ice covered fraction. The difference in mean annual discharge available for hydropower production between the two climate projections is now larger. Higher temperature increase for climate projection Echem A2 results in more rapid melting of glacier ice than for climate projection Echem B1 and larger contribution to streamflow as long as the glaciers are present, but also to earlier disappearance of glacier ice and consequently reduced streamflow when the glacier covered area is smaller.

For the case of constant glacier covered areas hydrological model results for the period 2071-2100 indicate a decrease in mean annual discharge available for hydropower production compared to the period 1981-2010 for catchments with a small fraction of the area covered with glacier ice. For catchments with a large fraction of the area covered with glacier ice there is an increase in mean annual discharge available for hydropower production. The increase in mean annual discharge available for hydropower production for catchments with large proportion of glacier covered area is larger for climate projection Echem A2 than for climate projection Echem B1.

The graphs in Appendix F show that the variability of streamflow do not change much during the 21<sup>st</sup> century. Results for mean annual discharge available for hydropower production for other assumptions regarding turbine capacity can be determined from the results presented as graphs in Appendix F following the procedure outlined above.



**Table 7.1 Mean annual discharge ( $10^6 \text{ m}^3/\text{year}$ ) available for hydropower production based on hydrological model results with precipitation and temperature input from climate projection Echam A2 downscaled to meteorological station sites assuming hydropower plant with capacity for annual inflow in the range 20 % - 200 % of mean annual inflow in the period 1981-2010. The glacier covered areas of the model are treated as constant, or time-variant with initial ice volumes modified by model mass balance results.**

<b>Station no.</b>	<b>Echam A2 1981-2010 constant glacier area</b>	<b>Echam A2 2021-2050 time-variant glacier area</b>	<b>Echam A2 2071-2100 time-variant glacier area</b>	<b>Echam A2 2071-2100 constant glacier area</b>
1121	4510	4463	4113	4113
1235	2279	2065	1605	2235
1246	160	151	114	114
1249	1310	1297	1085	1347
1253	591	571	461	666
1280	576	391	245	618
1314	10254	10559	8142	12558
1330	8249	8599	4952	10119
1349	7204	7537	4217	8865
1370	2679	2803	1688	3270
1418	3383	3491	3070	3961
1458	1538	1626	1583	1971
1549	1343	1422	677	1837
1621	8141	8287	5633	9324
1635	5915	6063	3474	7063
1650	1373	1401	327	1713
1740	8069	8284	6343	7952

**Table 7.2** Mean annual discharge ( $10^6 \text{ m}^3/\text{year}$ ) available for hydropower production based on hydrological model results with precipitation and temperature input from climate projection Echam B1 downscaled to meteorological station sites assuming hydropower plant with capacity for annual inflow in the range 20 % - 200 % of mean annual inflow in the period 1981-2010. The glacier covered areas of the model are treated as constant, or time-variant with initial ice volumes modified by model mass balance results.

Station no.	Echam B1 1981-2010 constant glacier area	Echam B1 2021-2050 time-variant glacier area	Echam B1 2071-2100 time-variant glacier area	Echam B1 2071-2100 constant glacier area
1121	5120	4826	4924	4924
1235	2371	2057	1812	2300
1246	168	149	138	138
1249	1423	1354	1238	1420
1253	614	569	478	649
1280	595	385	296	614
1314	10542	10769	8374	11763
1330	8411	8703	5146	9450
1349	7319	7607	4283	8274
1370	2725	2822	1709	3065
1418	3509	3582	3113	3801
1458	1573	1678	1474	1847
1549	1401	1467	786	1696
1621	8358	8373	5932	8987
1635	6053	6140	3552	7388
1650	1391	1415	338	1600
1740	8304	8356	7289	8432

## 8 Conclusions

The hydrological model has a high precision with regard to simulating observed streamflow for the period 1991-2008 when observed meteorological data are used as input. The agreement between observed streamflow data and model results with climate model data downscaled to meteorological station sites as input is also good, although it should be noted that the downscaled climate model time series used for driving the hydrological model in this case must be considered as individual realizations of the historical climate that differ from the observed records. The comparison in this case was done for monthly mean and multi-year mean monthly values. In spite of the fact that the day-to-day variations of observed precipitation and temperature data are not reproduced by the climate model signal, the strong seasonal character of meteorological conditions in Bhutan is correctly described and consequently the hydrological model reproduces the seasonal variations of observed streamflow. It can therefore be concluded that the hydrological model is well suited for describing the historical or present-day hydrological regimes of Bhutan, although floods and low flows are not correctly simulated. However, this is a general problem with hydrological modelling, frequently occurring values are simulated with higher precision than less frequent values and the results obtained in this work have the same precision in simulating extremes as many other studies using hydrological models. Also, data for extremes are often unreliable (Bronstert, 2004).

Hydrological precipitation-runoff models have several parameters which are effective at the scale of the computational elements of the model and therefore must be calibrated to the observable catchment responses which are the objectives of model predictions. If a precipitation-runoff model was a perfect description of catchment water balance dynamics, one would expect a much smaller set of parameter sets (Mroczkowski et al., 1997). As a result, there are uncertainties in model results caused by the hydrological model structure. In addition, the meteorological and hydrological data used during model calibration introduces additional uncertainty. However, the range of uncertainty for the model simulations in this work is small, most likely due to the strong seasonal character of meteorological processes leading to a well defined seasonal variation of streamflow. When climate change impacts on the hydrological regimes are to be described, the uncertainty caused by emission scenarios, climate models, downscaling methods, initial glacier ice volumes, glacier mass balance and glacier dynamics and possibly other conditions must also be taken into account. These factors increase the uncertainty in the model results presented in this study. Also, the inclusion of additional emission scenarios for greenhouse gases, several general circulation models, downscaling methods and hydrological model structures would lead to additional uncertainty, as all these factors influence the results. Several projections of future climate in the Fourth Assessment Report of the IPCC project increasing precipitation in the Tibetan plateau and southern Asia in the 21<sup>st</sup> century (Christensen et al., 2007). This would lead larger streamflow than the results of this study, although differences in temperature must also be taken into account.

Emission scenario A2 which has a higher concentration of greenhouse gases than emission scenario B1 leads to a larger temperature increase. The change in mean annual temperature from 1981 to 2050 averaged over all 17 sub-catchments studied in this work is approximately 1.4 °C for climate projections based on both emission scenarios. The

change in mean annual temperature from 1981 to 2100 averaged over all sub-catchments is approximately 4.9 °C for climate projection Echem A2 and 2.5 °C for climate projection Echem B1. This temperature increase will be accompanied by changes in cloud cover, precipitation, air humidity, radiation, wind and other meteorological elements. These changes will lead to changes in the land phase of the hydrological cycle with impacts on glacier mass balance, snow storage, soil moisture in the unsaturated zone, groundwater storage, evapotranspiration and runoff.

Hydrological model results show that mean annual precipitation sums for 1981-2010 varies from above 5000 mm/year in the southern, low-lying parts of Bhutan to below 500 mm/year in the northern, high-altitude parts. The changes in mean annual precipitation from 1981-2010 to 2021-2050 and 2071-2100 are mostly negative and the changes are larger by the end of the century than by the middle. Large negative changes are more frequent in southern parts of Bhutan. Precipitation changes from the control period 1981-2010 to the projection periods 2021-2050 and 2071-2100 are small for the winter (December, January, February), spring (March, April, May) and autumn (September, October, November) seasons. For the summer season (June, July, August) the changes are negative for both climate projections Echem A2 and Echem B1, but larger for Echem A2.

During the control period 1981-2100 there is no snow storage in low-lying areas in the historical or present-day climate, whereas mean annual maximum snow water equivalent may be larger than 500 mm of water in high-altitude areas. Temperature increase and reduced precipitation will lead to annual maximum values for snow water equivalent by the end of the century which are only one third of the values in the control climate for climate projection Echem A2. For climate projection Echem B1 the change in snow storage is probably smaller due to a smaller temperature decrease.

Results for evaporation, soil moisture deficit and groundwater storage for catchments 1330 Dobani and 1370 Yebesa for climate projection Echem A2 show that increasing temperatures result in a positive trend in evaporation in spite of reduced precipitation, while the combined effect of increasing temperature and reduces precipitation lead to increased soil moisture deficit and a negative trend in groundwater storage. In areas without glacier ice that melts, less water will be available for infiltration in the soil profile, whereas more water will be lost through evaporation. Soil moisture deficit will increase and groundwater storage will decrease.

The glacier covered areas of the catchments were treated in two ways by the hydrological model: (1) as constant assuming an inexhaustible reservoir of ice; and (2) as time-variant with initial ice volumes and glacier covered areas modified by model glacier mass balance. For the period 1981-2010 the model was run with constant glacier covered areas, whereas for the period 2011-2100 the model was run in both manners; with constant glacier covered areas, and with time-variant glacier covered areas allowing the elevation of the ice surface to increase or decrease due to net accumulation or ablation. It is not realistic to apply fixed glacier covered areas since model results for glacier mass balance are negative for most elevations in Bhutan during the entire period 1981-2100. However, until the middle of the 21<sup>st</sup> century negative glacier mass balance is not sufficiently large to melt more than small fractions of the glacier covered areas completely. The hydrological model did not change ice covered areas at all for the period 1981-2010 when time-variant glacier covered areas were applied and consequently it was run with constant

glacier covered areas for this period, assuming that information about initial ice volumes and glacier covered areas apply for the year 2011. Streamflow downstream of areas with glaciers will decline if glacier covered areas and the contribution to runoff from melting glacier ice is reduced. Glacier ice melting and mass balance is almost constant until the middle of the 21<sup>st</sup> century as a result of small changes in temperature. After the middle of the century glacier ice melt rates are higher due to increasing temperatures.

For most catchments streamflow is not changing much from 1981-2010 to 2021-2050. However, as a result of smaller precipitation amounts, in particular during summer, there is a reduction in streamflow for catchments with small glacier covered fraction since they will not receive a contribution to runoff from melting ice. The differences between simulations with input from climate projections Echem A2 and Echem B1 are small, but smaller precipitation amounts for EchemA2 leads to smaller streamflow than Echem B1. The catchments with largest glacier covered fraction will experience increased streamflow caused by increased contribution to runoff from glacier ice melt. For the period 2071-2100 there is a decline in precipitation compared to the period 1981-2010, most noticeable for the climate projection Echem A2. In combination with a reduction in glacier volume and area for hydrological model simulations with time-variant glacier covered areas this leads to a large reduction in streamflow. Catchments with a negligible glacier covered fraction will also experience reduced streamflow, but this is a result of precipitation change. Streamflow for the period 2071-2100 is in general smaller for climate projection Echem A2 than Echem B1, since Echem A2 have less precipitation.

The differences between streamflow for 2021-2050 based on simulations with constant and time-variant glacier covered areas are small, a consequence of the fact that glacier ice melting has only led to a small reduction in glacier covered areas during this period. Hydrological model simulations with constant glacier covered areas result in larger streamflow for the period 2071-2100 except for catchments with a small glacier covered fraction which will experience unchanged or slightly reduced streamflow.

Hydrological model simulations with time-variant glacier covered areas for periods 2021-2050 and 2071-2100 result in a decline in mean annual minimum streamflow. The reduction is larger for the period 2071-2100 than for the period 2021-2050 as a result of negative mass balance and reduction in glacier ice volume and area. Hydrological model simulations for period 2071-2100 with constant glacier covered area result in increasing mean annual minimum streamflow for many catchments as a result of higher temperatures and larger contribution from glacier ice melt. Catchments with a large glacier covered fraction experience a larger increase.

Hydrological model simulations for periods 2021-2050 with time-variant glacier covered areas and 2071-2100 with constant glacier covered areas result in increasing mean annual maximum streamflow for most catchments and there is a tendency for larger increase for catchments with a large glacier covered fraction. Hydrological model simulations for period 2071-2100 with time-variant glacier covered areas result in a decline in mean annual maximum streamflow for most catchments as a result of negative mass balance and reduction in glacier ice volume and area.

Mean annual discharge available for hydropower production has been estimated assuming a run-of-river hydropower plant at the outlet of each catchment with turbines with a capacity for annual inflow in the range 20 % - 200 % of mean annual inflow for the

period 1981-2010. The hydrological model simulations are transient, i.e. the hydrological model was run from 1981 until 2100, while results for the control and projection periods were extracted from the transient simulations.

The change in mean annual discharge available for hydropower production from 1981-2010 to 2021-2050 varies between 9 % decrease and 6 % increase for climate projections Echam A2 and between 13 % decrease and 7 % increase for climate projection Echam B1. The exception in both cases is catchment 1280 Lungtenphug which has a decrease of 32 % for A2 and a decrease of 35 % for B1. The results for this particular catchment is a consequence of the fact that elevations are small compared to other glacier covered catchments, resulting in higher temperatures and more rapid melting of glacier ice. The difference in mean annual discharge available for hydropower production between the two climate projections is small.

When glacier covered areas are treated as time-variant there is a reduction in glacier ice volume and area for the period 2071-2100. Combined with smaller precipitation amounts this leads to a decline in mean annual discharge available for hydropower production compared to the period 1981-2010 varying from -76 % to -4 %, the rate of change depending on the initial ice covered fraction.. The difference in mean annual discharge available for hydropower production between the two climate projections is now larger. Higher temperature increase for climate projection Echam A2 results in more rapid melting of glacier ice than for climate projection Echam B1 and larger contribution to streamflow as long as the glaciers are present, but also to earlier disappearance of glacier ice and consequently reduced streamflow when the glacier covered area is smaller.

For the case of constant glacier covered areas hydrological model results for the period 2071-2100 indicate a decrease in mean annual discharge available for hydropower production compared to the period 1981-2010 for catchments with a small fraction of the area covered with glacier ice. For catchments with a large fraction of the area covered with glacier ice there is an increase in mean annual discharge available for hydropower production. The increase in mean annual discharge available for hydropower production for catchments with large proportion of glacier covered area is larger for climate projection Echam A2 than for climate projection Echam B1.

Model results for the end of the 21<sup>st</sup> century with constant glacier covered areas are not realistic since glacier ice volume and area are expected to decrease, but they show that streamflow and hydropower production potential in the rivers of Bhutan are sensitive to the presence of glaciers and that smaller or larger change in glacier covered areas would have a large impact on projections of streamflow by the end of the 21<sup>st</sup> century.

The annual cycle of meteorological processes in Bhutan will not change during the 21<sup>st</sup> century in the sense that the largest amounts of precipitation will still occur during summer and the smallest during winter. At high altitudes temperature will remain below freezing point during the winter and precipitation will accumulate as snow. The annual cycle of streamflow follows the same pattern as in the present climate with low flow during winter and high flow during summer as a result of the combined effect of snowmelt and larger amounts of precipitation in the summer season than in the rest of the year. There is a relatively small change in the magnitude of streamflow until the middle of the 21<sup>st</sup> century, whereas changes are larger by the end of the 21<sup>st</sup> century due to melting of glacier ice.

# Acknowledgements

This study was performed with kind assistance and help from numerous people in Bhutan and Norway, in particular from Mr. Karma Chopel, Mr. Karma Dupchu and Mr. Hari Sharma at the Department of Energy of the Royal Government of Bhutan, Hydromet Services Division, and from Mr. David A. Wright, Ms. Gusong Ruan, Dr. Miriam Jackson and Dr. Ingjerd Haddeland at Norwegian Water Resources and Energy Directorate. Professor Ånund Killingtveit and Ms. Pratigya Pradhan at Norwegian University of Science and Technology provided valuable assistance with hydrological modelling of catchments in Bhutan.

# References

- Armstrong, R.L. 2010. The glaciers of the Hindu Kush-Himalayan Region. A summary of the science regarding glacier melt/retreat in the Himalayan, Hindu Kush, Karakoram, Pamir, and Tien Shan Mountain Ranges. International Centre for Integrated Mountain Development, Kathmandu, Nepal, 16 pp.
- Beldring, S. 2002. Multi-criteria validation of a precipitation-runoff model. *Journal of Hydrology* 257, 189-211.
- Beldring, S., Engeland, K., Roald, L.A., Sælthun, N.R., Voksø, A. 2003. Estimation of parameters in a distributed precipitation-runoff model for Norway. *Hydrology and Earth System Sciences* 7, 304-316.
- Bergström, S., and G. Sandberg, 1983: Simulation of groundwater response by conceptual models - three case studies. *Nordic Hydrology*, 14, 71-84.
- Bergström, S., 1995: The HBV model. *Computer Models of Watershed Hydrology*, V.P. Singh (Ed.), Water Resources Publications, Highlands Ranch, 443-476.
- Berthier, E., Arnaud, Y., Kumar, R., Sarfaraz, A., Wagnon, P., Chevallier, P. 2007. Remote sensing estimates of glacier mass balances in the Himachal Pradesh (Western Himalaya, India). *Remote Sensing of Environment* 108, 327-338.
- Bronstert, A. 2004. Rainfall-runoff modeling for assessing the impacts of climate and land use change. *Hydrological Processes* 18, 567-570.
- Christensen, J.H., Hewitson, B., Busuioc, A., Chen, A., Gao, X., Held, I., Jones, R., Kolli, R.K., Kwon, W.-T., Laprise, R., Magaña Rueda, V., Mearns, L., Menéndez, C.G., Räisänen, J., Rinke, A., Sarr, A., Whetton, P. 2007. Regional Climate Projections. In: Solomon, S., Qin, D., Manning, M., Chen, Z., Marquis, M., Averyt, K.B., Tignor, M. and Miller, H.L. (Eds.) *Climate Change 2007: The Physical Science Basis. Contribution of Working Group I to the Fourth Assessment Report of the Intergovernmental Panel on Climate Change*. Cambridge University Press, Cambridge, United Kingdom and New York, NY, USA, 847-940.
- Colleuille, H., Beldring, S., Mengistu, Z., Haugen, L.E., Øverlie, T., Andersen, J., Wong, W.K. Wong. 2008. Monitoring system for groundwater and soil water based on simulations and real-time observations: The Norwegian experience. XXV Nordic Hydrological Conference, Reykjavik, Nordic Hydrological Programme, Report no. 50, 329-339.
- Cruz, R.V., Harasawa, H., Lal, M., Wu, S., Anokhin, Y., Punsalmaa, B., Honda, Y., Jafari, M., Li, C., Huu Ninh, N. 2007. Asia. In: Parry, M.L., Canziani, O.F., Palutikof, J.P., van der Linden, P.J. Hanson, C.E. (Eds.) *Climate Change 2007: Impacts, Adaptation and Vulnerability. Contribution of Working Group II to the Fourth Assessment Report of the Intergovernmental Panel on Climate Change*, Cambridge University Press, Cambridge, UK, 469-506.



- Daly, C., Neilson, R.P. and Phillips, D.L. 1994. A statistical-topographic model for mapping precipitation over mountainous terrain. *Journal of Applied Meteorology*, 33, 140-158.
- Doherty, J., Brebber, L. and Whyte, P. 1998. PEST. Model independent parameter estimation. *Watermark Computing*, 185 pp.
- Dingman, S.L. 1994. *Physical Hydrology*, Prentice-Hall, New Jersey, 575 pp.
- Eriksson, M., Xu, J., Shresta, A.B., Vaidya, R.A., Nepal, S., Sandström, K. 2009. The changing Hiamalayas. Impacts of climate change on water resources and livelihood in the greater Himalayas. International Centre for Integrated Mountain Development, Kathmandu, Nepal, 24 pp.
- Giorgi F., Hewitson, B., Christensen J., Hulme, M., Von Storch, H., Whetton, P., Jones, R., Mearns, L. and Fu, C. 2001. Regional climate information – evaluation and projections. In: Houghton, J.T., Ding, Y., Griggs, D.J., Noguer, M., van der Linden, P.J., Dai, X., Maskell, K. and Johnson, C.A. (Eds.) *Climate change 2001: The Scientific Basis. Contribution of Working Group I to the Third Assessment Report of International Panel on Climate Change*. Cambridge University Press, Cambridge, 583-638.
- Gottschalk, L., Beldring, S., Engeland, K., Tallaksen, L., Sælthun, N.R., Kolberg, S. and Motovilov, Y. 2001. Regional/macroscale hydrological modelling: a Scandinavian experience. *Hydrological Sciences Journal*, 46, 963–982.
- Hagemann, S., Chen, C., Haerter, J.O., Heinke, J., Gerten, D., Piani, C. 2011: Impact of a statistical bias correction on the projected hydrological changes obtained from three GCMs and two hydrology models, *J. Hydrometeor.*, 10.1175/2011JHM1336.1, in press.
- Klemeš, V. 1986. Operational testing of hydrological simulation models. *Hydrological Sciences Journal*, 31, 13-24.
- Lettenmaier, D.P., Wood, A.W., Palmer, R.N., Wood, E.F. and Stakhiv, E.Z. 1999. Water resources implications of global warming: A U.S. regional perspective. *Climatic Change* 43, 537-579.
- Lindström, G., Johansson, B., Persson, M., Gardelin, M., Bergström, S. 1997. Development and test of the distributed HBV-96 model. *Journal of Hydrology* 201, 272-288.
- Jungclaus, J.H., Botzet, M., Haak, H., Keenlyside, N., Luo, J.-J., Latif, M., Marotzke, J., Mikolajewicz, U., Roeckner, E. 2006: Ocean circulation and tropical variability in the coupled model ECHAM5/MPI-OM. *J Climate*, 19, 3952-3972.
- McMahon, T.A. 1993. Hydrologic design for water use. In: Maidment, D.R. (Ed.), *Handbook of Hydrology*. McGraw-Hill, New York, 27.38-27.40.
- Matheussen, B., Kirschbaum, R.L., Goodman, I.A., O'Donnel, G.M. and Lettenmaier, D.P. 2000. Effects of land cover change on streamflow in the interior Columbia River Basin (USA and Canada). *Hydrological Processes*, 14, 867-885.
- Meehl, G.A., Stocker, T.F., Collins, W.D., Friedlingstein, P., Gaye, A.T., Gregory, J.M., Kitoh, A., Knutti, R., Murphy, J.M., Noda, A., Raper, S.C.B., Watterson, I.G., Weaver

- A.J. and Zhao, Z.-C. 2007. Global Climate Projections. In: Solomon, S., Qin, D., Manning, M., Chen, Z., Marquis, M., Averyt, K.B., Tignor, M. and Miller, H.L. (Eds.) *Climate Change 2007: The Physical Science Basis. Contribution of Working Group I to the Fourth Assessment Report of the Intergovernmental Panel on Climate Change.* Cambridge University Press, Cambridge, United Kingdom and New York, NY, USA, 747-843.
- Merz, B. and Plate, E.J. 1997. An analysis of the effects of spatial variability of soil and soil moisture on runoff. *Water Resources Research*, 33, 2909-2922.
- Middelkoop, H., Daamen, K., Gellens, D., Grabs, W., Kwadijk, J.C.J., Lang, H., Parmet, B.W.A.H., Schädler, B., Schulla, J. and Wilke, K. 2001. Impact of climate change on hydrological regimes and water resources management in the Rhine basin, *Climatic Change* 49, 105-128.
- Molnar, P., Tapponnier, P. 1977. The collision between India and Eurasia. In: Bolt, B.A. (Ed.) *Earthquakes and Volcanoes.* Scientific American. Freeman, San Fransisco, 62-73.
- Mool, P.K., Wangda, D., Bajracharya, S.R., Kunzang, K., Gurung, D.R., Joshi, D.R. 2001. Inventory of glaciers, glacial lakes and glacial lake outburst floods. Monitoring and early warning systems in the Hindu Kush-Himalayan region. International Centre for Integrated Mountain Development in cooperation with United Nations Environment Programme, Regional Resource Centre – Asia and the Pacific. Kathmandu, Nepal,. ISBN 92 115 362 1, 127 pp.
- Mroczkowski, M., Raper, G.P., Kuczera, G. 1997. The quest for more powerful validation of conceptual catchment models. *Water Resources Research* 33, 2325-2335.
- Naden, P.S. 1993. A routing model for continental-scale hydrology. In: Wilkinson, W.B. (Ed.), *Macroscale Modelling of the Hydrosphere.* IAHS Publication 214, 67-79
- Nakićenović, N., Alcamo, J., Davis, G., de Vries, B., Fenhann, J., Gaffin, S., Gregory, K., Grübler, A., Jung, T.Y., Kram, T., La Rovere, E.L., Michaelis, L., Mori, S., Morita, T., Pepper, W., Pitcher, H., Price, L., Riahi, K., Roehrl, A., Rogner, H.-H., Sankovski, A., Schlesinger, M., Shukla, P., Smith, S., Swart, R., van Rooijen, S., Victor, N., Dadi, Z. 2000. *IPCC Special Report on Emission Scenarios.* Cambridge Univ. Press, Cambridge, United Kingdom, 599 pp.
- Piani, C., Weedon, G.P., Best, M., Gomes, S.M., Viterbo, P., Hagemann, S., Haerter, J.O. 2010. Statistical bias correction of global simulated daily precipitation and temperature for the application of hydrological models. *Journal of Hydrology* 395, 3-4, 199-215, doi:10.1016/j.jhydrol.2010.10.024
- Peixoto, J.P., Oort, A.H. 1992. *Physics of climate.* American Institute of Physics, New York, 520 s.
- Pradhan, P. 2008. Hydrological studies in Punatsangchhu river, Bhutan. Master Thesis in Hydropower Development (Hydrology). Norwegian University of Science and Technology, Department of Hydraulic and Environmental Engineering. Trondheim, Norway, 57 pp.

- Rees, G., Sullivan, C., O'Regan, D. 2004. SAGARMATHA. Snow and glacier aspects of water resources management in the Himalayas. Final Technical Report: Volume 1, Project Overview. Centre for Ecology and Hydrology, Wallingford, United Kingdom, 104 pp.
- Reynard, N.S., Prudhomme, C. and Crooks, S.M. 2001. The flood characteristics of large U.K. Rivers: Potential effects of changing climate and land use. *Climatic Change* 48:343-359.
- Roeckner, E., Brokopf, R., Esch, M., Giorgetta, M., Hagemann, S., Kornblueh, L., Manzini, E., Schlese, U., Schulzweida, U. 2006. Sensitivity of Simulated Climate to Horizontal and Vertical Resolution in the ECHAM5 Atmosphere Model. *J. Climate*, 19, 3771–3791.
- Sharma, E., Chettri, N., Tse-ring, K., Shrestha, A.B., Jing, F., Mool, P., Eriksson, M. 2009. Climate change impacts and vulnerability in the Eastern Himalayas. International Centre for Integrated Mountain Development, Kathmandu, Nepal, 28 pp.
- Solomon, S., Qin, D., Manning, M., Chen, Z., Marquis, M., Averyt, K.B., Tignor, M., Miller, H.L. (Eds.). 2007. *Climate Change 2007. The Physical Science Basis. Contribution of Working Group I to the Fourth Assessment Report of the Intergovernmental Panel on Climate Change*, Cambridge University Press, Cambridge, United Kingdom and New York, NY, USA.
- Sorooshian, S. and Gupta, V.K. 1995. Model calibration. In: Singh, V.P. (Ed.), *Computer Models of Watershed Hydrology*. Water Resources Publications, Highlands Ranch, 23-68.
- Sælthun, N.R. 1996. The Nordic HBV model. Norwegian Water Resources and Energy Administration Publication 7, Oslo, 26 pp.
- Trenberth, K.E., Jones, P.D., Ambenje, P., Bojariu, R., Easterling, D., Klein Tank, A., Parker, D., Rahimzadeh, F., Renwick, J.A., Rusticucci, M., Soden, B. and Zhai, P. 2007. Observations: Surface and Atmospheric Climate Change. In: Solomon, S., Qin, D., Manning, M., Chen, Z., Marquis, M., Averyt, K.B., Tignor, M. and Miller, H.L. (Eds.) *Climate Change 2007: The Physical Science Basis. Contribution of Working Group I to the Fourth Assessment Report of the Intergovernmental Panel on Climate Change*. Cambridge University Press, Cambridge, United Kingdom and New York, NY, USA, 235-335.
- Węglarczyk, S. 1998. The interdependence and applicability of some statistical quality measures for hydrological models. *Journal of Hydrology*, 206, 98-103.
- Wilby, R.L., Harris, I. 2006. A framework for assessing uncertainties in climate change impacts: low flow scenarios for the River Thames, UK. *Water Resources Research* 42, W02419, doi:10.1029/2005WR004065.
- Wood, A.W., Leung, L.R., Sridhar, V. and Lettenmaier, D.P. 2004. Hydrologic implications of dynamical and statistical approaches to downscaling climate model outputs. *Clim. Change* 62: 189-216.

# **Appendix A Evaluation of hydrological model with observed meteorological data input**

Figures A1-A4: Hydrological model results for daily streamflow based on observed meteorological data from the station network of Hydromet Services Division. Temperature and precipitation input data have been modified by the hydrological model according to temperature lapse rates and precipitation elevation gradients determined during model calibration. Streamflow simulations are compared to observed hydrological data. The glacier covered-areas of the model are treated as constant.

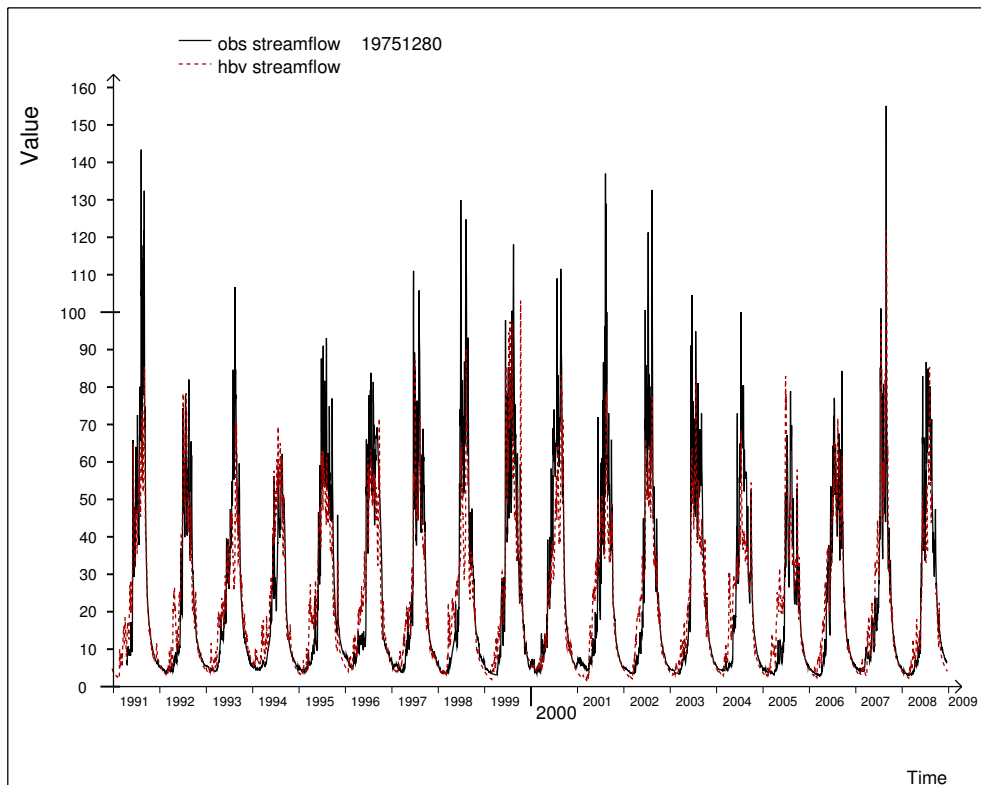
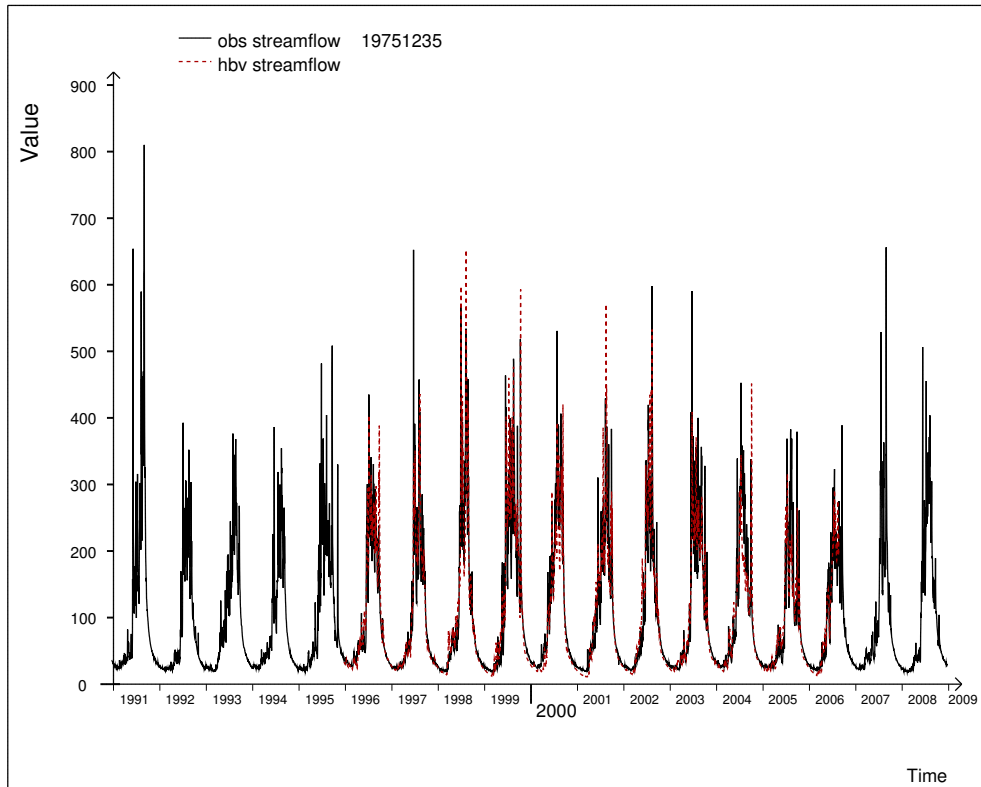


Figure A1. Observed (black) and simulated with HBV model (red) daily streamflow ( $\text{m}^3/\text{s}$ ) for catchments 1235 Chimakoti (top) and 1280 Lungtenphug (bottom) for the period 1991-2008.

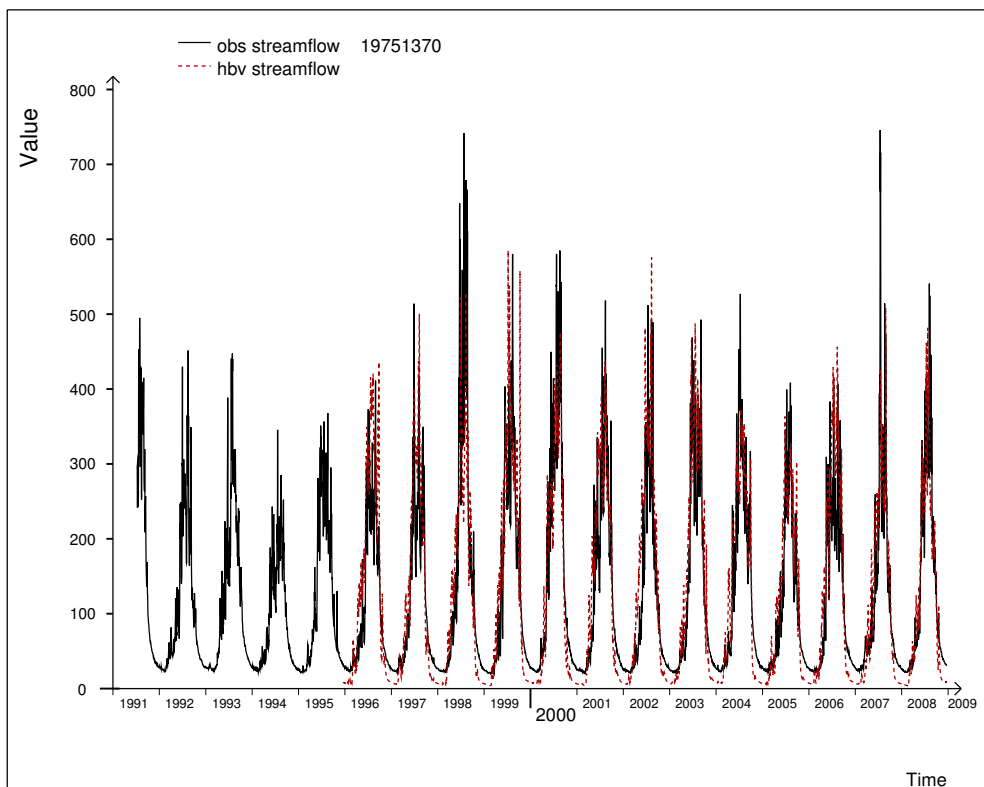
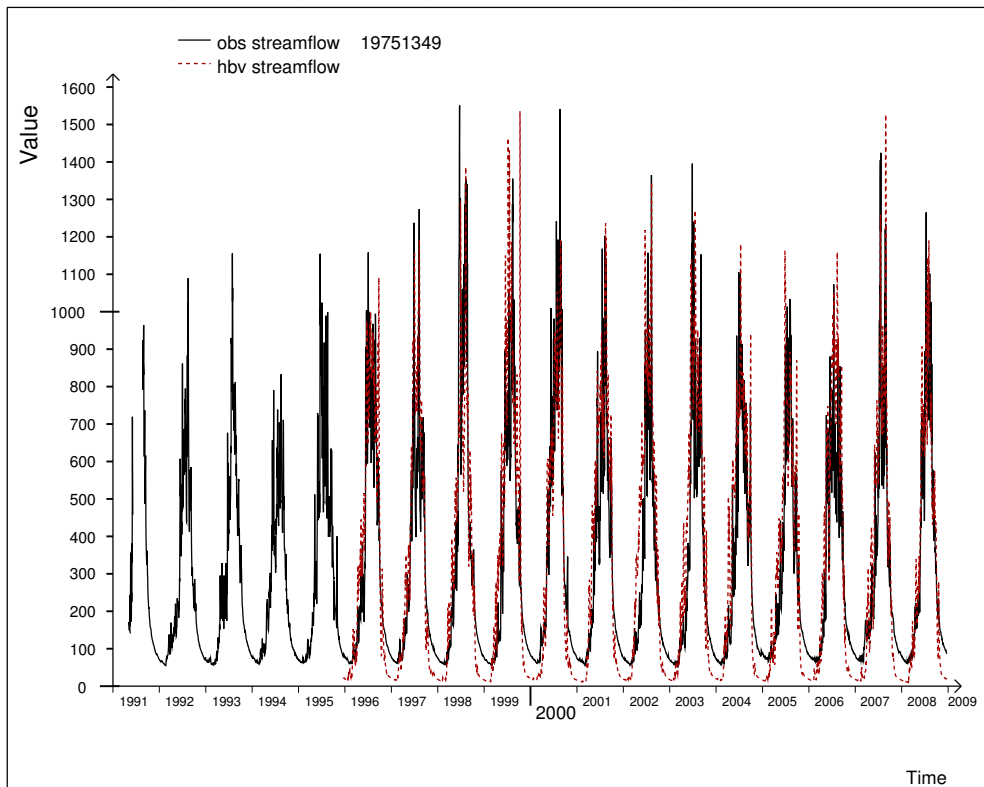


Figure A2. Observed (black) and simulated with HBV model (red) daily streamflow ( $\text{m}^3/\text{s}$ ) for catchments 1349 Wangdirapids (top) and 1370 Yebesa (bottom) for the period 1991-2008.

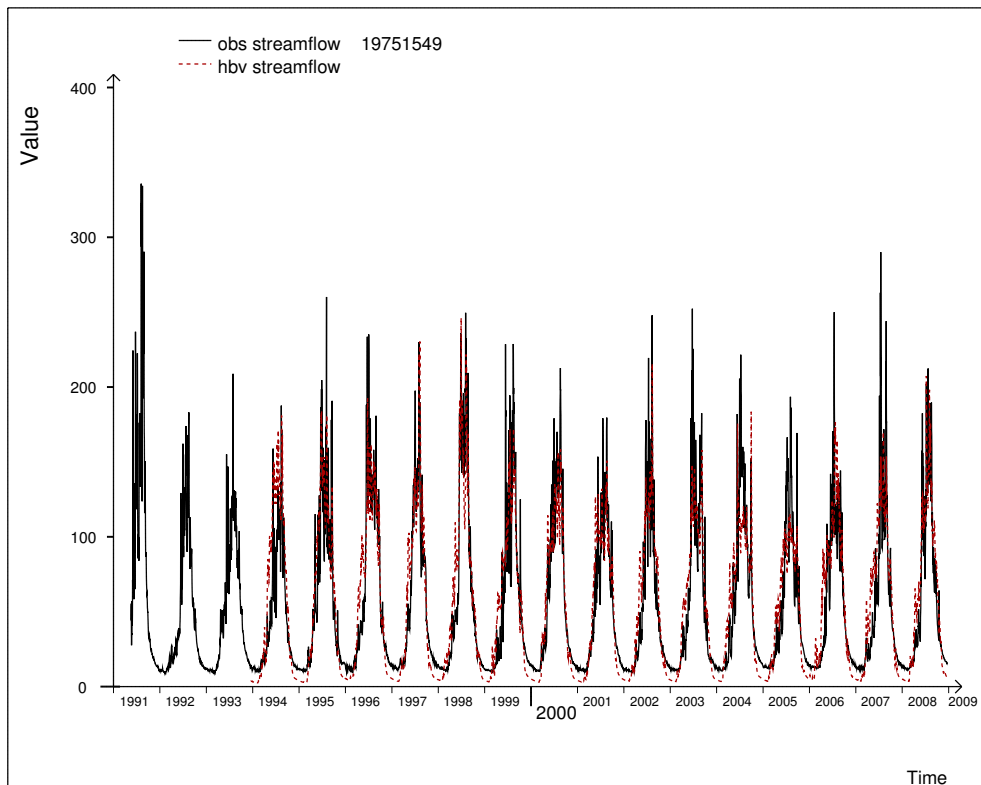
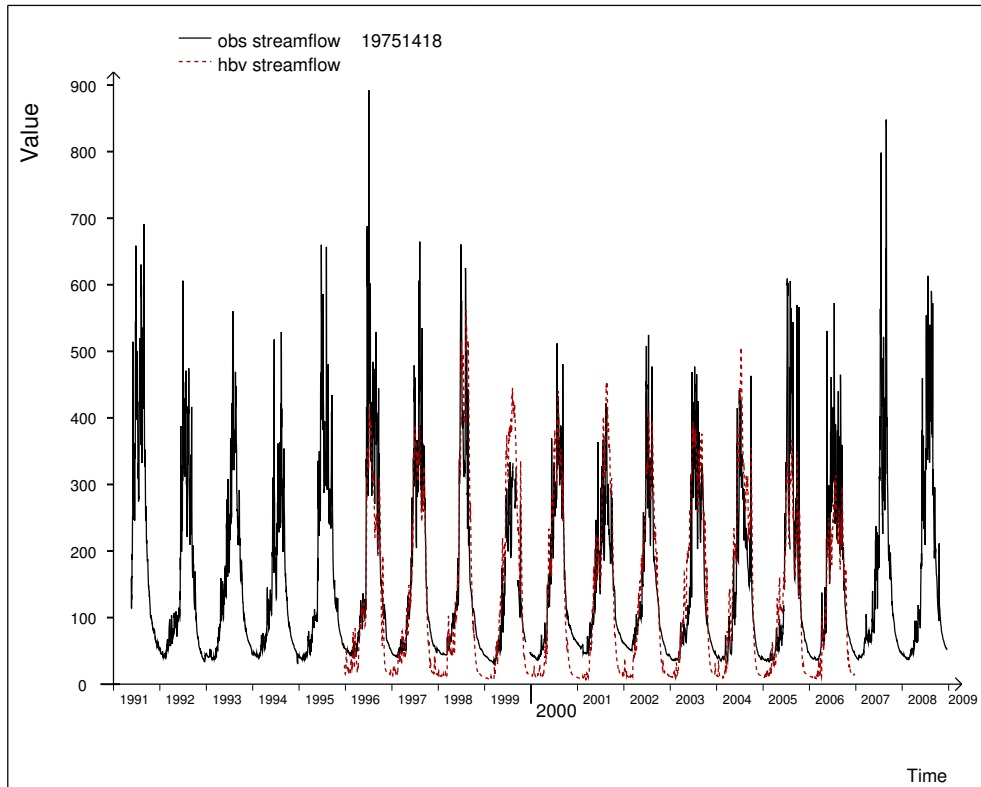


Figure A3. Observed (black) and simulated with HBV model (red) daily streamflow ( $\text{m}^3/\text{s}$ ) for catchments 1418 Tingtibi (top) and 1549 Kurje (bottom) for the period 1991-2008.

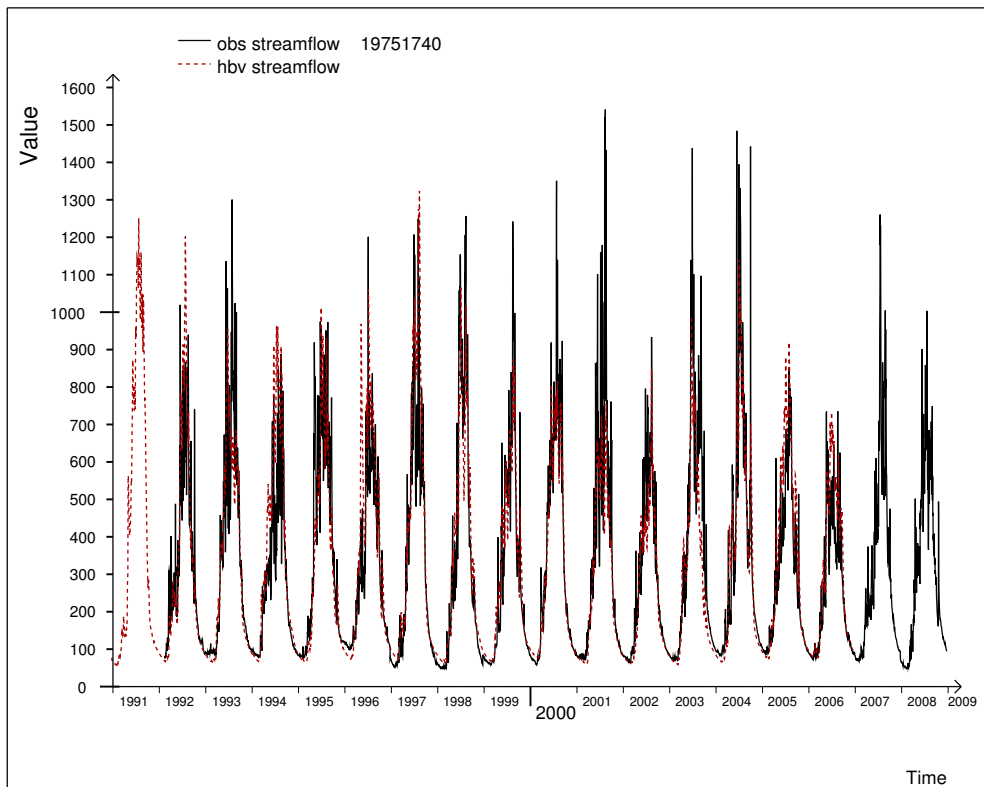
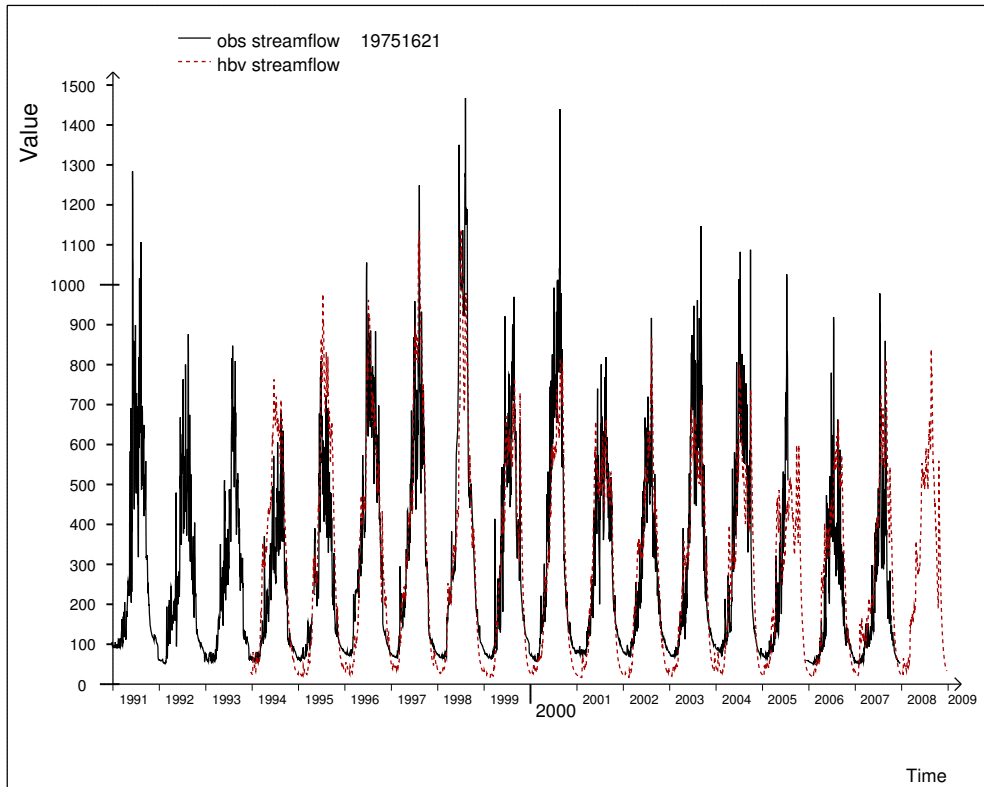


Figure A4. Observed (black) and simulated with HBV model (red) daily streamflow ( $\text{m}^3/\text{s}$ ) for catchments 1621 Kurizampa (top) and 1740 Uzorong (bottom) for the period 1991-2008.



# **Appendix B Evaluation of hydrological model with input from climate projection Echem B1**

Figures B1-B6: HBV hydrological model results based on downscaled climate model data from projection Echem B1 for the control period 1991-2008. Streamflow simulations are compared to observed hydrological data. Hydrological model results and observed streamflow data have been aggregated to monthly values and multi-year mean monthly values, i.e. the average of each calendar month for all years. The glacier covered-areas of the model are treated as constant.

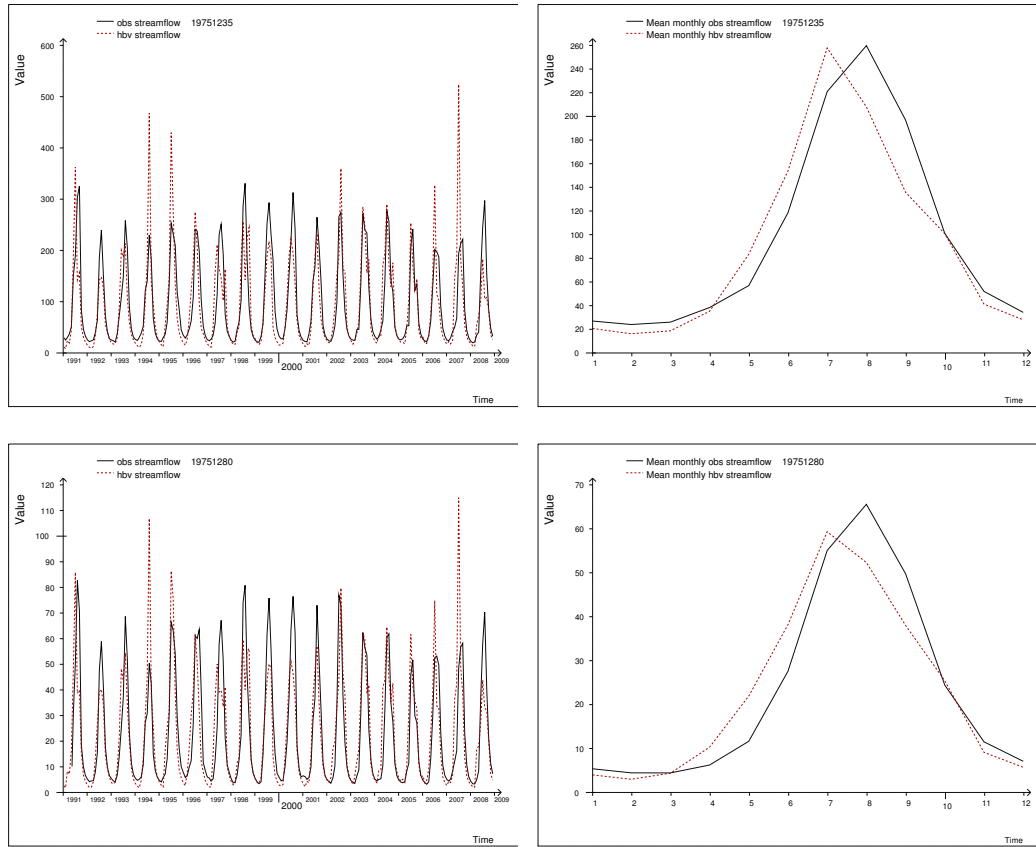


Figure B1. Observed (black) and simulated with HBV model (red) monthly streamflow ( $\text{m}^3/\text{s}$ ) for catchments 1235 Chimakoti (top left) and 1280 Lungtenphug (bottom left) for the period 1991-2008 based on downscaled climate model data from projection Echem B1.

Observed (black) and simulated with HBV model (red) multi-year mean monthly streamflow ( $\text{m}^3/\text{s}$ ) for catchments 1235 Chimakoti (top right) and 1280 Lungtenphug (bottom right) for the period 1991-2008 based on downscaled climate model data from projection Echem B1.

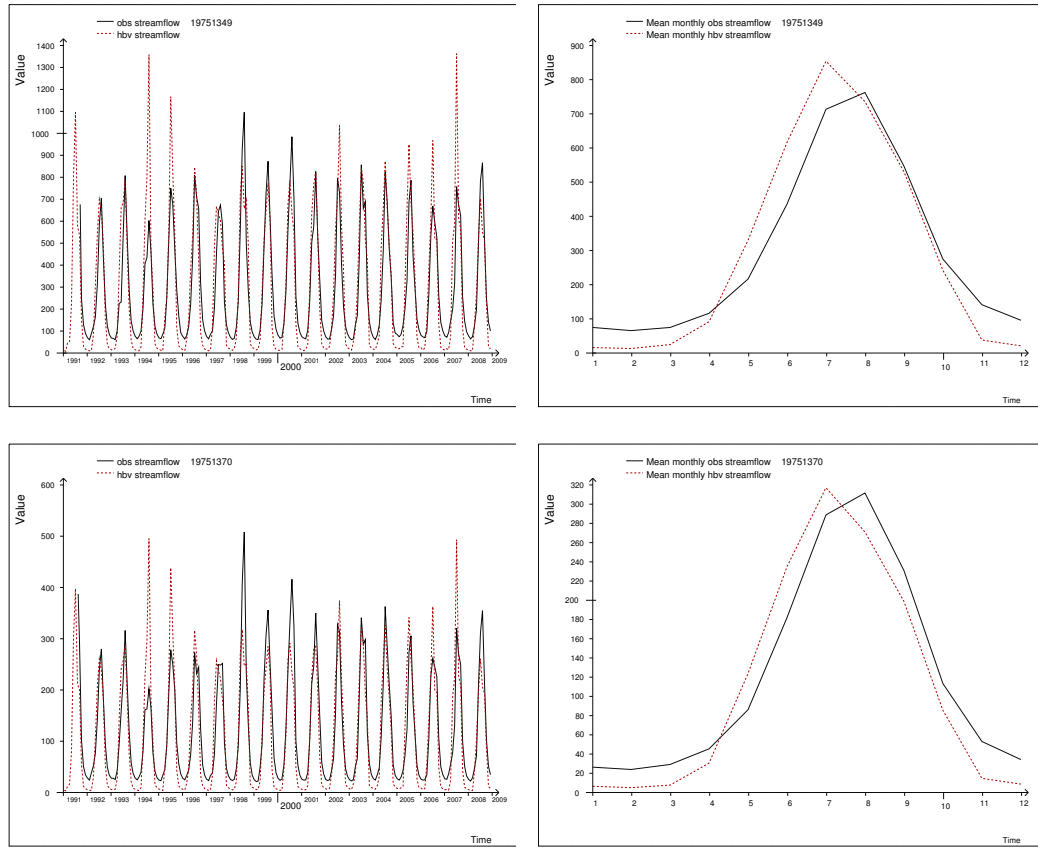


Figure B2. Observed (black) and simulated with HBV model (red) monthly streamflow ( $\text{m}^3/\text{s}$ ) for catchments 1349 Wangdirapids (top left) and 1370 Yebesa (bottom left) for the period 1991-2008 based on downscaled climate model data from projection Echam B1.

Observed (black) and simulated with HBV model (red) multi-year mean monthly streamflow ( $\text{m}^3/\text{s}$ ) for catchments 1349 Wangdirapids (top right) and 1370 Yebesa (bottom right) for the period 1991-2008 based on downscaled climate model data from projection Echam B1.

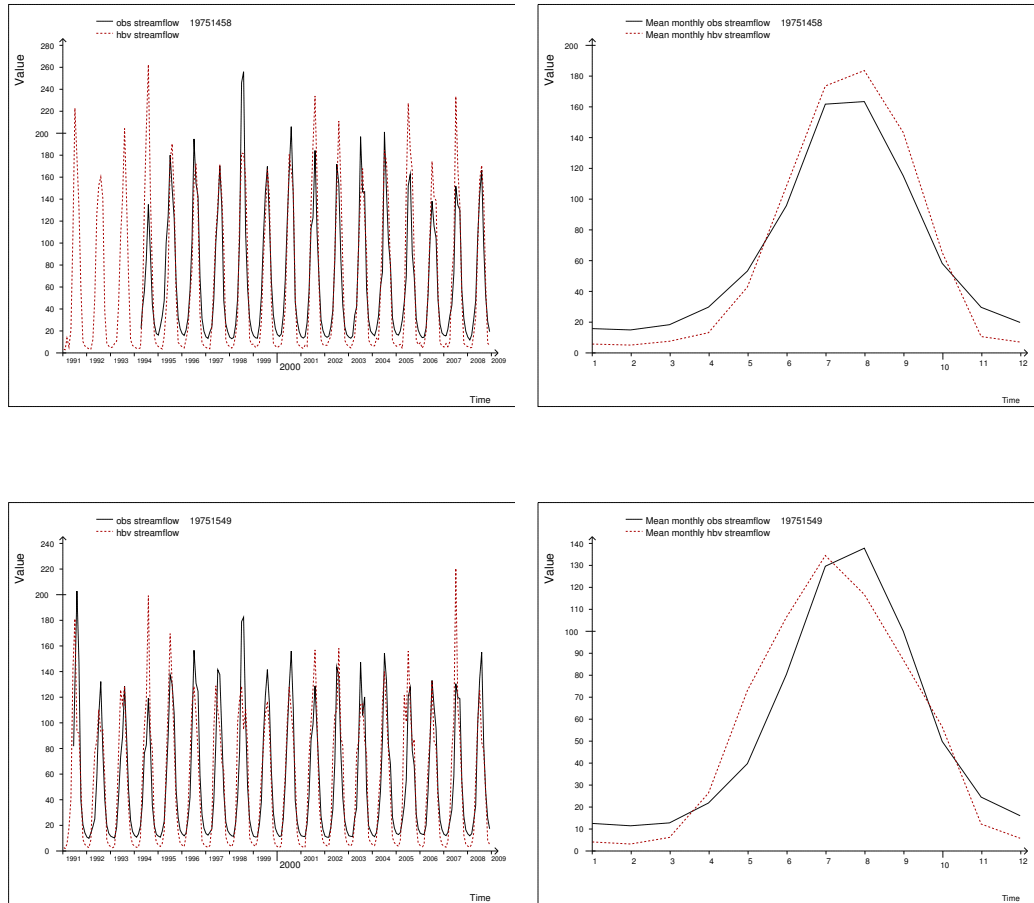


Figure B3. Observed (black) and simulated with HBV model (red) monthly streamflow ( $\text{m}^3/\text{s}$ ) for catchments 1458 Bjizam (top left) and 1549 Kurjey (bottom left) for the period 1991-2008 based on downscaled climate model data from projection Echam B1.

Observed (black) and simulated with HBV model (red) multi-year mean monthly streamflow ( $\text{m}^3/\text{s}$ ) for catchments 1458 Bjizam (top right) and 1549 Kurjey (bottom right) for the period 1991-2008 based on downscaled climate model data from projection Echam B1.

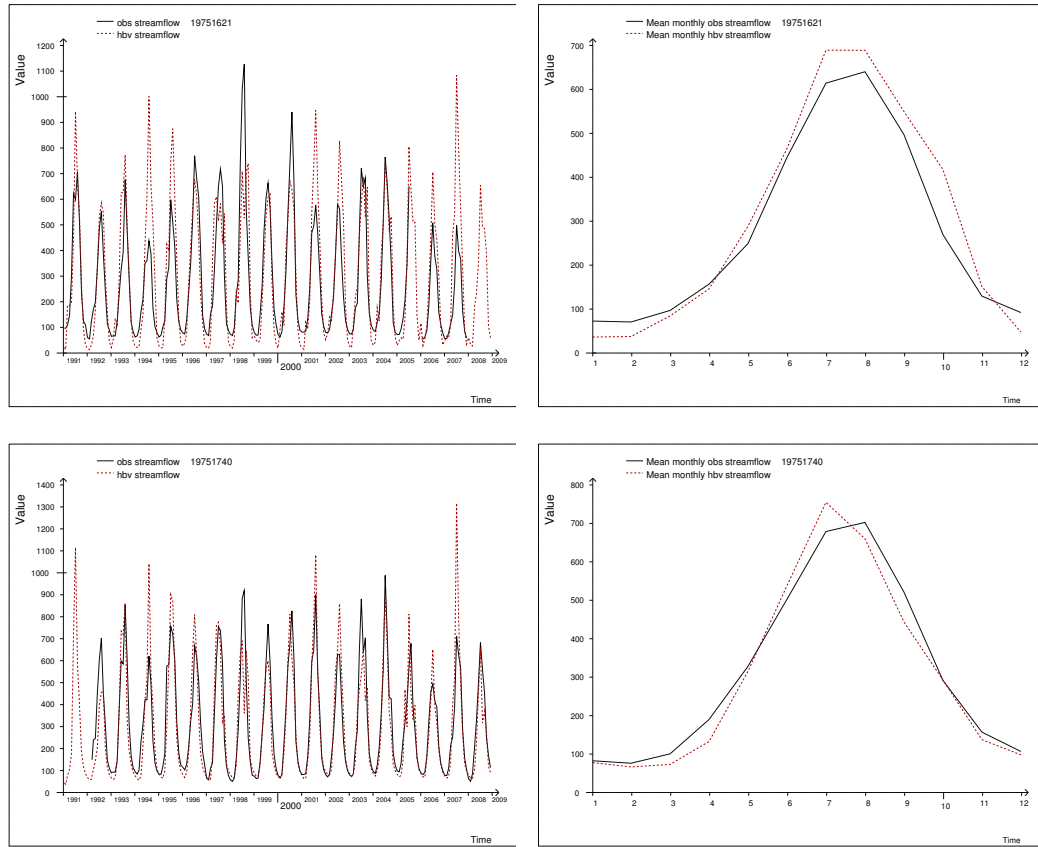


Figure B4. Observed (black) and simulated with HBV model (red) monthly streamflow ( $\text{m}^3/\text{s}$ ) for catchments 1621 Kurizampa (top left) and 1740 Uzorong (bottom left) for the period 1991-2008 based on downscaled climate model data from projection Echam B1.

Observed (black) and simulated with HBV model (red) multi-year mean monthly streamflow ( $\text{m}^3/\text{s}$ ) for catchments 1621 Kurizampa (top right) and 1740 Uzorong (bottom right) for the period 1991-2008 based on downscaled climate model data from projection Echam B1.

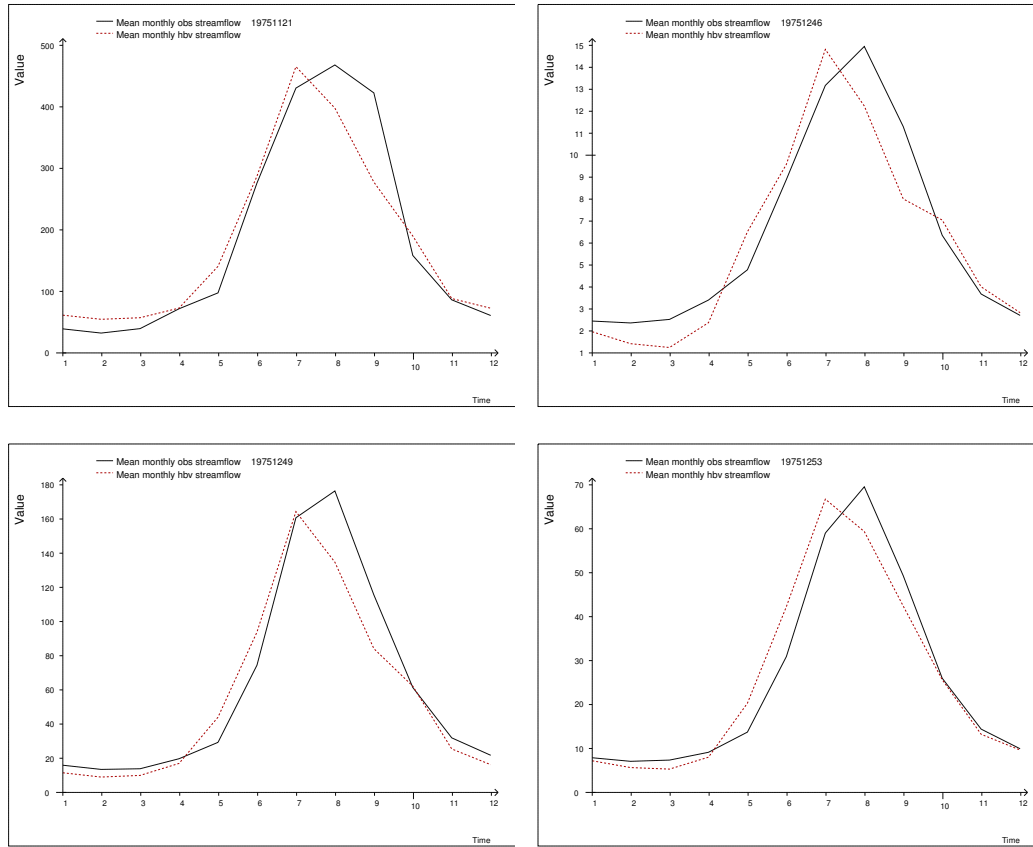


Figure B5. Observed (black) and simulated with HBV model (red) multi-year mean monthly streamflow ( $\text{m}^3/\text{s}$ ) for catchments 1121 Doyagang (top left), 1246 Haa (top right), 1249 Damchhu (bottom left) and 1253 Paro (bottom right) for the period 1991-2008 based on downscaled climate model data from projection Echem B1.

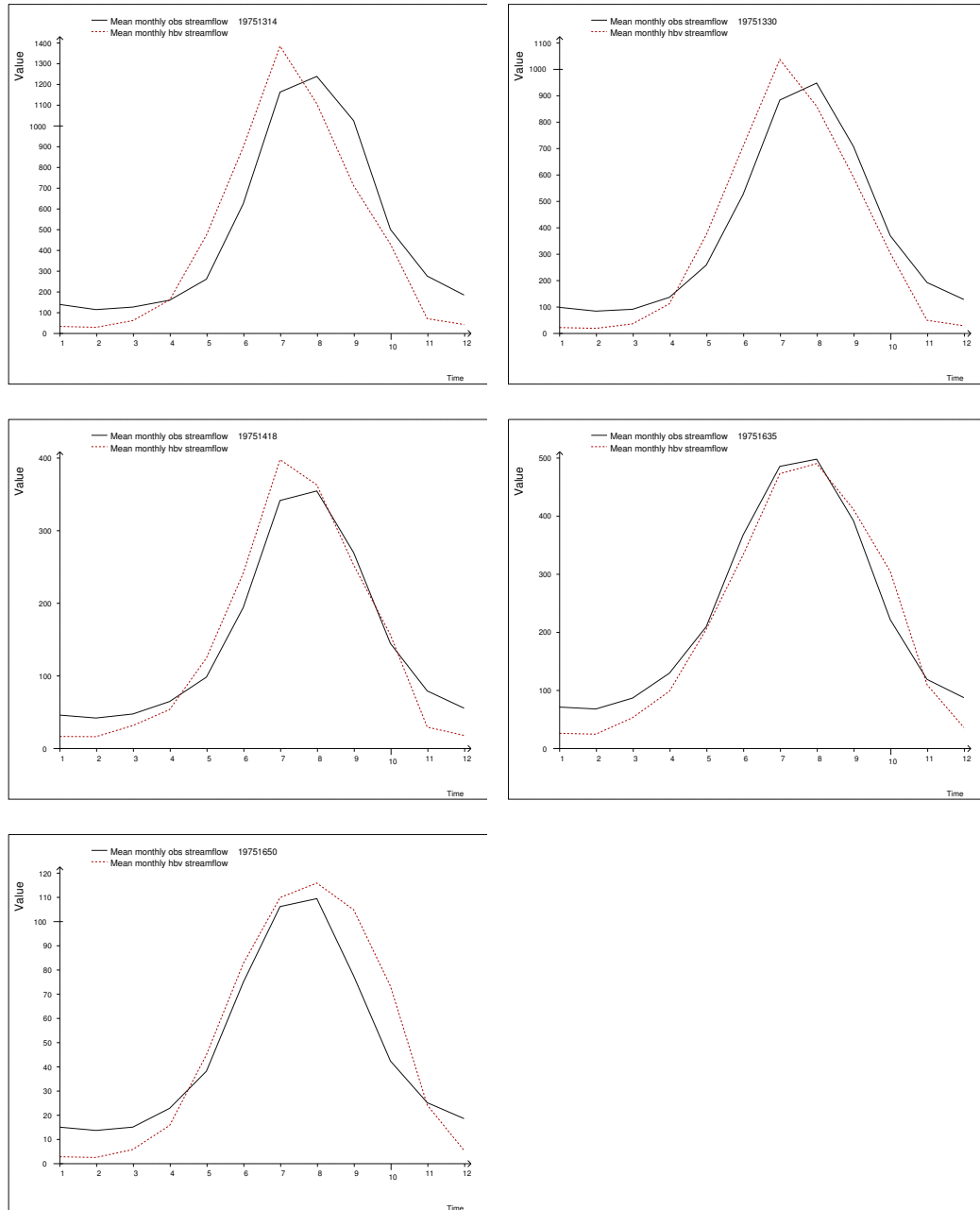


Figure B6. Observed (black) and simulated with HBV model (red) multi-year mean monthly streamflow ( $\text{m}^3/\text{s}$ ) for catchments 1314 Kerabari (top left), 1330 Dobani (top right), 1418 Tingtibi (middle left), 1635 Autsho (middle right) and 1650 Sumpa (bottom) for the period 1991-2008 based on downscaled climate model data from projection Echam B1.

# **Appendix C Seasonal precipitation change and mean daily streamflow for climate projections Echem A2 and B1**

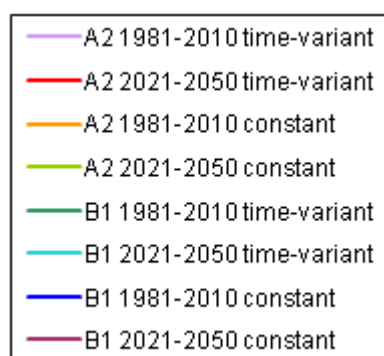
Figures C1-C17: HBV hydrological model results based on downscaled climate model data from projections Echem A2 and Echem B1 for the periods 1981-2010, 2021-2050 and 2071-2100 as input. Temperature and precipitation input data have been modified by the hydrological model according to temperature lapse rates and precipitation elevation gradients determined during model calibration. Precipitation averaged over all model grid cells within a sub-catchment is presented as multi-year mean seasonal change, i.e. the change in the average of each season of the year for all years in each period from the control period 1981-2010 to each projection period 2021-2050 and 2071-2100. The seasons are winter (December, January, February), spring (March, April, May), summer (June, July, August) and autumn (September, October, November). Hydrological model results for streamflow at the outlet of each sub-catchment have been aggregated to multi-year mean daily values, i.e. the average of each day of the year for all years in each period. The glacier covered areas of the model are treated as constant, or time-variant with initial ice volumes modified by model mass balance results for glacier covered grid cells.



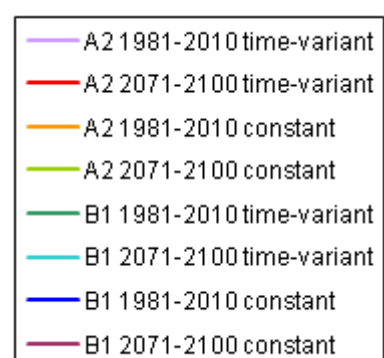
Legend precipitation:



Legend streamflow 1981-2010 vs. 2021-2050:



Legend streamflow 1981-2010 vs. 2071-2100:



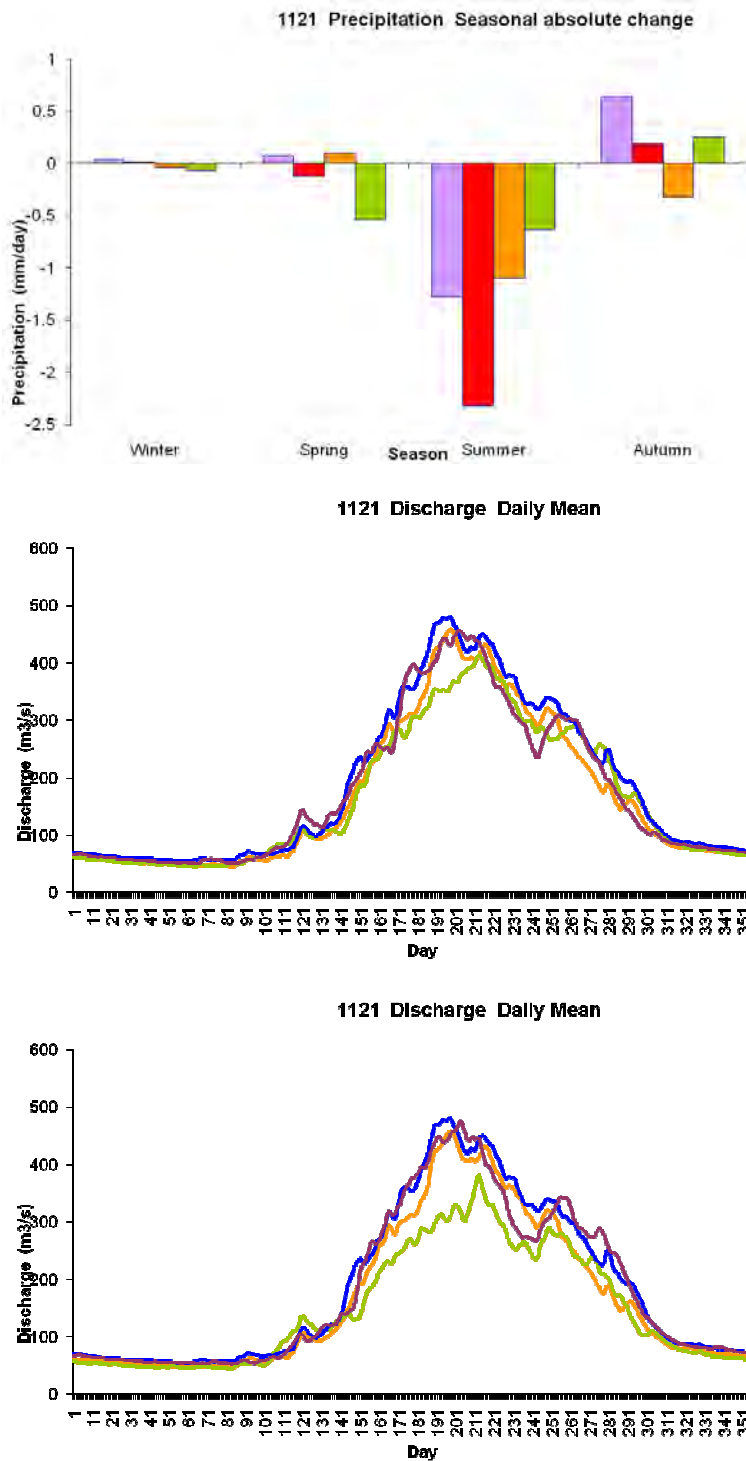


Figure C1. Hydrological model results for catchment 1121 Doyagan with precipitation and temperature input from climate projections Echam A2 and B1 downscaled to meteorological station sites. Top: seasonal precipitation (mm/day) for periods 1981-2010, 2021-2050 and 2071-2100. Middle: multi-year mean daily streamflow ( $\text{m}^3/\text{s}$ ) for periods 1981-2010 and 2021-2050. Bottom: multi-year mean daily streamflow ( $\text{m}^3/\text{s}$ ) for periods 1981-2010 and 2071-2100. The glacier covered areas of the model are treated as constant, or time-variant with initial ice volumes modified by model mass balance results.

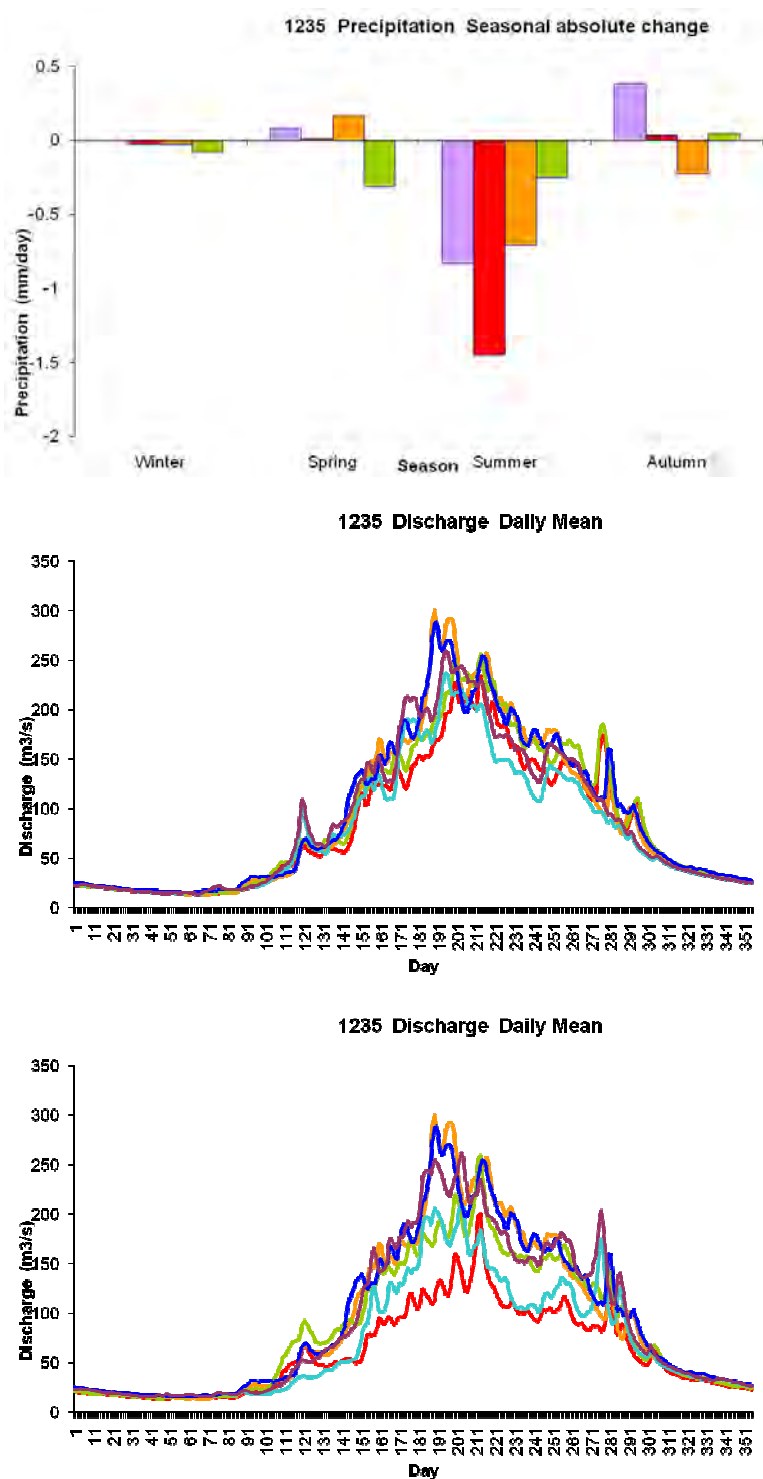


Figure C2. Hydrological model results for catchment 1235 Chimakoti with precipitation and temperature input from climate projections Echam A2 and B1 downscaled to meteorological station sites. Top: seasonal precipitation (mm/day) for periods 1981-2010, 2021-2050 and 2071-2100. Middle: multi-year mean daily streamflow ( $\text{m}^3/\text{s}$ ) for periods 1981-2010 and 2021-2050. Bottom: multi-year mean daily streamflow ( $\text{m}^3/\text{s}$ ) for periods 1981-2010 and 2071-2100. The glacier covered areas of the model are treated as constant, or time-variant with initial ice volumes modified by model mass balance results.

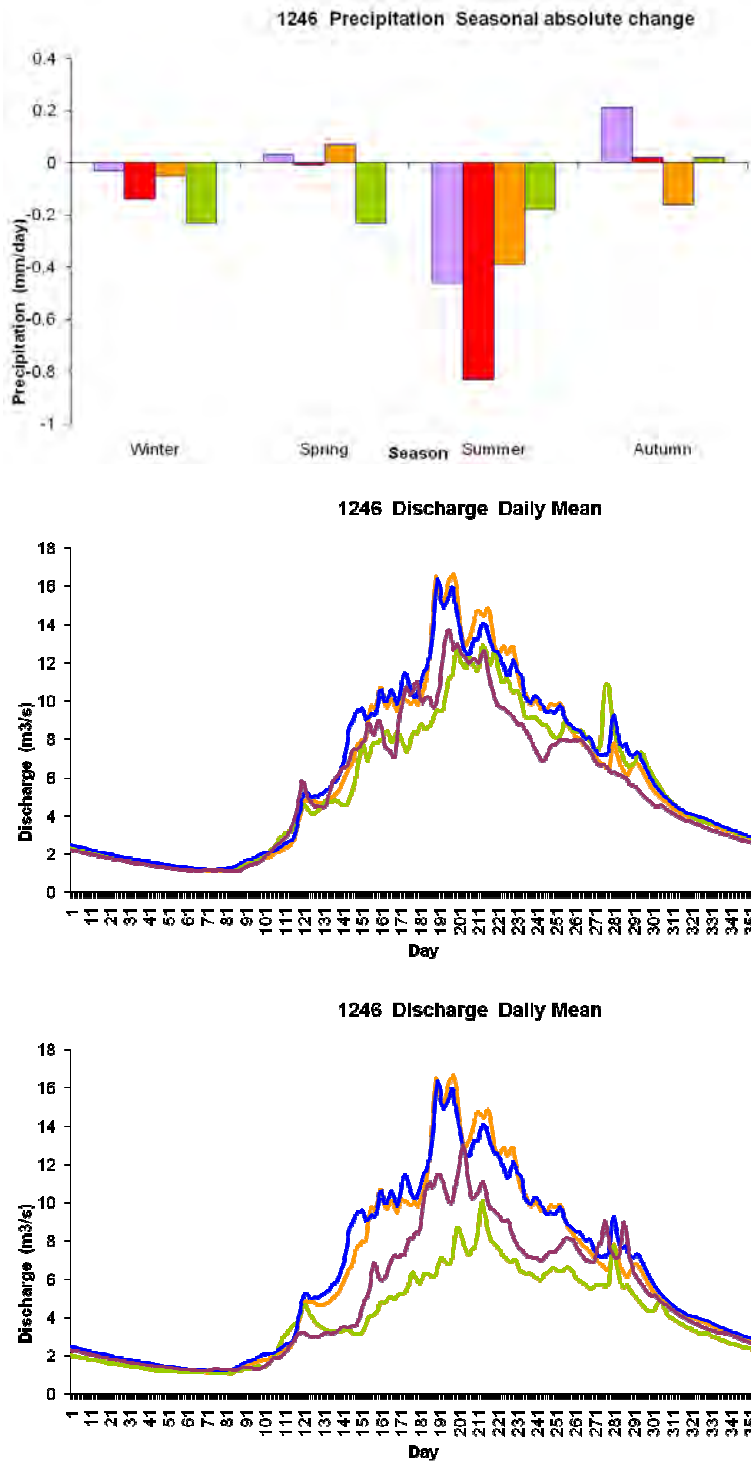


Figure C3. Hydrological model results for catchment 1246 Haa with precipitation and temperature input from climate projections Echam A2 and B1 downscaled to meteorological station sites. Top: seasonal precipitation (mm/day) for periods 1981-2010, 2021-2050 and 2071-2100. Middle: multi-year mean daily streamflow ( $\text{m}^3/\text{s}$ ) for periods 1981-2010 and 2021-2050. Bottom: multi-year mean daily streamflow ( $\text{m}^3/\text{s}$ ) for periods 1981-2010 and 2071-2100. The glacier covered areas of the model are treated as constant, or time-variant with initial ice volumes modified by model mass balance.

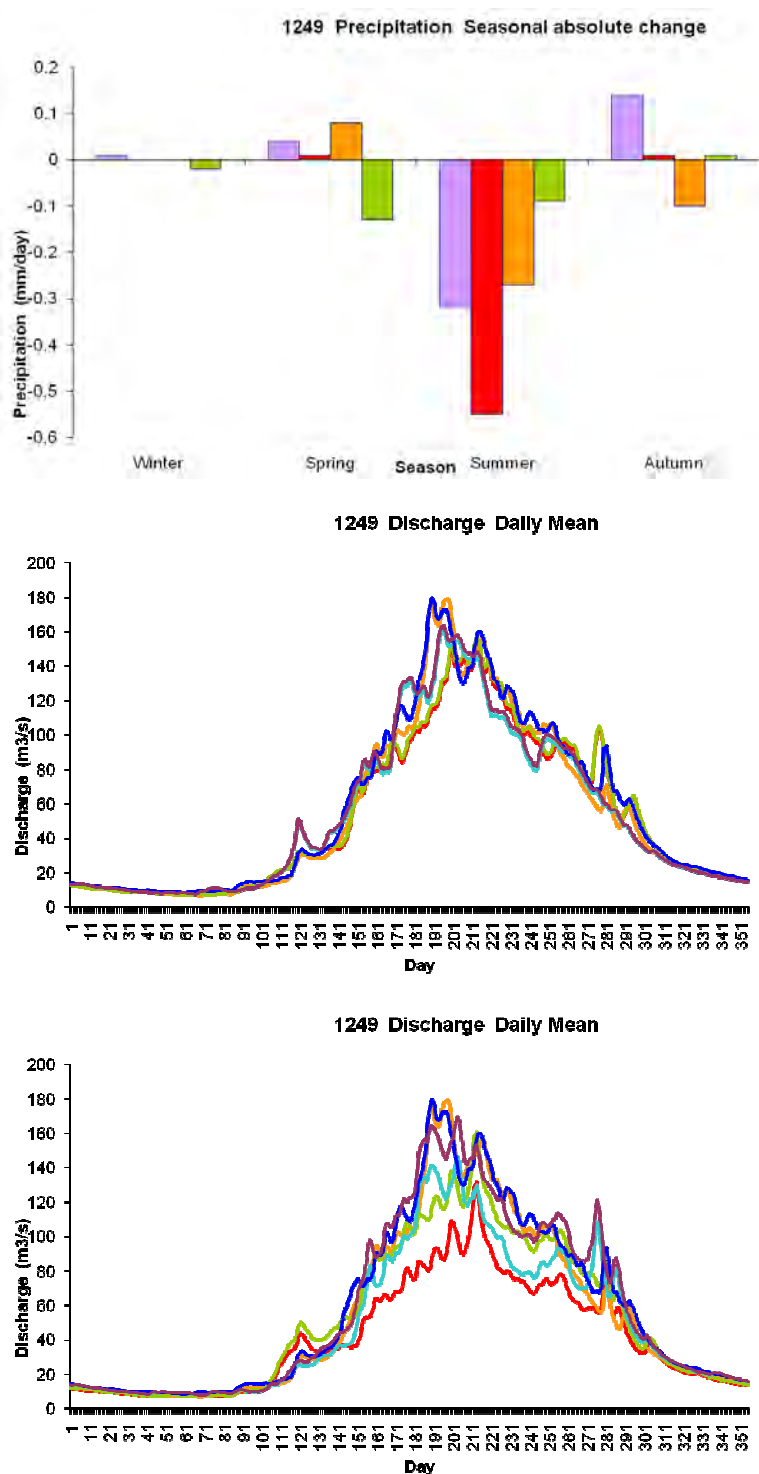


Figure C4. Hydrological model results for catchment 1249 Damchhu with precipitation and temperature input from climate projections Echam A2 and B1 downscaled to meteorological station sites. Top: seasonal precipitation (mm/day) for periods 1981-2010, 2021-2050 and 2071-2100. Middle: multi-year mean daily streamflow ( $\text{m}^3/\text{s}$ ) for periods 1981-2010 and 2021-2050. Bottom: multi-year mean daily streamflow ( $\text{m}^3/\text{s}$ ) for periods 1981-2010 and 2071-2100. The glacier covered areas of the model are treated as constant, or time-variant with initial ice volumes modified by model mass balance results.

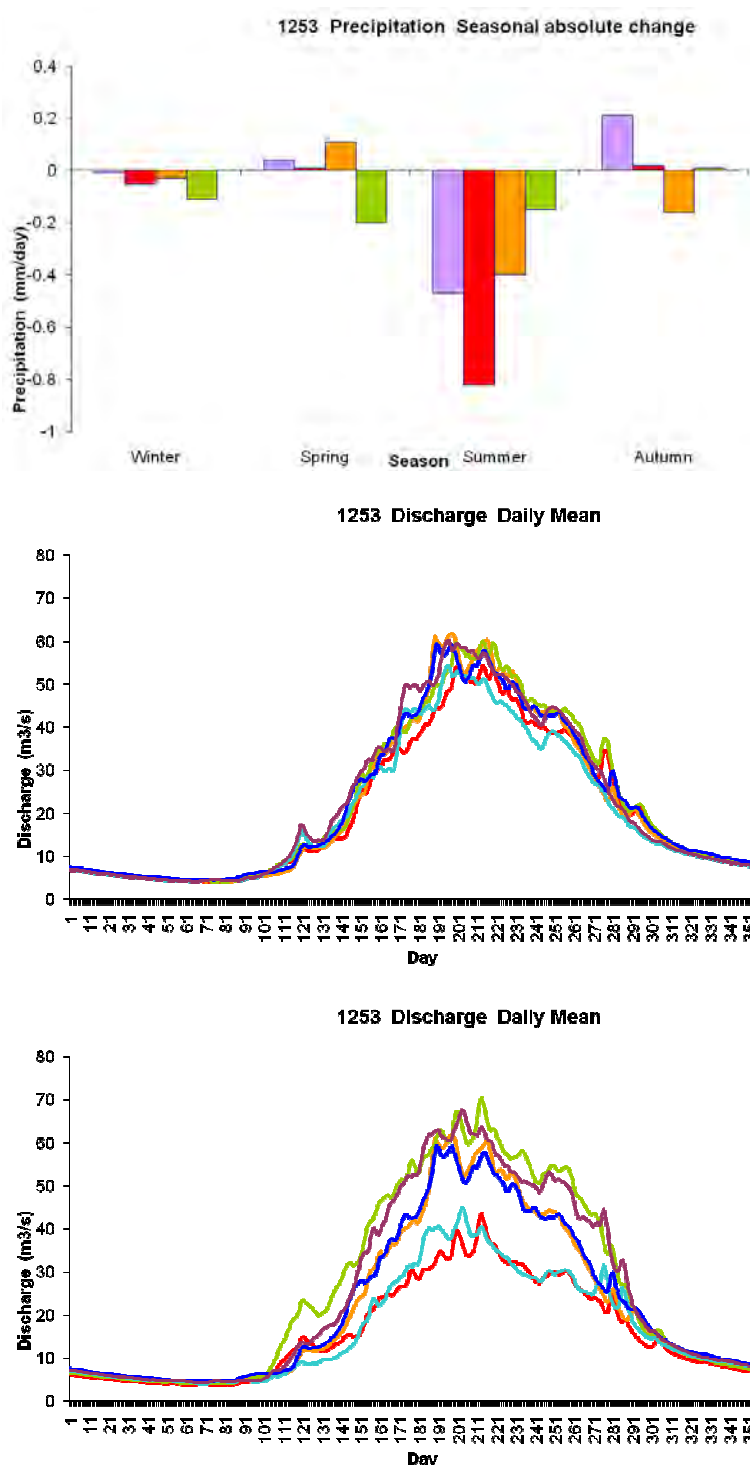


Figure C5. Hydrological model results for catchment 1253 Paro with precipitation and temperature input from climate projections Echam A2 and B1 downscaled to meteorological station sites. Top: seasonal precipitation (mm/day) for periods 1981-2010, 2021-2050 and 2071-2100. Middle: multi-year mean daily streamflow ( $\text{m}^3/\text{s}$ ) for periods 1981-2010 and 2021-2050. Bottom: multi-year mean daily streamflow ( $\text{m}^3/\text{s}$ ) for periods 1981-2010 and 2071-2100. The glacier covered areas of the model are treated as constant, or time-variant with initial ice volumes modified by model mass balance results.

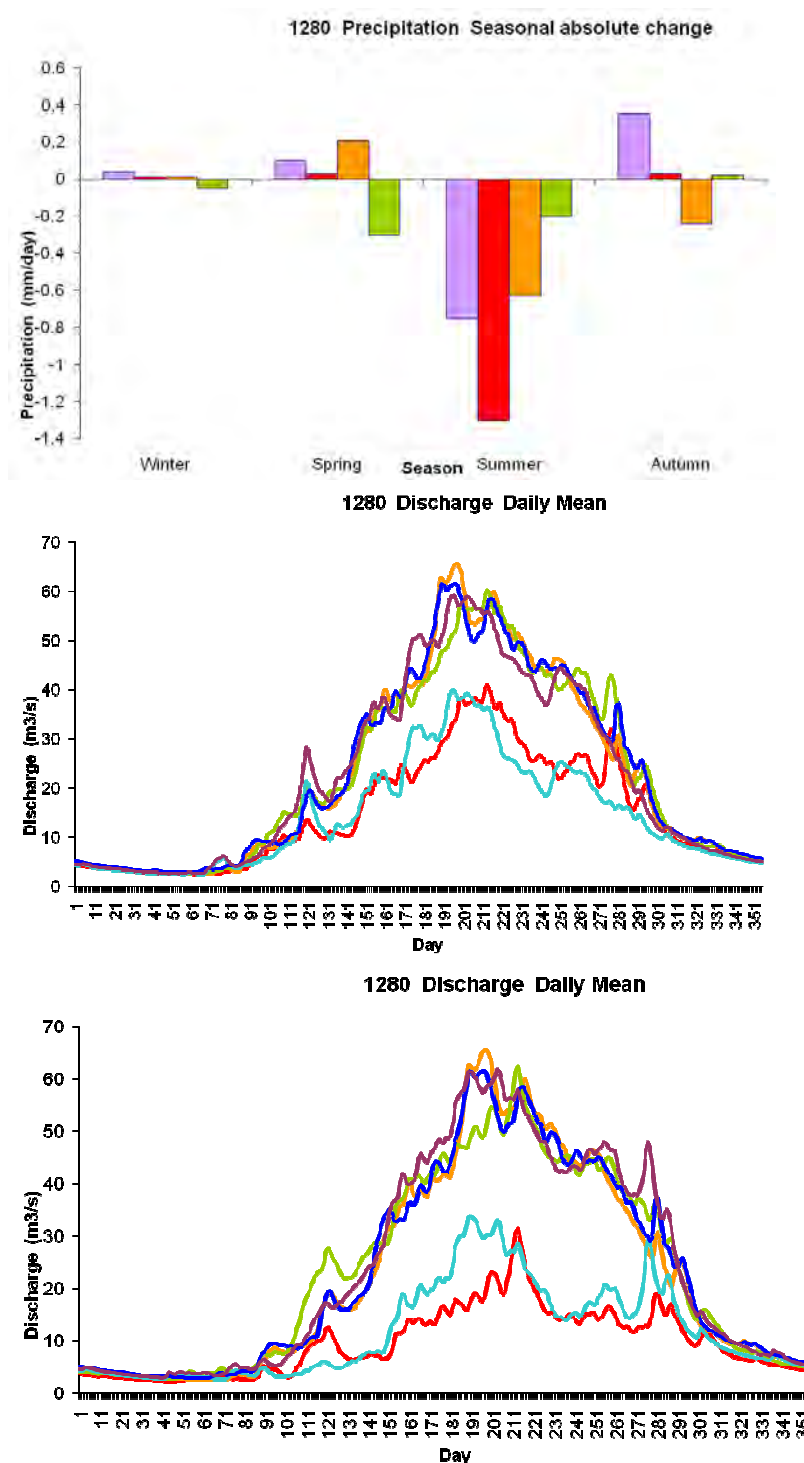


Figure C6. Hydrological model results for catchment 1280 Lungtenphug with precipitation and temperature input from climate projections Ecam A2 and B1 downscaled to meteorological station sites. Top: seasonal precipitation (mm/day) for periods 1981-2010, 2021-2050 and 2071-2100. Middle: multi-year mean daily streamflow (m<sup>3</sup>/s) for periods 1981-2010 and 2021-2050. Bottom: multi-year mean daily streamflow (m<sup>3</sup>/s) for periods 1981-2010 and 2071-2100. The glacier covered areas of the model are treated as constant, or time-variant with initial ice volumes modified by model mass balance results.

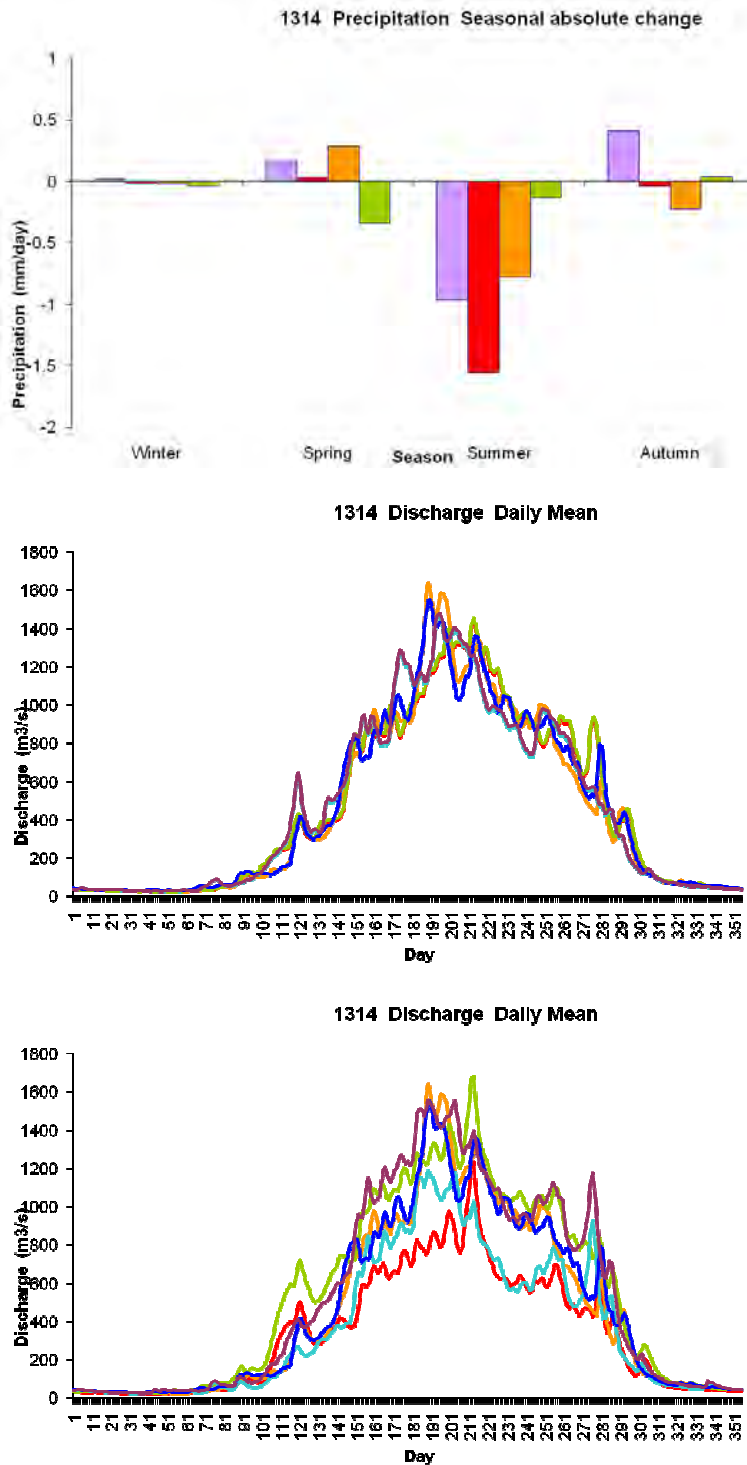


Figure C7. Hydrological model results for catchment 1314 Kerabari with precipitation and temperature input from climate projections Echam A2 and B1 downscaled to meteorological station sites. Top: seasonal precipitation (mm/day) for periods 1981-2010, 2021-2050 and 2071-2100. Middle: multi-year mean daily streamflow ( $\text{m}^3/\text{s}$ ) for periods 1981-2010 and 2021-2050. Bottom: multi-year mean daily streamflow ( $\text{m}^3/\text{s}$ ) for periods 1981-2010 and 2071-2100. The glacier covered areas of the model are treated as constant, or time-variant with initial ice volumes modified by model mass balance results.



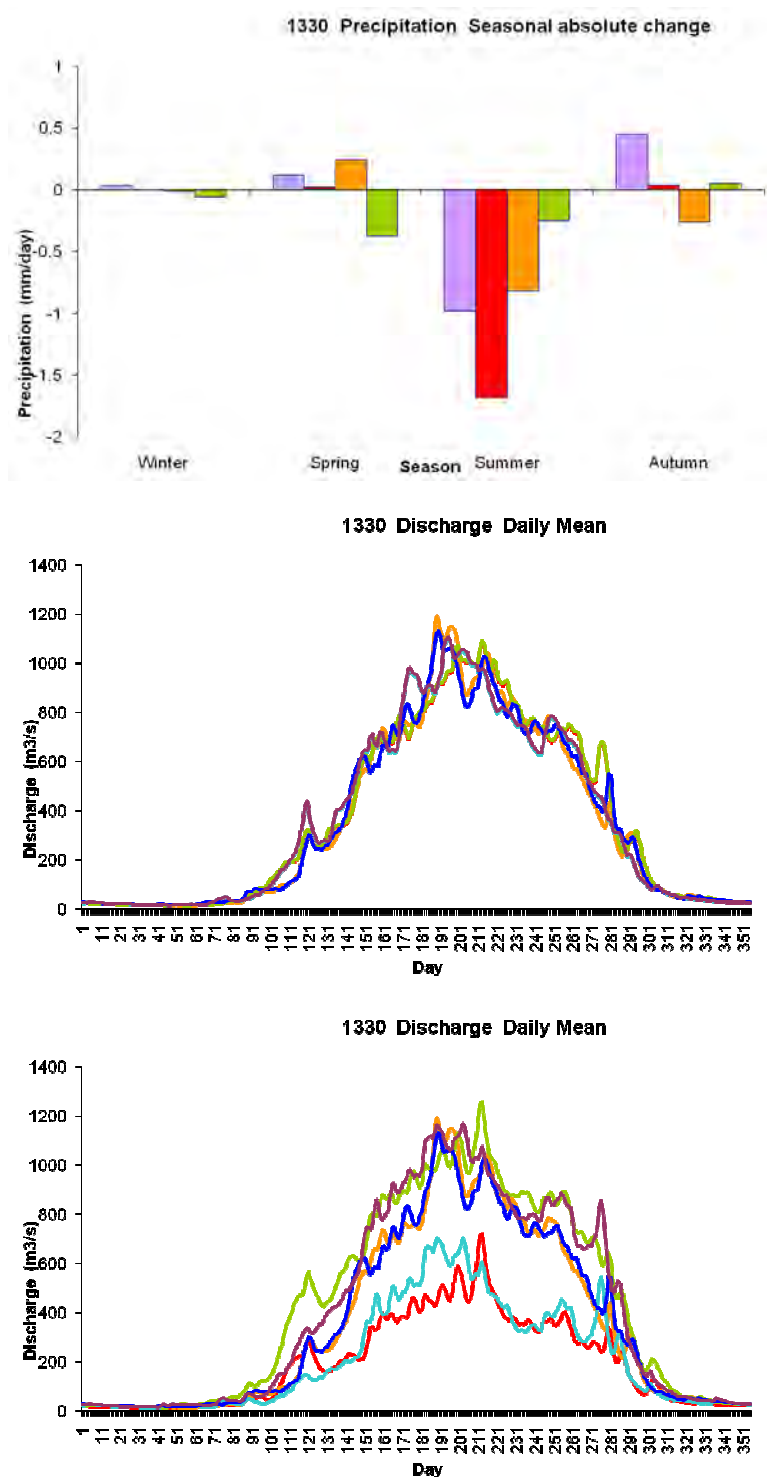


Figure C8. Hydrological model results for catchment 1330 Dobani with precipitation and temperature input from climate projections Echam A2 and B1 downscaled to meteorological station sites. Top: seasonal precipitation (mm/day) for periods 1981-2010, 2021-2050 and 2071-2100. Middle: multi-year mean daily streamflow ( $\text{m}^3/\text{s}$ ) for periods 1981-2010 and 2021-2050. Bottom: multi-year mean daily streamflow ( $\text{m}^3/\text{s}$ ) for periods 1981-2010 and 2071-2100. The glacier covered areas of the model are treated as constant, or time-variant with initial ice volumes modified by model mass balance results.

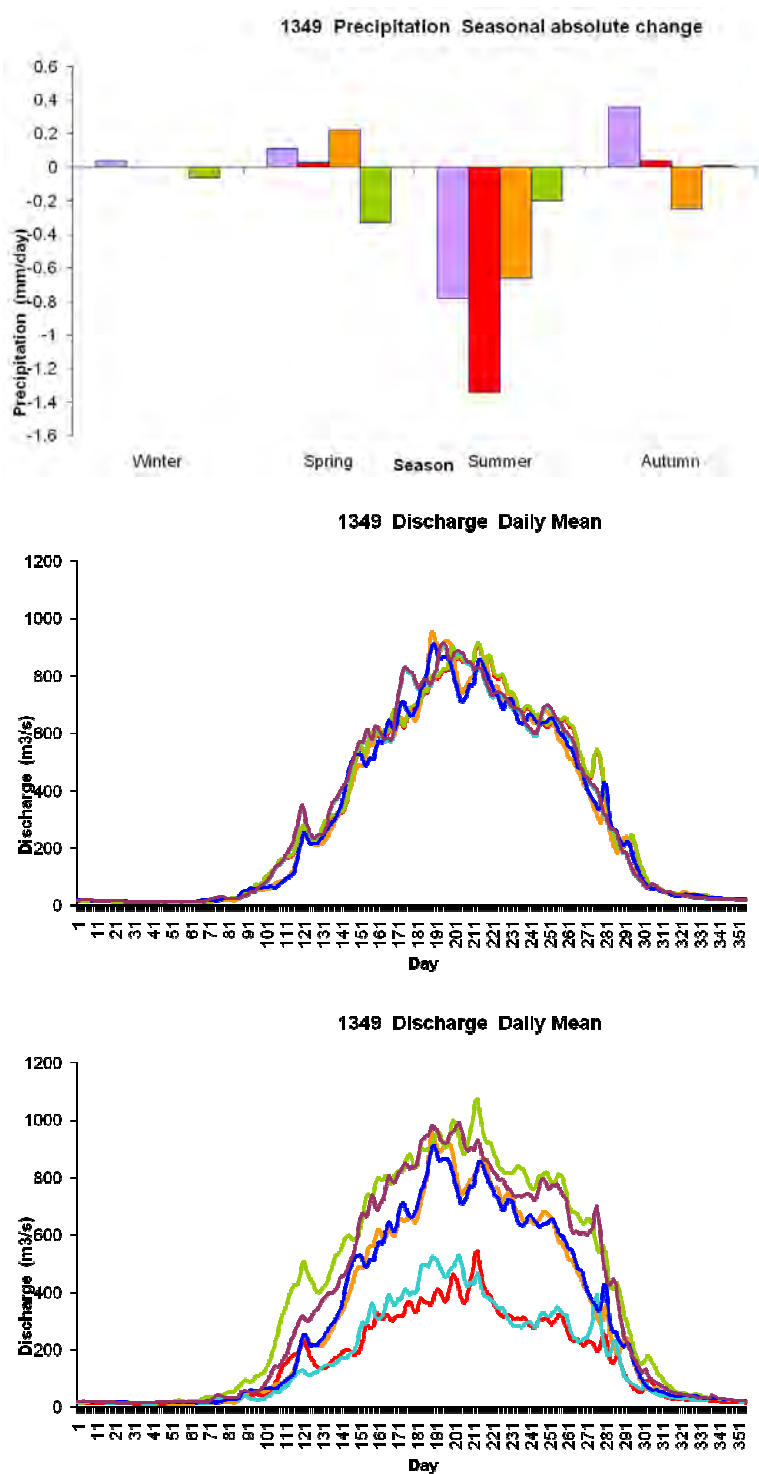


Figure C9. Hydrological model results for catchment 1349 Wangdirapids with precipitation and temperature input from climate projections Echam A2 and B1 downscaled to meteorological station sites. Top: seasonal precipitation (mm/day) for periods 1981-2010, 2021-2050 and 2071-2100. Middle: multi-year mean daily streamflow ( $\text{m}^3/\text{s}$ ) for periods 1981-2010 and 2021-2050. Bottom: multi-year mean daily streamflow ( $\text{m}^3/\text{s}$ ) for periods 1981-2010 and 2071-2100. The glacier covered areas of the model are treated as constant, or time-variant with initial ice volumes modified by model mass balance results.

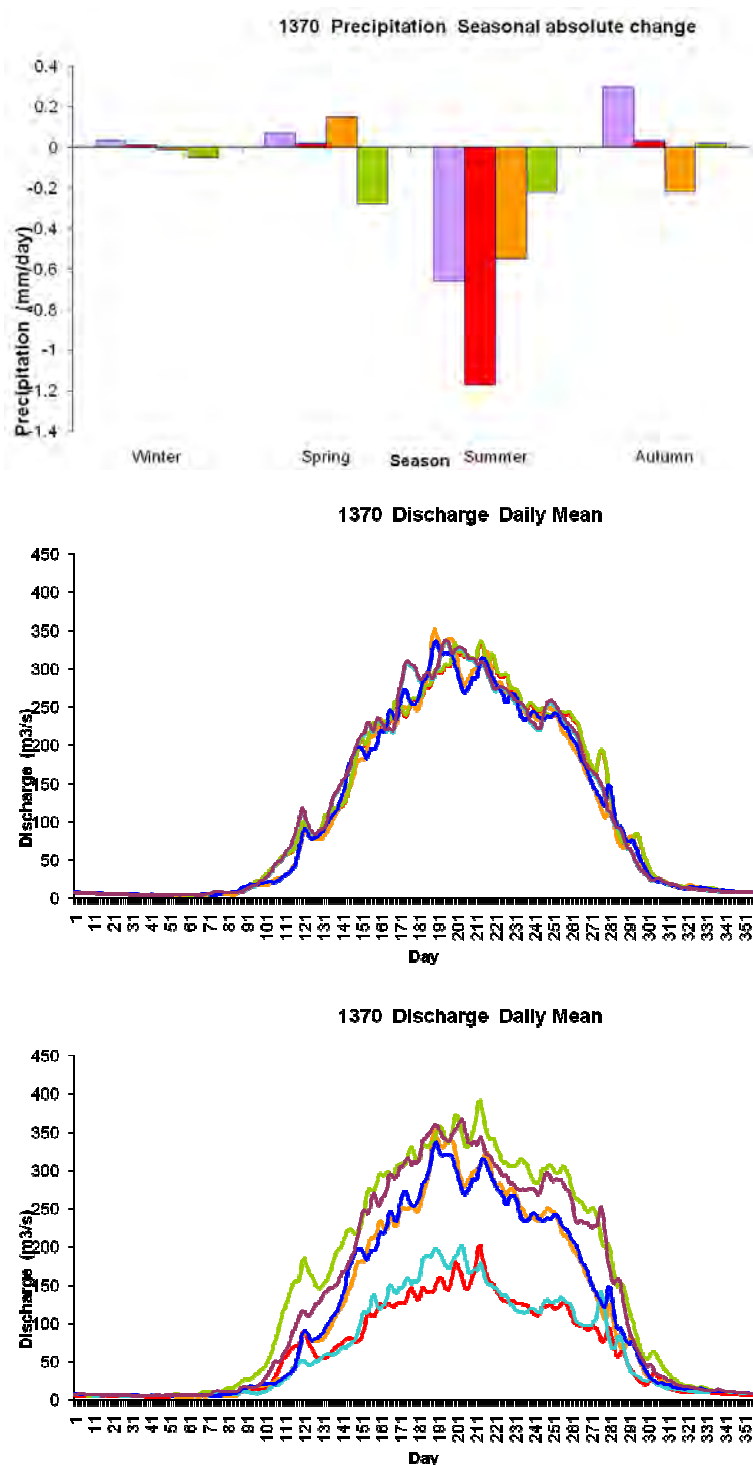


Figure C10. Hydrological model results for catchment 1370 Yebesa with precipitation and temperature input from climate projections Echam A2 and B1 downscaled to meteorological station sites. Top: seasonal precipitation (mm/day) for periods 1981-2010, 2021-2050 and 2071-2100. Middle: multi-year mean daily streamflow ( $\text{m}^3/\text{s}$ ) for periods 1981-2010 and 2021-2050. Bottom: multi-year mean daily streamflow ( $\text{m}^3/\text{s}$ ) for periods 1981-2010 and 2071-2100. The glacier covered areas of the model are treated as constant, or time-variant with initial ice volumes modified by model mass balance results.

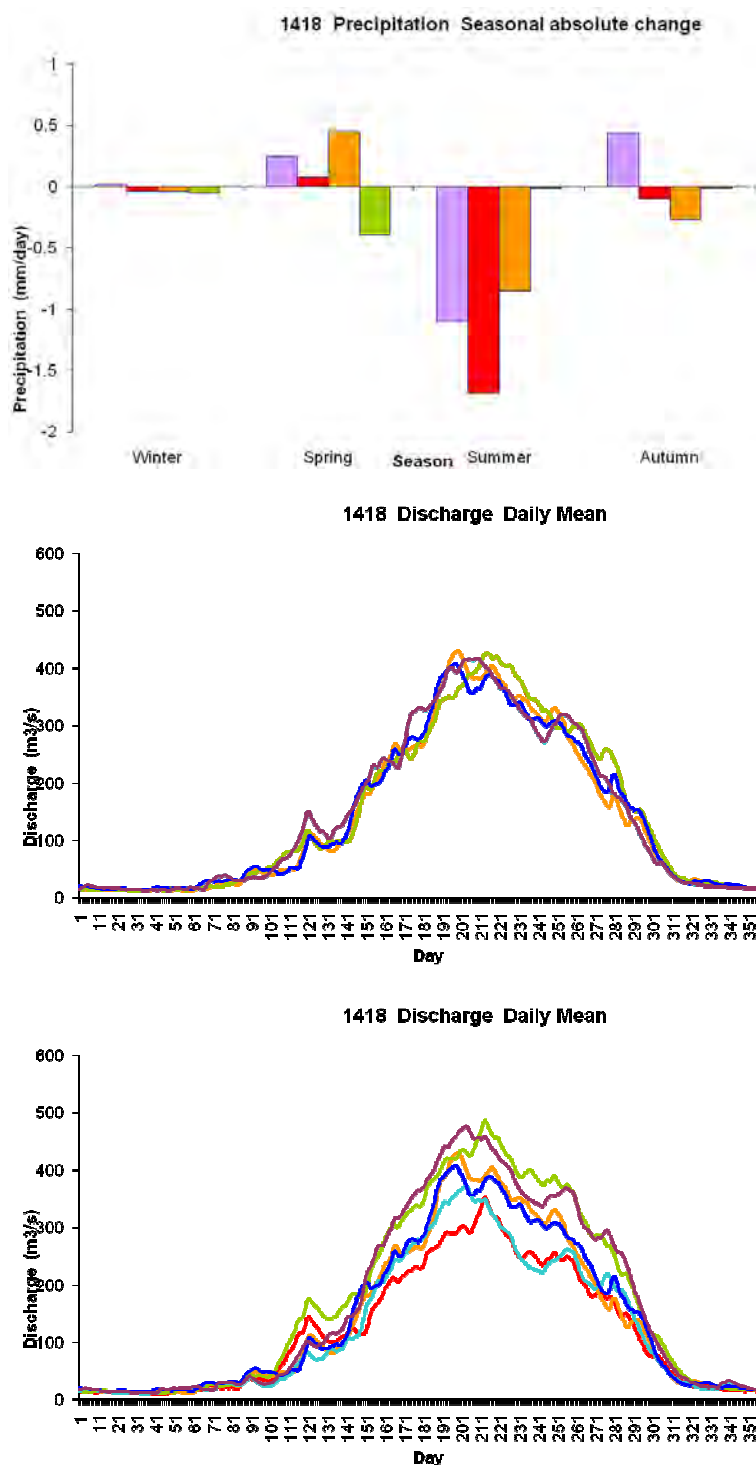


Figure C11. Hydrological model results for catchment 1418 Tingtibi with precipitation and temperature input from climate projections Echam A2 and B1 downscaled to meteorological station sites. Top: seasonal precipitation (mm/day) for periods 1981-2010, 2021-2050 and 2071-2100. Middle: multi-year mean daily streamflow ( $\text{m}^3/\text{s}$ ) for periods 1981-2010 and 2021-2050. Bottom: multi-year mean daily streamflow ( $\text{m}^3/\text{s}$ ) for periods 1981-2010 and 2071-2100. The glacier covered areas of the model are treated as constant, or time-variant with initial ice volumes modified by model mass balance results.

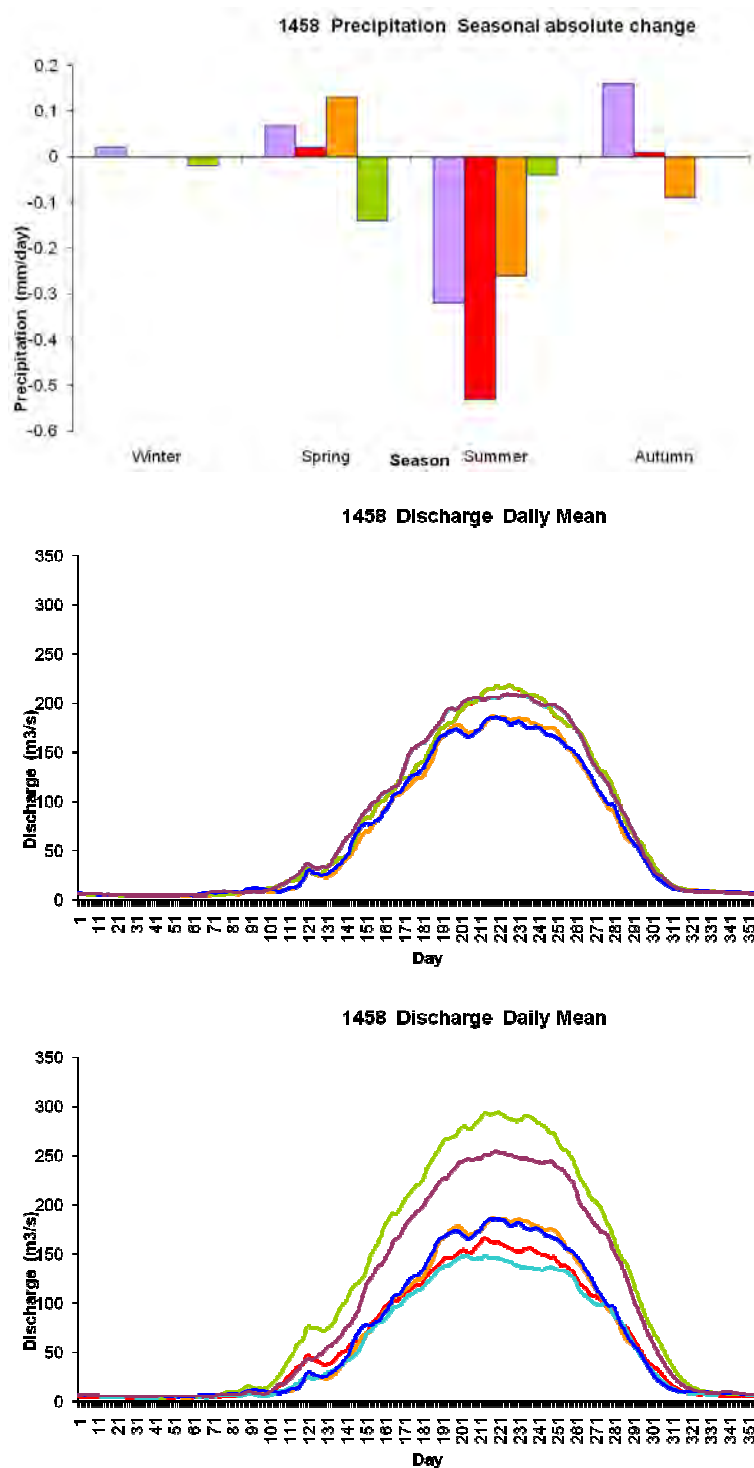


Figure C12. Hydrological model results for catchment 1458 Bjizam with precipitation and temperature input from climate projections Echam A2 and B1 downscaled to meteorological station sites. Top: seasonal precipitation (mm/day) for periods 1981-2010, 2021-2050 and 2071-2100. Middle: multi-year mean daily streamflow ( $\text{m}^3/\text{s}$ ) for periods 1981-2010 and 2021-2050. Bottom: multi-year mean daily streamflow ( $\text{m}^3/\text{s}$ ) for periods 1981-2010 and 2071-2100. The glacier covered areas of the model are treated as constant, or time-variant with initial ice volumes modified by model mass balance results.

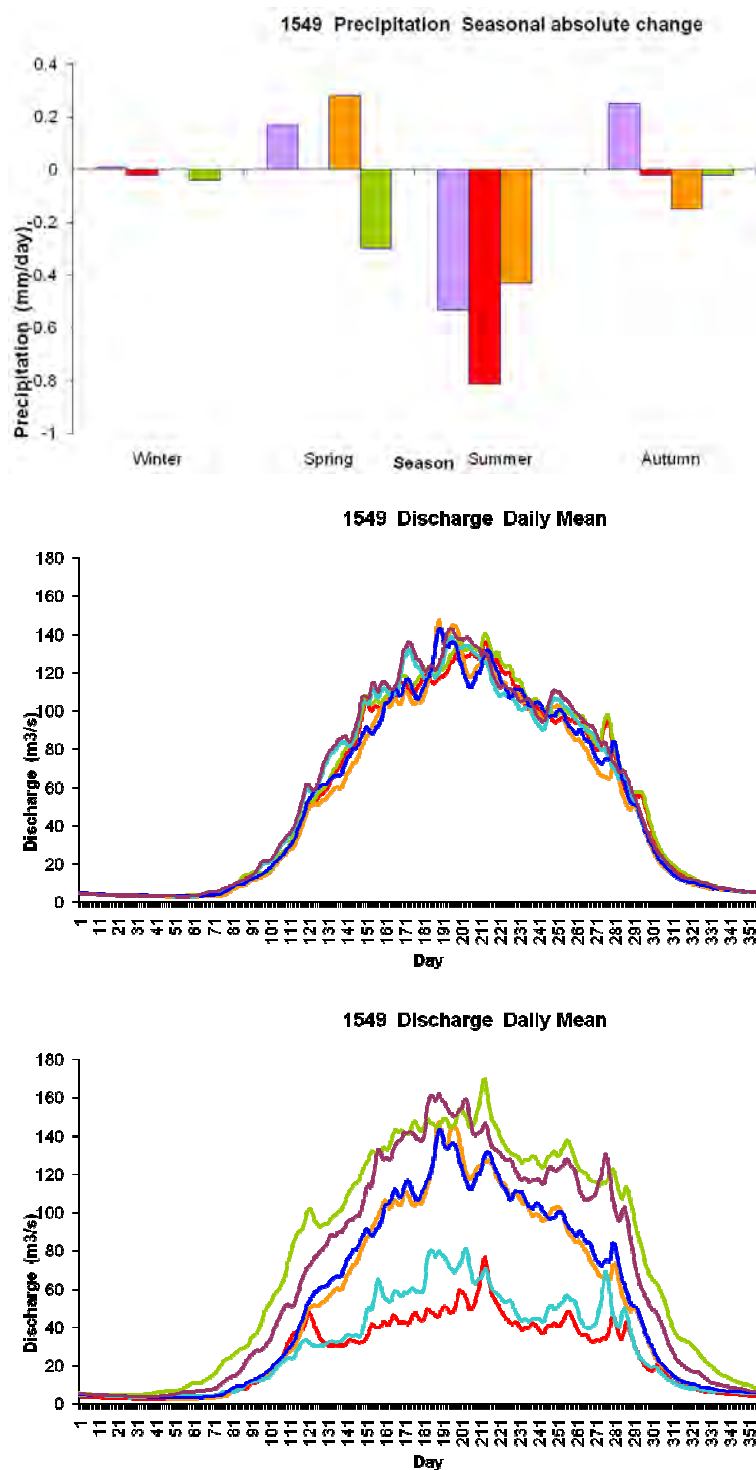


Figure C13. Hydrological model results for catchment 1549 Kurje with precipitation and temperature input from climate projections Echam A2 and B1 downscaled to meteorological station sites. Top: seasonal precipitation (mm/day) for periods 1981-2010, 2021-2050 and 2071-2100. Middle: multi-year mean daily streamflow ( $\text{m}^3/\text{s}$ ) for periods 1981-2010 and 2021-2050. Bottom: multi-year mean daily streamflow ( $\text{m}^3/\text{s}$ ) for periods 1981-2010 and 2071-2100. The glacier covered areas of the model are treated as constant, or time-variant with initial ice volumes modified by model mass balance results.

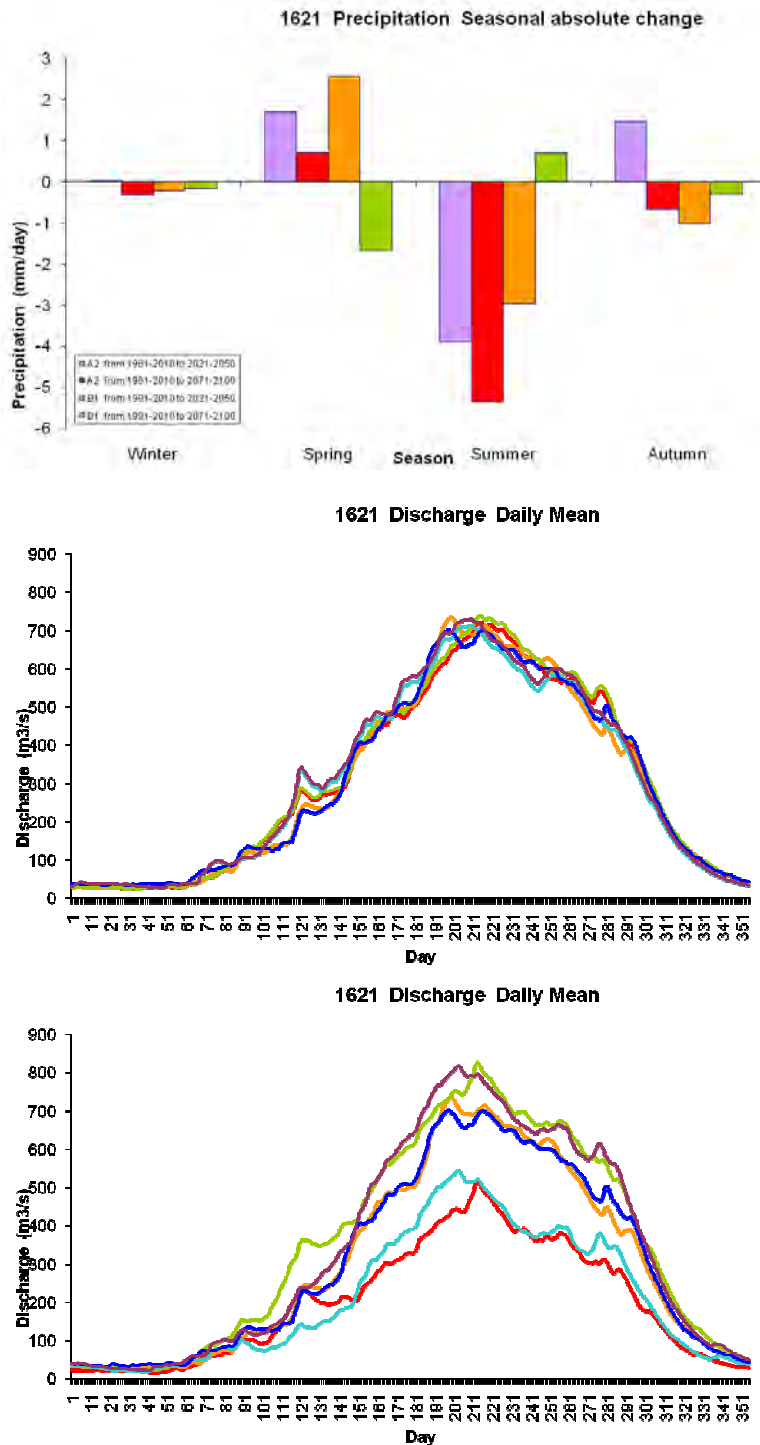


Figure C14. Hydrological model results for catchment 1621 Kurizampa with precipitation and temperature input from climate projections Echem A2 and B1 downscaled to meteorological station sites. Top: seasonal precipitation (mm/day) for periods 1981-2010, 2021-2050 and 2071-2100. Middle: multi-year mean daily streamflow ( $\text{m}^3/\text{s}$ ) for periods 1981-2010 and 2021-2050. Bottom: multi-year mean daily streamflow ( $\text{m}^3/\text{s}$ ) for periods 1981-2010 and 2071-2100. The glacier covered areas of the model are treated as constant, or time-variant with initial ice volumes modified by model mass balance results.

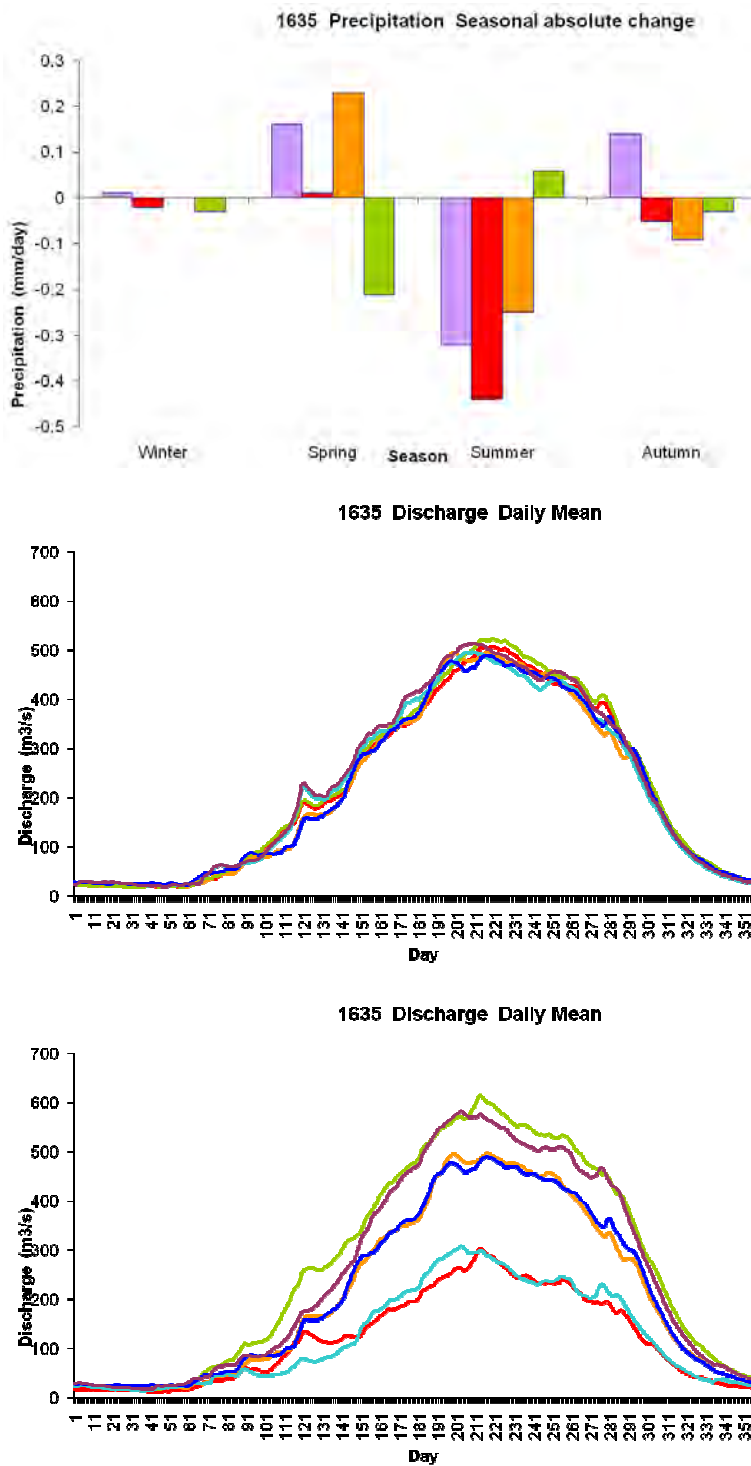


Figure C15. Hydrological model results for catchment 1635 Autsho with precipitation and temperature input from climate projections Echam A2 and B1 downscaled to meteorological station sites. Top: seasonal precipitation (mm/day) for periods 1981-2010, 2021-2050 and 2071-2100. Middle: multi-year mean daily streamflow ( $\text{m}^3/\text{s}$ ) for periods 1981-2010 and 2021-2050. Bottom: multi-year mean daily streamflow ( $\text{m}^3/\text{s}$ ) for periods 1981-2010 and 2071-2100. The glacier covered areas of the model are treated as constant, or time-variant with initial ice volumes modified by model mass balance results.



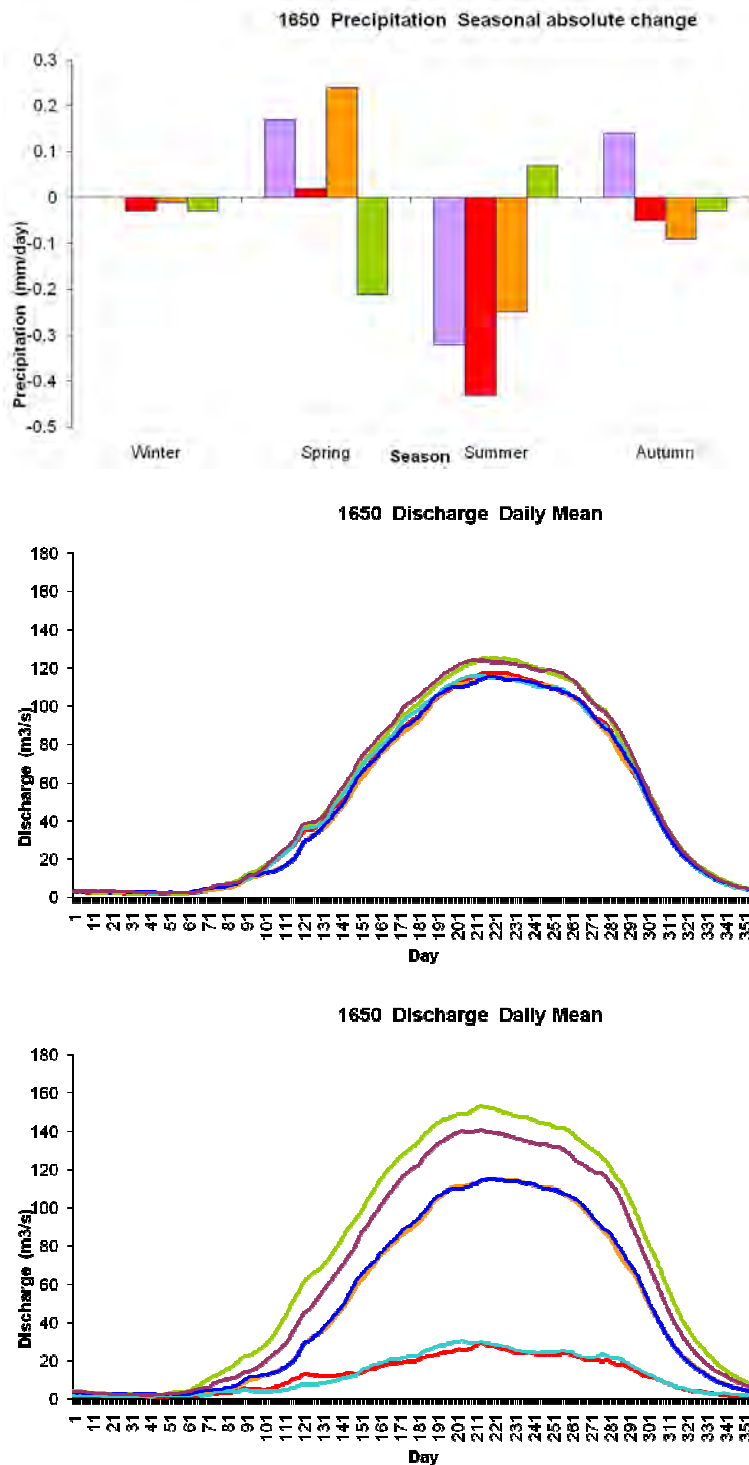


Figure C16. Hydrological model results for catchment 1650 Sumpa with precipitation and temperature input from climate projections Echam A2 and B1 downscaled to meteorological station sites. Top: seasonal precipitation (mm/day) for periods 1981-2010, 2021-2050 and 2071-2100. Middle: multi-year mean daily streamflow ( $\text{m}^3/\text{s}$ ) for periods 1981-2010 and 2021-2050. Bottom: multi-year mean daily streamflow ( $\text{m}^3/\text{s}$ ) for periods 1981-2010 and 2071-2100. The glacier covered areas of the model are treated as constant, or time-variant with initial ice volumes modified by model mass balance results.

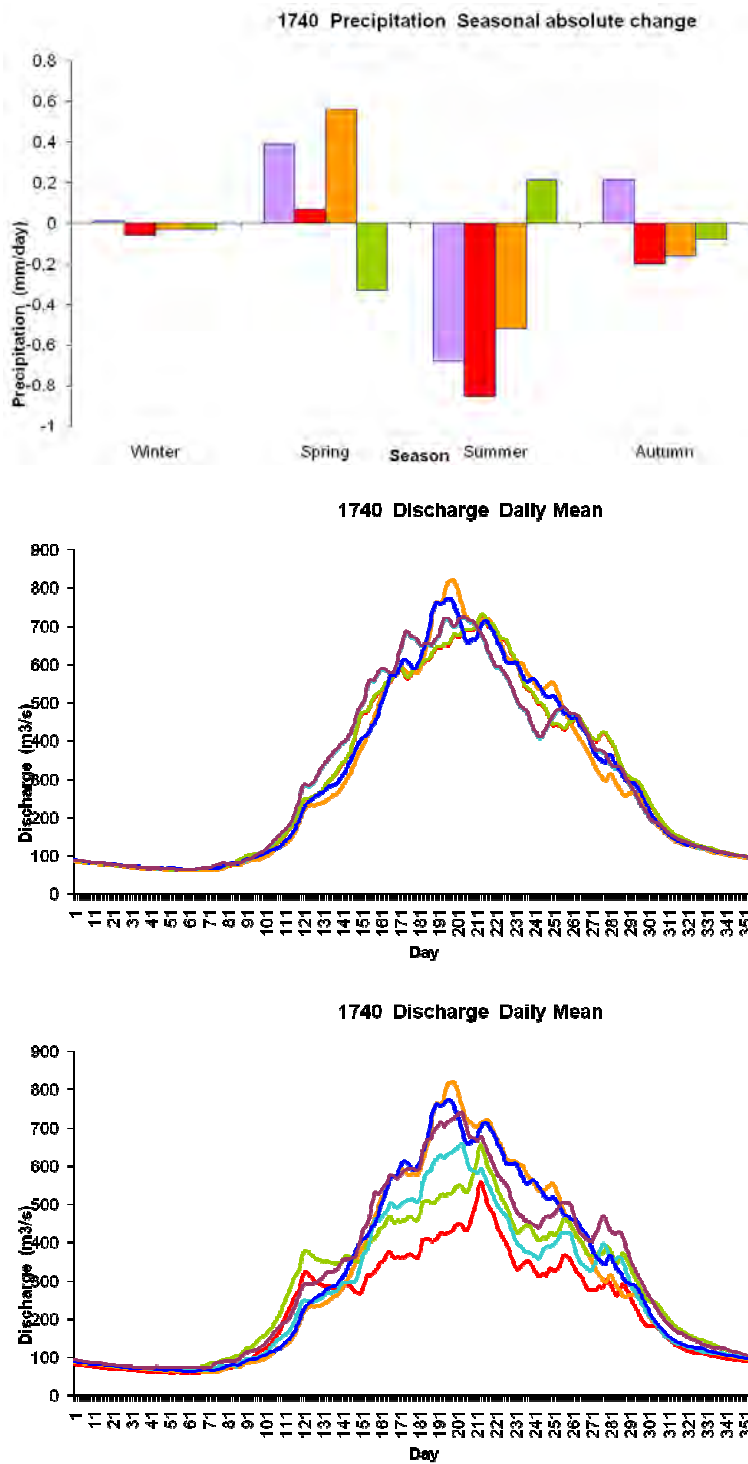


Figure C17. Hydrological model results for catchment 1740 Uzorong with precipitation and temperature input from climate projections Echam A2 and B1 downscaled to meteorological station sites. Top: seasonal precipitation (mm/day) for periods 1981-2010, 2021-2050 and 2071-2100. Middle: multi-year mean daily streamflow ( $\text{m}^3/\text{s}$ ) for periods 1981-2010 and 2021-2050. Bottom: multi-year mean daily streamflow ( $\text{m}^3/\text{s}$ ) for periods 1981-2010 and 2071-2100. The glacier covered areas of the model are treated as constant, or time-variant with initial ice volumes modified by model mass balance results.

# **Appendix D Hydrological model results for period 1981-2100 based on climate projection Echem A2**

HBV hydrological model results based on downscaled climate model data from projection Echem A2 for the period 1981-2100 as input. Temperature and precipitation input data have been modified by the hydrological model according to temperature lapse rates and precipitation elevation gradients for each sub-catchment determined during model calibration.

Figures D1-D8: Catchments 1330 Dobani and 1370 Yebesa. Annual mean temperature, annual precipitation sum, annual evaporation sum, annual sum of snow water equivalent, annual sum of soil moisture deficit and annual sum of groundwater storage based on daily model results averaged over all model grid cells within each sub-catchment. Hydrological model results for streamflow at the outlet of each catchment have been aggregated to mean annual values, i.e. the average of each day of the year for every year. The glacier covered areas of the model are treated as constant, or time-variant with initial ice volumes modified by model mass balance results for glacier covered grid cells. The trend line is plotted if there is a significant trend at the 5 % level based on Student's t-test.

Figures D9-D23: Catchments 1121 Doyagang, 1235 Chimakoti, 1246 Haa, 1249 Damchhu, 1253 Paro, 1280 Lungtenphug, 1314 Kerabari, 1349 Wangdirapids, 1418 Tingtibi, 1458 Bjizam, 1549 Kurjey, 1621 Kurizampa, 1635 Autsho, 1650 Sumpa and 1740 Uzorong. Hydrological model results for streamflow at the outlet of each catchment have been aggregated to mean annual values, i.e. the average of each day of the year for every year. The glacier covered areas of the model are treated as constant, or time-variant with initial ice volumes modified by model mass balance results for glacier covered grid cells. The trend line is plotted if there is a significant trend at the 5 % level.

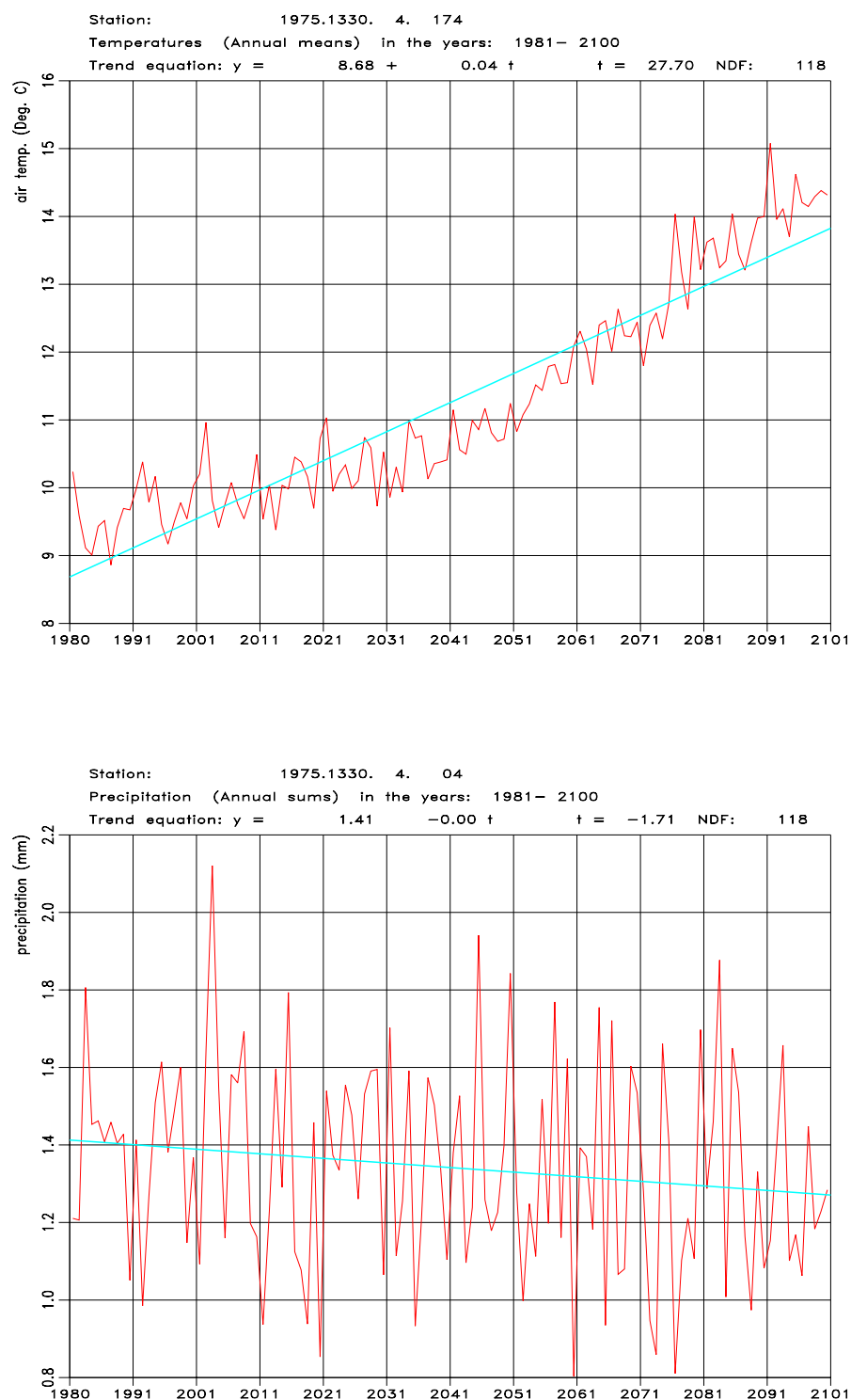


Figure D1. Hydrological model results for period 1981-2100 for catchment 1330 Dobani with precipitation and temperature input from climate projection Echam A2 downscaled to meteorological station sites. Top: annual mean temperature (°C). Bottom: annual precipitation sum (metres).

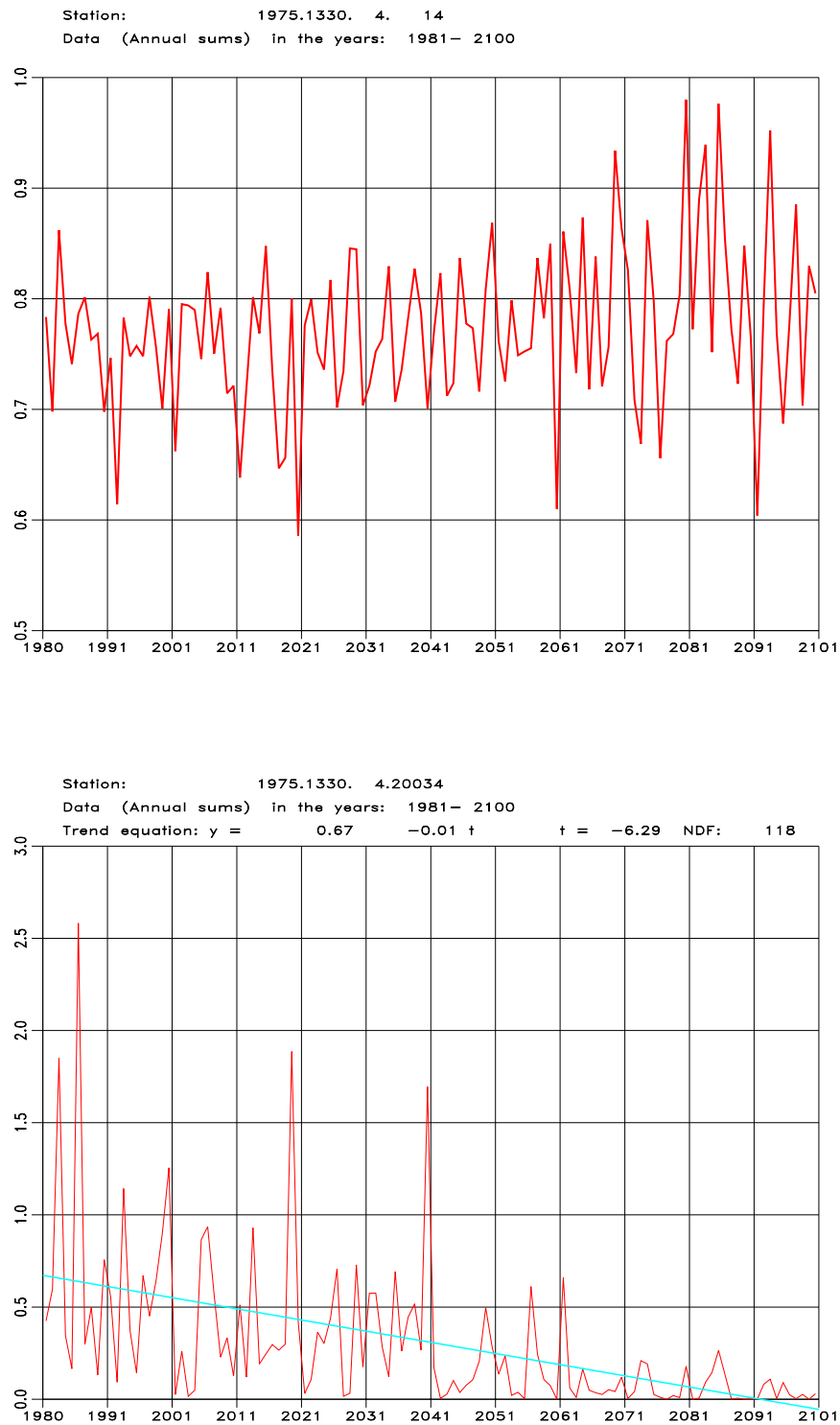


Figure D2. Hydrological model results for period 1981-2100 for catchment 1330 Dobani with precipitation and temperature input from climate projection Echam A2 downscaled to meteorological station sites. Top: annual evaporation sum (metres). Bottom: annual sum of snow water equivalent (metres).

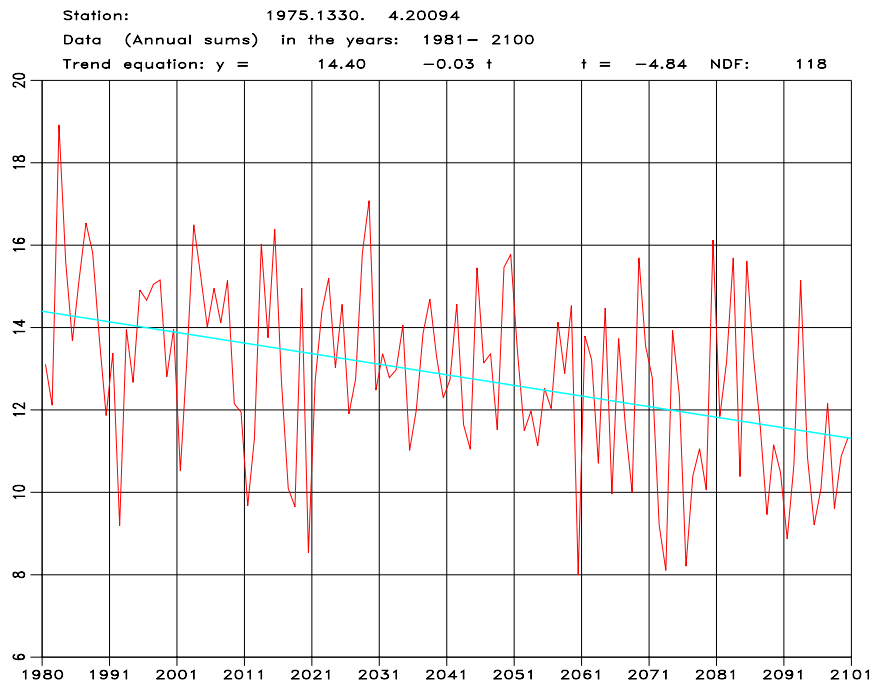
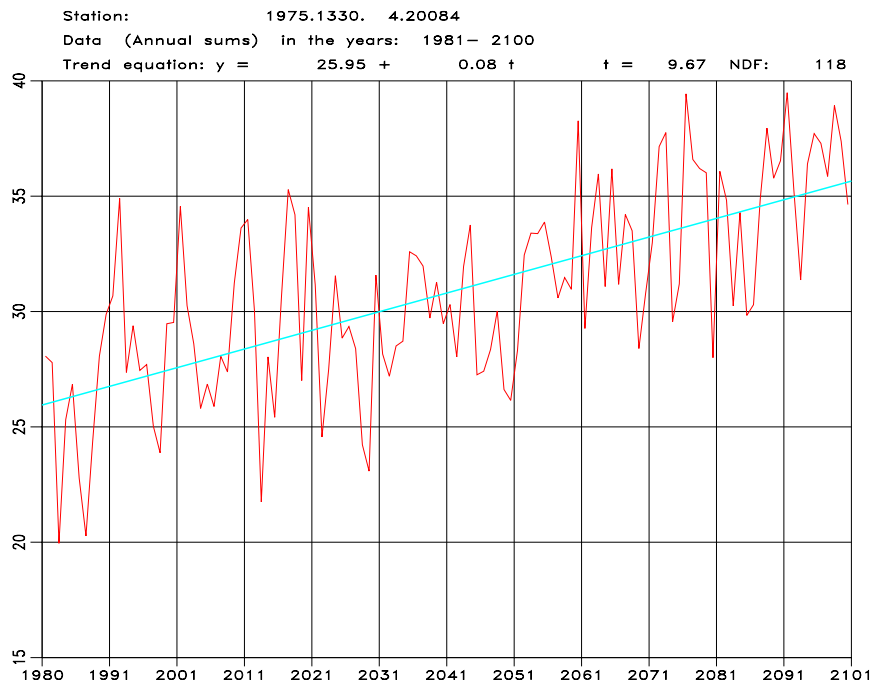


Figure D3. Hydrological model results for period 1981-2100 for catchment 1330 Dobani with precipitation and temperature input from climate projection Echam A2 downscaled to meteorological station sites. Top: annual sum of soil moisture deficit (metres). Bottom: annual sum of groundwater storage (metres).

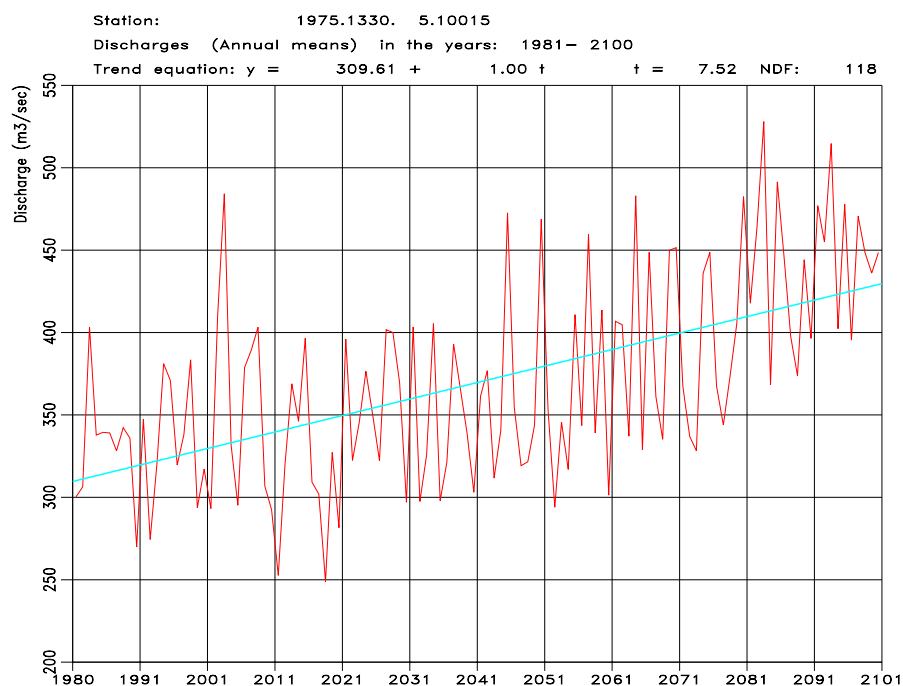
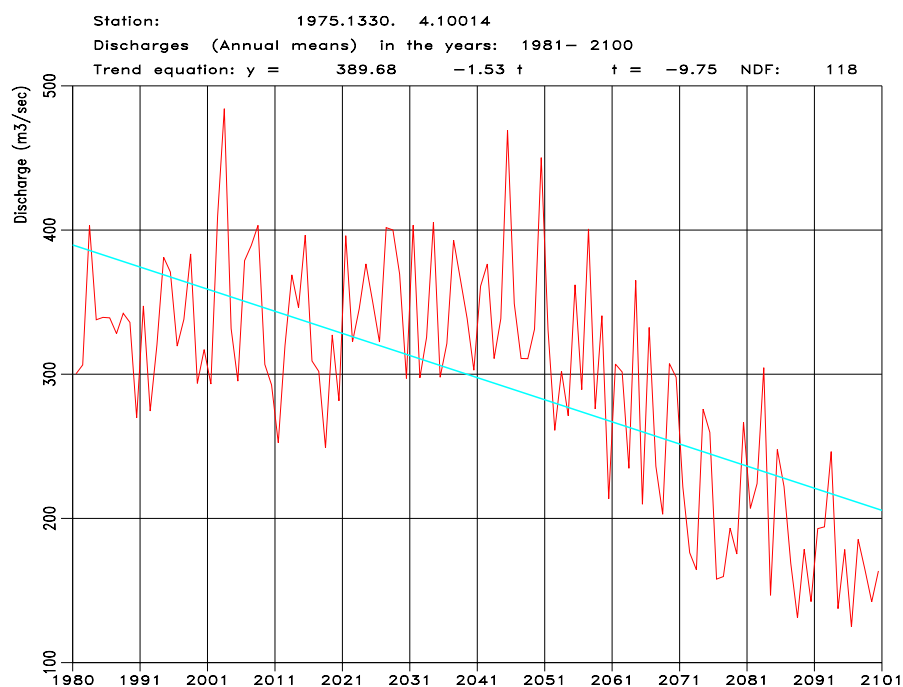


Figure D4. Hydrological model results for annual mean streamflow ( $\text{m}^3/\text{s}$ ) for period 1981-2100 for catchment 1330 Dobani with precipitation and temperature input from climate projection Echam A2 downscaled to meteorological station sites. Glacier covered areas are treated as time-variant (top) and as constant (bottom).

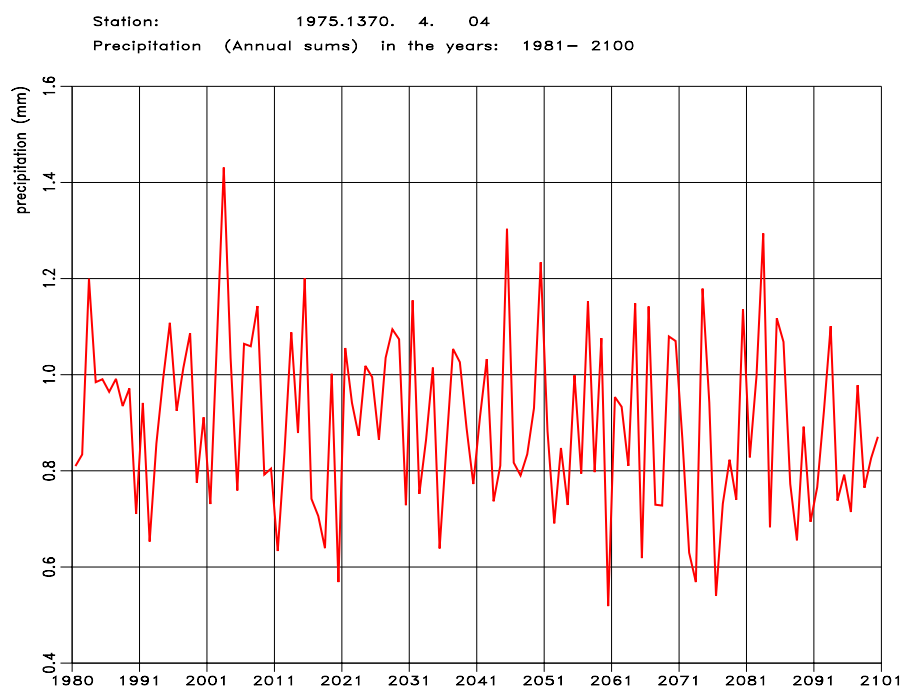
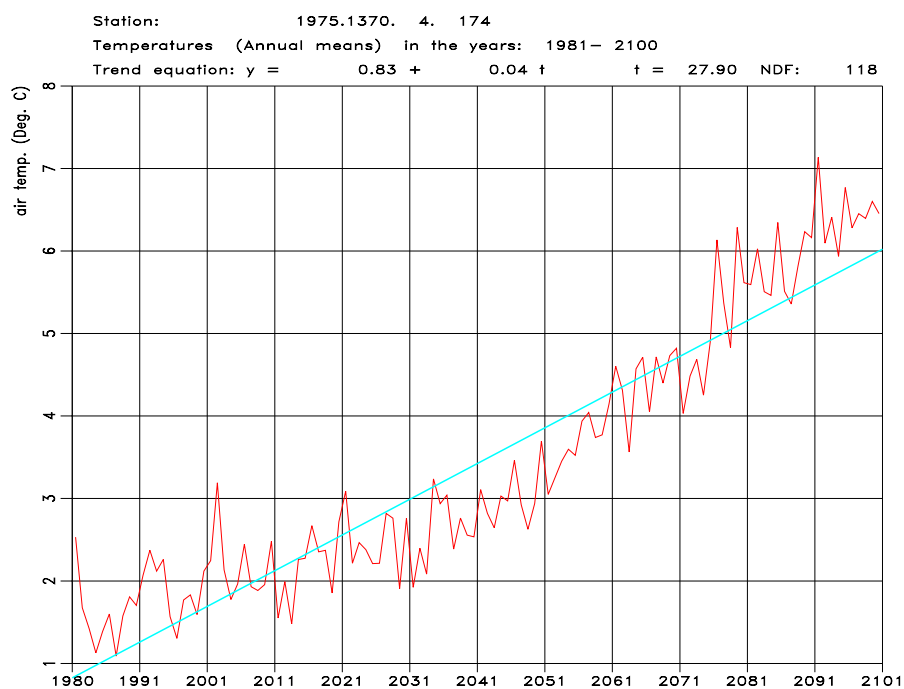


Figure D5. Hydrological model results for period 1981-2100 for catchment 1370 Yebesa with precipitation and temperature input from climate projection Echam A2 downscaled to meteorological station sites. Top: annual mean temperature (°C). Bottom: annual precipitation sum (metres).



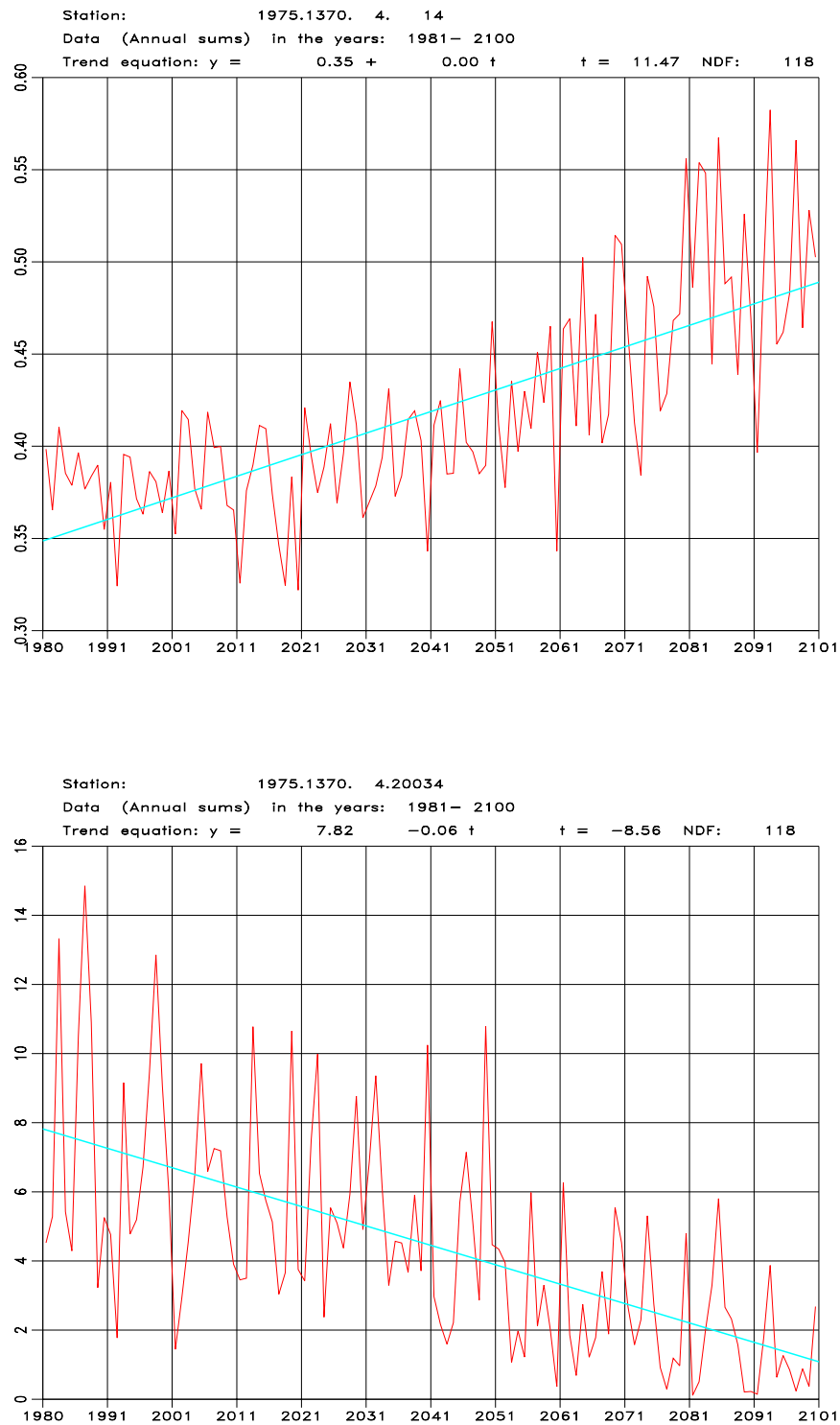


Figure D6. Hydrological model results for period 1981-2100 for catchment 1370 Yebesa with precipitation and temperature input from climate projection Echam A2 downscaled to meteorological station sites. Top: annual evaporation sum (metres). Bottom: annual sum of snow water equivalent (metres).

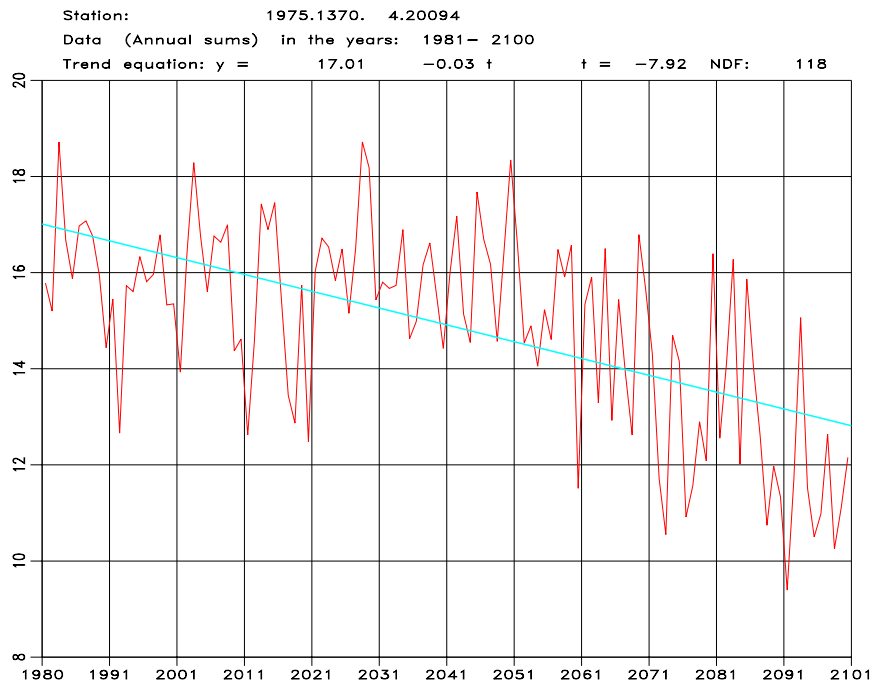
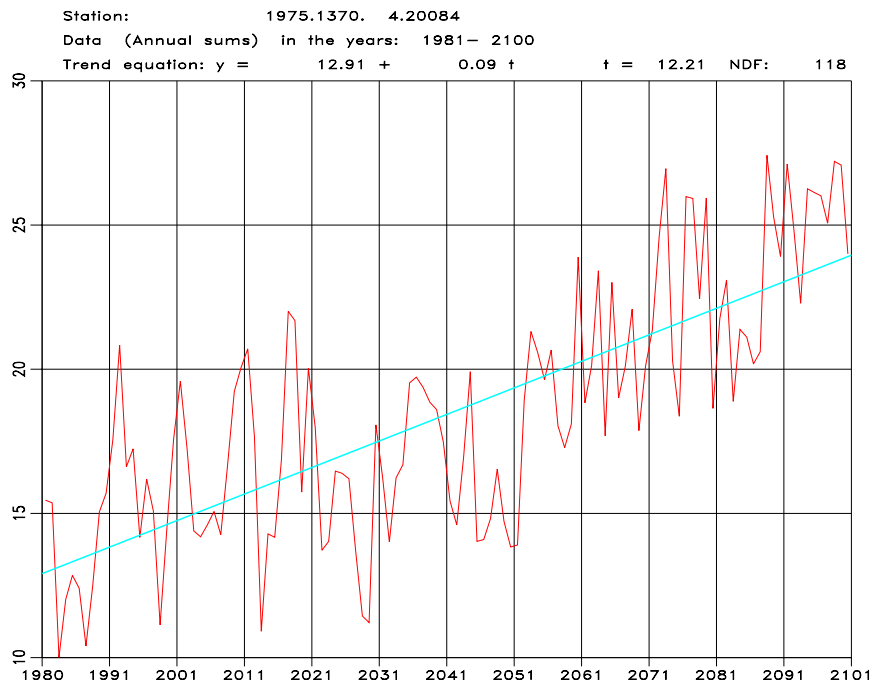


Figure D7. Hydrological model results for period 1981-2100 for catchment 1370 Yebesa with precipitation and temperature input from climate projection Echam A2 downscaled to meteorological station sites. Top: annual sum of soil moisture deficit (metres). Bottom: annual sum of groundwater storage (metres).

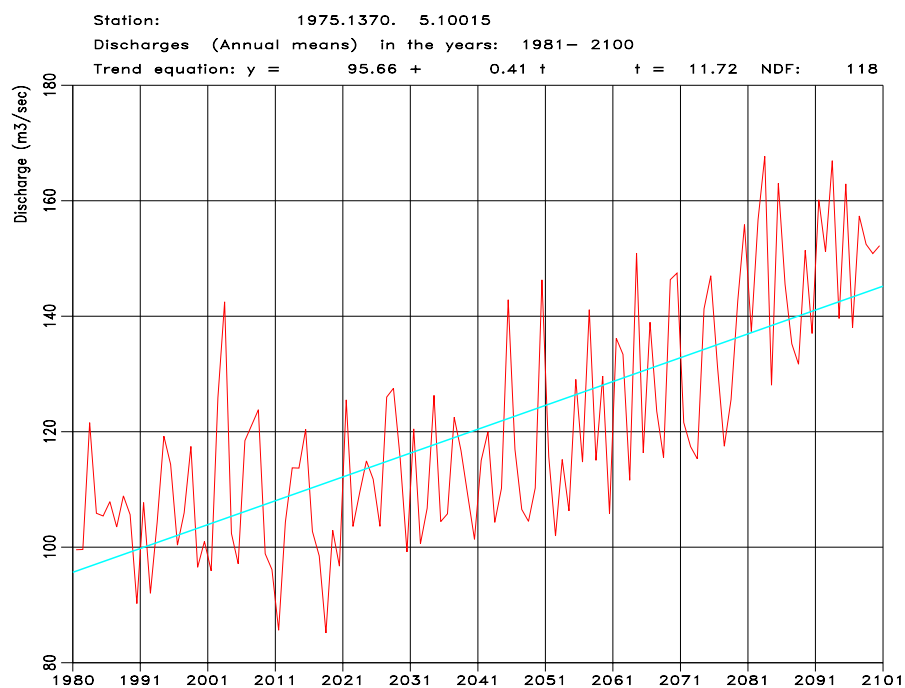
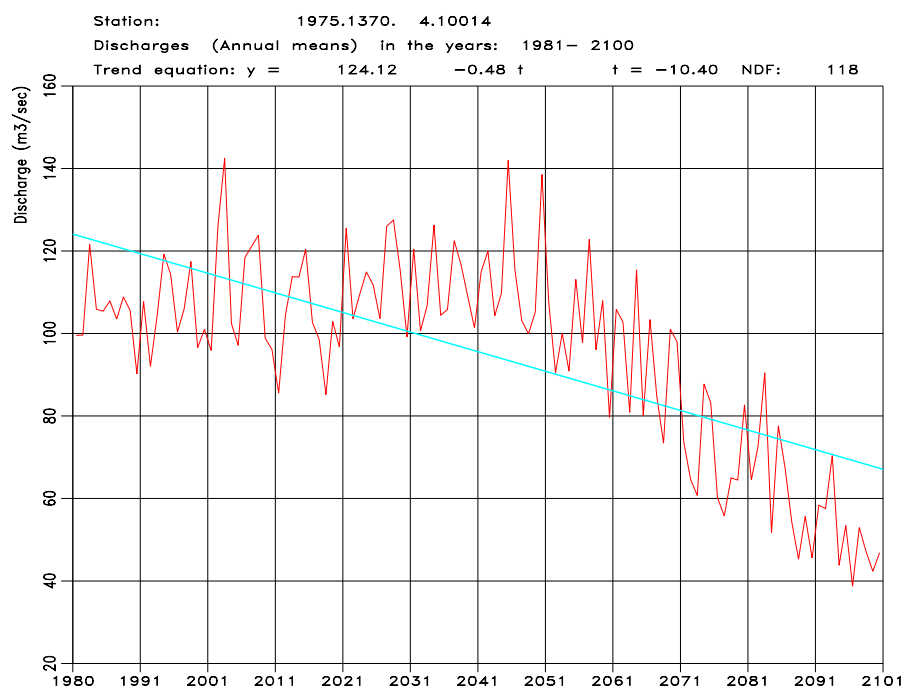


Figure D8. Hydrological model results for annual mean streamflow ( $\text{m}^3/\text{s}$ ) for period 1981-2100 for catchment 1370 Yebesa with precipitation and temperature input from climate projection Echam A2 downscaled to meteorological station sites. Glacier covered areas are treated as time-variant (top) and as constant (bottom).

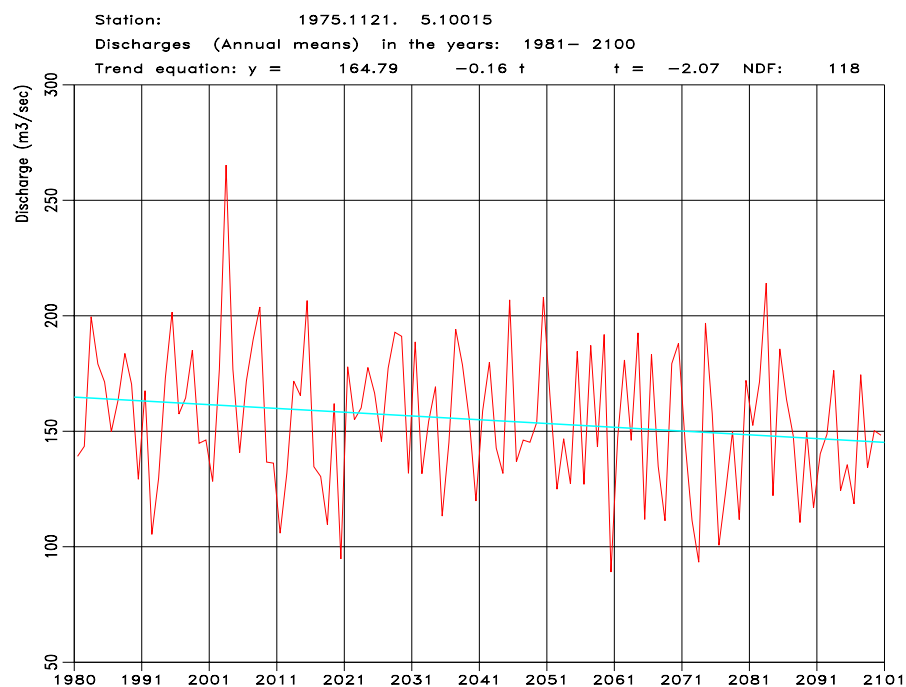
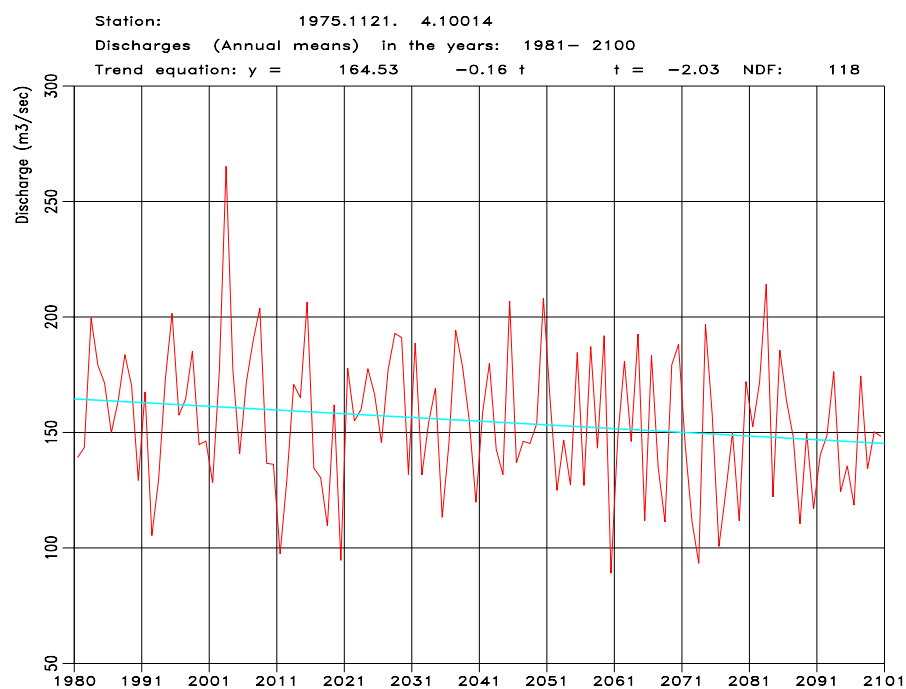


Figure D9. Hydrological model results for annual mean streamflow ( $\text{m}^3/\text{s}$ ) for period 1981-2100 for catchment 1121 Doyagang with precipitation and temperature input from climate projection Echem A2 downscaled to meteorological station sites. Glacier covered areas are treated as time-variant (top) and as constant (bottom).

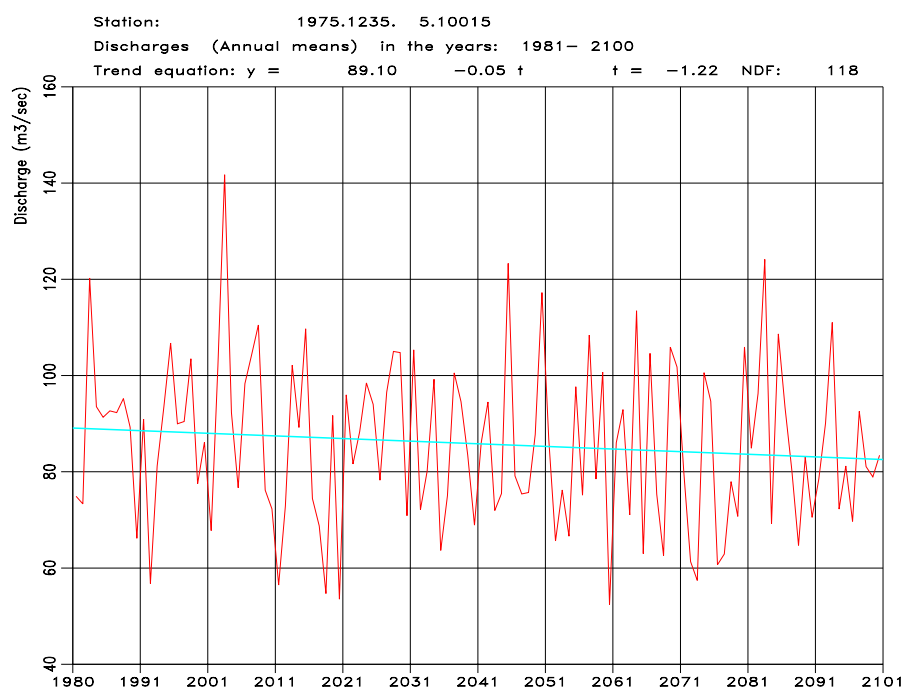
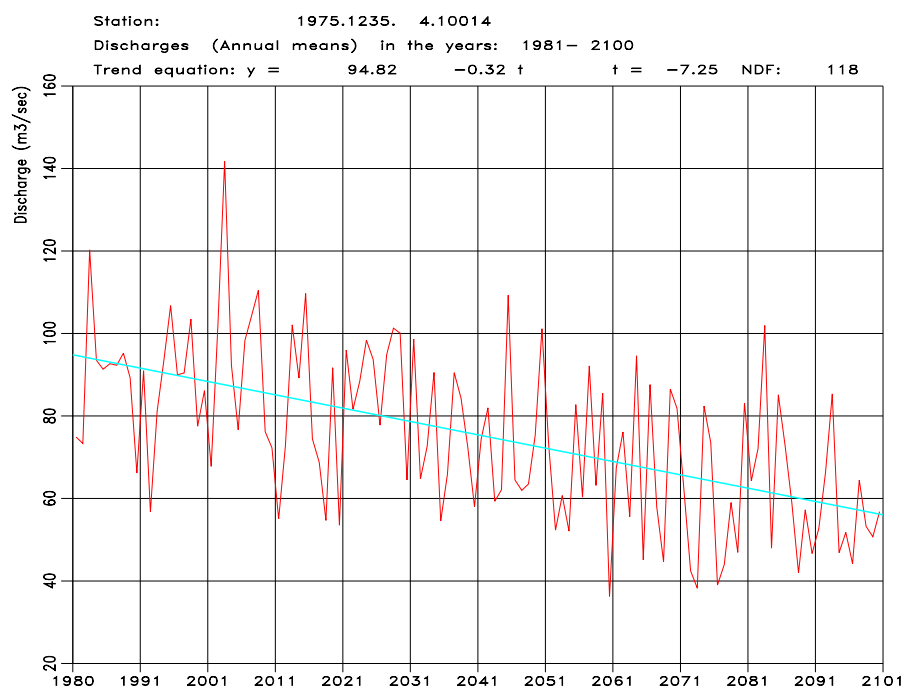


Figure D10. Hydrological model results for annual mean streamflow ( $\text{m}^3/\text{s}$ ) for period 1981–2100 for catchment 1235 Chimakoti with precipitation and temperature input from climate projection Echem A2 downscaled to meteorological station sites. Glacier covered areas are treated as time-variant (top) and as constant (bottom).

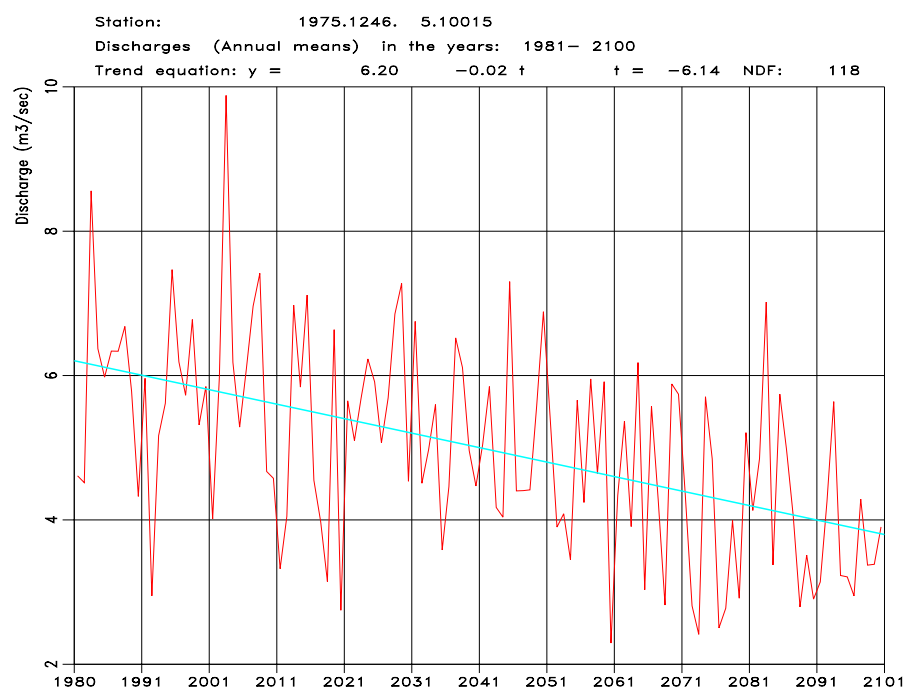
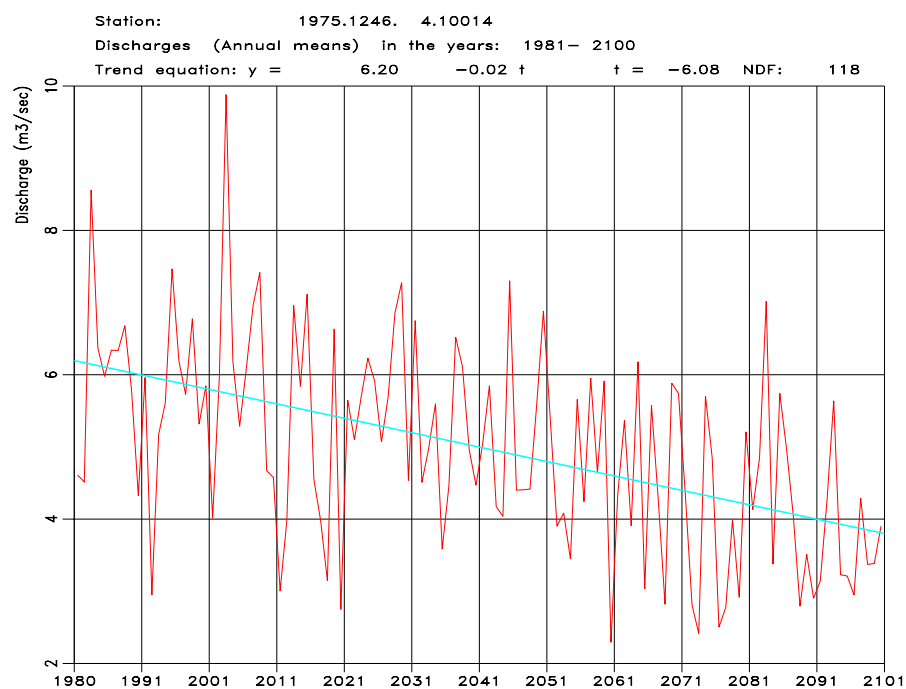


Figure D11. Hydrological model results for annual mean streamflow ( $\text{m}^3/\text{s}$ ) for period 1981-2100 for catchment 1246 Haa with precipitation and temperature input from climate projection Echem A2 downscaled to meteorological station sites. Glacier covered areas are treated as time-variant (top) and as constant (bottom).

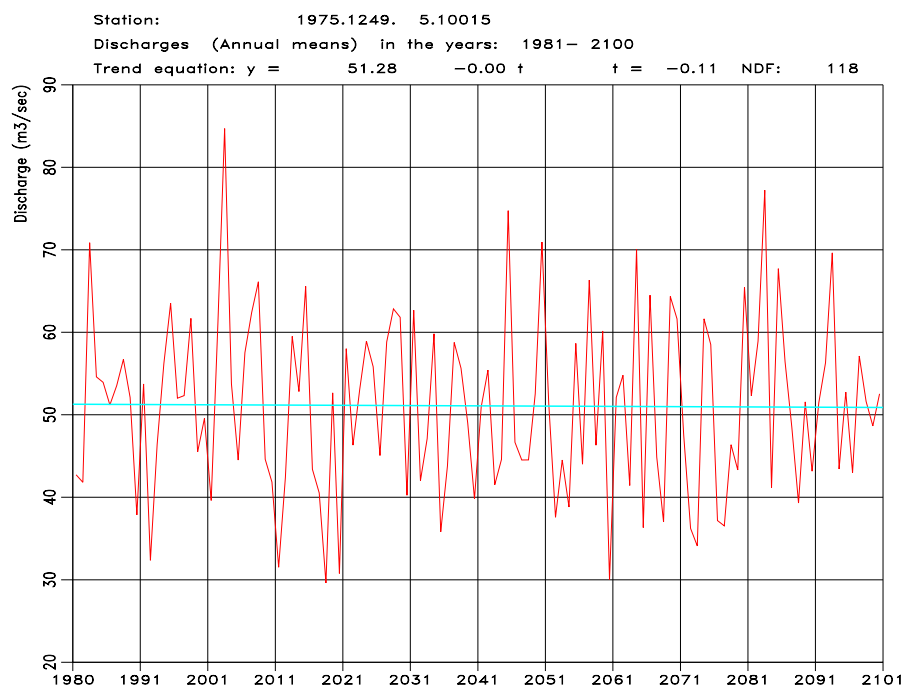
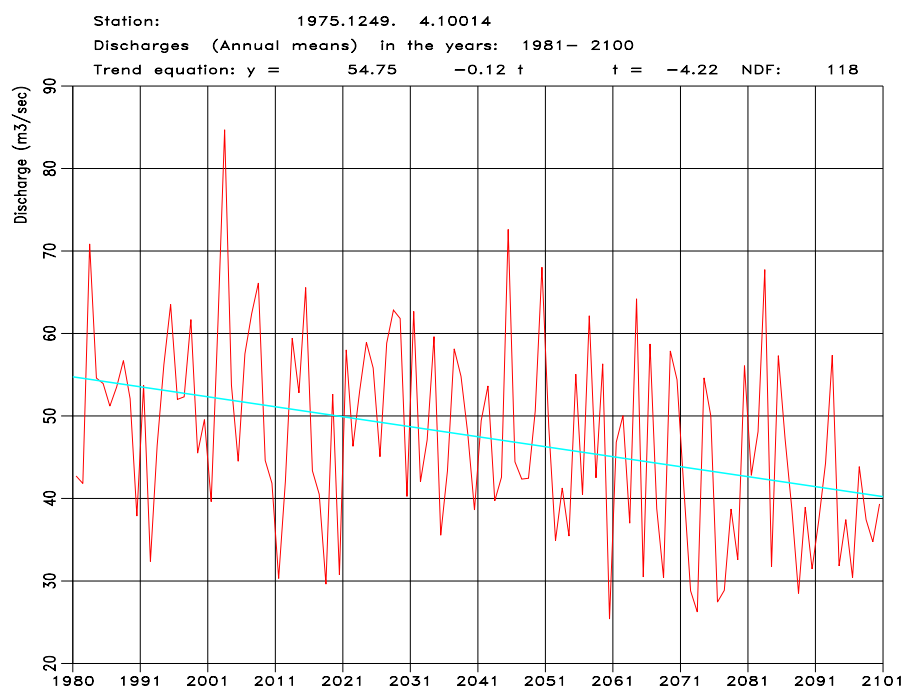


Figure D12. Hydrological model results for annual mean streamflow ( $\text{m}^3/\text{s}$ ) for period 1981–2100 for catchment 1249 Damchhu with precipitation and temperature input from climate projection Echem A2 downscaled to meteorological station sites. Glacier covered areas are treated as time-variant (top) and as constant (bottom).

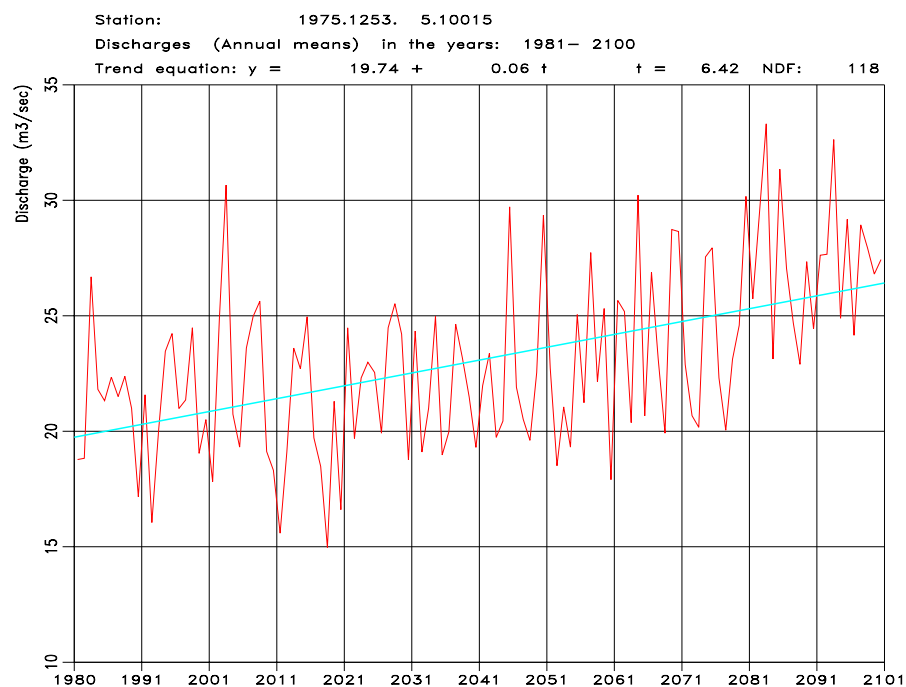
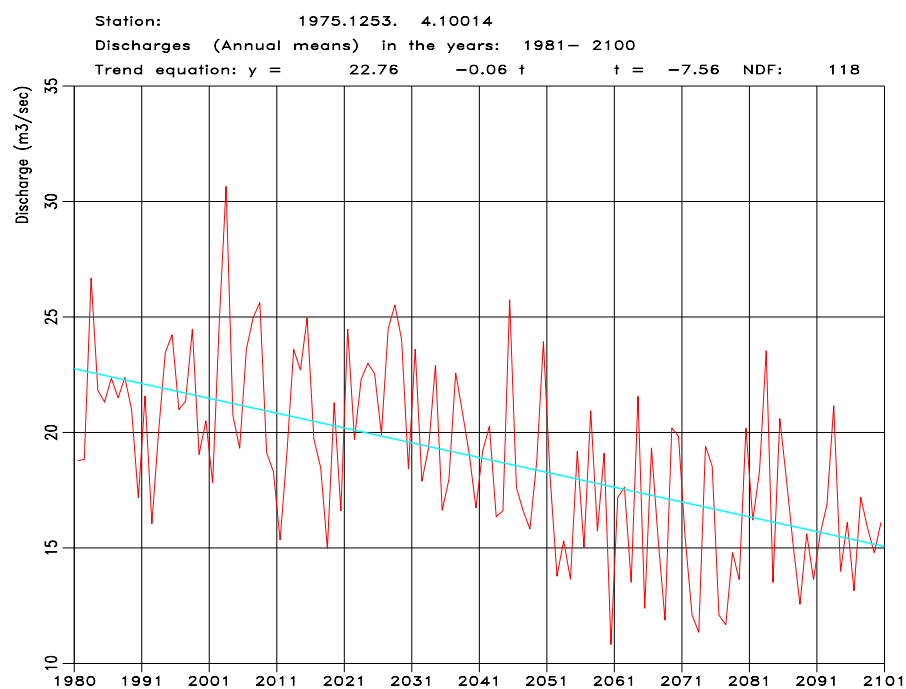


Figure D13. Hydrological model results for annual mean streamflow ( $\text{m}^3/\text{s}$ ) for period 1981-2100 for catchment 1253 Paro with precipitation and temperature input from climate projection Echem A2 downscaled to meteorological station sites. Glacier covered areas are treated as time-variant (top) and as constant (bottom).



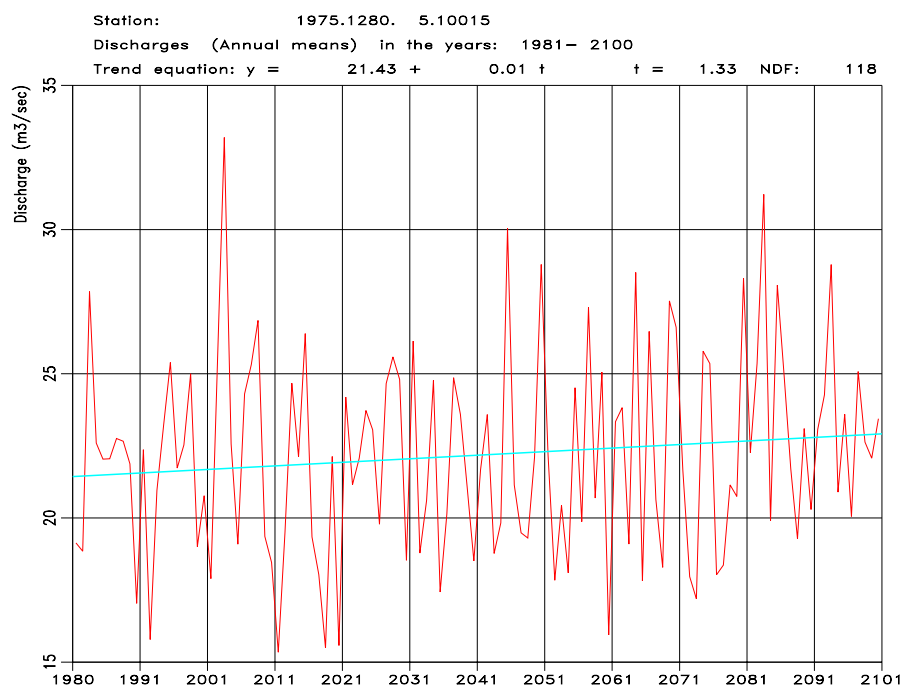
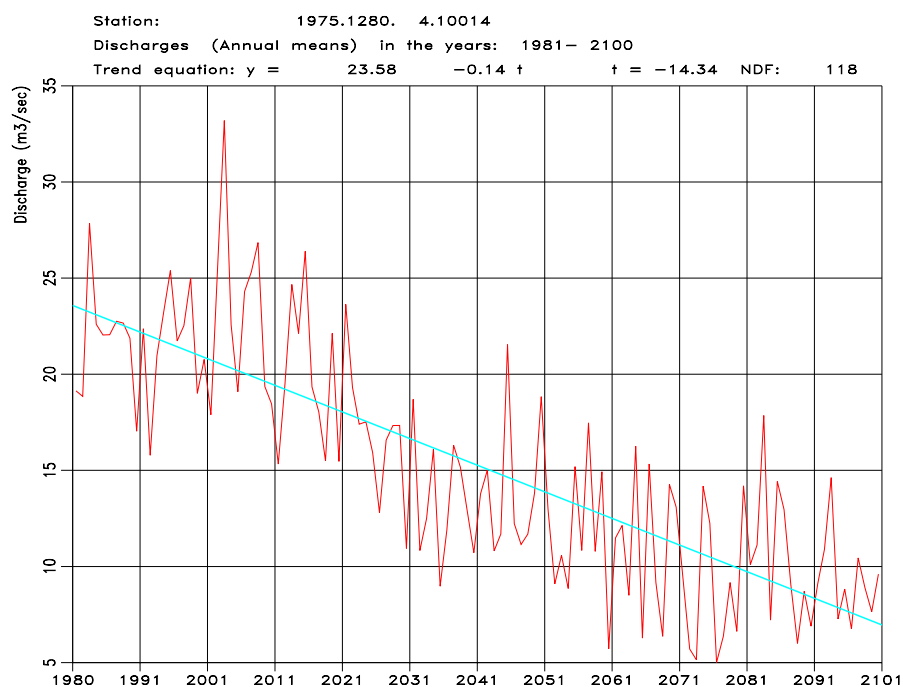


Figure D14. Hydrological model results for annual mean streamflow ( $\text{m}^3/\text{s}$ ) for period 1981-2100 for catchment 1280 Lungtenphug with precipitation and temperature input from climate projection Ecam A2 downscaled to meteorological station sites. Glacier covered areas are treated as time-variant (top) and as constant (bottom).

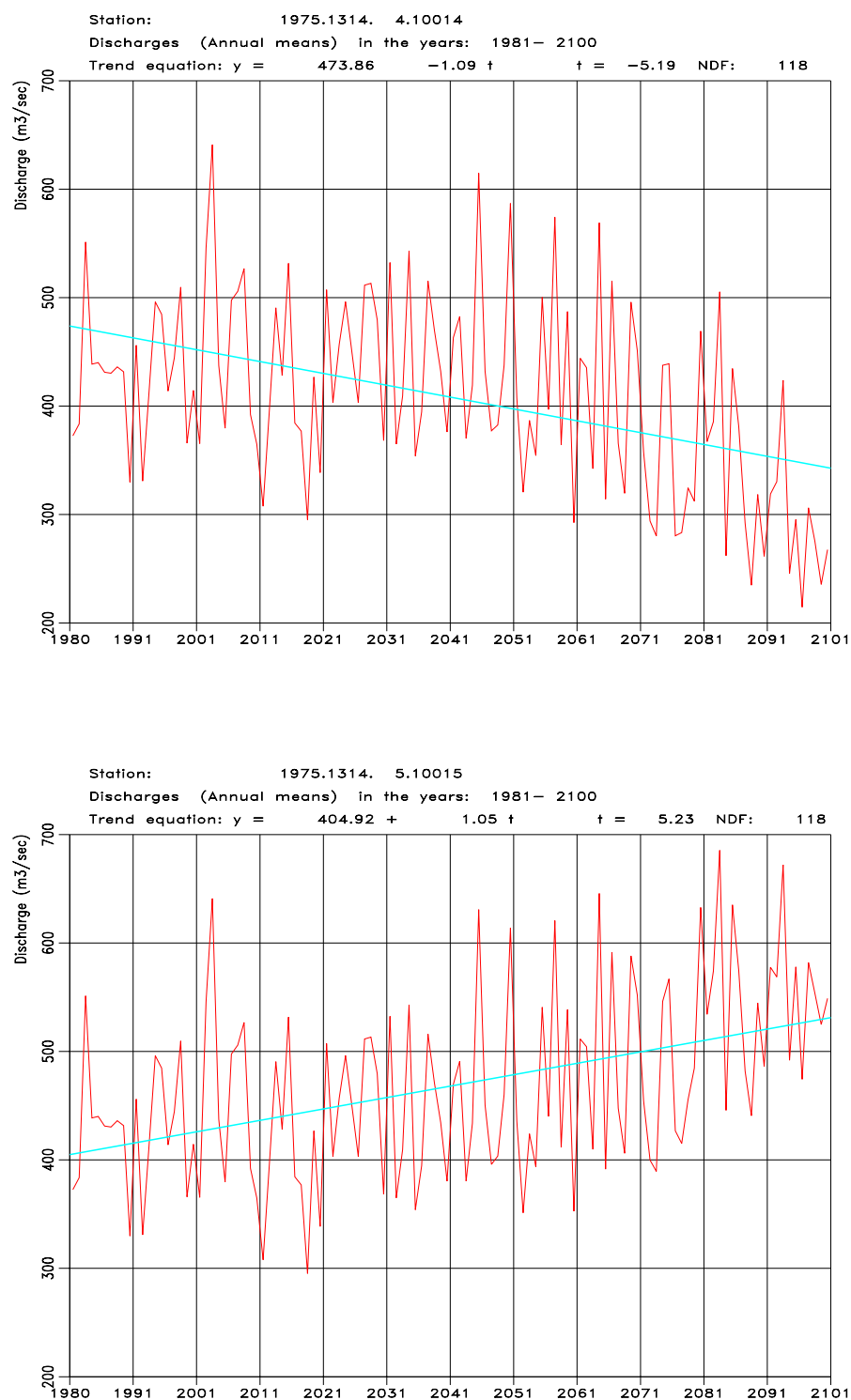


Figure D15. Hydrological model results for annual mean streamflow ( $\text{m}^3/\text{s}$ ) for period 1981-2100 for catchment 1314 Kerabari with precipitation and temperature input from climate projection Echem A2 downscaled to meteorological station sites. Glacier covered areas are treated as time-variant (top) and as constant (bottom).

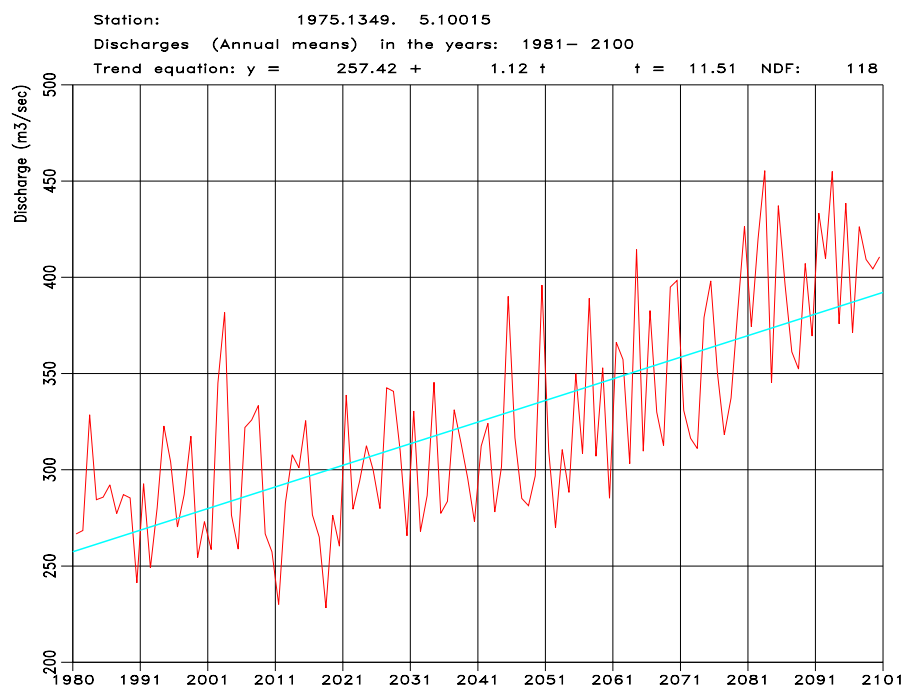
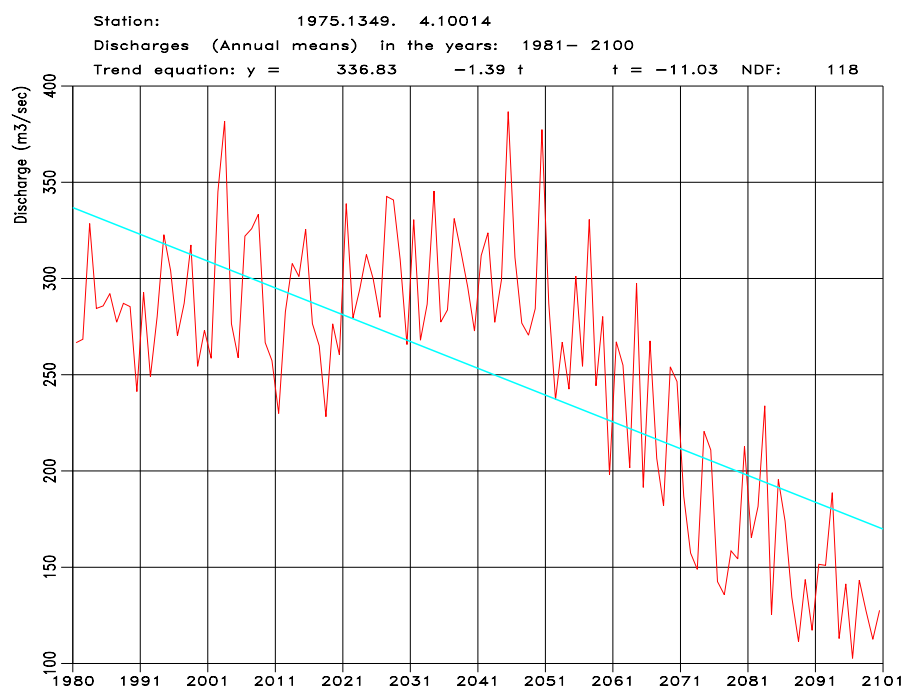


Figure D16. Hydrological model results for annual mean streamflow ( $\text{m}^3/\text{s}$ ) for period 1981–2100 for catchment 1349 Wangdirapids with precipitation and temperature input from climate projection Echam A2 downscaled to meteorological station sites. Glacier covered areas are treated as time-variant (top) and as constant (bottom).

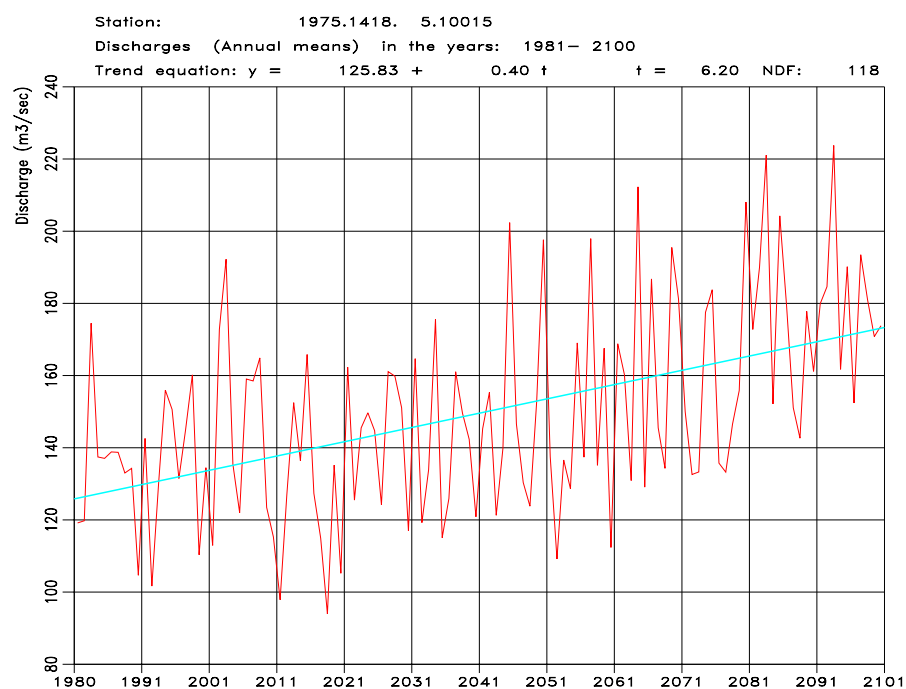
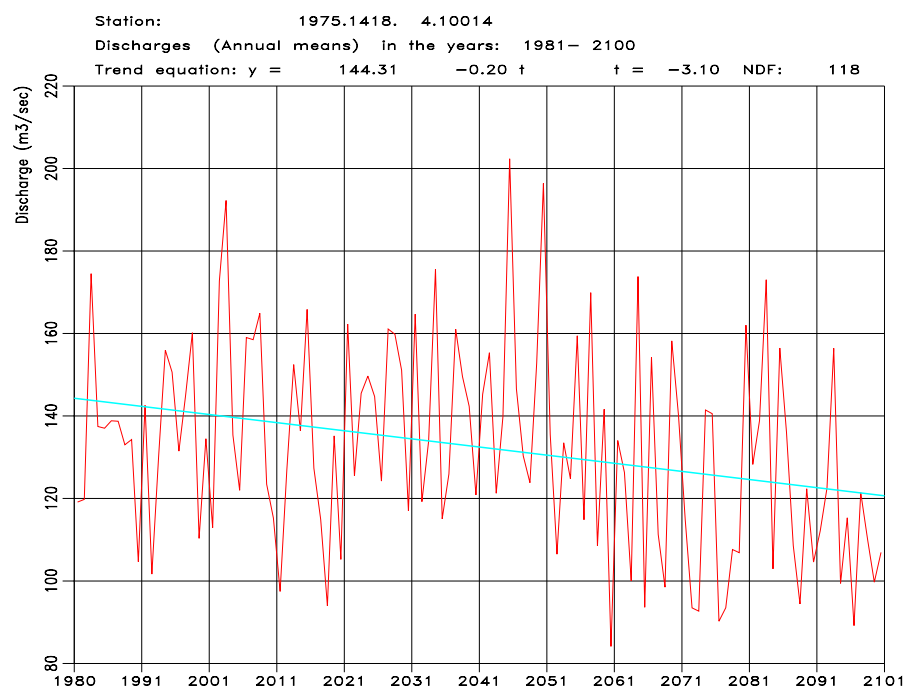


Figure D17. Hydrological model results for annual mean streamflow ( $\text{m}^3/\text{s}$ ) for period 1981-2100 for catchment 1418 Tingtibi with precipitation and temperature input from climate projection Echem A2 downscaled to meteorological station sites. Glacier covered areas are treated as time-variant (top) and as constant (bottom).

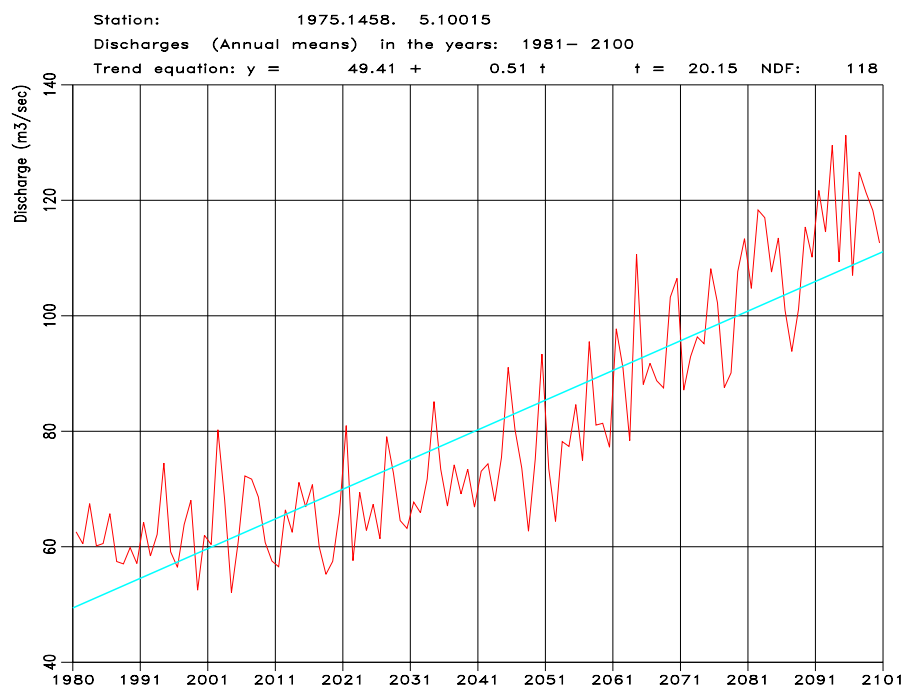
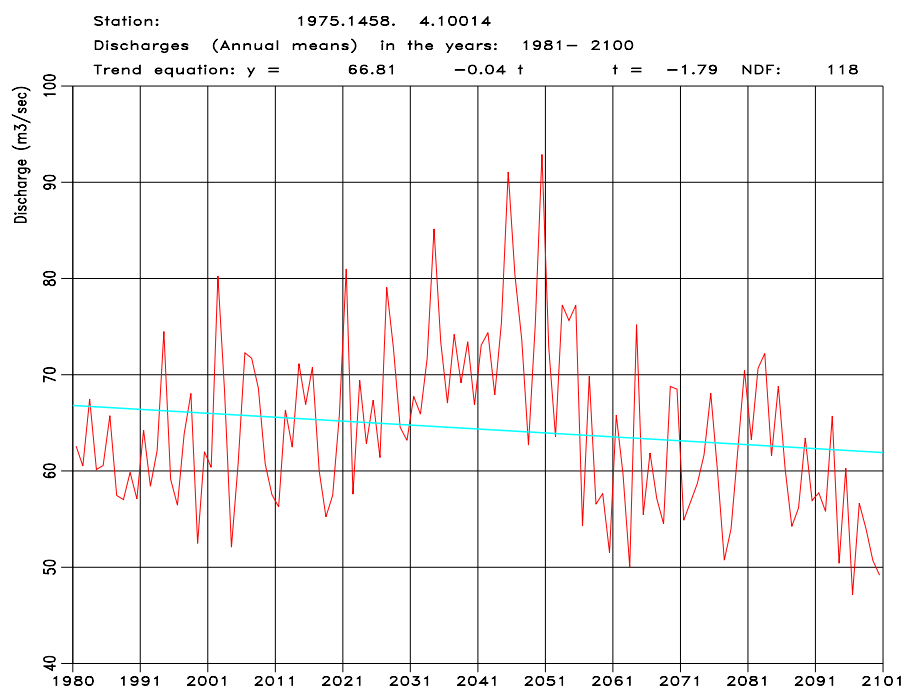


Figure D18. Hydrological model results for annual mean streamflow ( $\text{m}^3/\text{s}$ ) for period 1981–2100 for catchment 1458 Bjizam with precipitation and temperature input from climate projection Echem A2 downscaled to meteorological station sites. Glacier covered areas are treated as time-variant (top) and as constant (bottom).

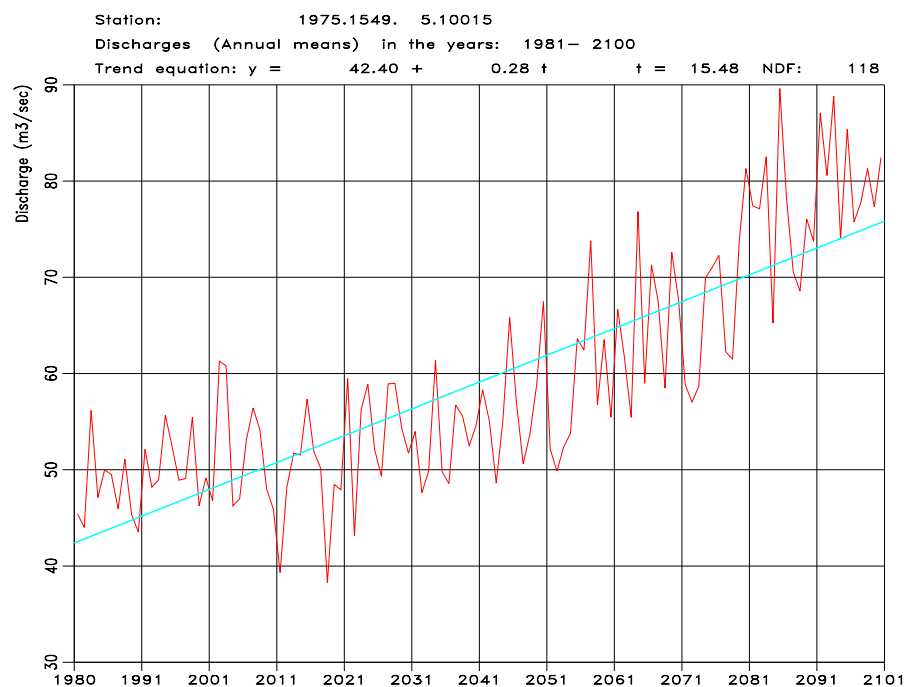
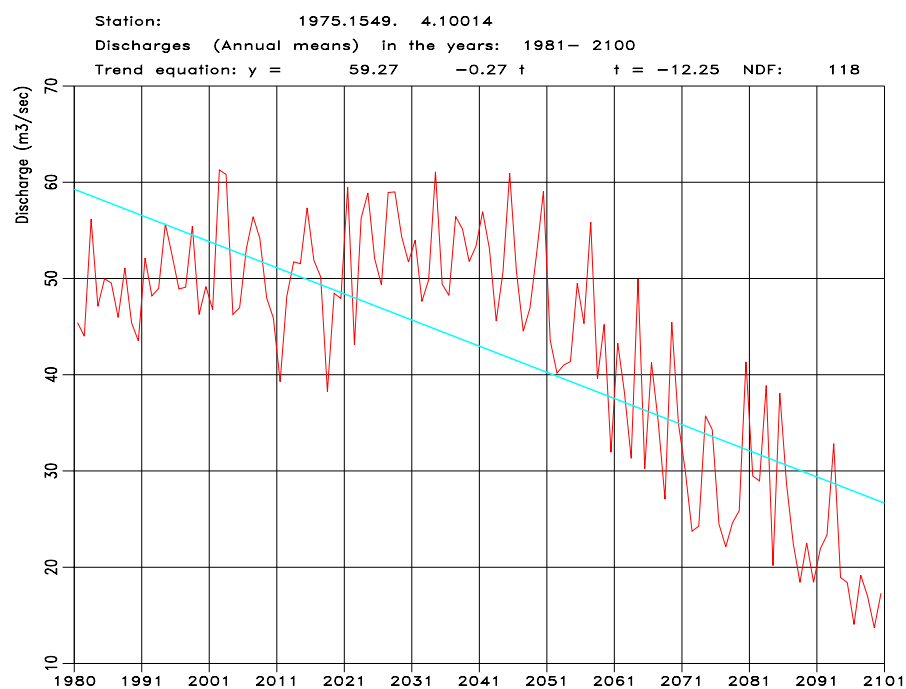


Figure D19. Hydrological model results for annual mean streamflow ( $\text{m}^3/\text{s}$ ) for period 1981-2100 for catchment 1549 Kurje with precipitation and temperature input from climate projection Echem A2 downscaled to meteorological station sites. Glacier covered areas are treated as time-variant (top) and as constant (bottom).

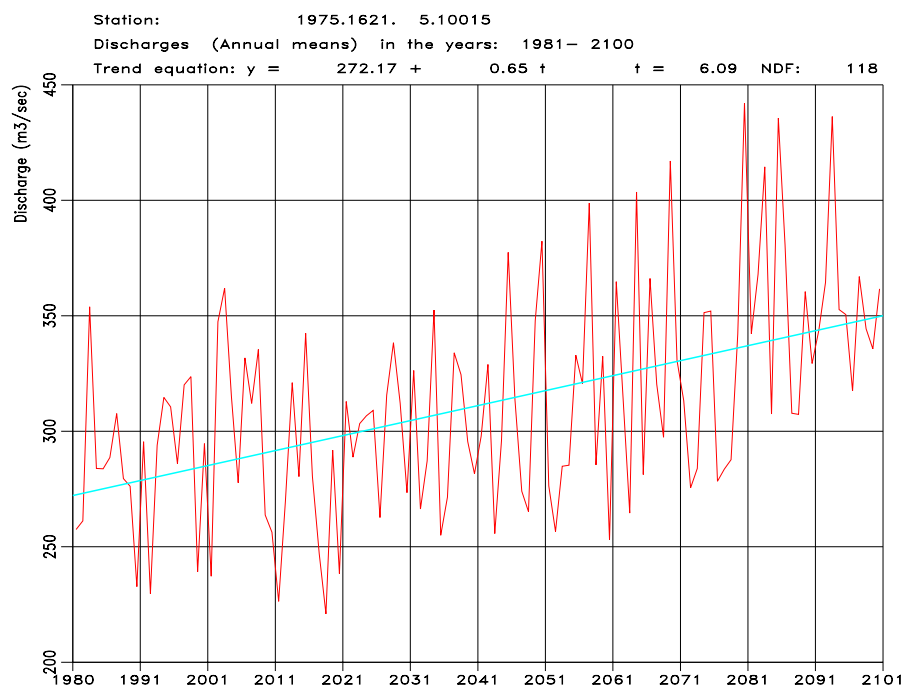
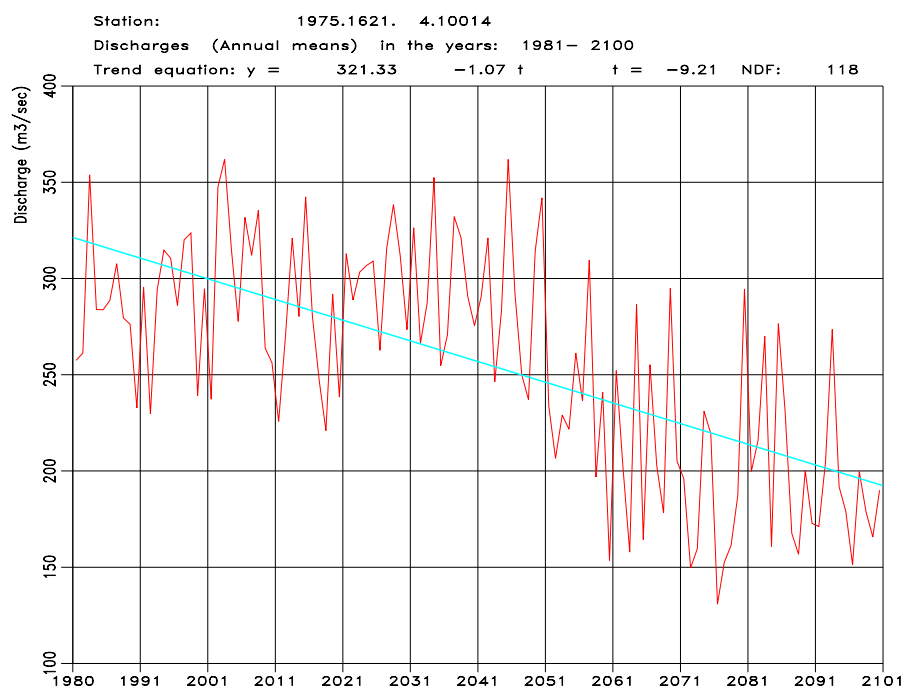


Figure D20. Hydrological model results for annual mean streamflow ( $\text{m}^3/\text{s}$ ) for period 1981–2100 for catchment 1621 Kurizampa with precipitation and temperature input from climate projection Echem A2 downscaled to meteorological station sites. Glacier covered areas are treated as time-variant (top) and as constant (bottom).

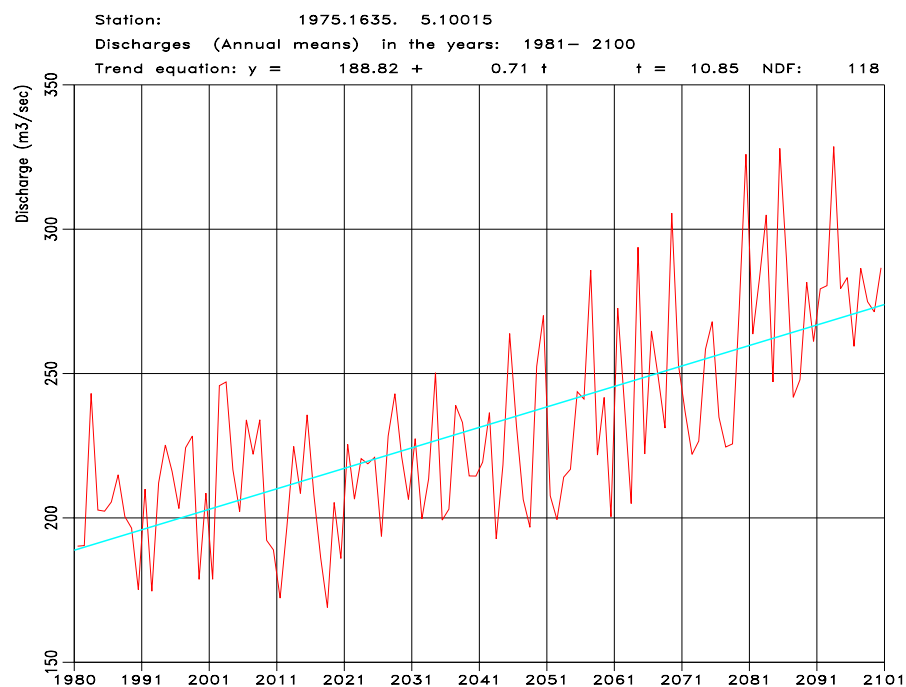
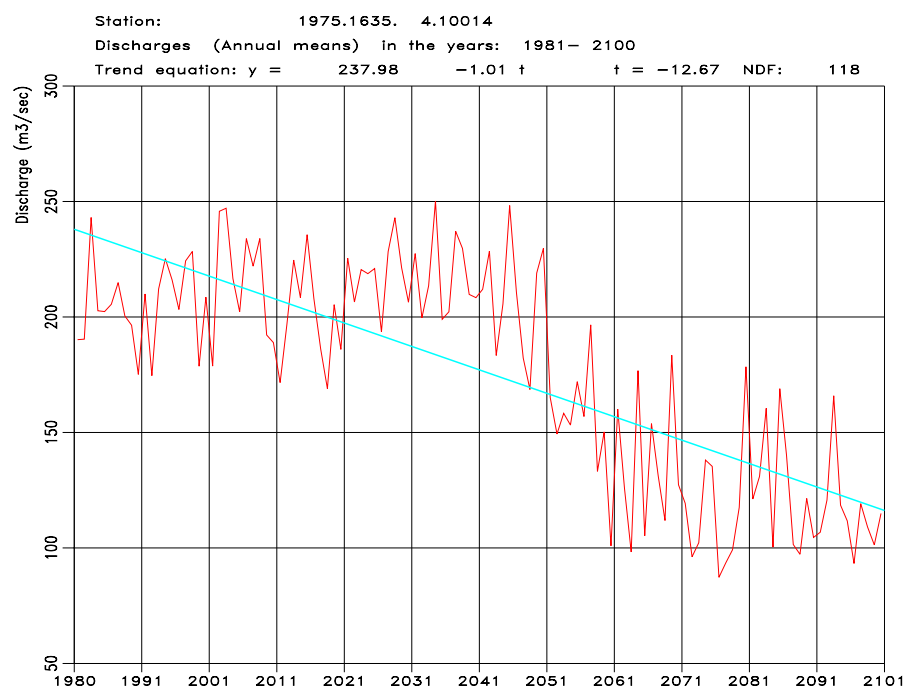


Figure D21. Hydrological model results for annual mean streamflow ( $\text{m}^3/\text{s}$ ) for period 1981-2100 for catchment 1635 Autsho with precipitation and temperature input from climate projection Echem A2 downscaled to meteorological station sites. Glacier covered areas are treated as time-variant (top) and as constant (bottom).



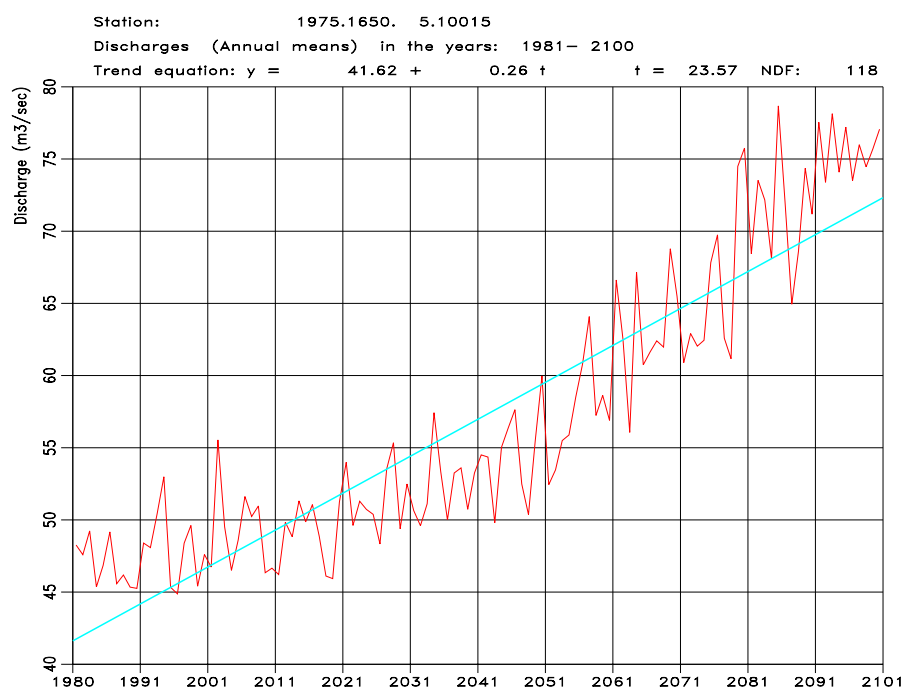
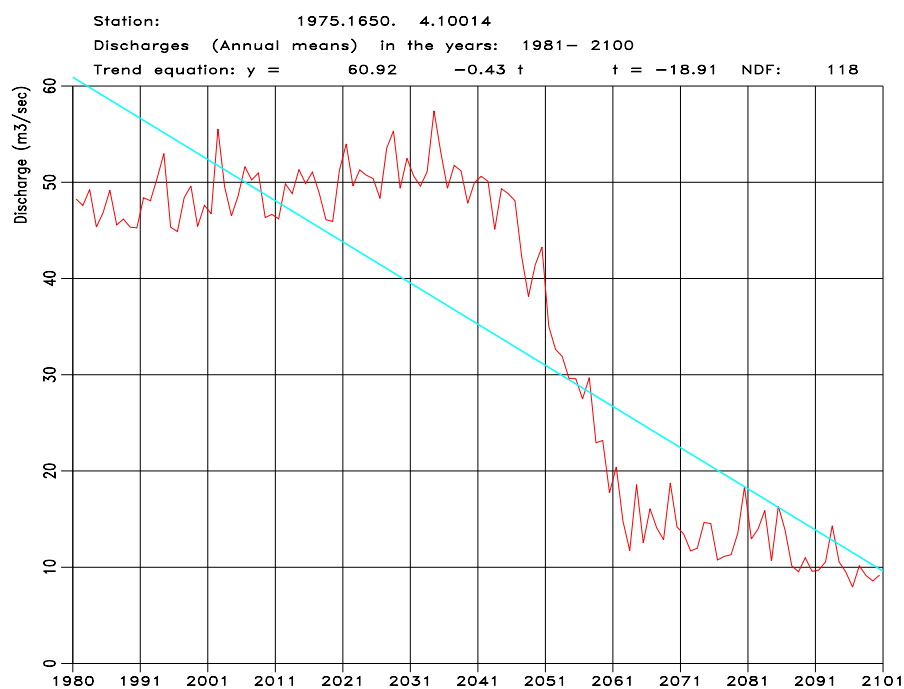


Figure D22. Hydrological model results for annual mean streamflow ( $\text{m}^3/\text{s}$ ) for period 1981–2100 for catchment 1650 Sumpa with precipitation and temperature input from climate projection Echem A2 downscaled to meteorological station sites. Glacier covered areas are treated as time-variant (top) and as constant (bottom).

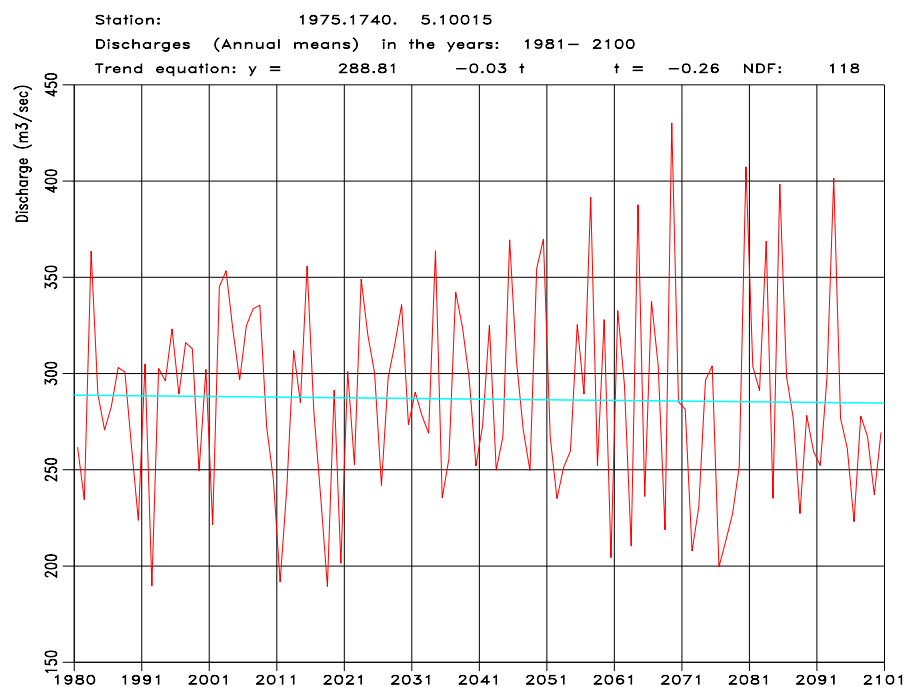
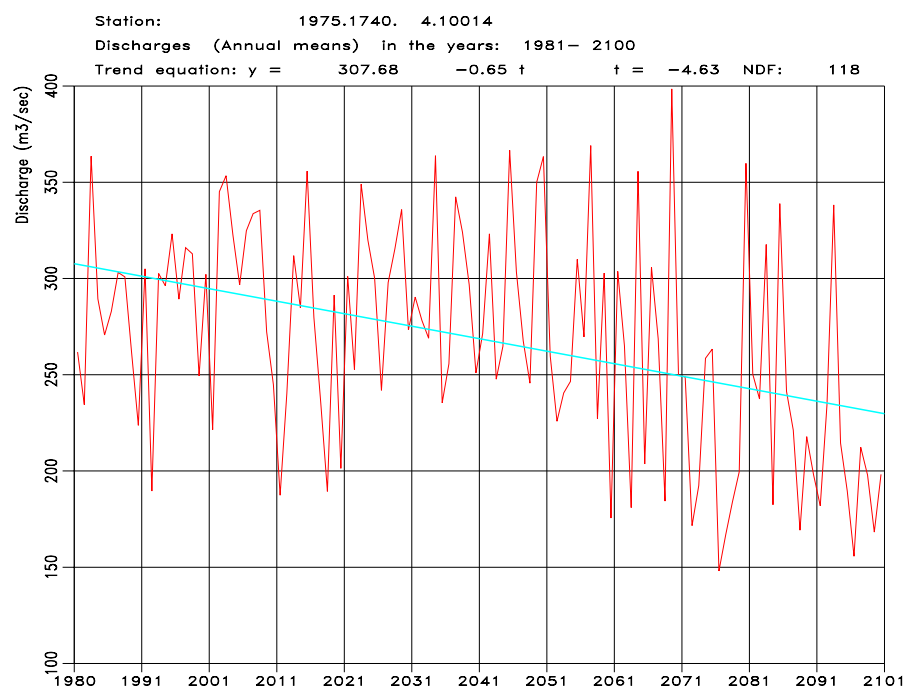


Figure D23. Hydrological model results for annual mean streamflow ( $\text{m}^3/\text{s}$ ) for period 1981-2100 for catchment 1740 Uzorong with precipitation and temperature input from climate projection Echem A2 downscaled to meteorological station sites. Glacier covered areas are treated as time-variant (top) and as constant (bottom).

# **Appendix E Maps of hydrological model results for Bhutan based on climate projection Echam A2**

Figures E1-E14: HBV hydrological model results based on downscaled climate model data from projection Echam A2 for the period 1981-2100 as input. Temperature and precipitation input data have been modified by the hydrological model according to temperature lapse rates and precipitation elevation gradients for each sub-catchment determined during model calibration. Model results for temperature, precipitation, runoff, snow water equivalent and glacier ice thickness for the period 1981-2010 and changes from 1981-2010 to 2021-2050 and from 1981-2010 to 2071 to 2100 are shown as maps. Temperature and water balance simulations have been performed with the HBV hydrological model for 1 km<sup>2</sup> grid cells with daily time step and mean values for periods of 30 year have been determined. The glacier covered areas of the model are treated as constant for the period 1981-2010, and as time-variant with initial ice volumes for glacier covered grid cells modified by model mass balance results for the period 2011-2100.

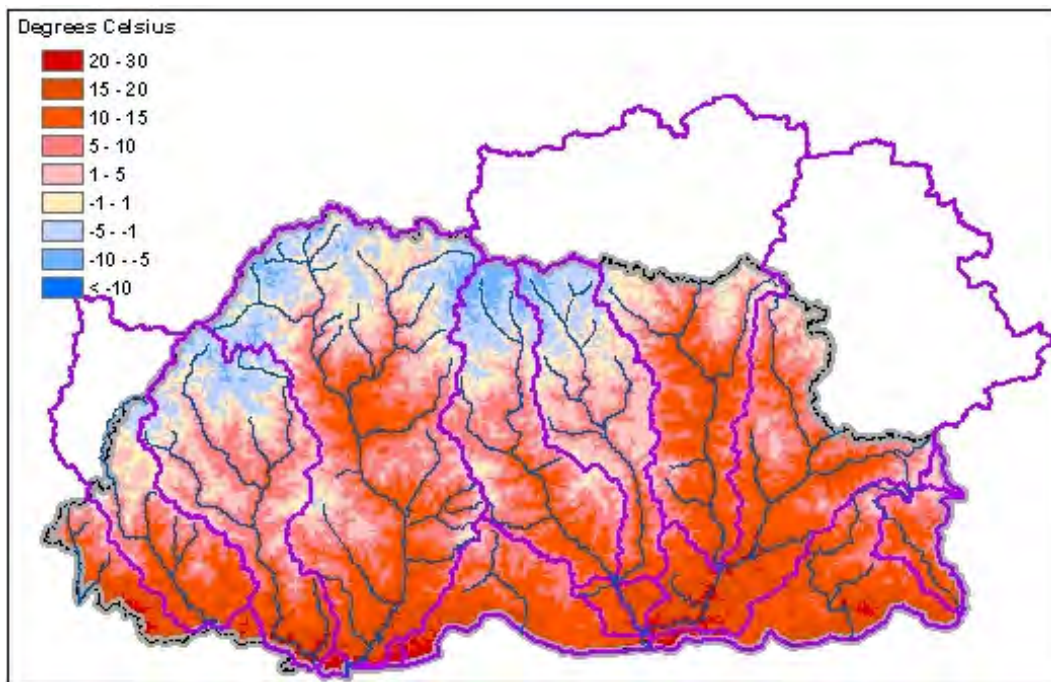


Figure E1. Hydrological model results for mean annual temperature (°C) for the period 1981-2010 based on input from climate projection Echam A2.

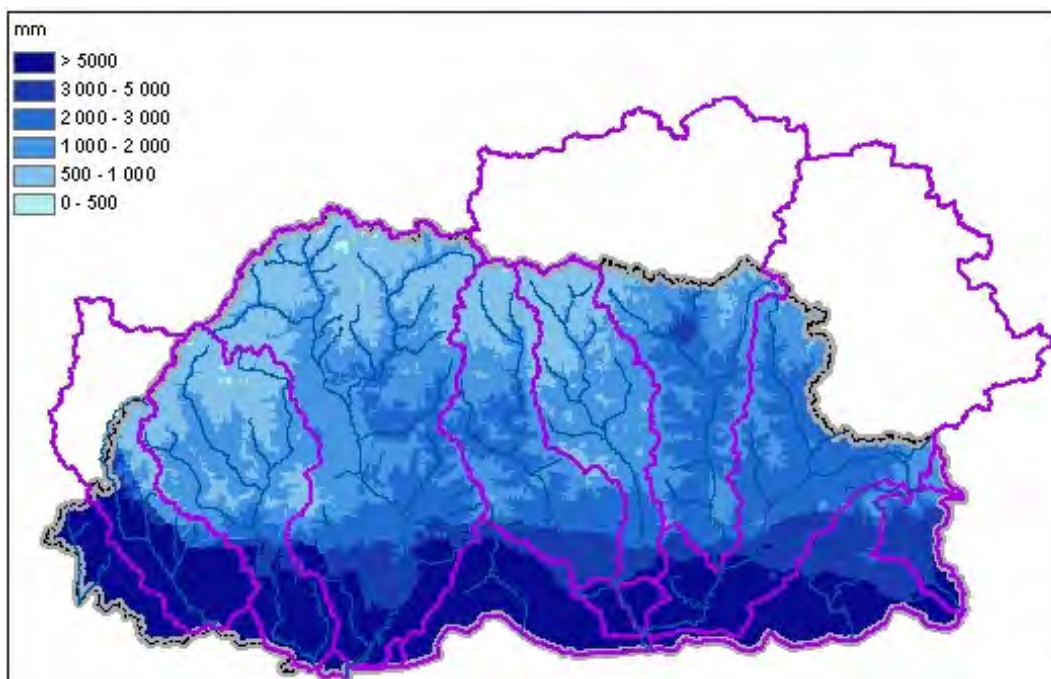


Figure E2. Hydrological model results for mean annual precipitation (mm) for the period 1981-2010 based on input from climate projection Echam A2.

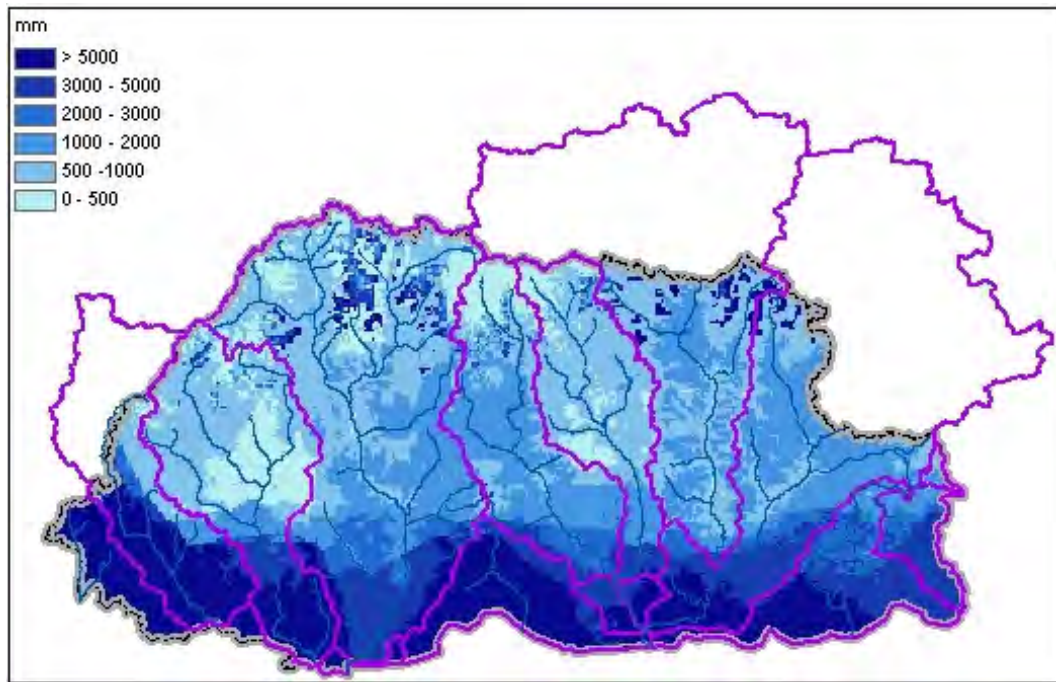


Figure E3. Hydrological model results for mean annual runoff (mm) for the period 1981-2010 based on input from climate projection ECHAM A2. The glacier covered areas are treated as constant.

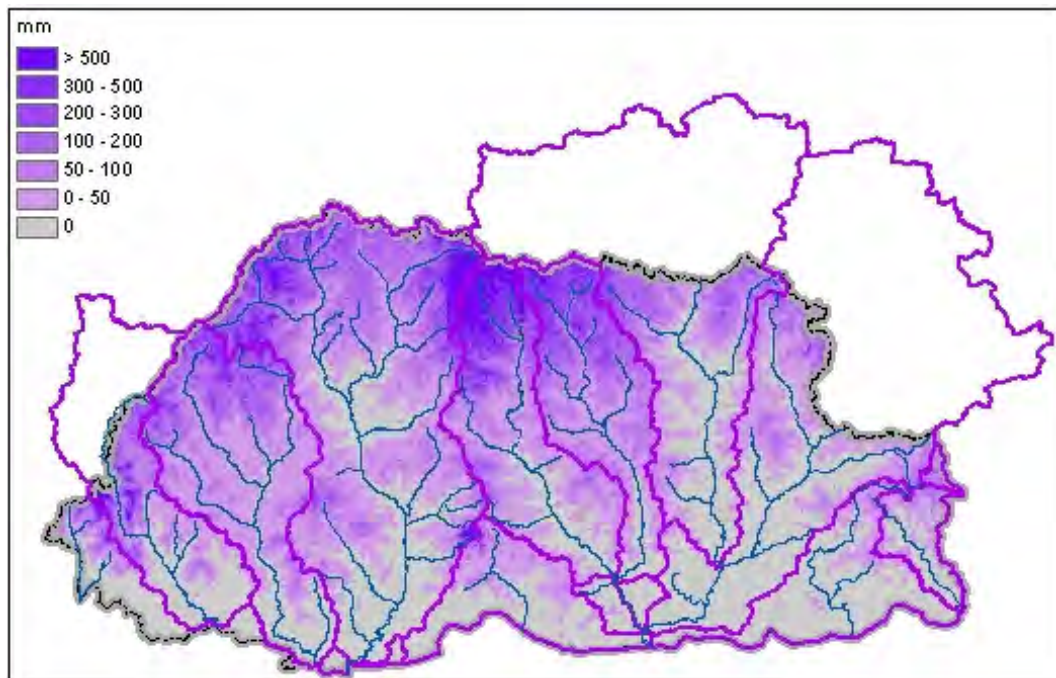


Figure E4. Hydrological model results for mean annual maximum snow water equivalent (mm) for the period 1981-2010 based on input from climate projection ECHAM A2.



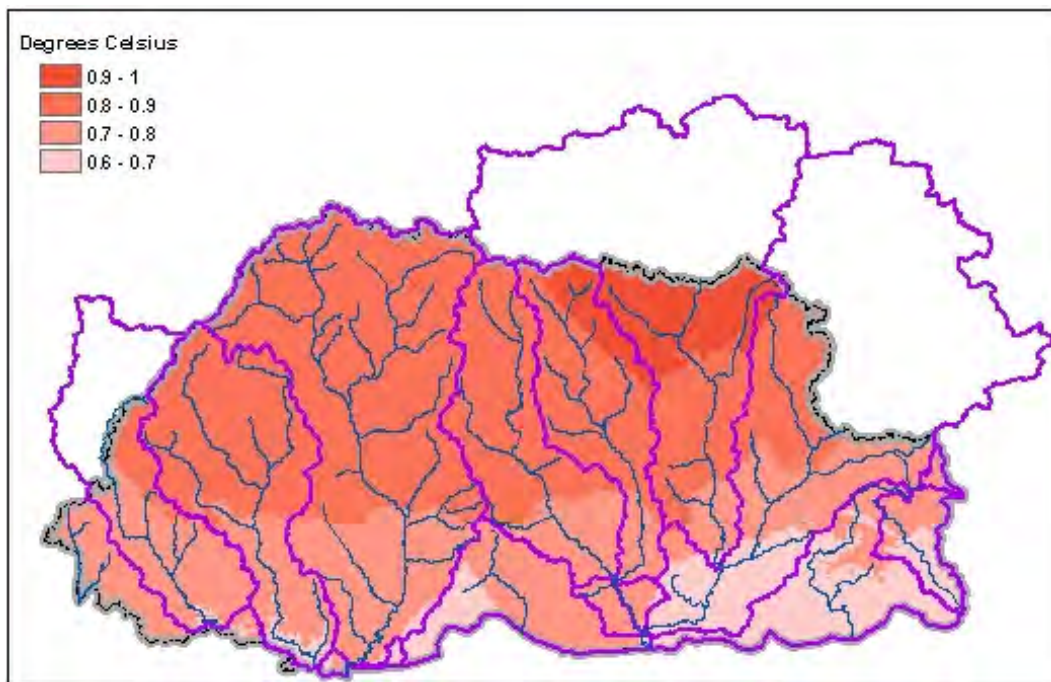


Figure E5. Hydrological model results for change in mean annual temperature (°C) from 1981-2010 to 2021-2050 based on input from climate projection Echam A2.

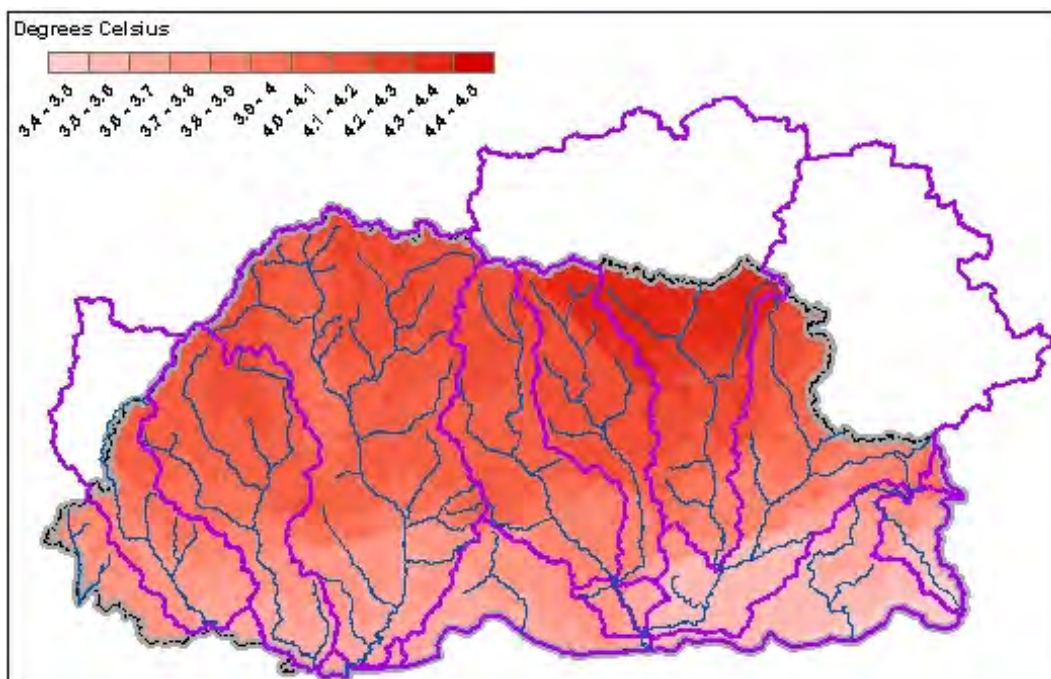


Figure E6. Hydrological model results for change in mean annual temperature (°C) from 1981-2010 to 2071-2100 based on input from climate projection Echam A2.

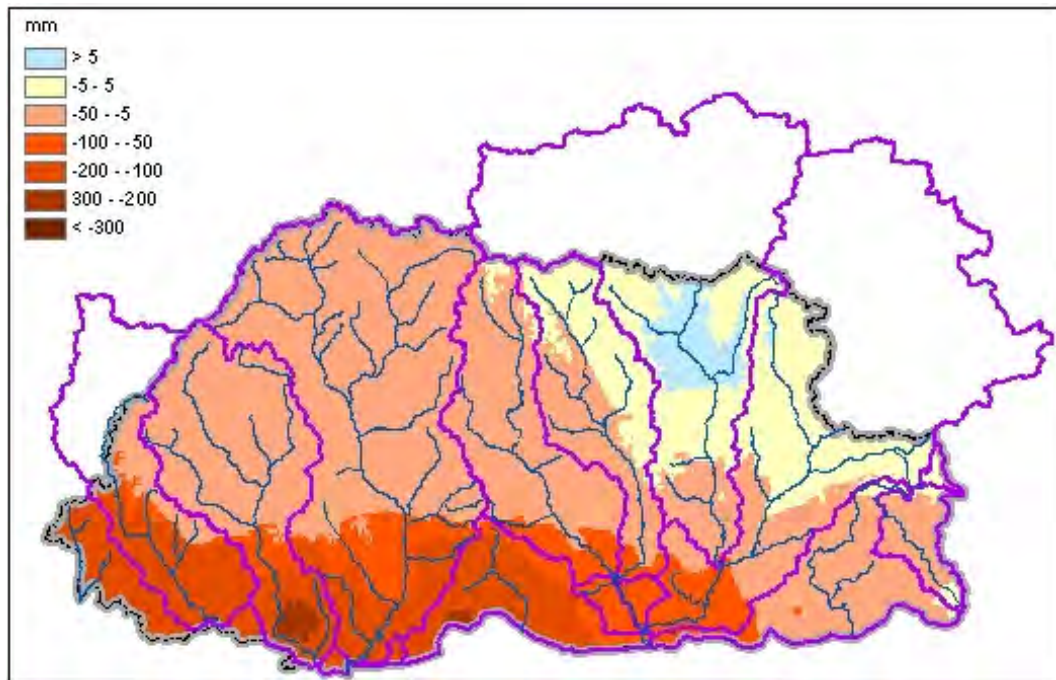


Figure E7. Hydrological model results for change in mean annual precipitaton (mm) from 1981-2010 to 2021-2050 based on input from climate projection Echam A2.

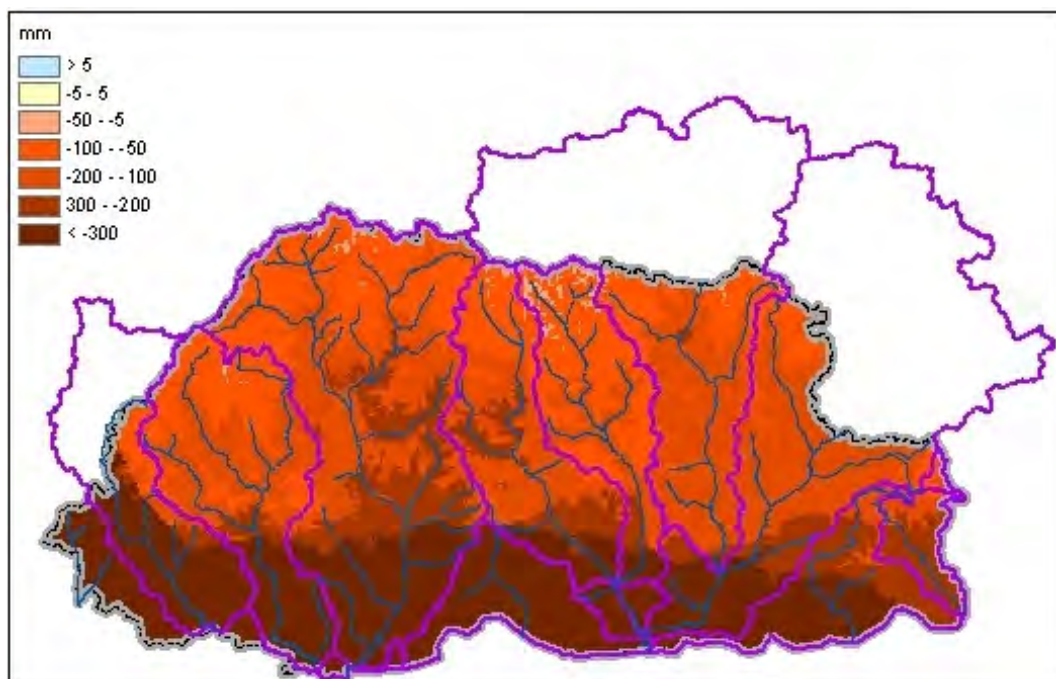


Figure E8. Hydrological model results for change in mean annual precipitaton (mm) from 1981-2010 to 2071-2100 based on input from climate projection Echam A2.



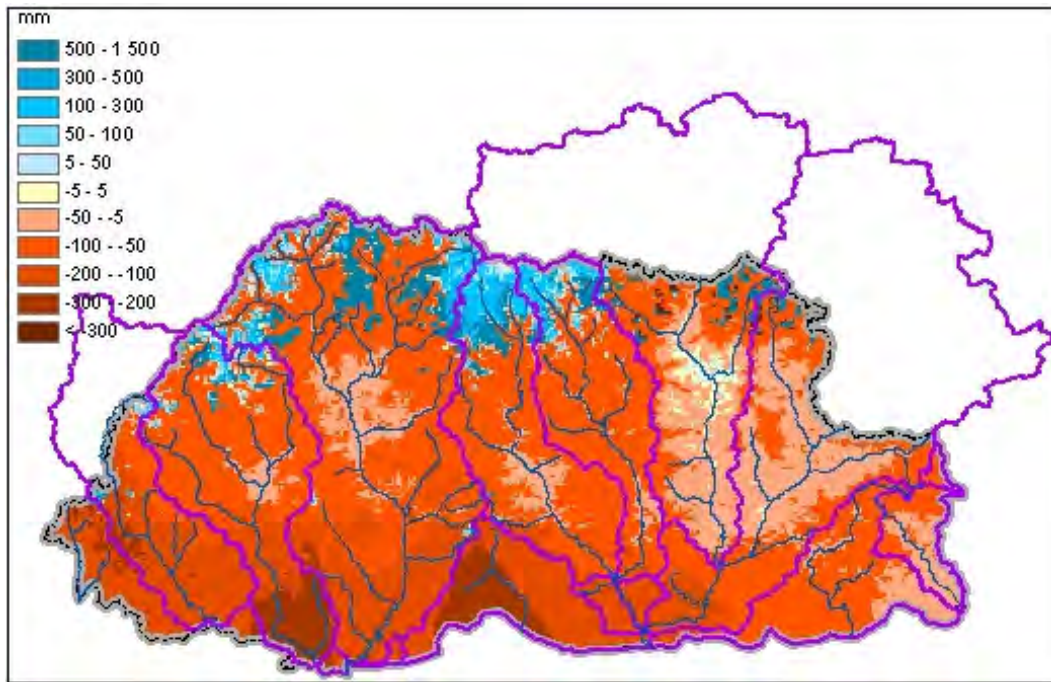


Figure E9. Hydrological model results for change in mean annual runoff (mm) from 1981-2010 to 2021-2050 based on input from climate projection Echam A2. The glacier covered areas are treated as time-variant.

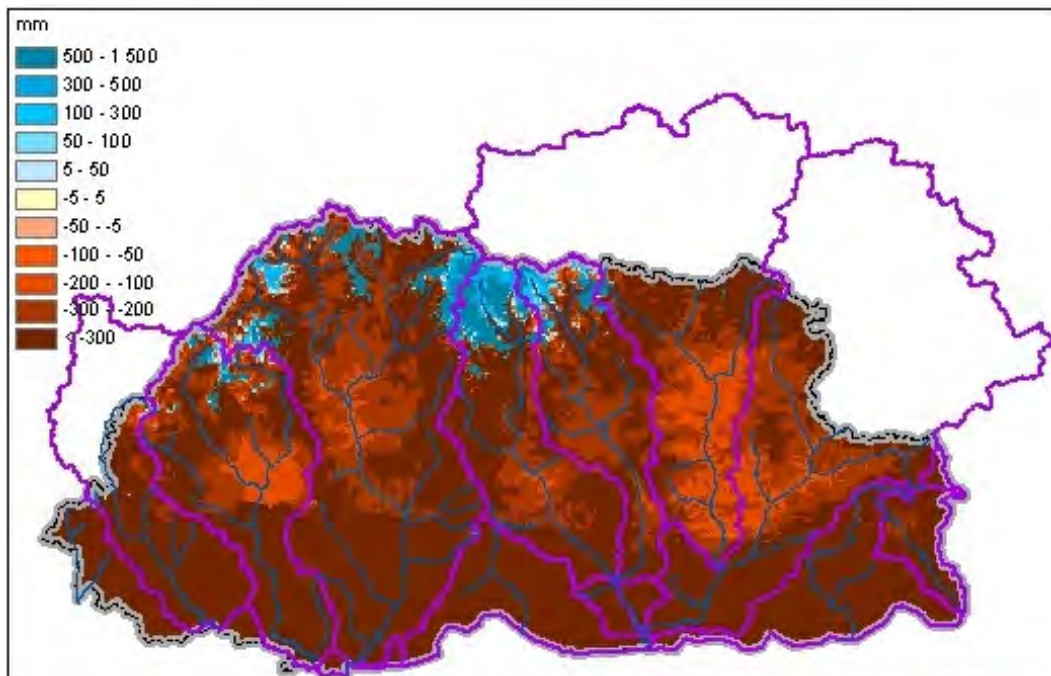


Figure E10. Hydrological model results for change in mean annual runoff (mm) from 1981-2010 to 2071-2100 based on input from climate projection Echam A2. The glacier covered areas are treated as time-variant.



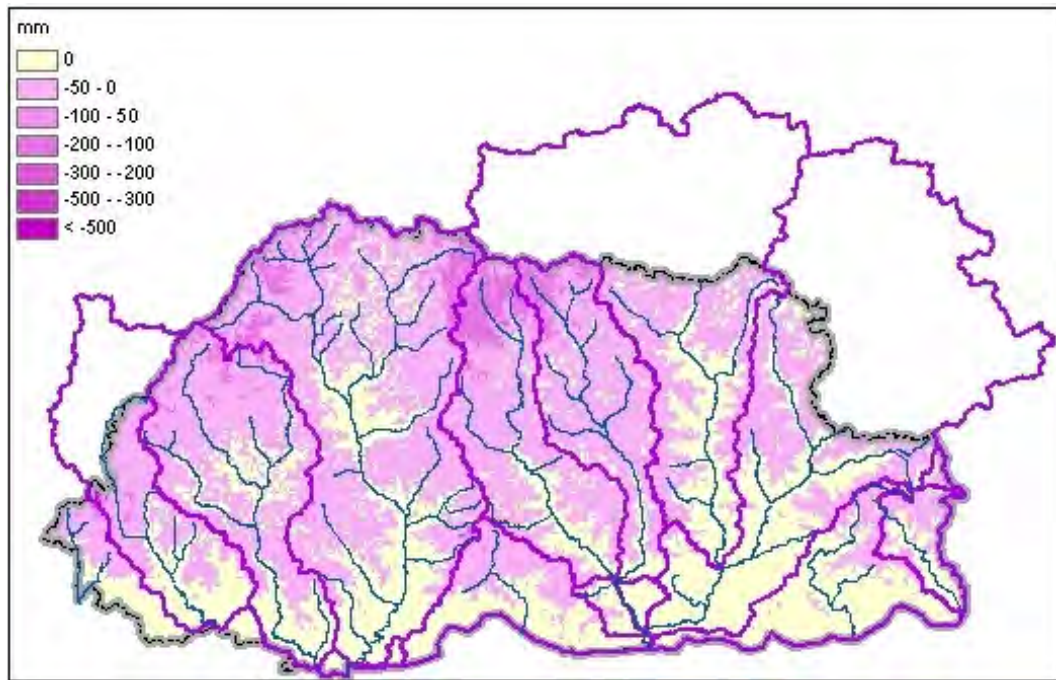


Figure E11. Hydrological model results for change in mean annual maximum snow water equivalent (mm) from 1981-2010 to 2021-2050 based on input from climate projection Ecam A2.

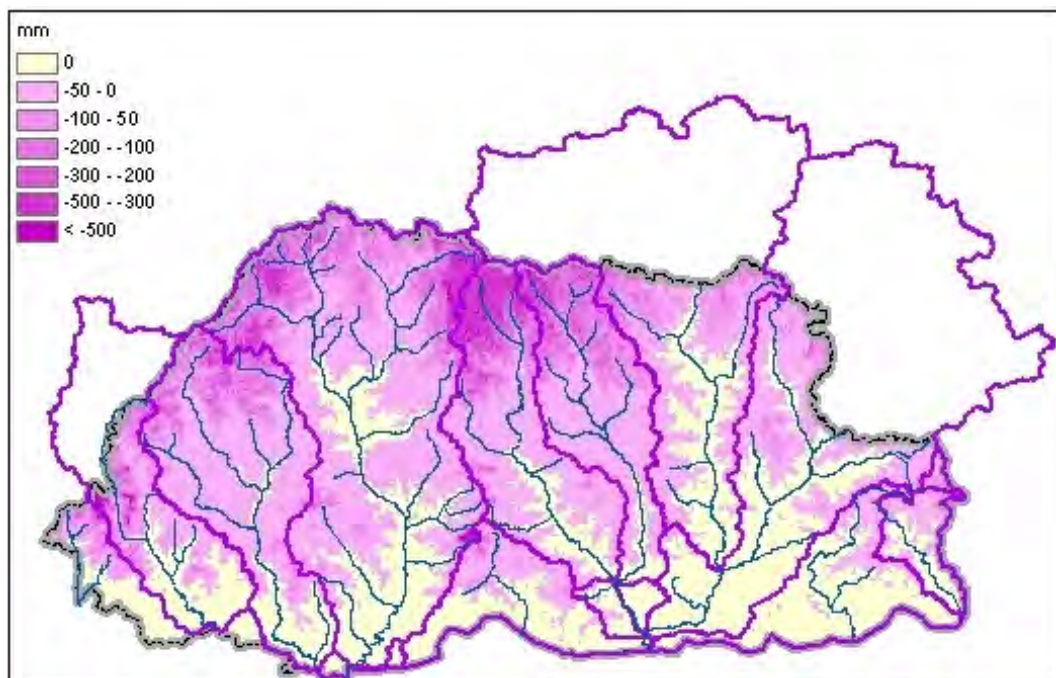


Figure E12. Hydrological model results for change in mean annual maximum snow water equivalent (mm) from 1981-2010 to 2021-2100 based on input from climate projection Ecam A2.

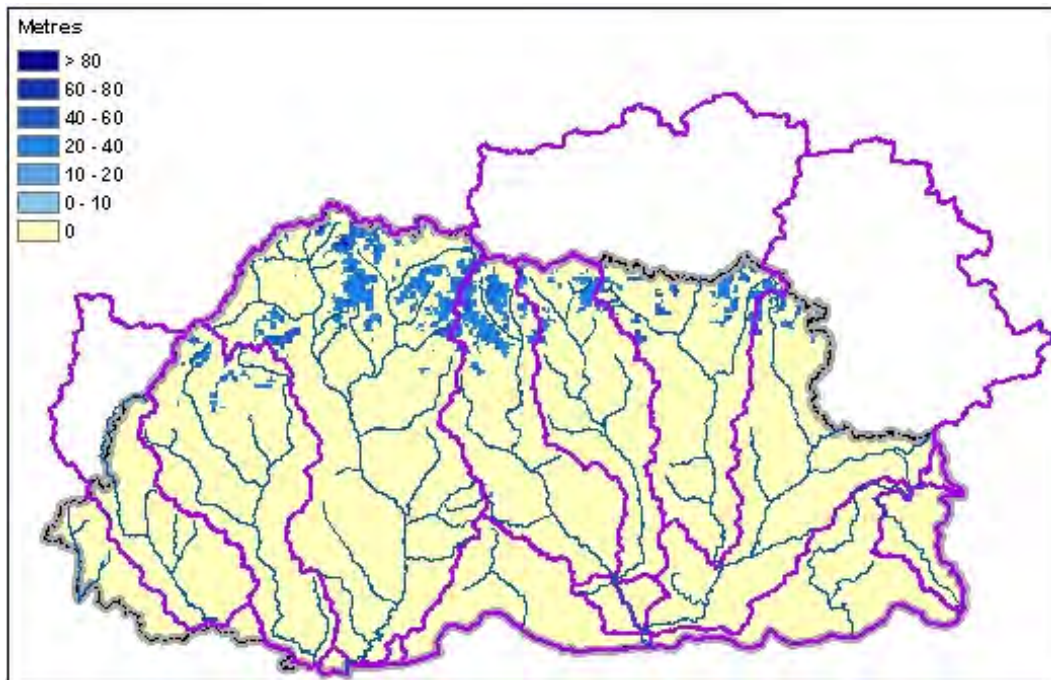


Figure E13. Glacier ice thickness (metres) and glacier covered areas at the end of year 2010 based on data from ICIMOD. Glacier ice thickness is used as initial values for hydrological model simulations for the period 2011-2100.

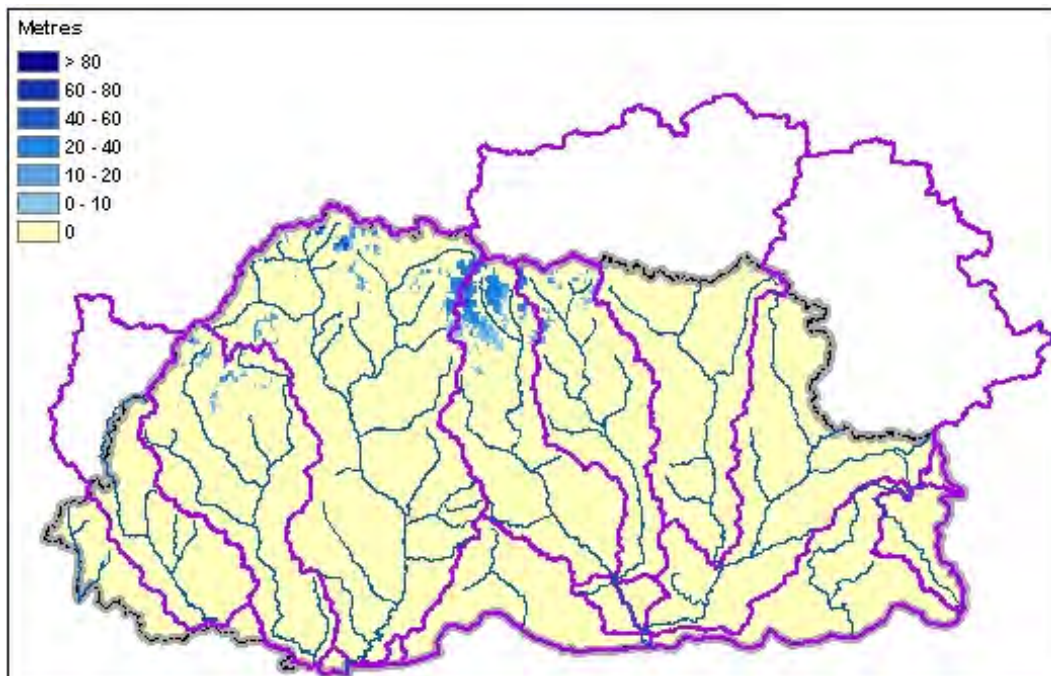


Figure E14. Glacier ice thickness (metres) and glacier covered areas at the end of year 2100 based on hydrological model simulations for the period 2011-2100 with input from climate projection ECHAM A2. The glacier covered areas are treated as time-variant.

# **Appendix F   Flow duration curves based on climate projection Echam B1**

Figures F1-F34: Flow duration curves (red) , sum lower integrated curves (green) and installed capacity curves (blue) for the periods 1981-2010, 2021-2050 and 2071-2100 based on hydrological modelling with input from climate projection Echam B1 downscaled to meteorological station sites. The hydrological model was run with constant glacier covered areas for the period 1981-2010, with time-variant glacier covered areas for the period 2021-2050 and with both constant and glacier covered areas for the period 2071-2100. The streamflow values have been normalized by dividing by mean annual streamflow for each simulation period. The maximum value plotted in the graph is 300 % of mean annual streamflow, although the flow duration curve comprises higher streamflow.

The flow duration curve presents the exceedance probability of streamflow, i.e. the fraction of time over the entire record that different streamflow values are exceeded

Sum lower is the integrated volume of discharge below a given streamflow value.

Diversion capacity is the fraction of the integrated volume of discharge that can be diverted by a construction with installed capacity equal to a given streamflow value.

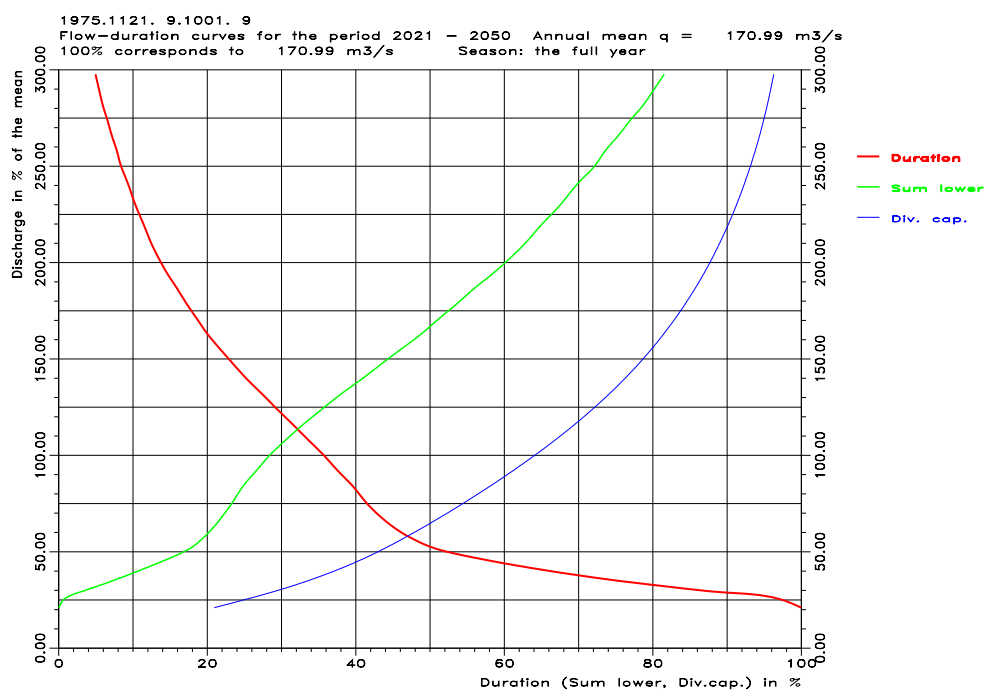
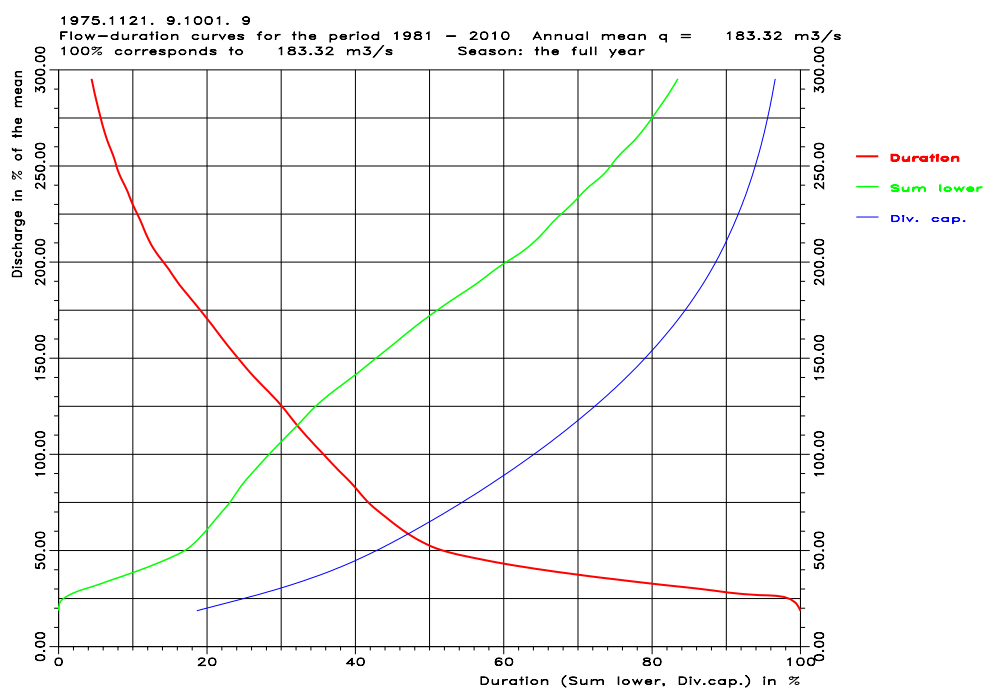


Figure F1. Curves for flow duration (red), sum lower (green) and diversion capacity (blue) for catchment 1121 Doyagang with precipitation and temperature input from climate projection Ecam B1. Top: 1981-2010, constant glacier area, annual mean  $183 \text{ m}^3/\text{s}$ . Bottom: 2021-2050, time-variant glacier area, annual mean  $171 \text{ m}^3/\text{s}$ .

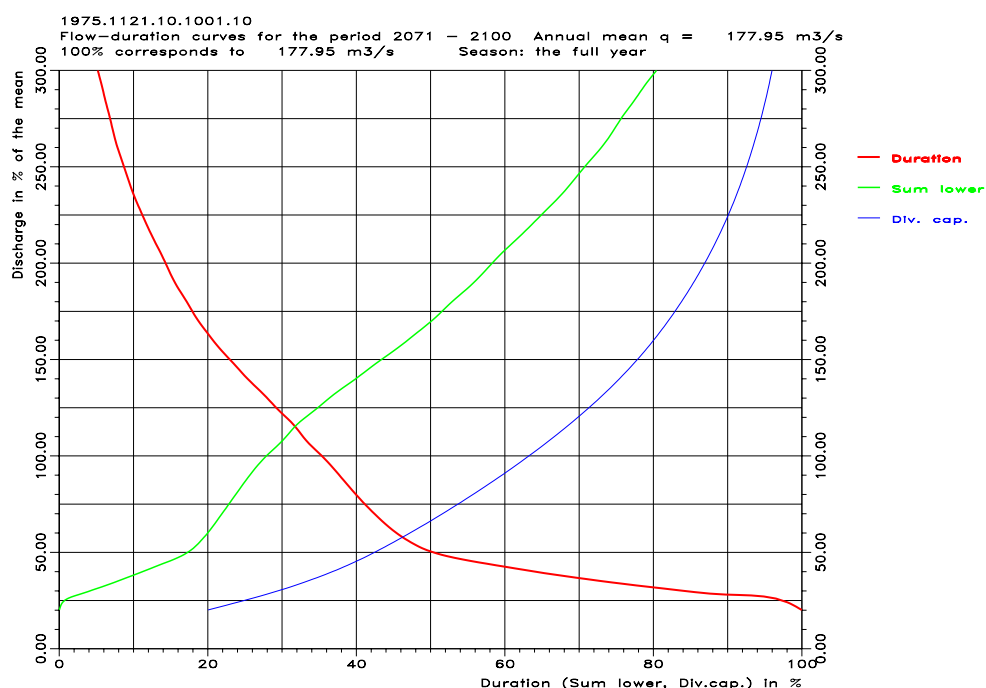
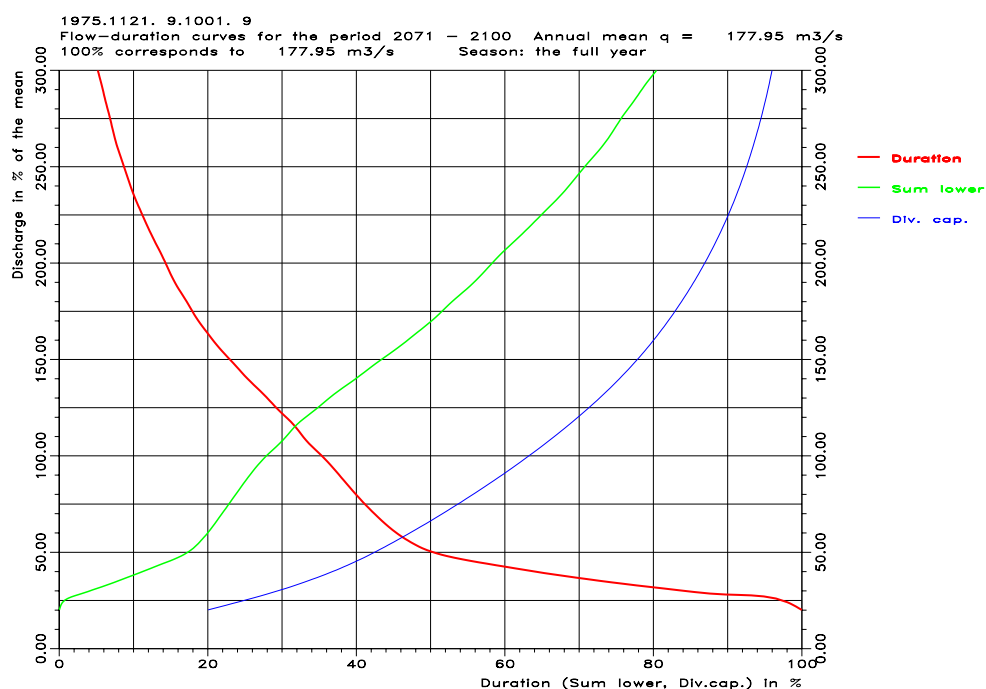


Figure F2. Curves for flow duration (red), sum lower (green) and diversion capacity (blue) for catchment 1121 Doyagang with precipitation and temperature input from climate projection Ecam B1. Top: 2071-2100, time-variant glacier area, annual mean 178 m<sup>3</sup>/s. Bottom: 2071-2100, constant glacier area, annual mean 178 m<sup>3</sup>/s.

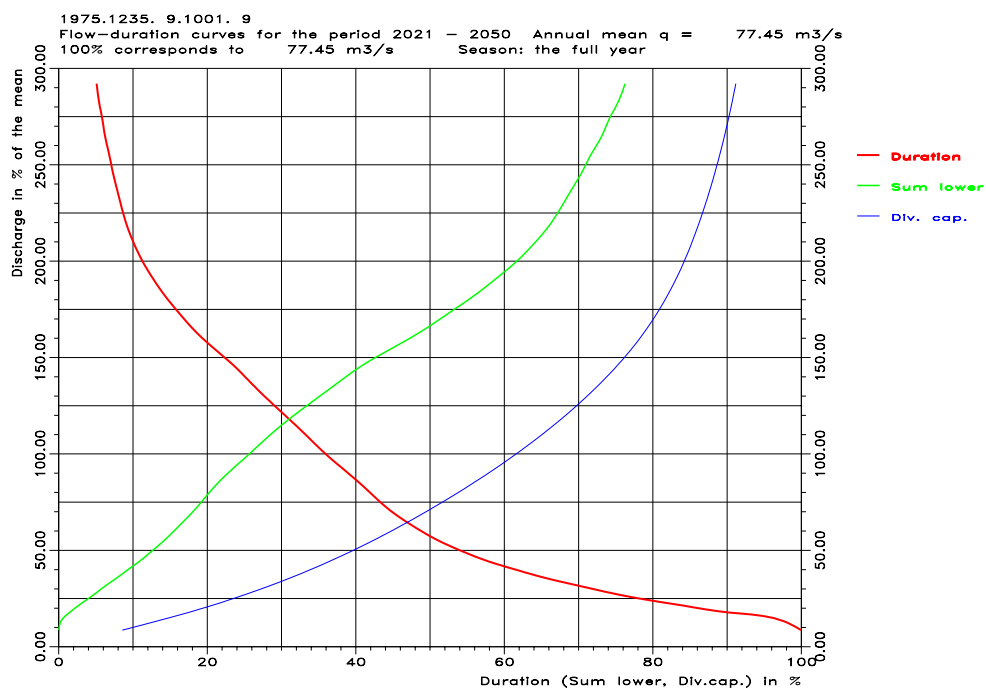
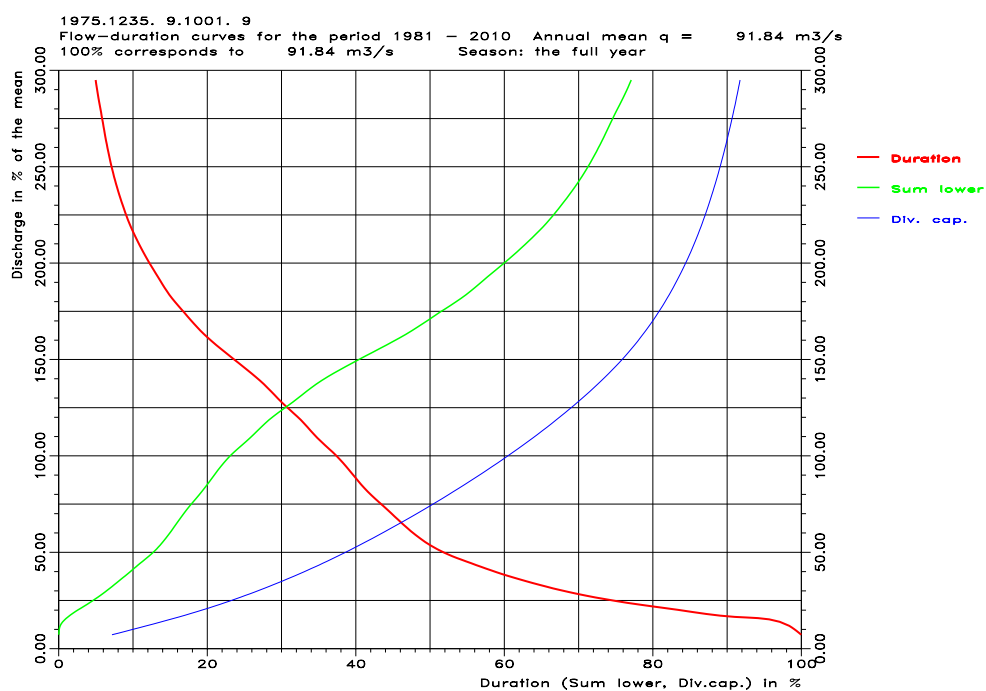


Figure F3. Curves for flow duration (red), sum lower (green) and diversion capacity (blue) for catchment 1235 Chimakoti with precipitation and temperature input from climate projection Echem B1. Top: 1981-2010, constant glacier area, annual mean  $92 \text{ m}^3/\text{s}$ . Bottom: 2021-2050, time-variant glacier area, annual mean  $77 \text{ m}^3/\text{s}$ .



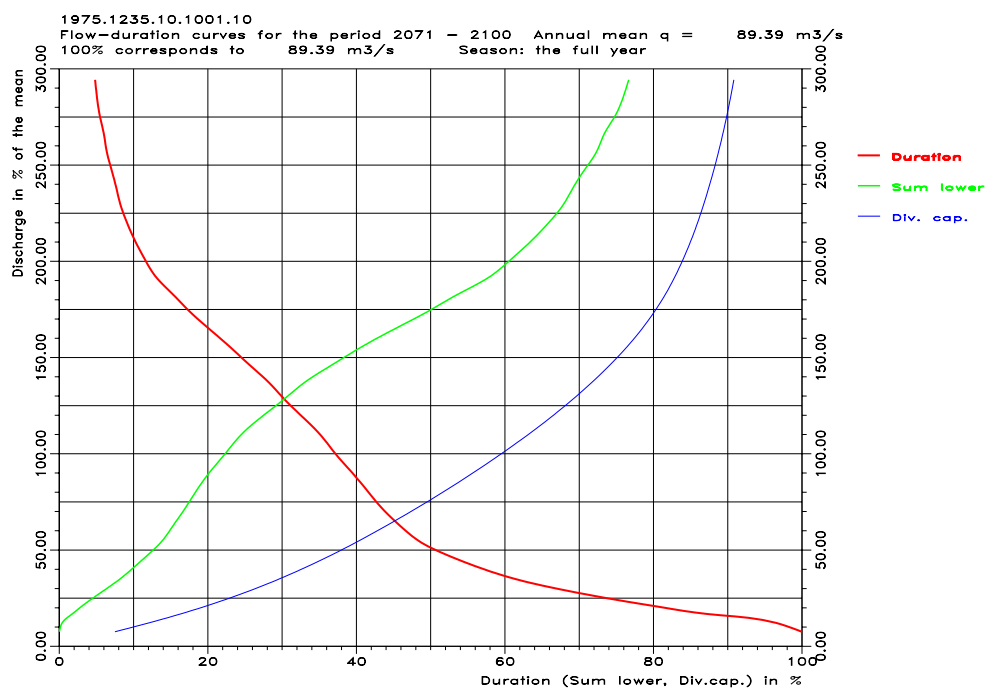
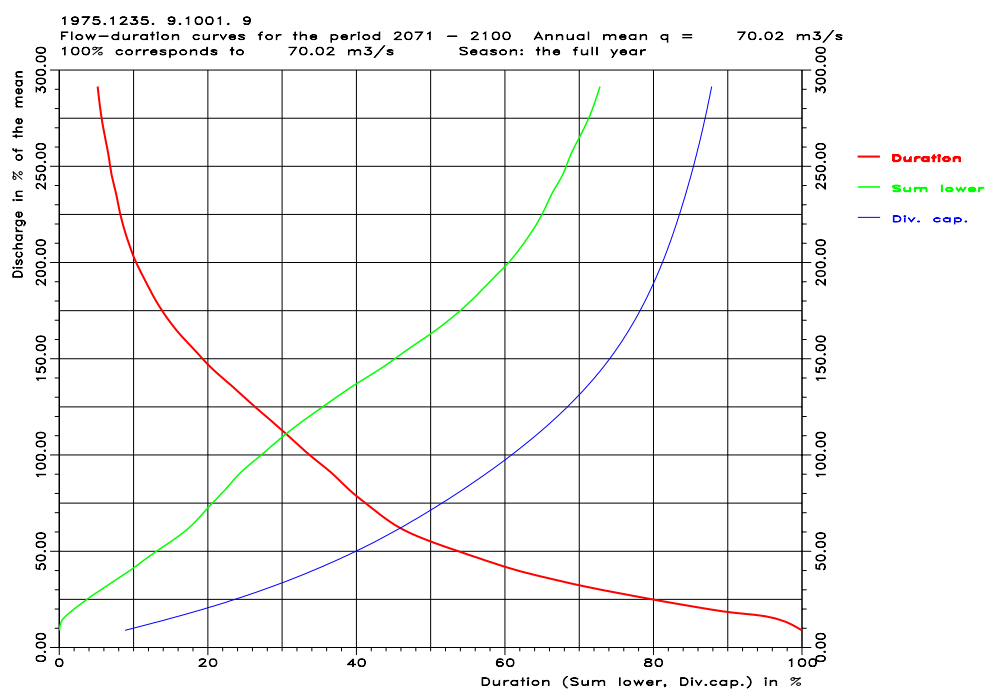


Figure F4. Curves for flow duration (red), sum lower (green) and diversion capacity (blue) for catchment 1235 Chimakoti with precipitation and temperature input from climate projection Ecam B1. Top: 2071-2100, time-variant glacier area, annual mean 70 m<sup>3</sup>/s. Bottom: 2071-2100, constant glacier area, annual mean 89 m<sup>3</sup>/s.

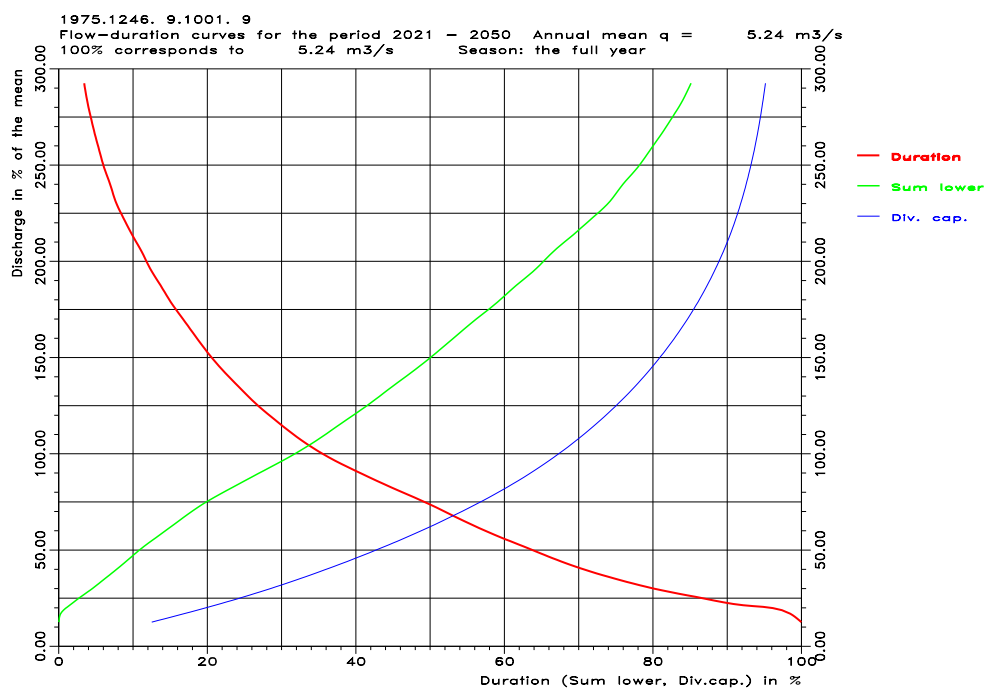
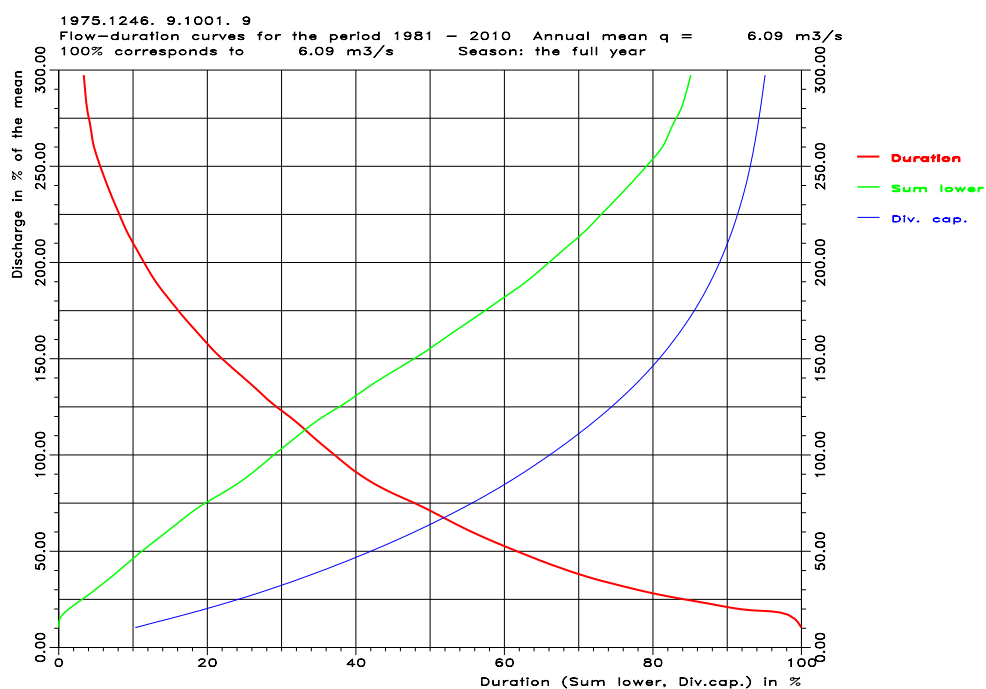


Figure F5. Curves for flow duration (red), sum lower (green) and diversion capacity (blue) for catchment 1246 Haa with precipitation and temperature input from climate projection Ecam B1. Top: 1981-2010, constant glacier area, annual mean  $6.1 \text{ m}^3/\text{s}$ . Bottom: 2021-2050, time-variant glacier area, annual mean  $5.2 \text{ m}^3/\text{s}$ .



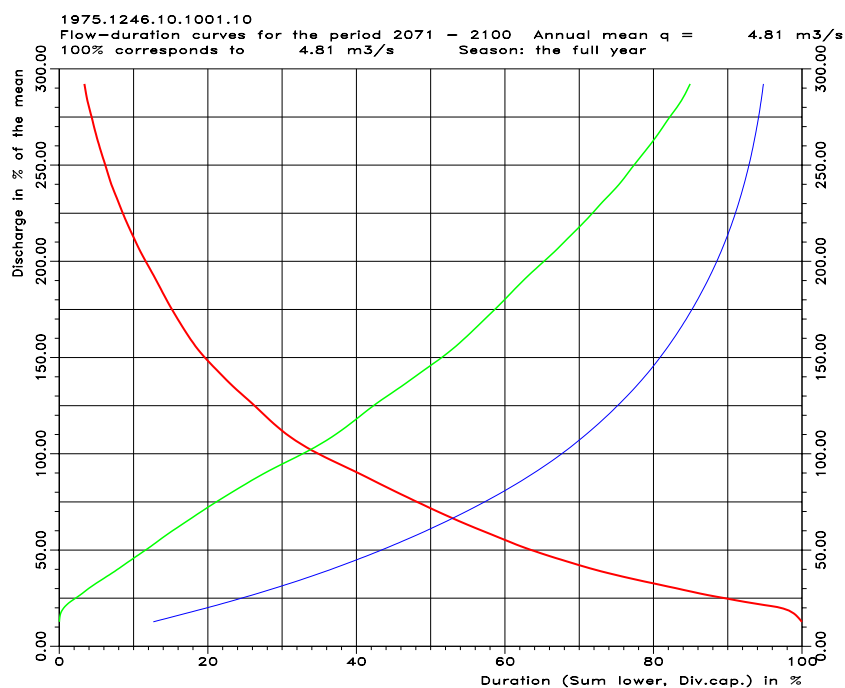
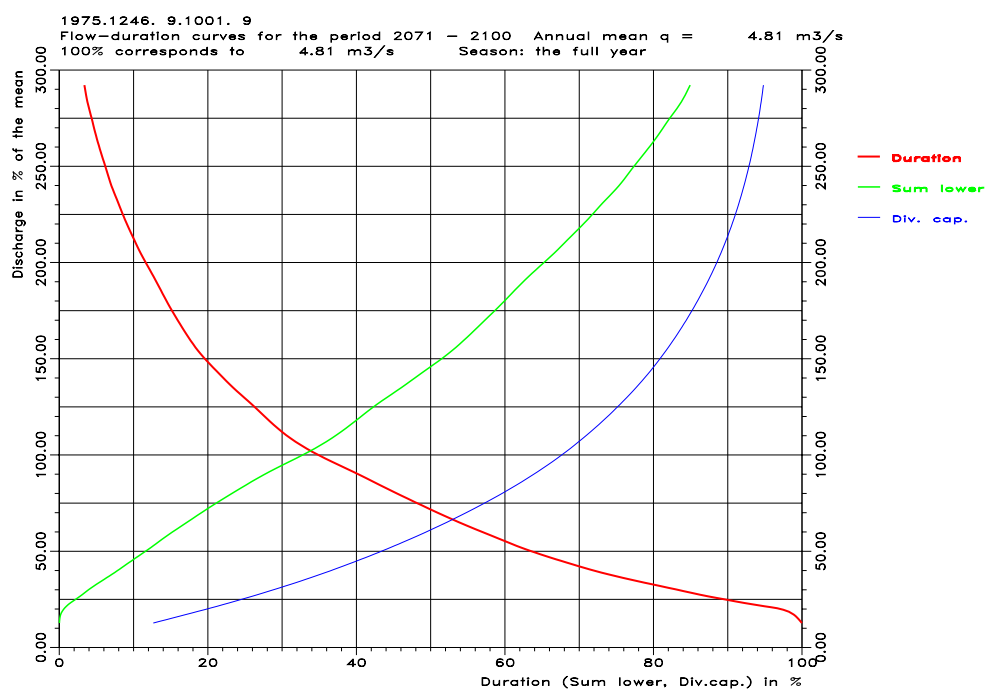


Figure F6. Curves for flow duration (red), sum lower (green) and diversion capacity (blue) for catchment 1246 Haa with precipitation and temperature input from climate projection Echam B1. Top: 2071-2100, time-variant glacier area, annual mean 4.8 m<sup>3</sup>/s. Bottom: 2071-2100, constant glacier area, annual mean 4.8 m<sup>3</sup>/s.

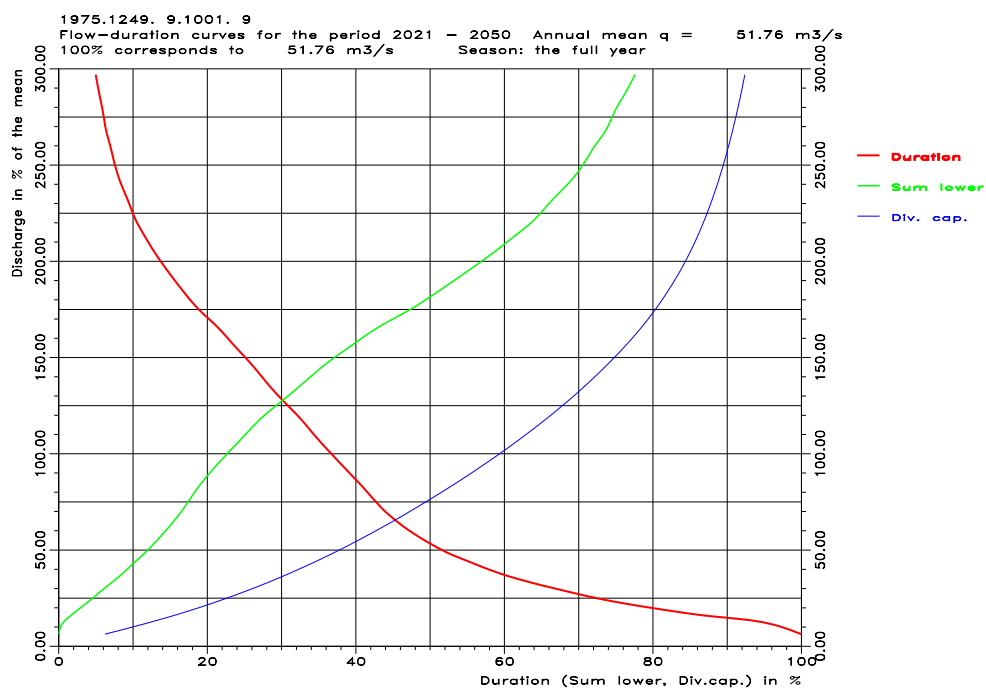
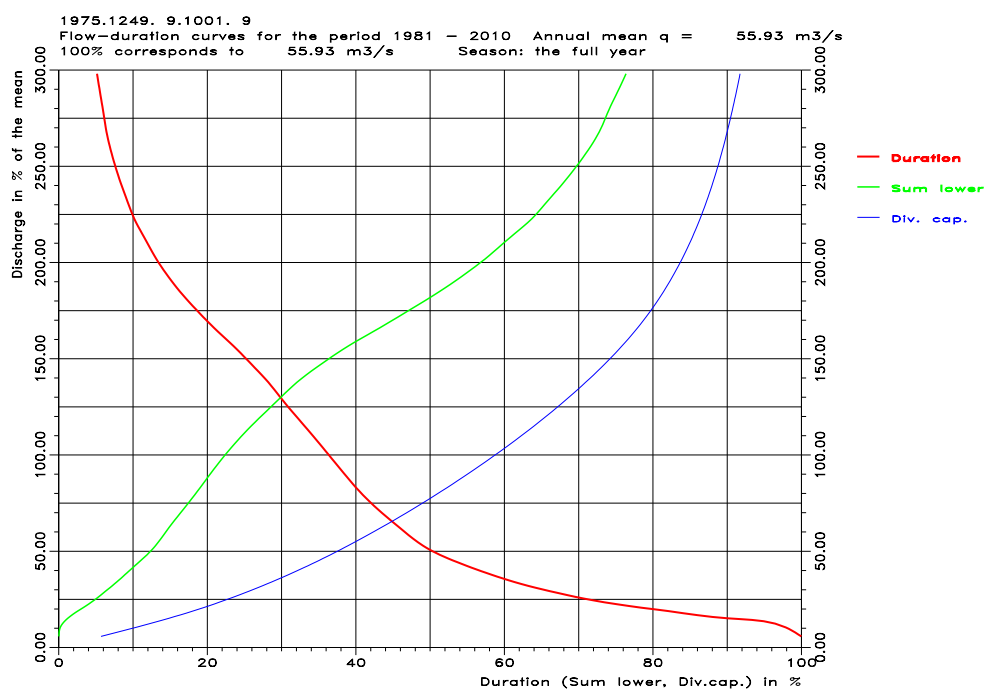


Figure F7. Curves for flow duration (red), sum lower (green) and diversion capacity (blue) for catchment 1249 Damchhu with precipitation and temperature input from climate projection Ecam B1. Top: 1981-2010, constant glacier area, annual mean  $56 \text{ m}^3/\text{s}$ . Bottom: 2021-2050, time-variant glacier area, annual mean  $52 \text{ m}^3/\text{s}$ .

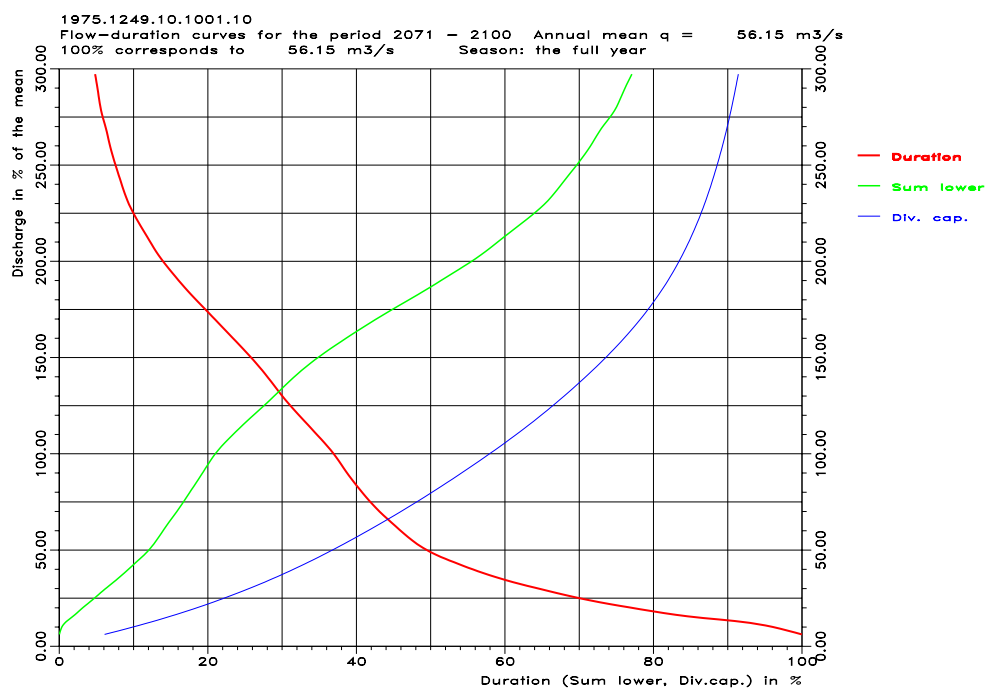
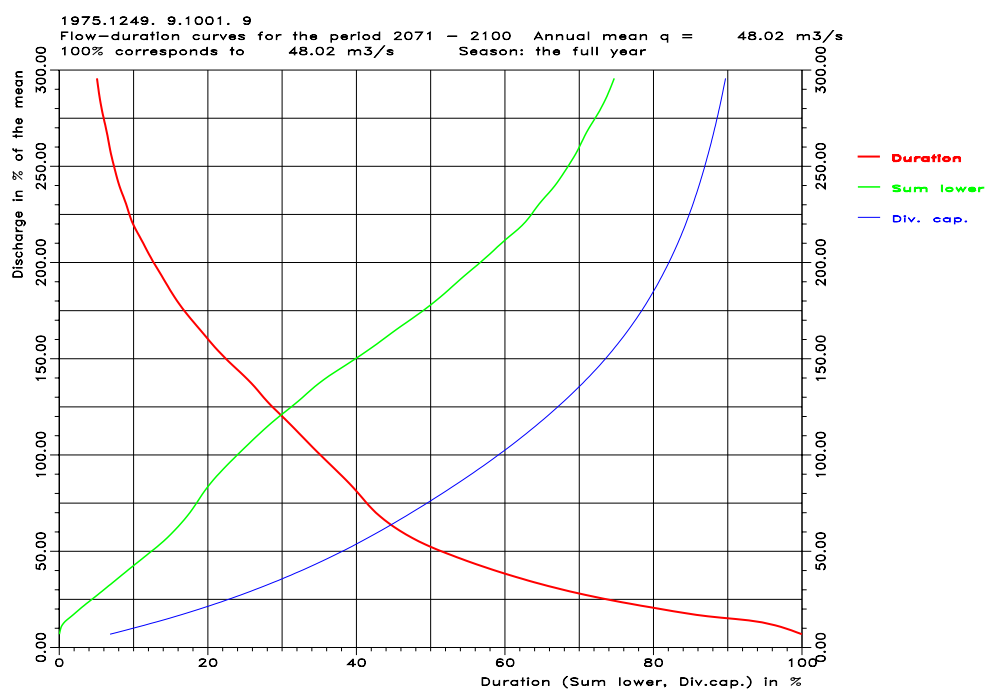


Figure F8. Curves for flow duration (red), sum lower (green) and diversion capacity (blue) for catchment 1249 Damchhu with precipitation and temperature input from climate projection Echam B1. Top: 2071-2100, time-variant glacier area, annual mean 48 m<sup>3</sup>/s. Bottom: 2071-2100, constant glacier area, annual mean 56 m<sup>3</sup>/s.

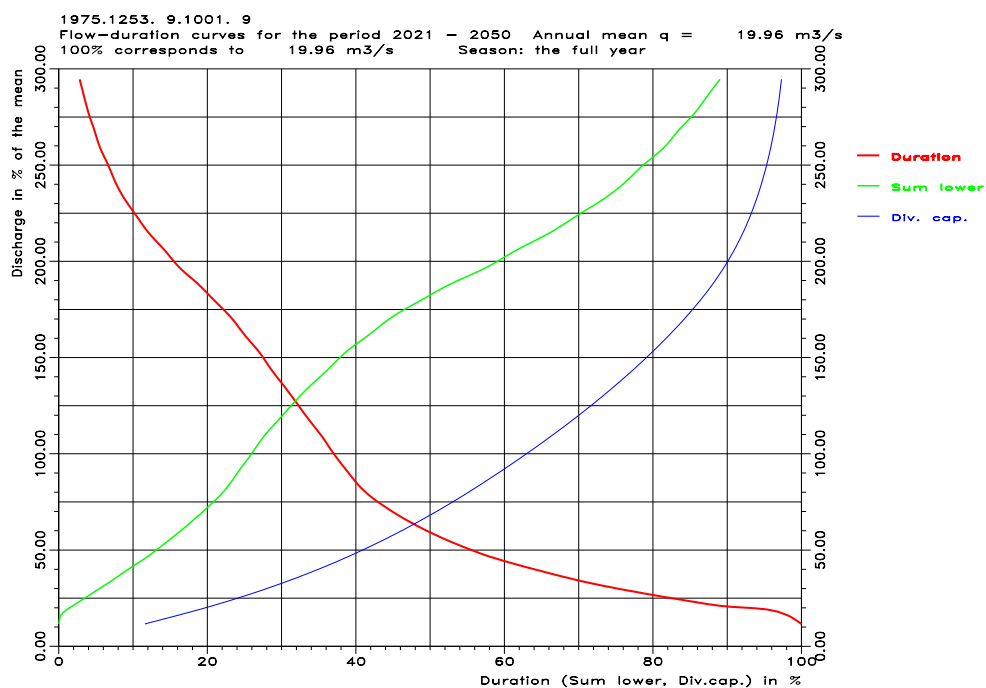
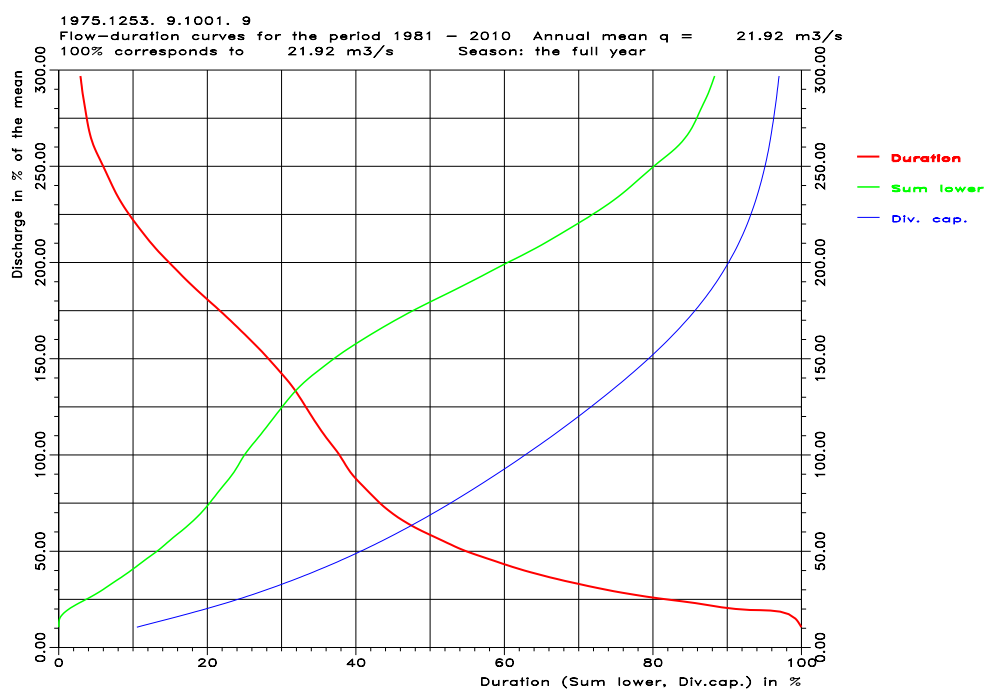


Figure F9. Curves for flow duration (red), sum lower (green) and diversion capacity (blue) for catchment 1253 Paro with precipitation and temperature input from climate projection Ecam B1. Top: 1981-2010, constant glacier area, annual mean  $22 \text{ m}^3/\text{s}$ . Bottom: 2021-2050, time-variant glacier area, annual mean  $20 \text{ m}^3/\text{s}$ .

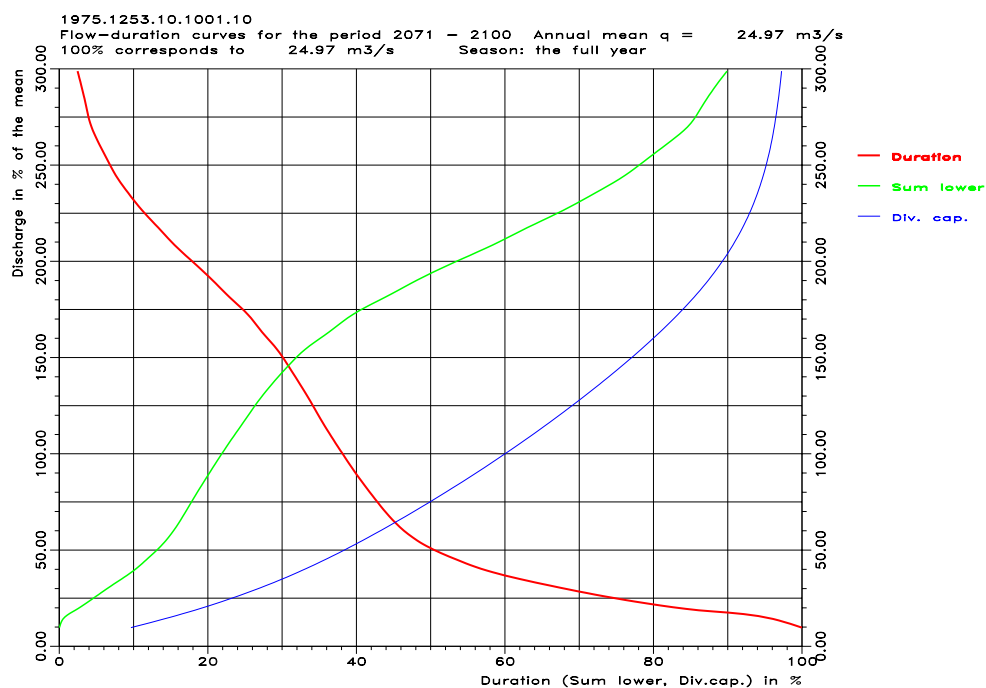
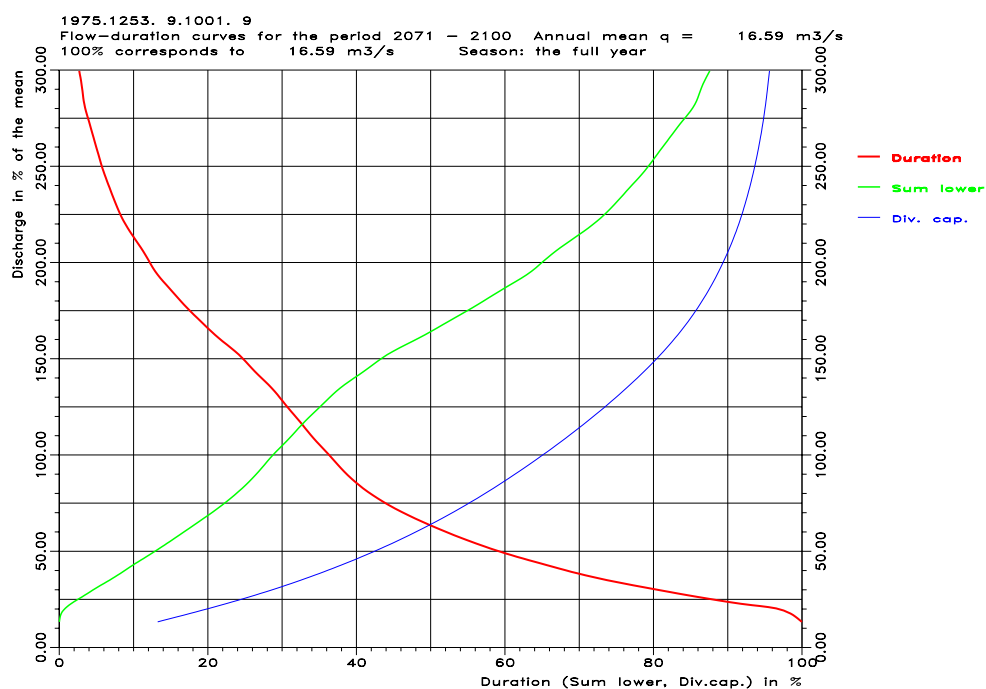


Figure F10. Curves for flow duration (red), sum lower (green) and diversion capacity (blue) for catchment 1253 Paro with precipitation and temperature input from climate projection Echam B1. Top: 2071-2100, time-variant glacier area, annual mean  $17 \text{ m}^3/\text{s}$ . Bottom: 2071-2100, constant glacier area, annual mean  $25 \text{ m}^3/\text{s}$ .

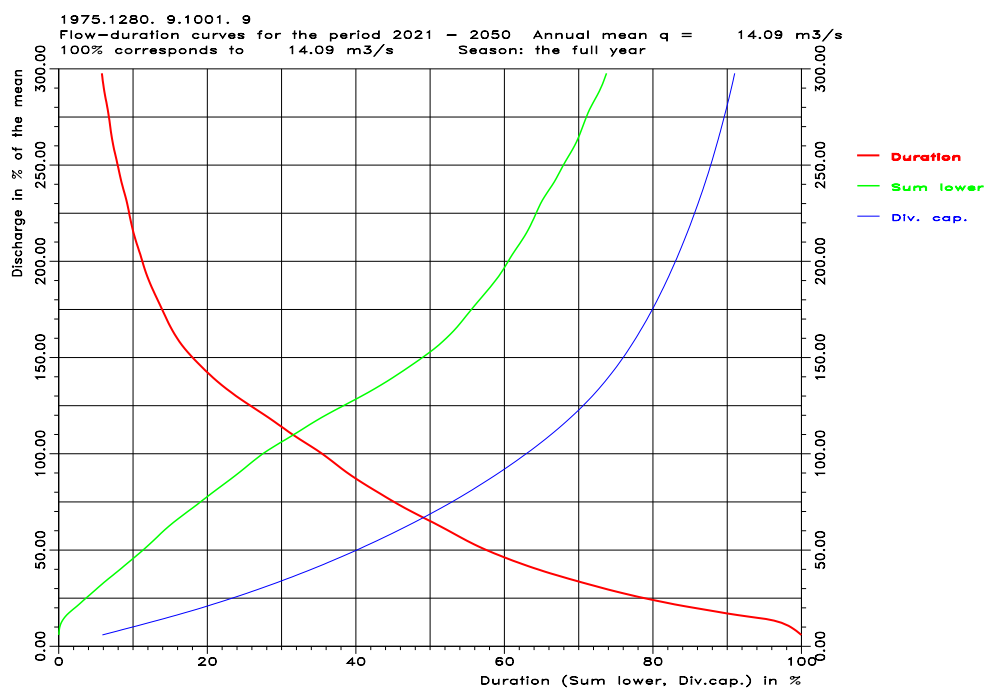
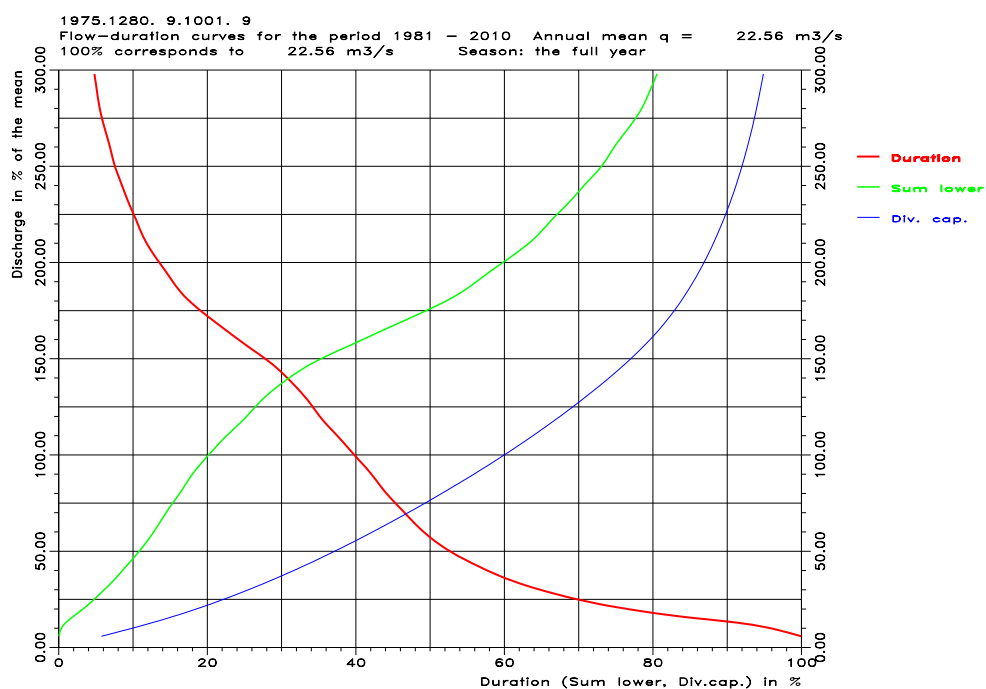


Figure F11. Curves for flow duration (red), sum lower (green) and diversion capacity (blue) for catchment 1280 Lungtenphug with precipitation and temperature input from climate projection Echem B1. Top: 1981-2010, constant glacier area, annual mean  $23 \text{ m}^3/\text{s}$ . Bottom: 2021-2050, time-variant glacier area, annual mean  $14 \text{ m}^3/\text{s}$ .

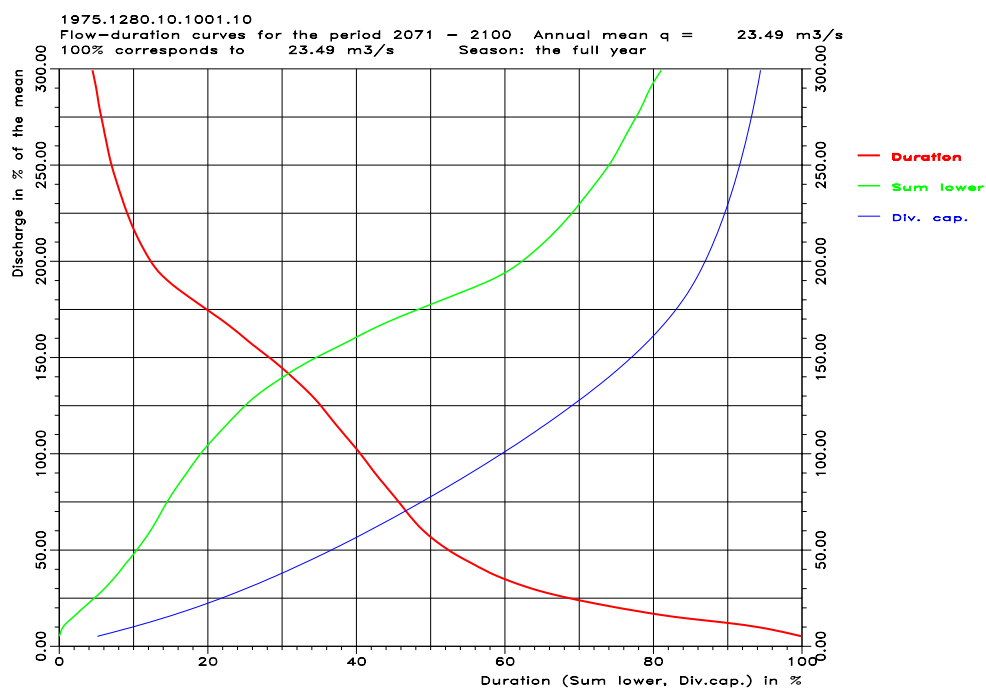
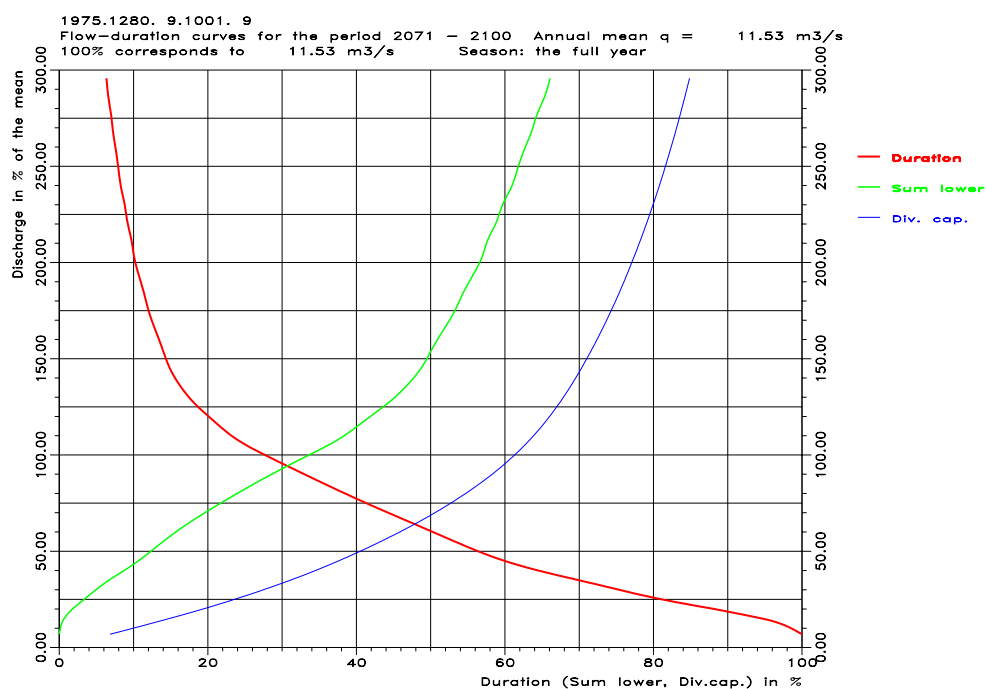


Figure F12. Curves for flow duration (red), sum lower (green) and diversion capacity (blue) for catchment 1280 Lungtenphug with precipitation and temperature input from climate projection Echam B1. Top: 2071-2100, time-variant glacier area, annual mean 12 m<sup>3</sup>/s. Bottom: 2071-2100, constant glacier area, annual mean 23 m<sup>3</sup>/s.

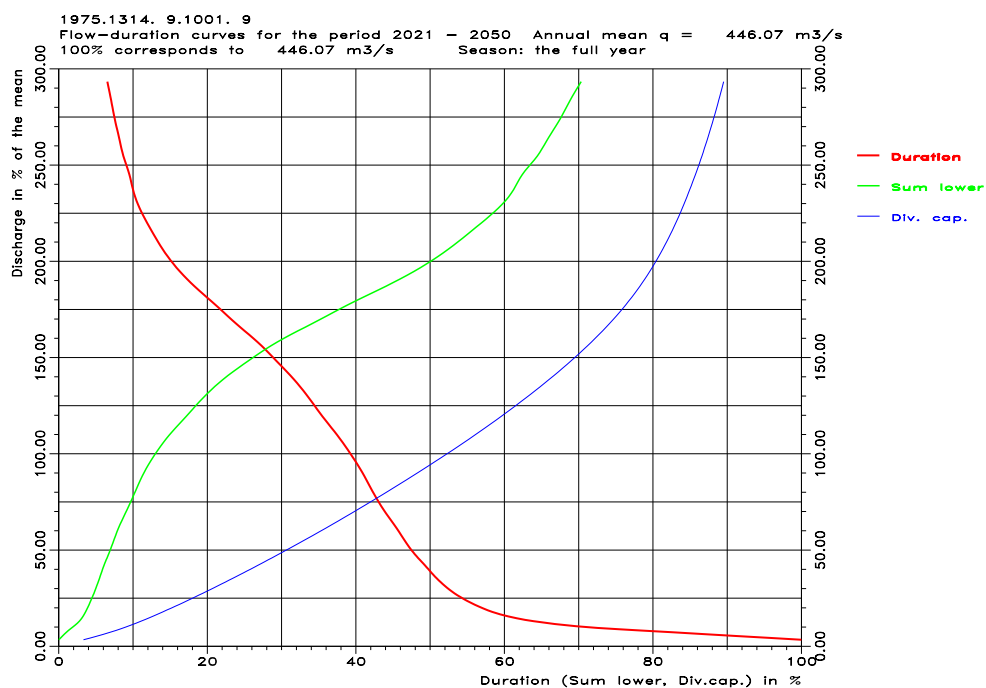
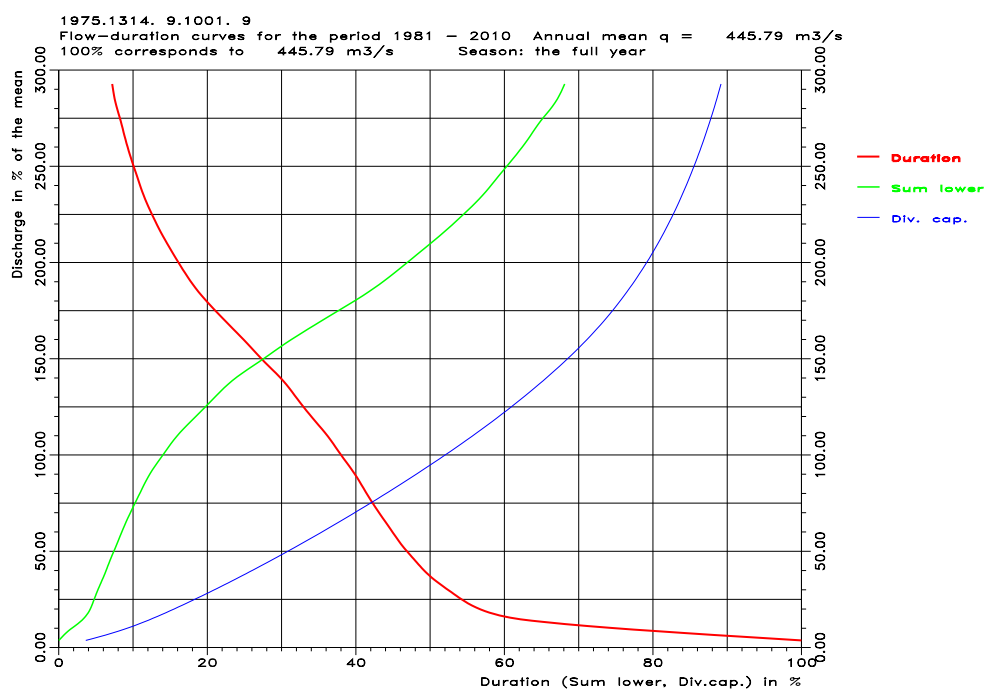


Figure F13. Curves for flow duration (red), sum lower (green) and diversion capacity (blue) for catchment 1314 Kerabari with precipitation and temperature input from climate projection Echam B1. Top: 1981-2010, constant glacier area, annual mean  $446 \text{ m}^3/\text{s}$ . Bottom: 2021-2050, time-variant glacier area, annual mean  $446 \text{ m}^3/\text{s}$ .



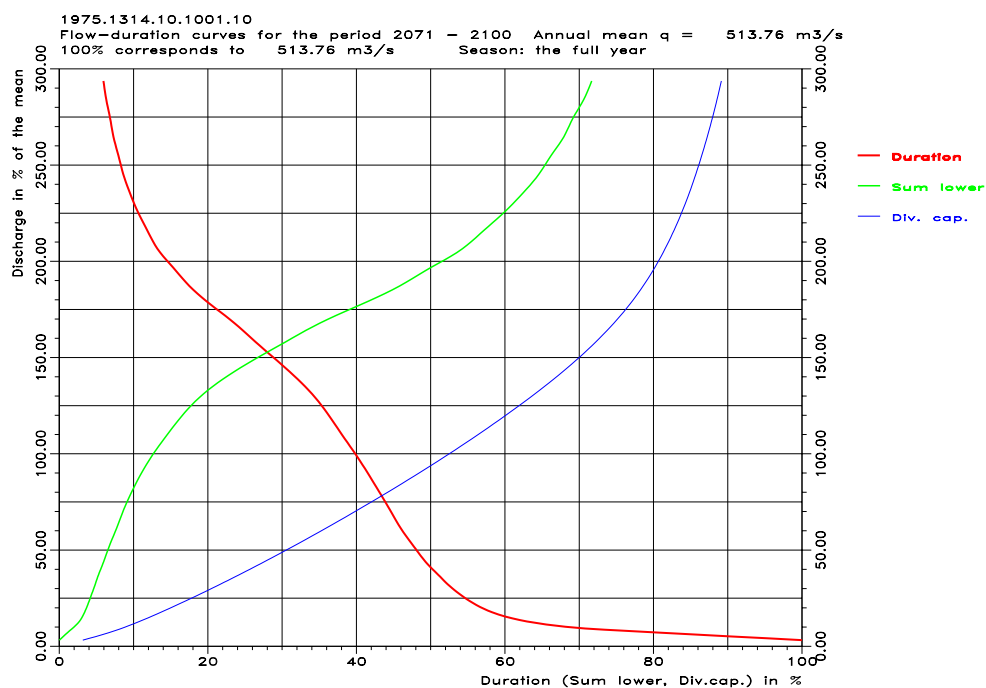
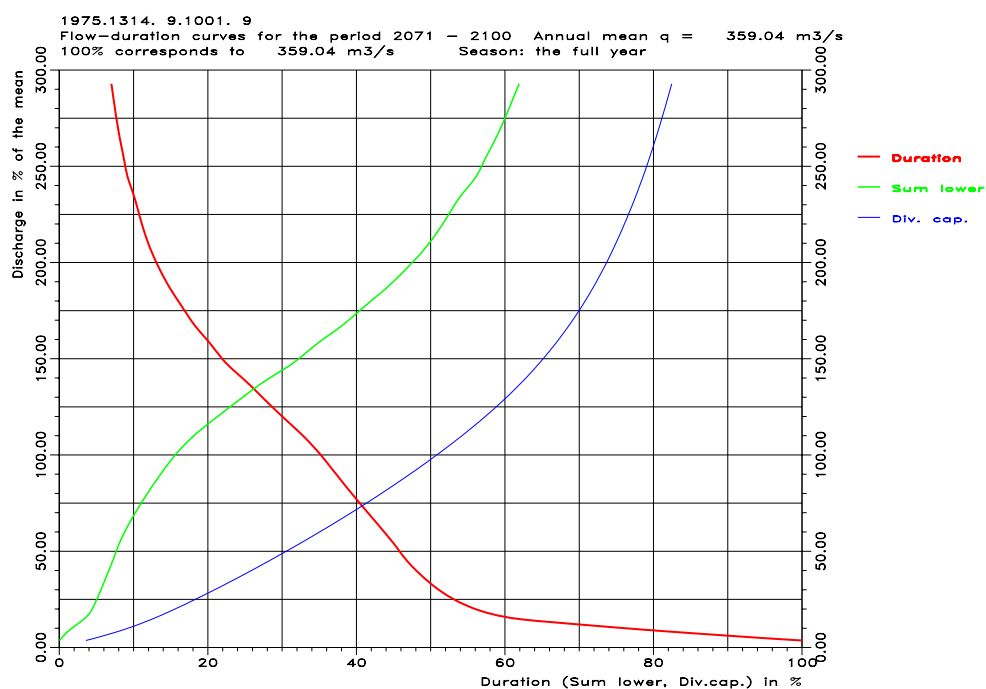


Figure F14. Curves for flow duration (red), sum lower (green) and diversion capacity (blue) for catchment 1314 Kerabari with precipitation and temperature input from climate projection Echam B1. Top: 2071-2100, time-variant glacier area, annual mean 359 m<sup>3</sup>/s. Bottom: 2071-2100, constant glacier area, annual mean 614 m<sup>3</sup>/s.

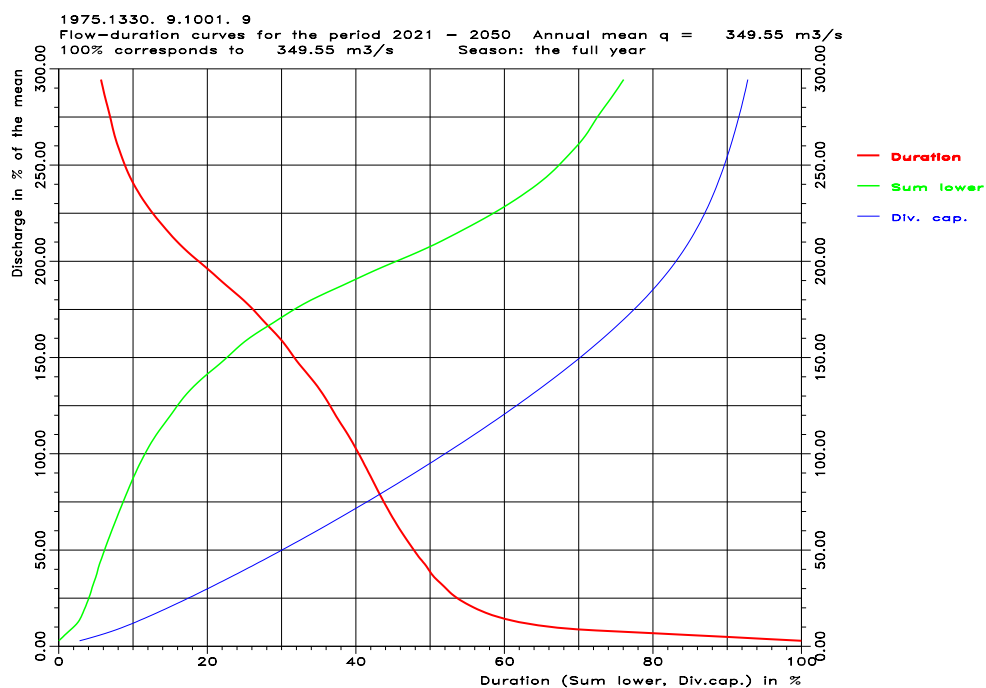
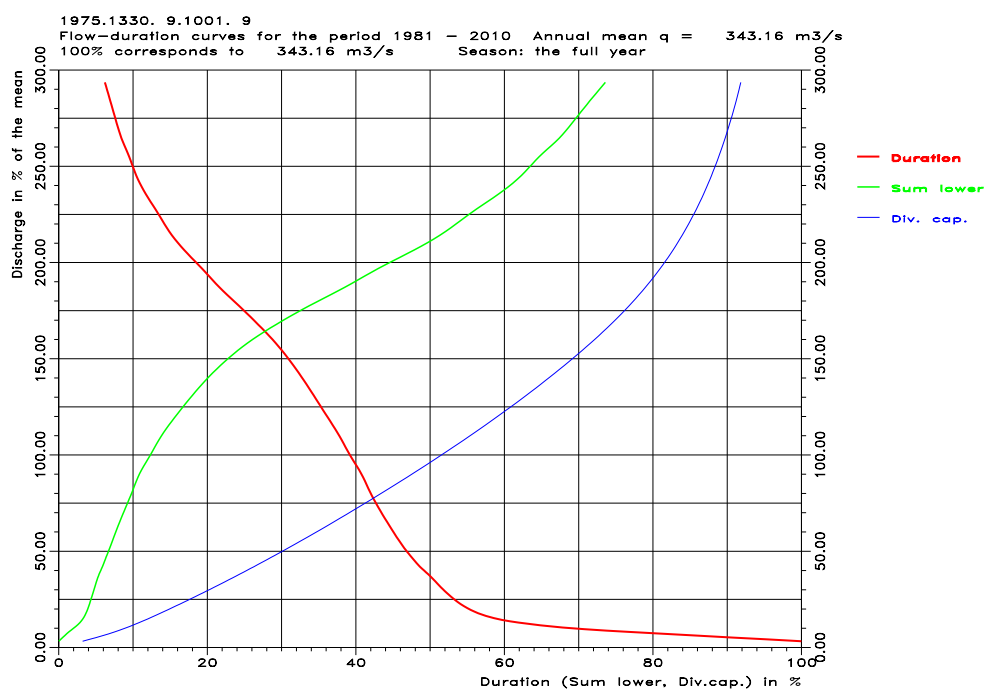


Figure F15. Curves for flow duration (red), sum lower (green) and diversion capacity (blue) for catchment 1330 Dobani with precipitation and temperature input from climate projection Ecam B1. Top: 1981-2010, constant glacier area, annual mean  $343 \text{ m}^3/\text{s}$ . Bottom: 2021-2050, time-variant glacier area, annual mean  $350 \text{ m}^3/\text{s}$ .

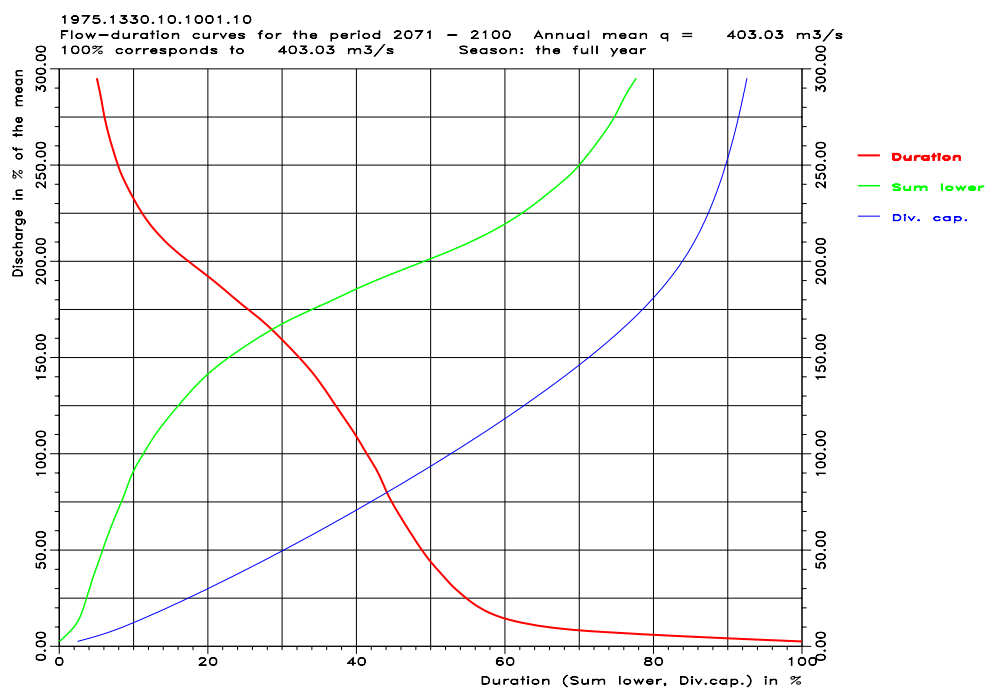
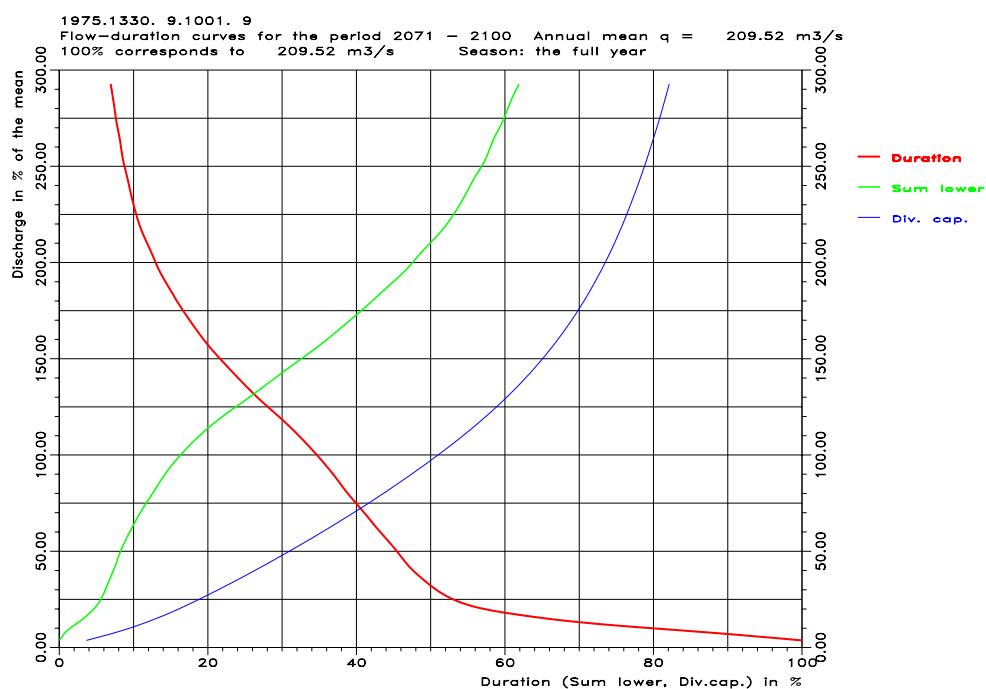


Figure F16. Curves for flow duration (red), sum lower (green) and diversion capacity (blue) for catchment 1330 Dobani with precipitation and temperature input from climate projection Echam B1. Top: 2071-2100, time-variant glacier area, annual mean 210 m<sup>3</sup>/s. Bottom: 2071-2100, constant glacier area, annual mean 403 m<sup>3</sup>/s.

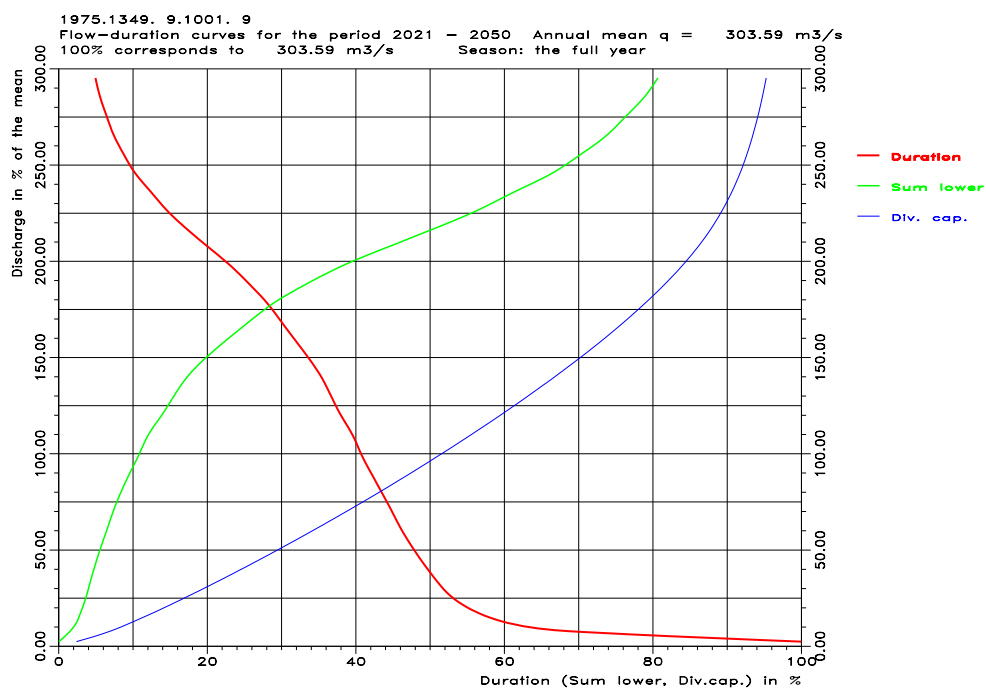
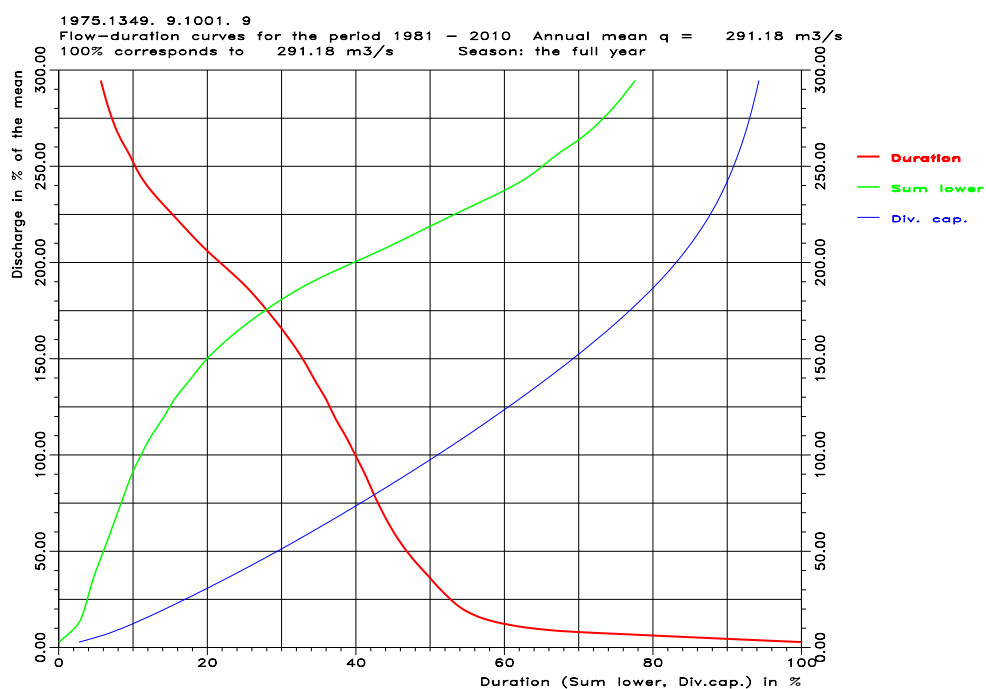


Figure F17. Curves for flow duration (red), sum lower (green) and diversion capacity (blue) for catchment 1349 Wangdirapids with precipitation and temperature input from climate projection Echem B1. Top: 1981-2010, constant glacier area, annual mean  $291 \text{ m}^3/\text{s}$ . Bottom: 2021-2050, time-variant glacier area, annual mean  $304 \text{ m}^3/\text{s}$ .

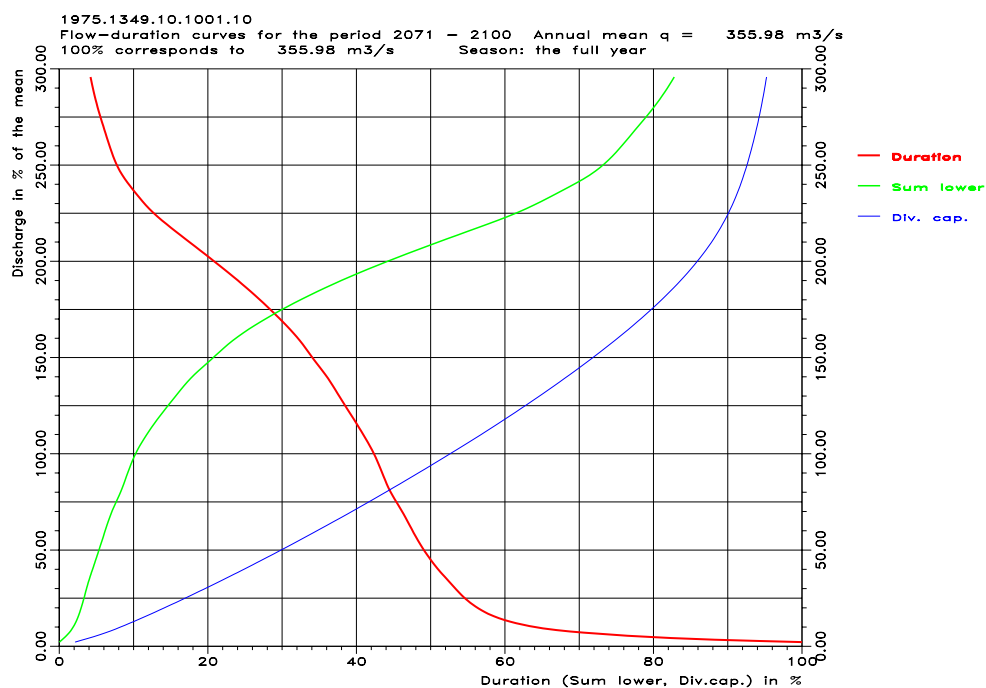
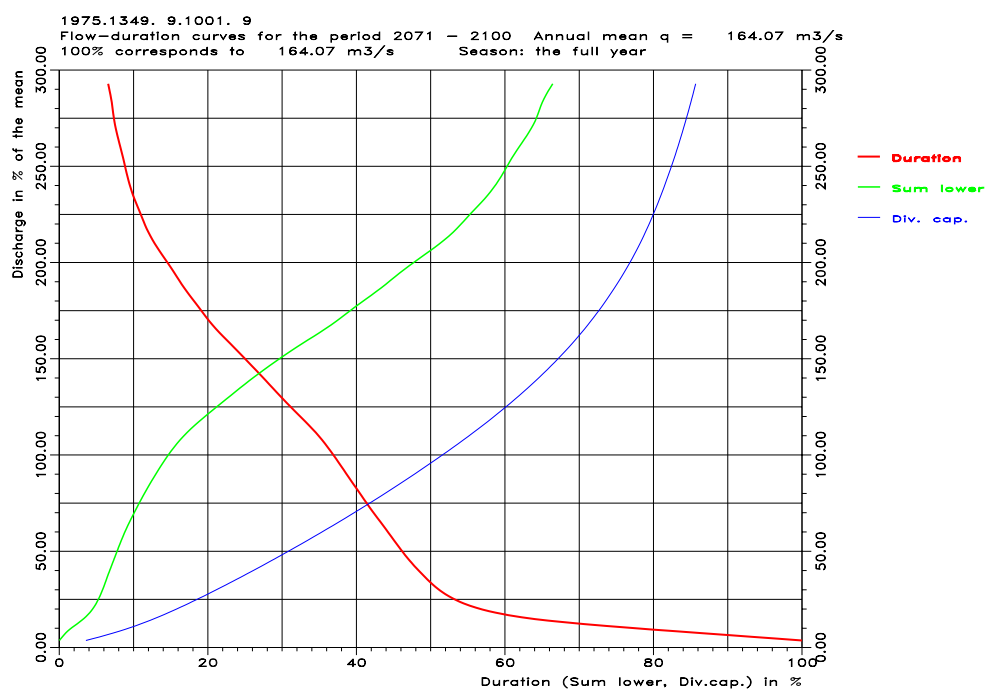


Figure F18. Curves for flow duration (red), sum lower (green) and diversion capacity (blue) for catchment 1349 Wangdirapids with precipitation and temperature input from climate projection Ecam B1. Top: 2071-2100, time-variant glacier area, annual mean  $164 \text{ m}^3/\text{s}$ . Bottom: 2071-2100, constant glacier area, annual mean  $356 \text{ m}^3/\text{s}$ .

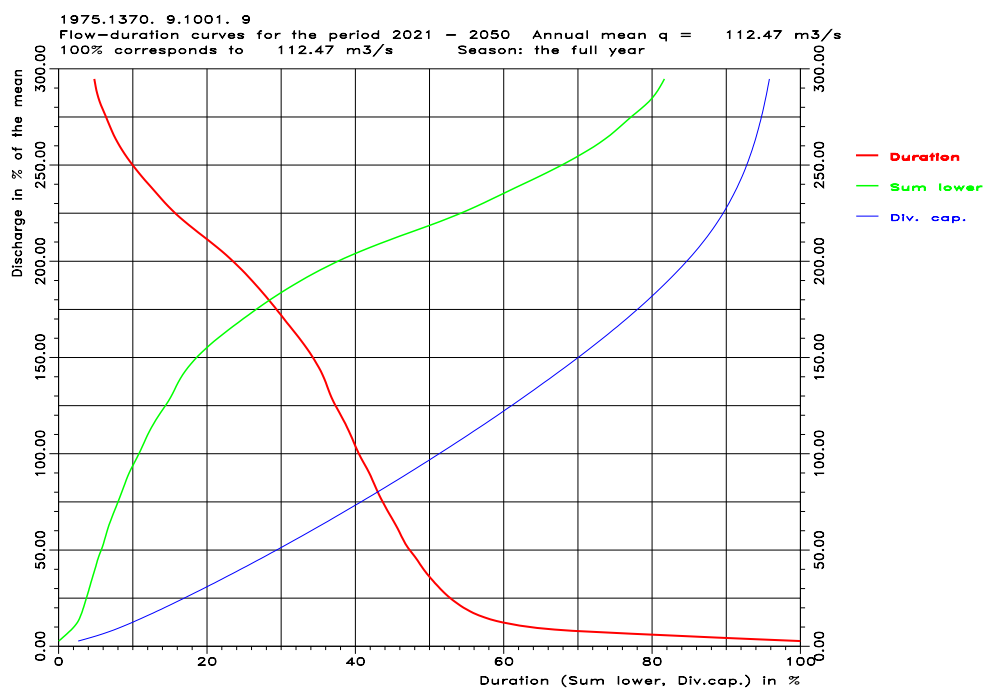
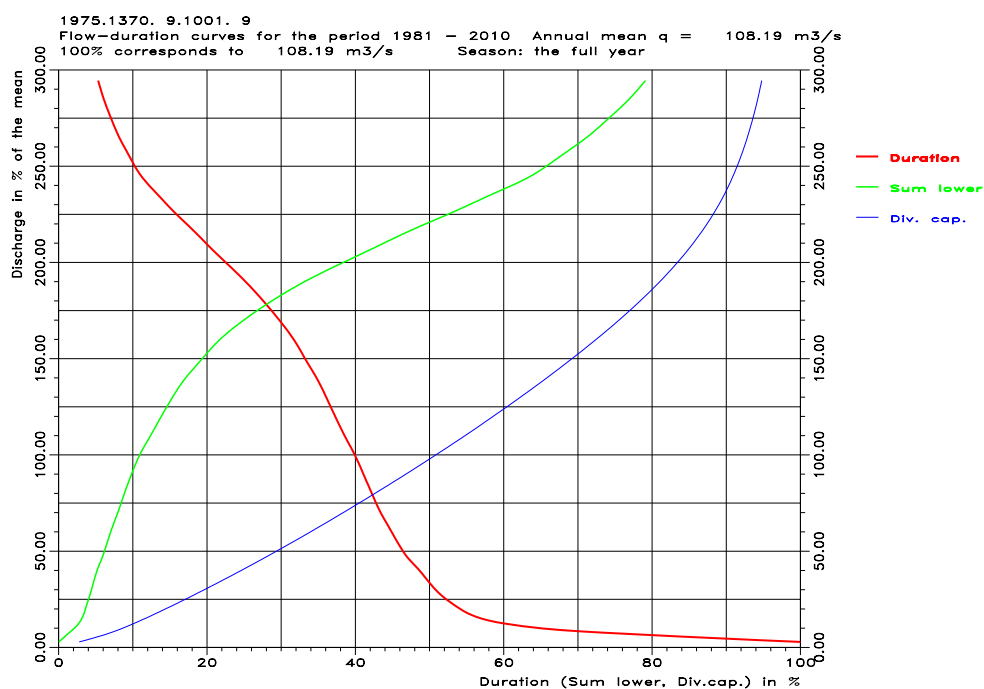


Figure F19. Curves for flow duration (red), sum lower (green) and diversion capacity (blue) for catchment 1370 Yebesa with precipitation and temperature input from climate projection Echam B1. Top: 1981-2010, constant glacier area, annual mean  $108 \text{ m}^3/\text{s}$ . Bottom: 2021-2050, time-variant glacier area, annual mean  $112 \text{ m}^3/\text{s}$

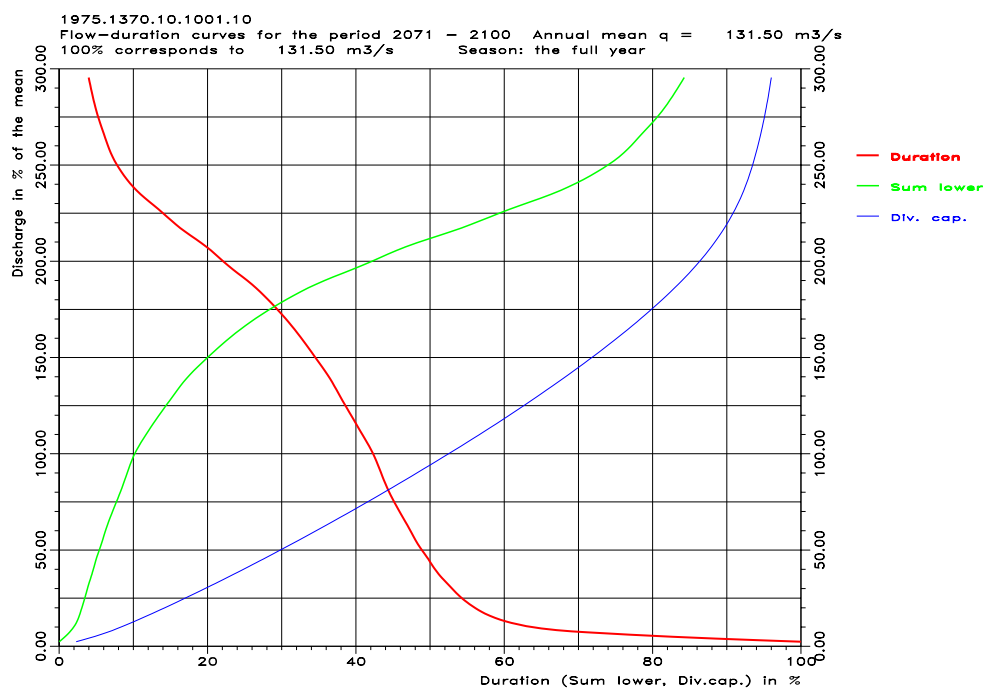
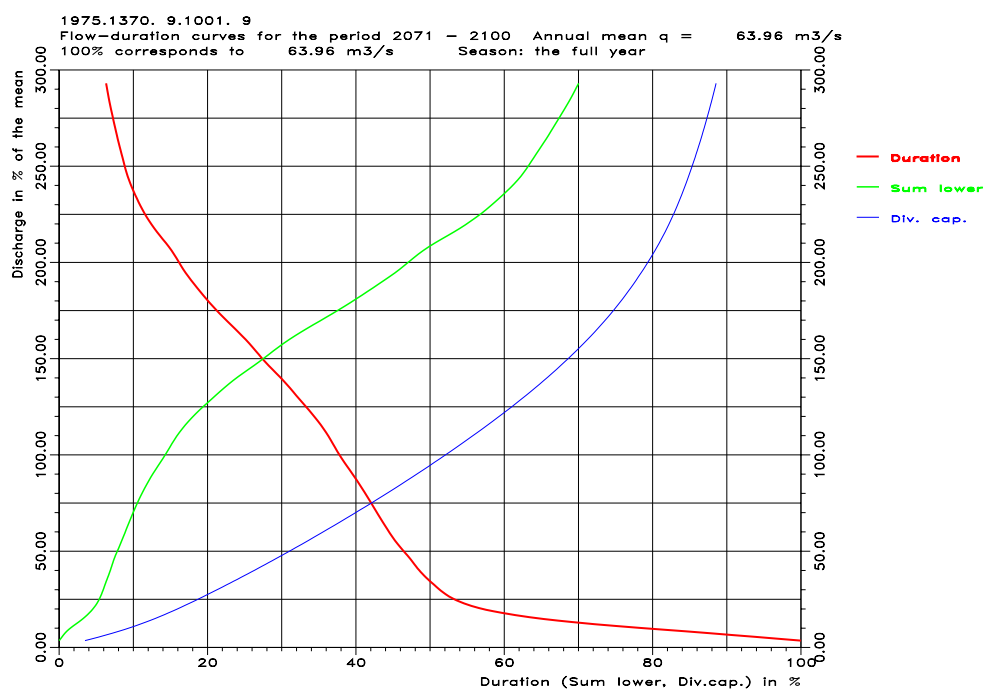


Figure F20. Curves for flow duration (red), sum lower (green) and diversion capacity (blue) for catchment 1370 Yebesa with precipitation and temperature input from climate projection Echam B1. Top: 2071-2100, time-variant glacier area, annual mean 64 m<sup>3</sup>/s. Bottom: 2071-2100, constant glacier area, annual mean 132 m<sup>3</sup>/s.

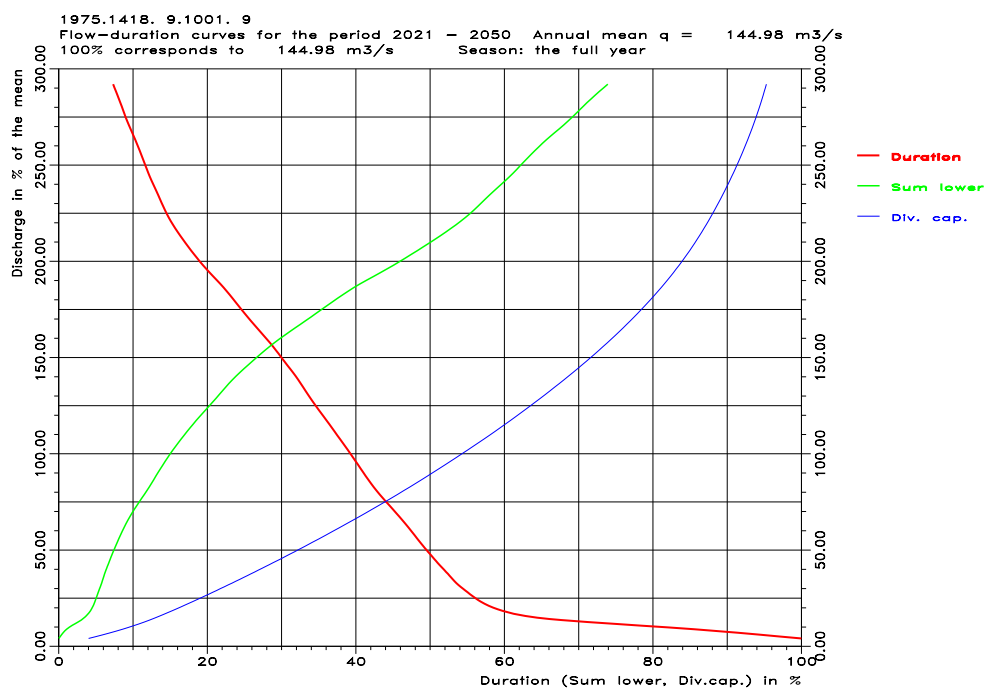
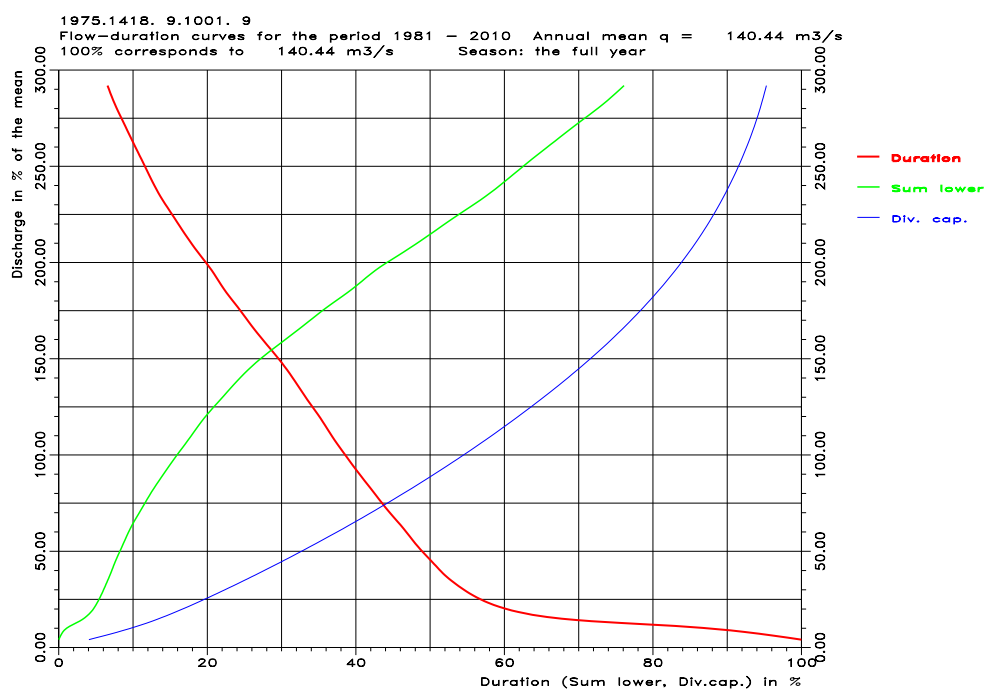


Figure F21. Curves for flow duration (red), sum lower (green) and diversion capacity (blue) for catchment 1418 Tingtibi with precipitation and temperature input from climate projection Ecam B1. Top: 1981-2010, constant glacier area, annual mean  $140 \text{ m}^3/\text{s}$ . Bottom: 2021-2050, time-variant glacier area, annual mean  $145 \text{ m}^3/\text{s}$ .



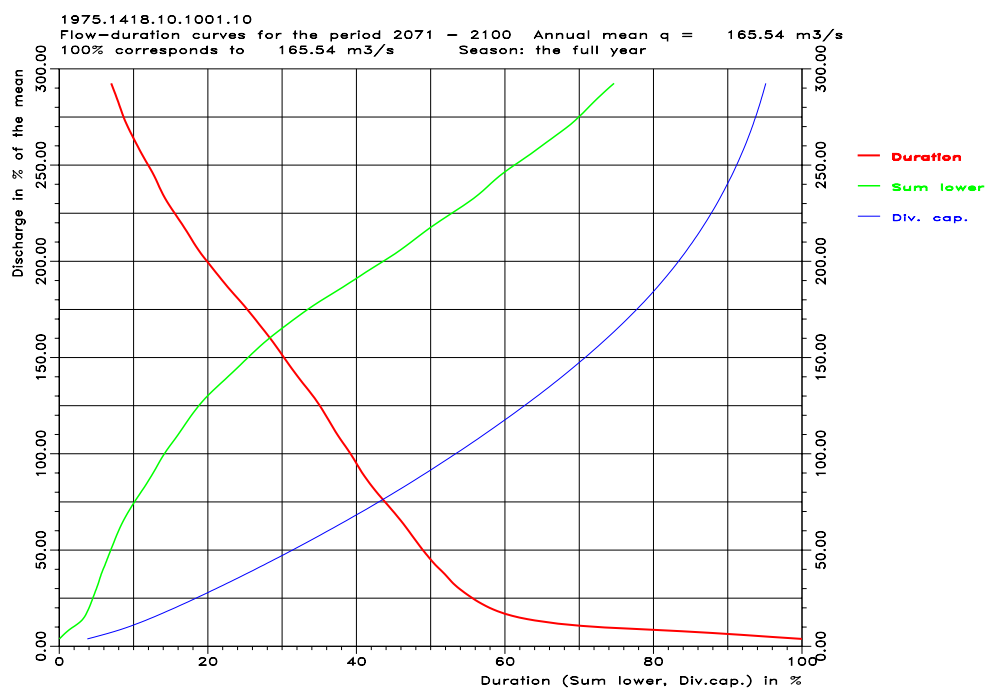
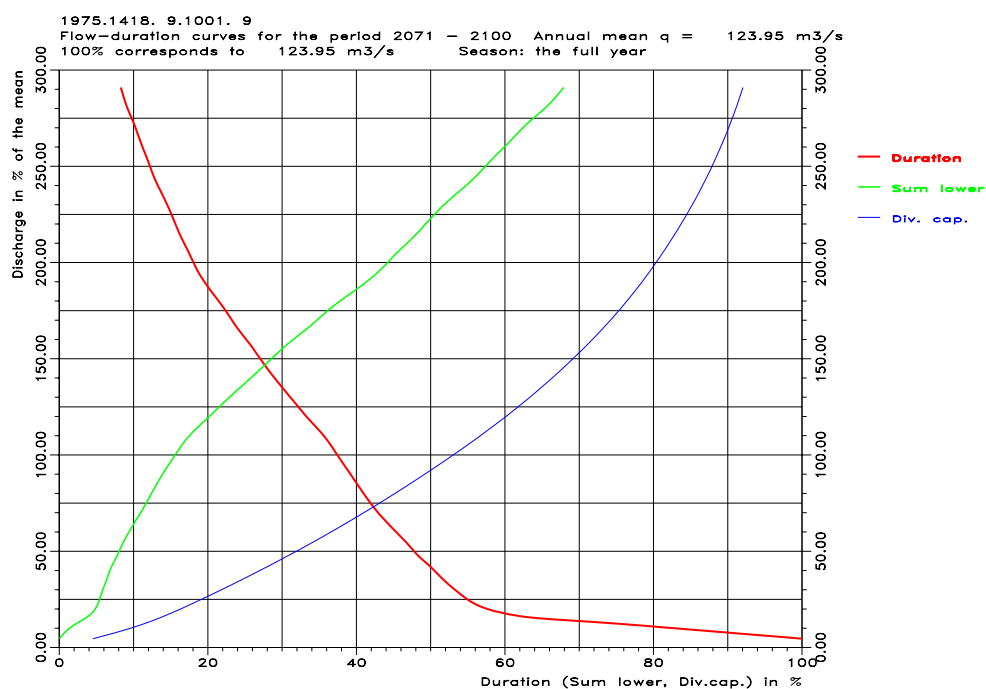


Figure F22. Curves for flow duration (red), sum lower (green) and diversion capacity (blue) for catchment 1418 Tingtibi with precipitation and temperature input from climate projection Echam B1. Top: 2071-2100, time-variant glacier area, annual mean 124 m<sup>3</sup>/s. Bottom: 2071-2100, constant glacier area, annual mean 166 m<sup>3</sup>/s.

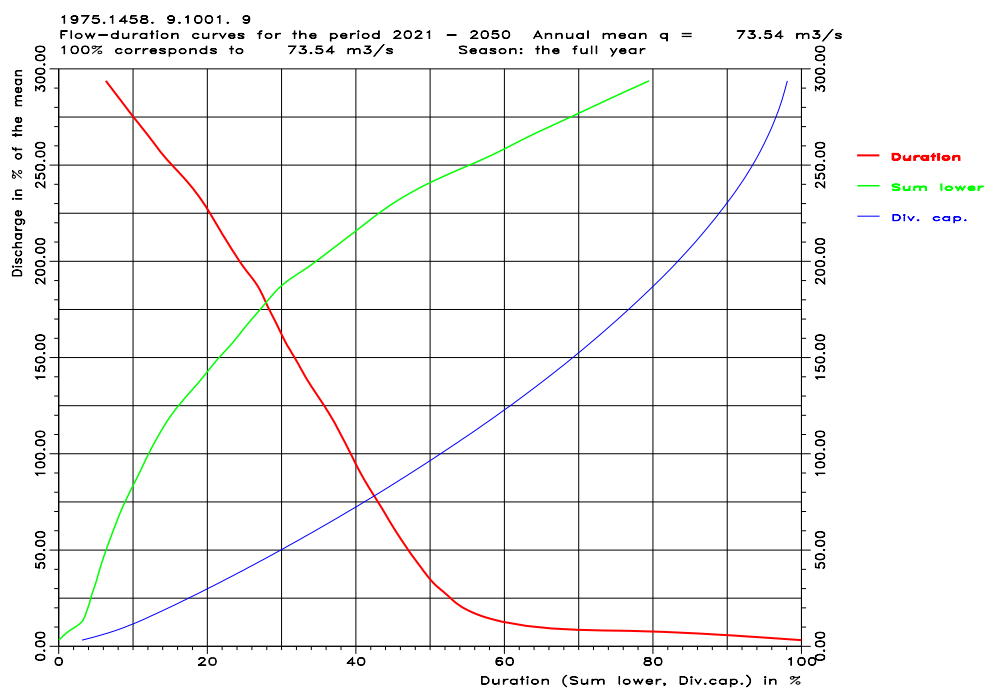
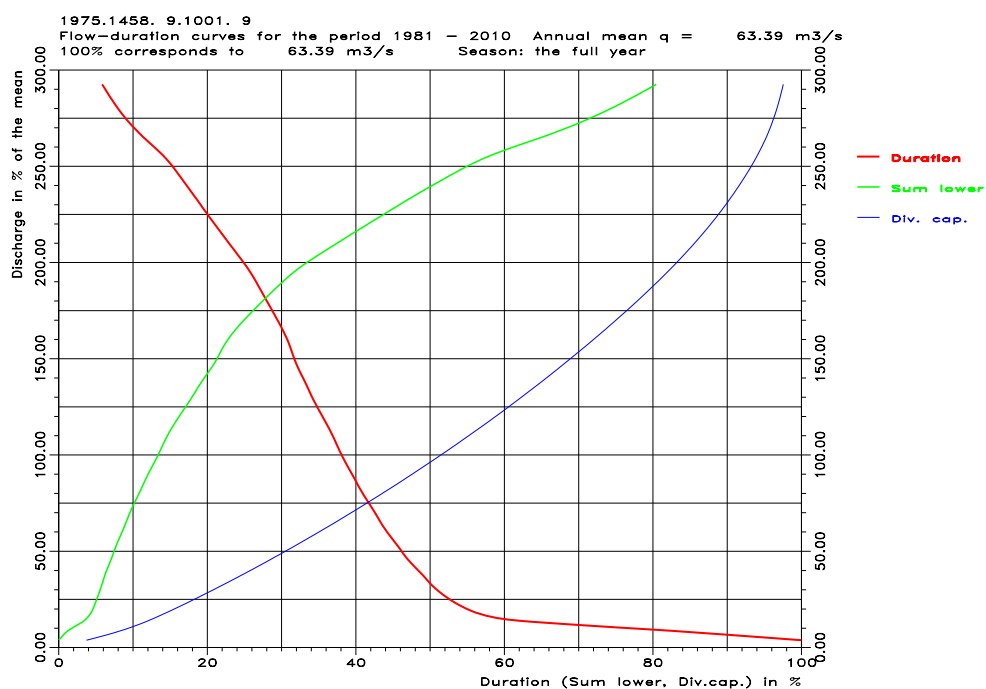


Figure F23. Curves for flow duration (red), sum lower (green) and diversion capacity (blue) for catchment 1458 Bjizam with precipitation and temperature input from climate projection Echam B1. Top: 1981-2010, constant glacier area, annual mean  $63 \text{ m}^3/\text{s}$ . Bottom: 2021-2050, time-variant glacier area, annual mean  $74 \text{ m}^3/\text{s}$ .

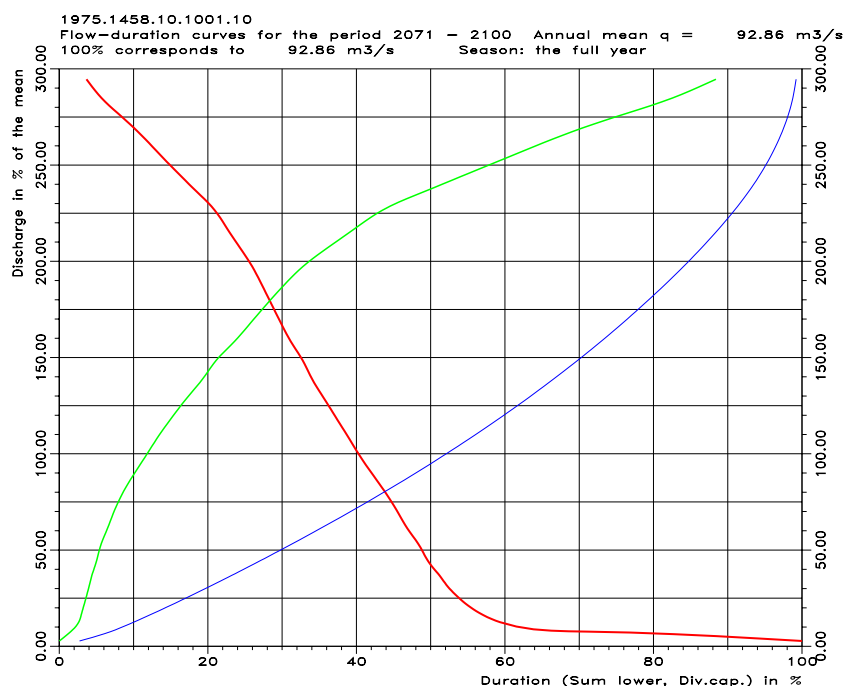
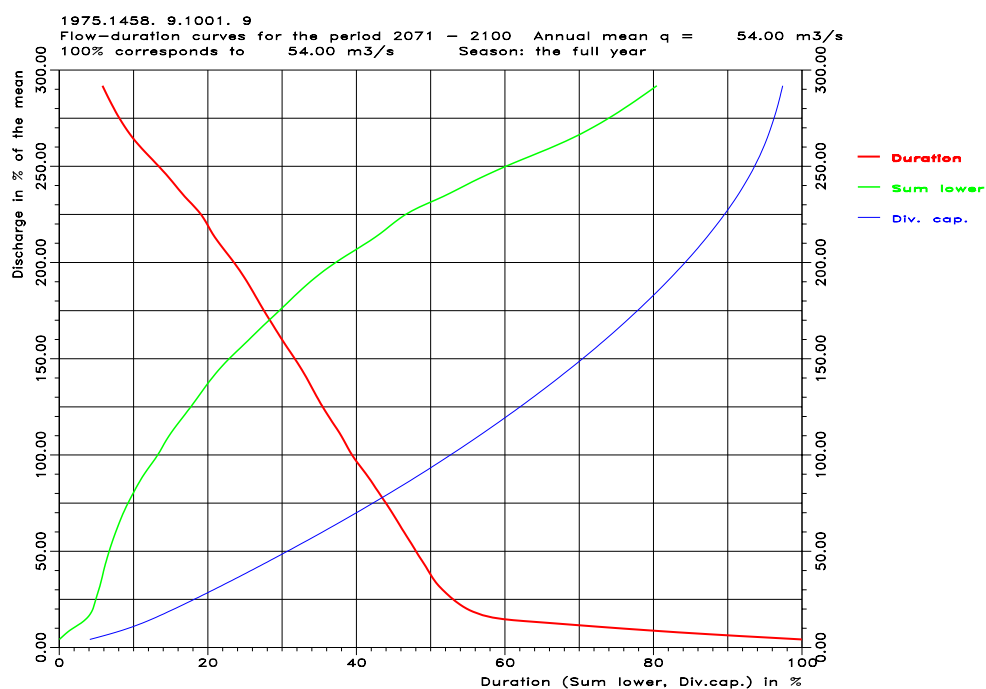


Figure F24. Curves for flow duration (red), sum lower (green) and diversion capacity (blue) for catchment 1458 Bjizam with precipitation and temperature input from climate projection Echam B1. Top: 2071-2100, time-variant glacier area, annual mean 54 m<sup>3</sup>/s. Bottom: 2071-2100, constant glacier area, annual mean 93 m<sup>3</sup>/s.

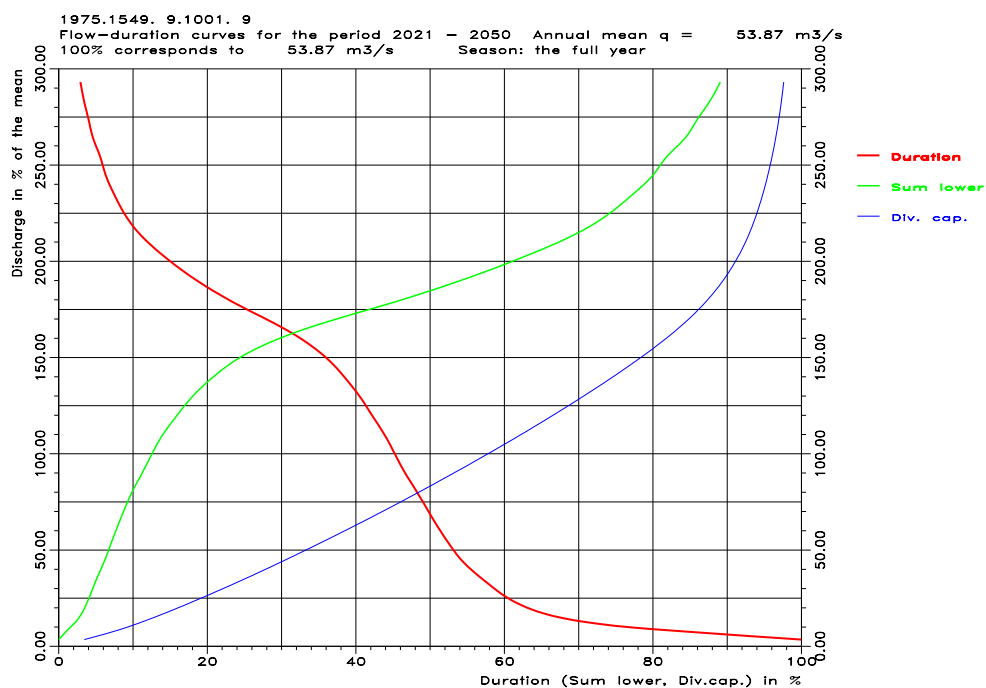
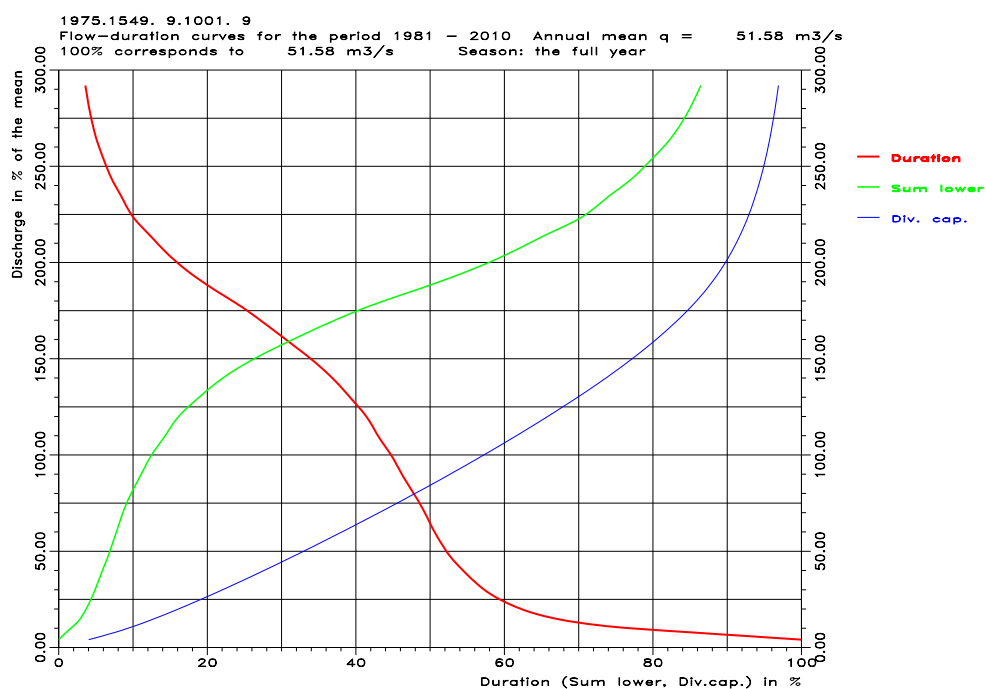


Figure F25. Curves for flow duration (red), sum lower (green) and diversion capacity (blue) for catchment 1549 Kurjey with precipitation and temperature input from climate projection Echam B1. Top: 1981-2010, constant glacier area, annual mean  $52 \text{ m}^3/\text{s}$ . Bottom: 2021-2050, time-variant glacier area, annual mean  $54 \text{ m}^3/\text{s}$ .

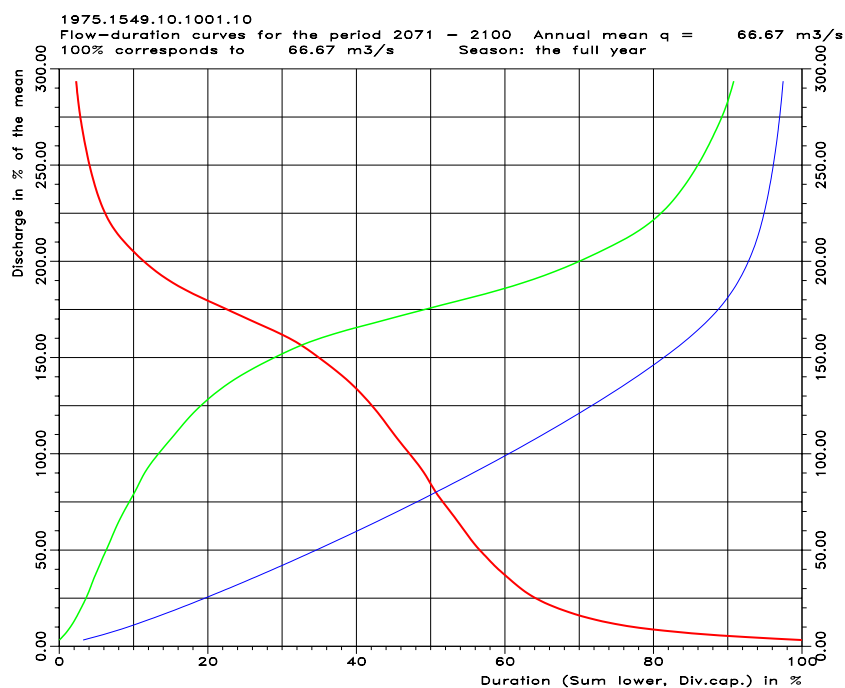
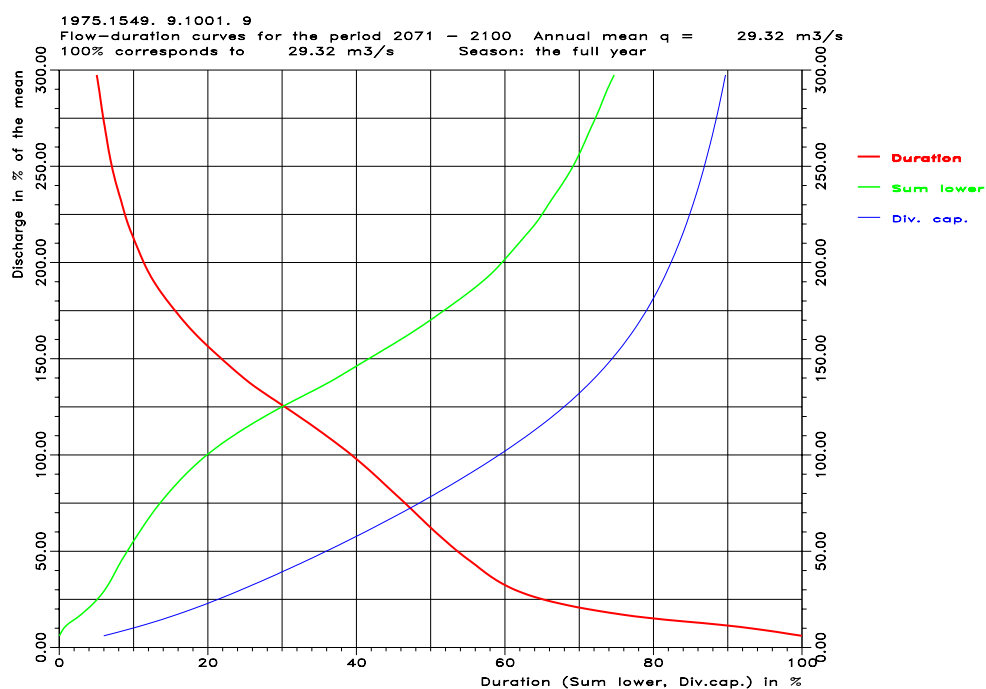


Figure F26. Curves for flow duration (red), sum lower (green) and diversion capacity (blue) for catchment 1549 Kurje with precipitation and temperature input from climate projection Echam B1. Top: 2071-2100, time-variant glacier area, annual mean 29 m<sup>3</sup>/s. Bottom: 2071-2100, constant glacier area, annual mean 67 m<sup>3</sup>/s.

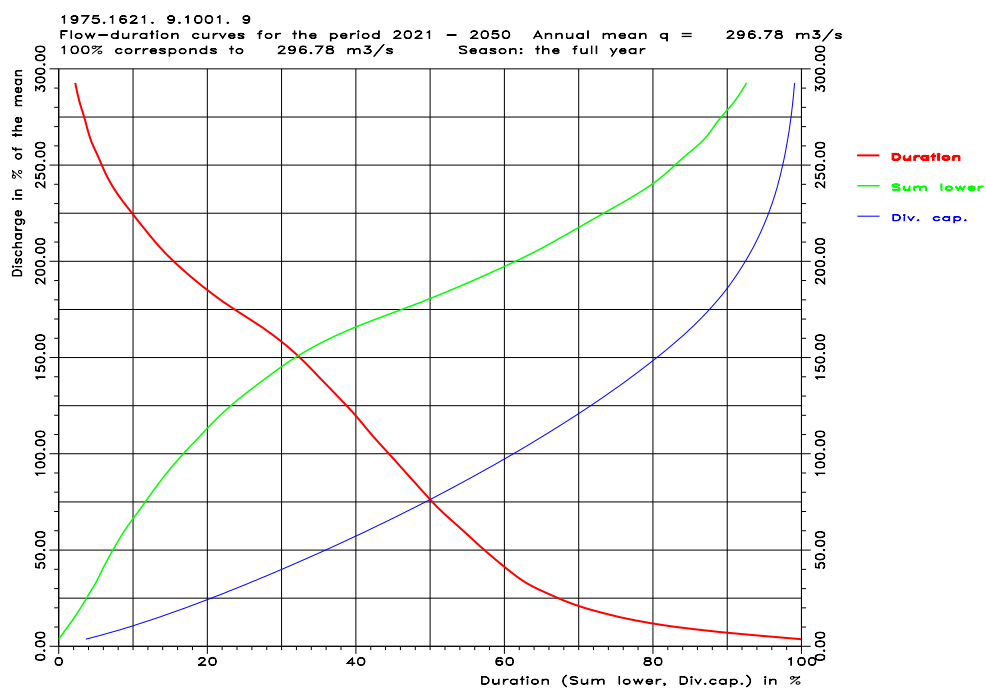
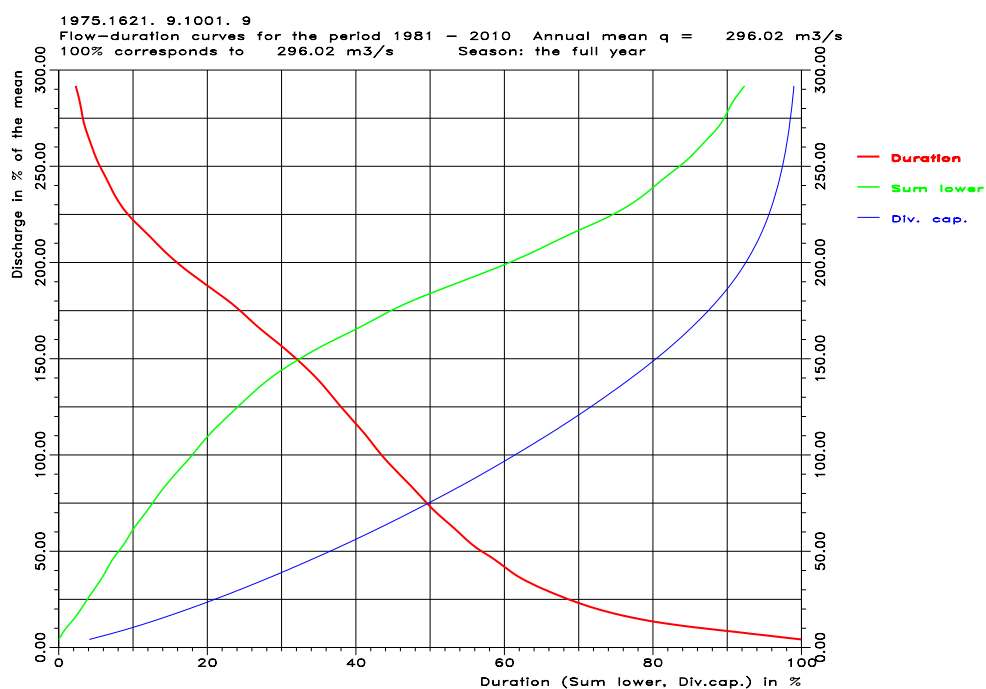


Figure F27. Curves for flow duration (red), sum lower (green) and diversion capacity (blue) for catchment 1621 Kurizampa with precipitation and temperature input from climate projection Echem B1. Top: 1981-2010, constant glacier area, annual mean  $296 \text{ m}^3/\text{s}$ . Bottom: 2021-2050, time-variant glacier area, annual mean  $297 \text{ m}^3/\text{s}$ .

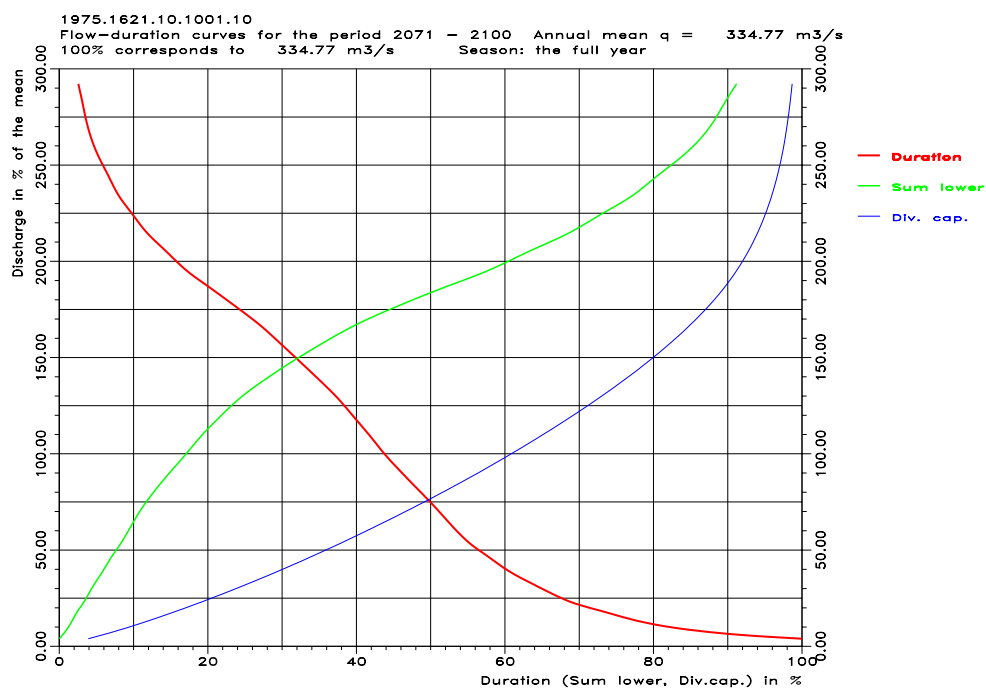
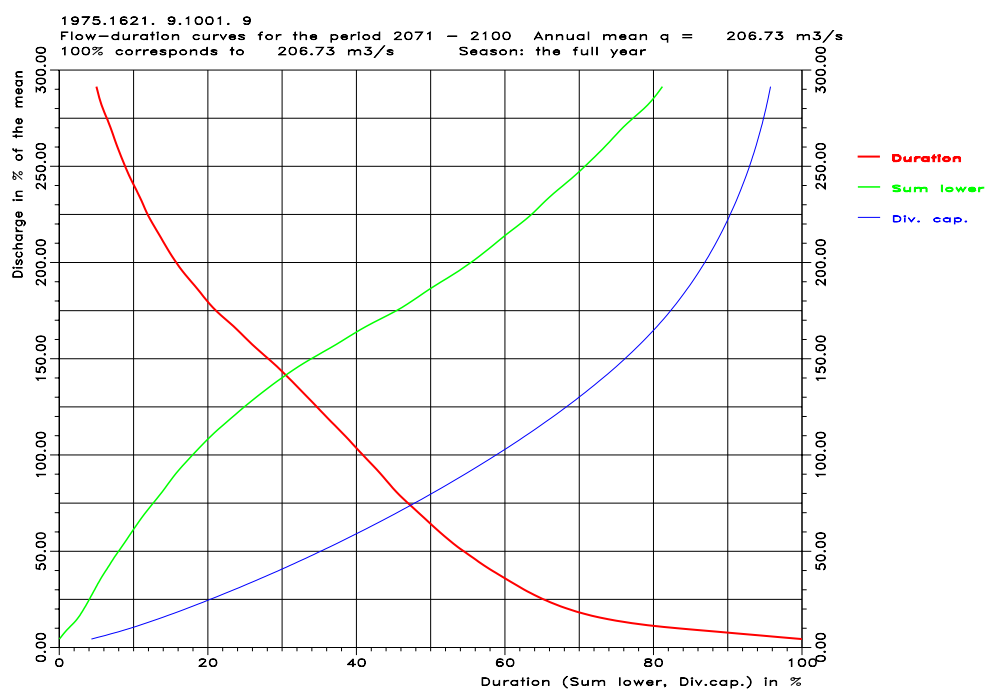


Figure F28. Curves for flow duration (red), sum lower (green) and diversion capacity (blue) for catchment 1621 Kurizampa with precipitation and temperature input from climate projection Echam B1. Top: 2071-2100, time-variant glacier area, annual mean 209 m<sup>3</sup>/s. Bottom: 2071-2100, constant glacier area, annual mean 335 m<sup>3</sup>/s.

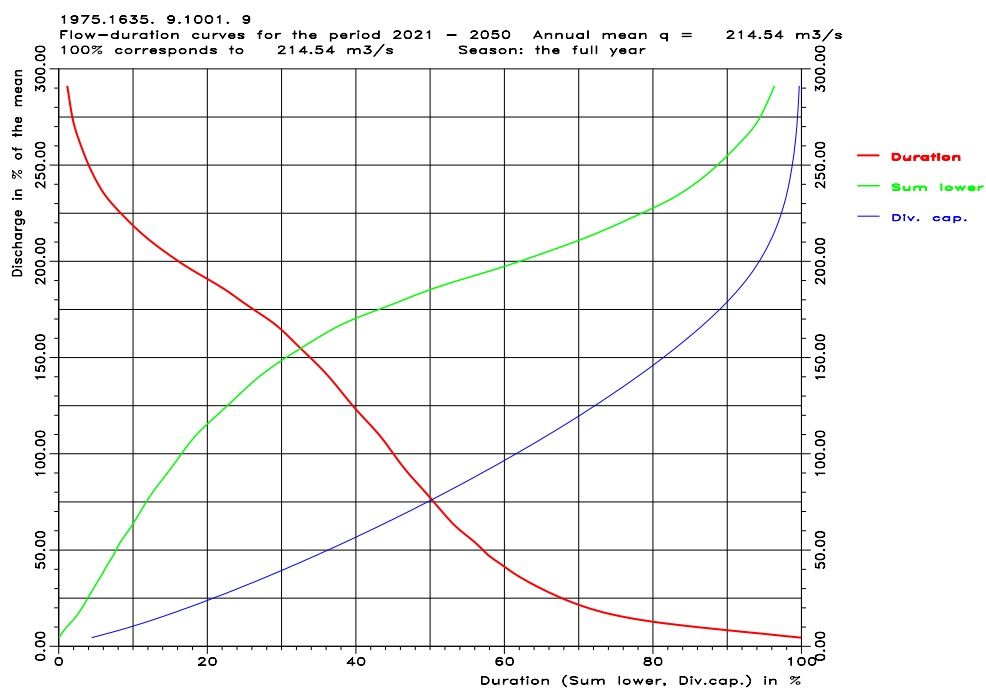
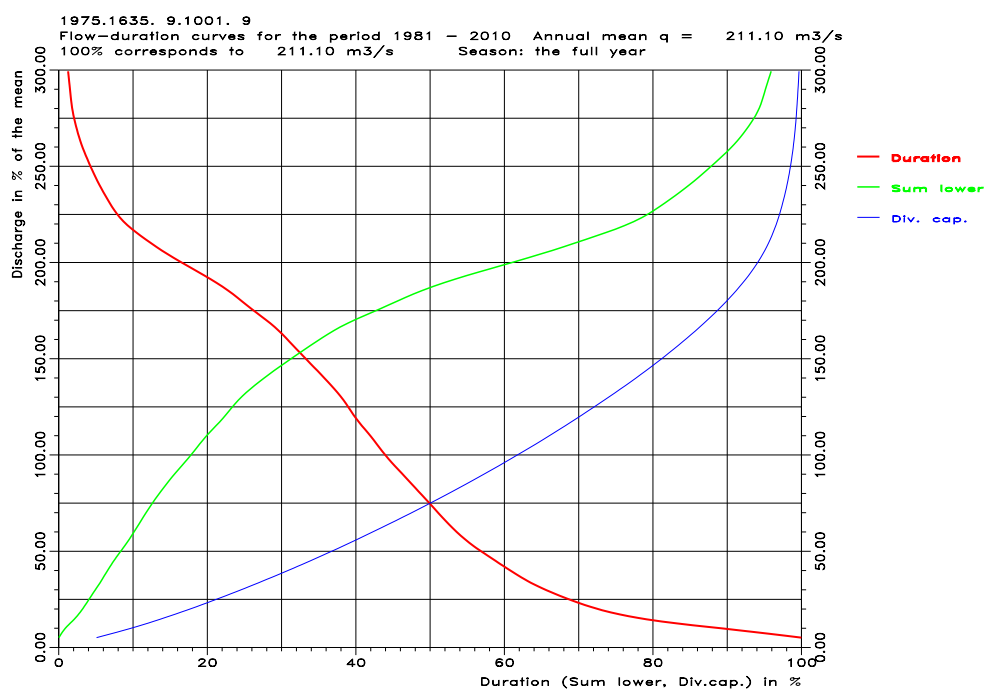


Figure F29. Curves for flow duration (red), sum lower (green) and diversion capacity (blue) for catchment 1635 Autsho with precipitation and temperature input from climate projection Echam B1. Top: 1981-2010, constant glacier area, annual mean  $211 \text{ m}^3/\text{s}$ . Bottom: 2021-2050, time-variant glacier area, annual mean  $215 \text{ m}^3/\text{s}$ .



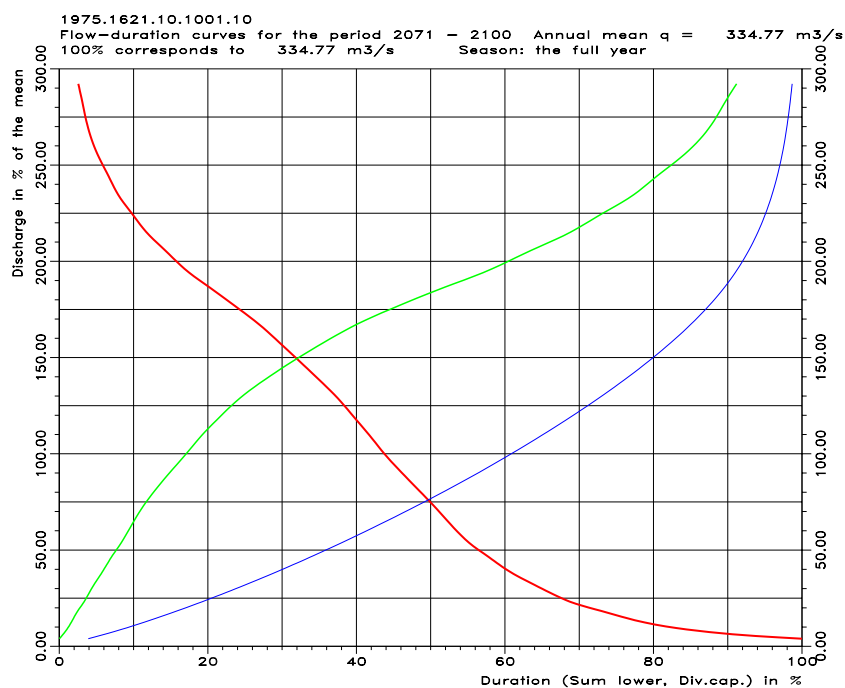
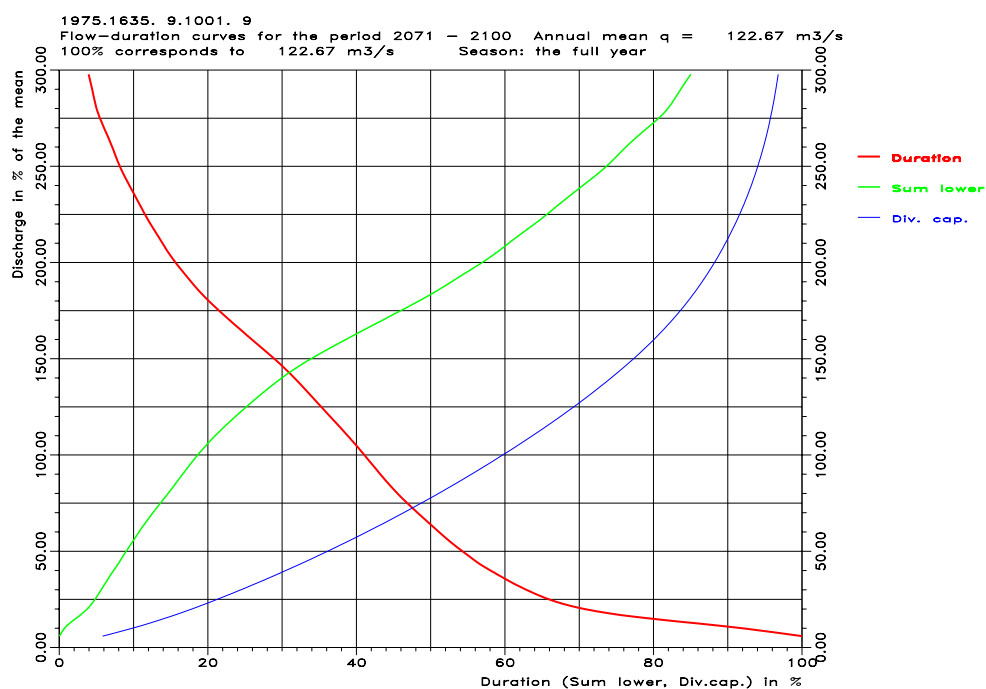


Figure F30. Curves for flow duration (red), sum lower (green) and diversion capacity (blue) for catchment 1635 Autsho with precipitation and temperature input from climate projection Echam B1. Top: 2071-2100, time-variant glacier area, annual mean 123 m<sup>3</sup>/s. Bottom: 2071-2100, constant glacier area, annual mean 335 m<sup>3</sup>/s.

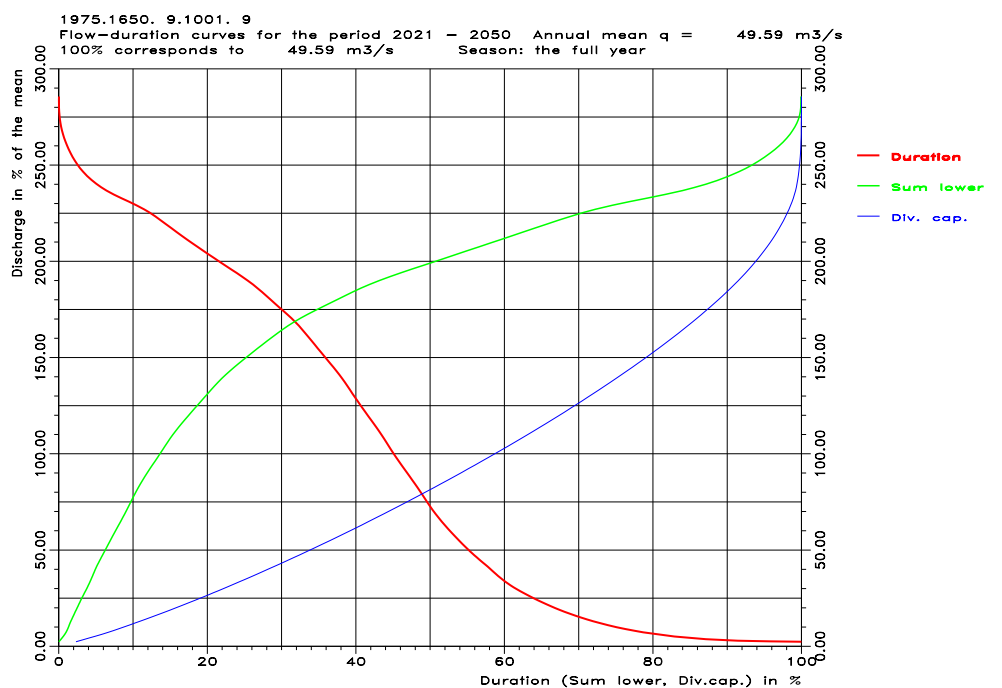
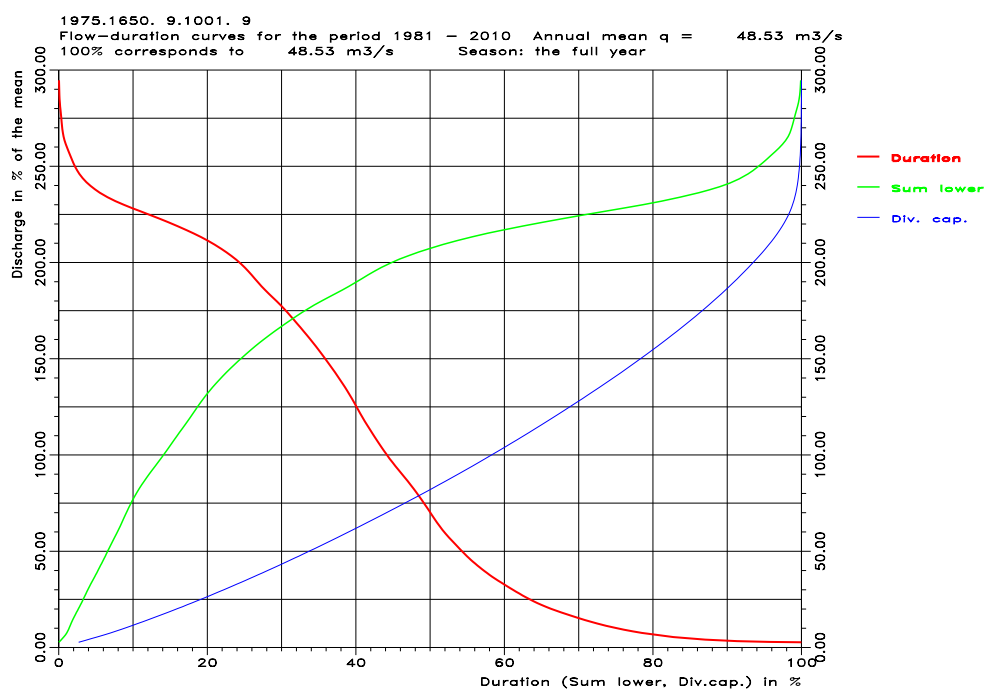


Figure F31. Curves for flow duration (red), sum lower (green) and diversion capacity (blue) for catchment 1650 Sumpa with precipitation and temperature input from climate projection Ecam B1. Top: 1981-2010, constant glacier area, annual mean  $49 \text{ m}^3/\text{s}$ . Bottom: 2021-2050, time-variant glacier area, annual mean  $50 \text{ m}^3/\text{s}$ .

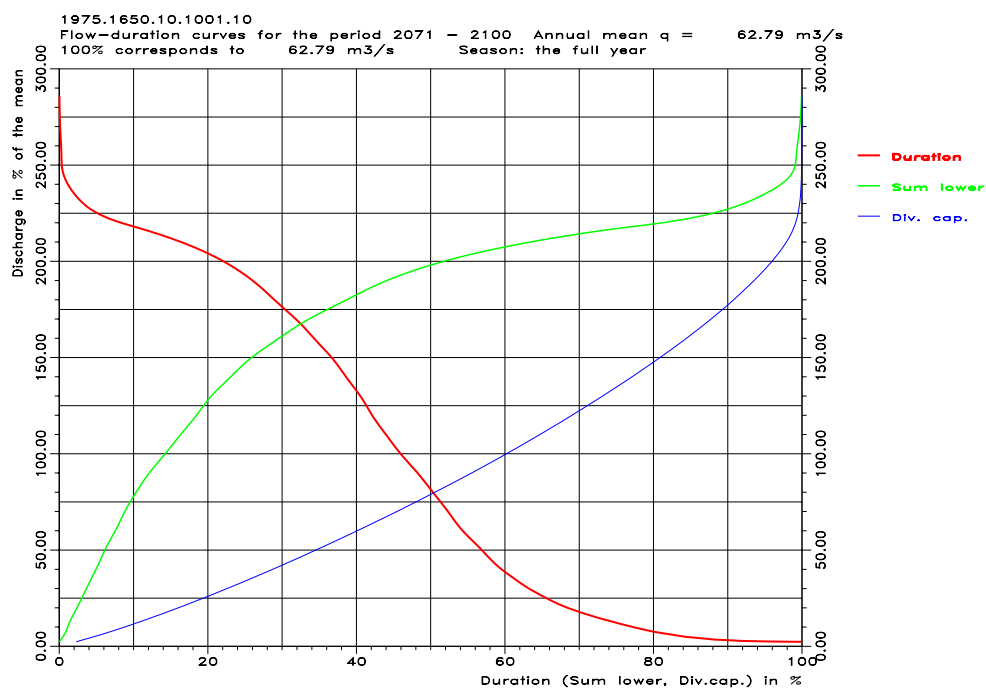
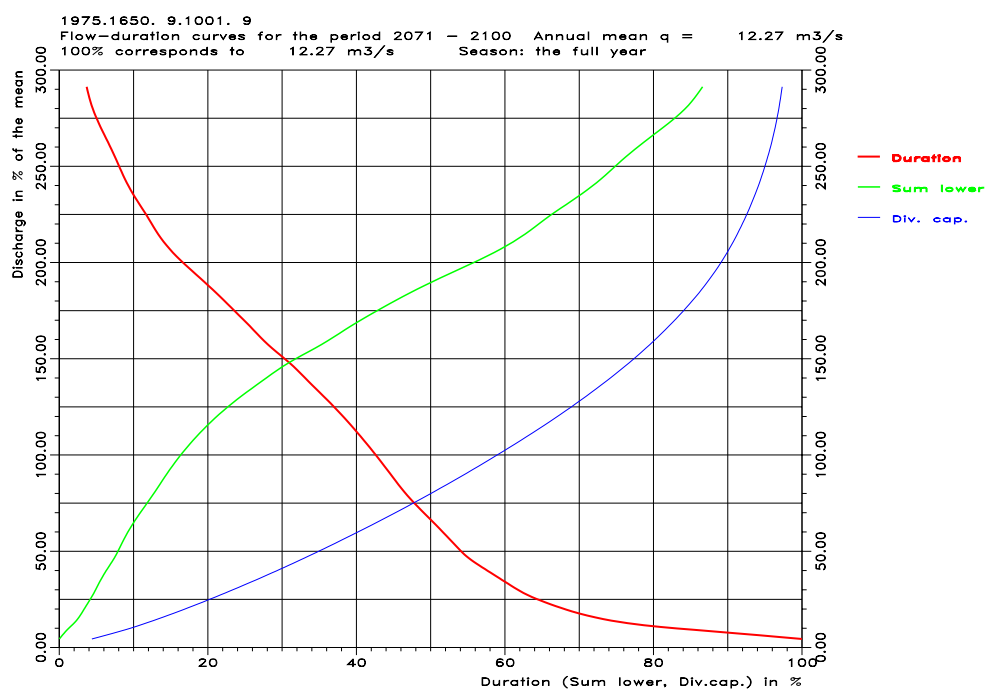


Figure F32. Curves for flow duration (red), sum lower (green) and diversion capacity (blue) for catchment 1650 Sumpa with precipitation and temperature input from climate projection Echam B1. Top: 2071-2100, time-variant glacier area, annual mean 12 m<sup>3</sup>/s. Bottom: 2071-2100, constant glacier area, annual mean 63 m<sup>3</sup>/s.

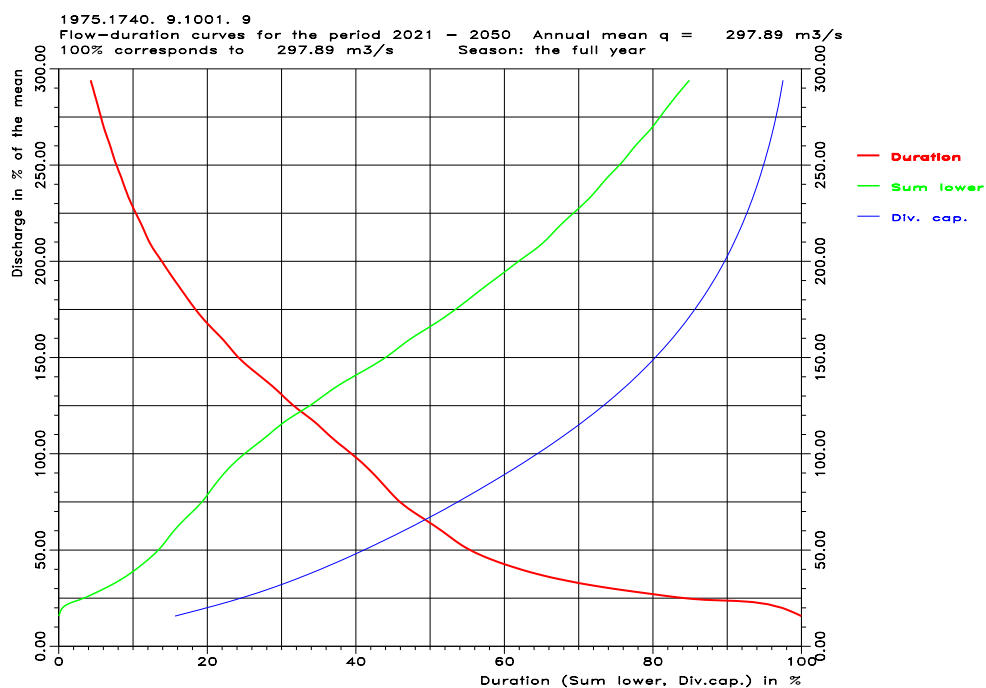
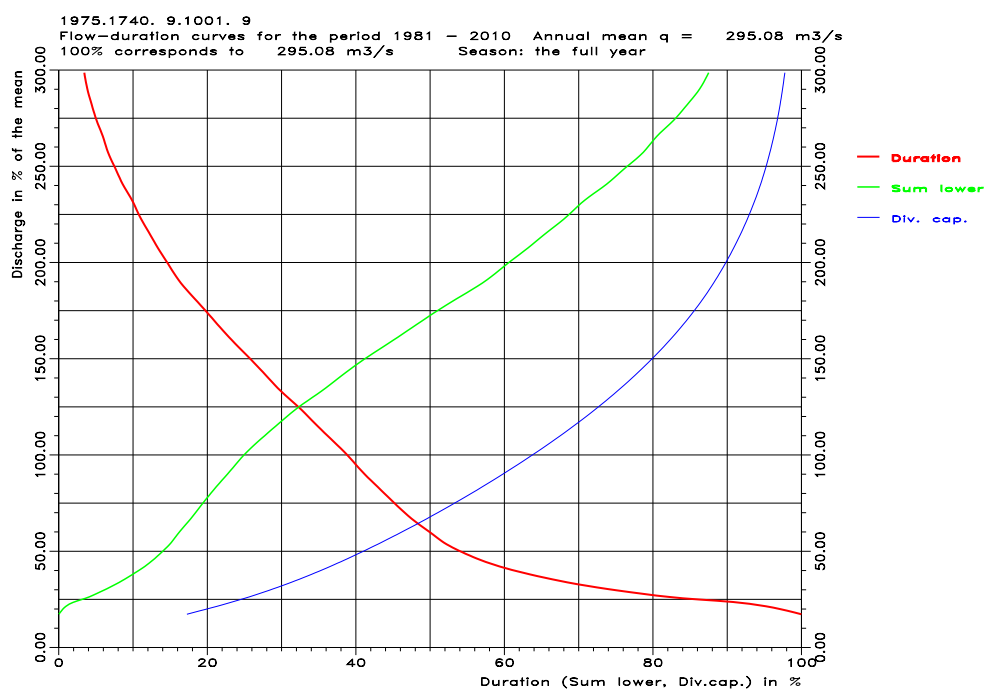


Figure F33. Curves for flow duration (red), sum lower (green) and diversion capacity (blue) for catchment 1740 Uzorong with precipitation and temperature input from climate projection Echam B1. Top: 1981-2010, constant glacier area, annual mean  $295 \text{ m}^3/\text{s}$ . Bottom: 2021-2050, time-variant glacier area, annual mean  $298 \text{ m}^3/\text{s}$ .

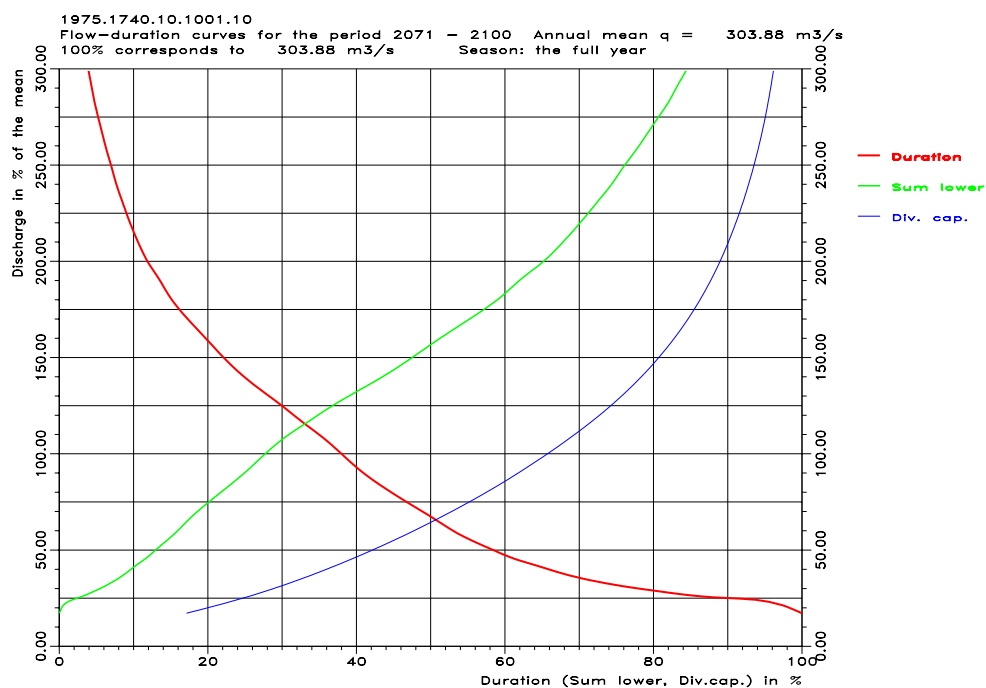
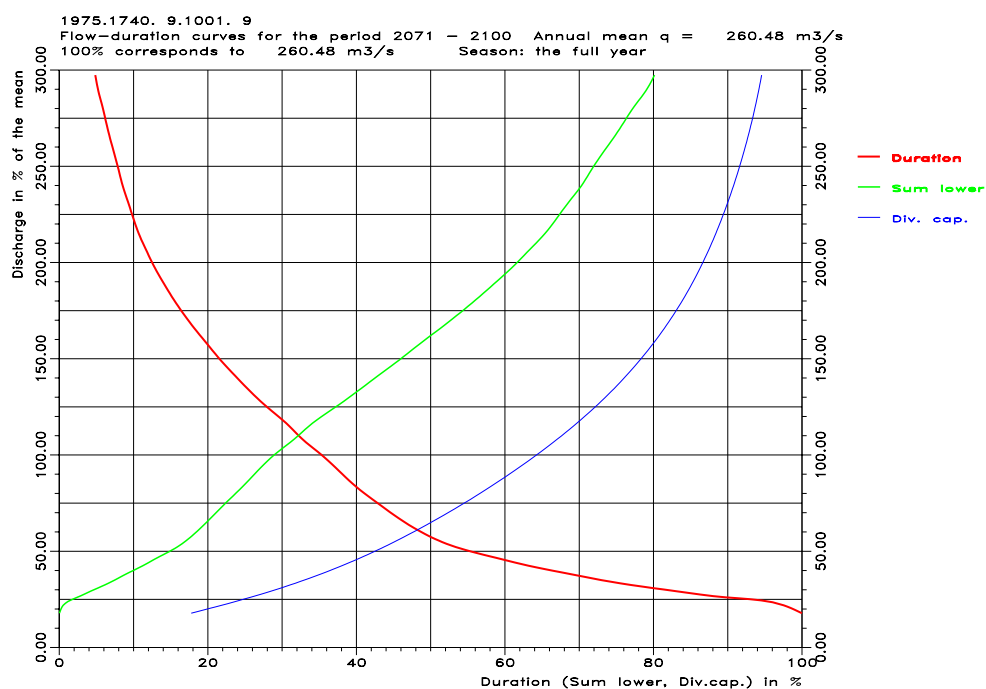


Figure F34. Curves for flow duration (red), sum lower (green) and diversion capacity (blue) for catchment 1740 Uzorong with precipitation and temperature input from climate projection Echam B1. Top: 2071-2100, time-variant glacier area, annual mean 260 m<sup>3</sup>/s. Bottom: 2071-2100, constant glacier area, annual mean 304 m<sup>3</sup>/s.



## **Published in the Report series 2010**

- Nr. 1 Representation of catchment hydrology, water balance, runoff and discharge in the JULES and SURFEX land surface models. Tuomo Saloranta (26 s.)
- Nr. 2 Mapping of selected markets with Nodal pricing or similar systems Australia, New Zealand and North American power markets. Vivi Mathiesen (Ed.) (44 s.)
- Nr. 3 Glaciological investigations in Norway in 2010: Bjarne Kjøllmoen (Ed.) (99 s.)
- Nr. 4 Climate change impacts on the flow regimes of rivers in Bhutan and possible consequences for hydropower development. Stein Beldring (Ed.) (153 s.)









Norwegian  
Water Resources and  
Energy Directorate

Norwegian Water Resources  
and Energy Directorate

Middelthunsgate 29  
PB. 5091 Majorstuen,  
N-0301 Oslo Norway

Telephone: +47 09575  
Internet: [www.nve.no](http://www.nve.no)